

**The fate of potassium and ash from biomass combustion and
their impact on the degradation of monoethanolamine (MEA)
for carbon capture**

Diarmaid Clery

Submitted in accordance with the requirements for the degree of Doctor of
Philosophy as part of the integrated PhD with MSc in Bioenergy

Centre of Doctoral Training in Bioenergy,
School of Chemical and Process Engineering,
And School of Chemistry,
The University of Leeds

May 2019

The candidate confirms that the work submitted is his own except where work which has formed part of jointly authored publications has been included. The contribution of the candidate and the other authors to this work has been explicitly indicated below. The candidate confirms that appropriate credit has been given within the thesis where reference has been made to the work of others.

Chapter 4 is based on the work from the jointly authored publication below. The candidate is the first author of the publication with the project supervisors as the co-authors.

Chapter 4

Clery, D., Mason, P.E., Rayner, C.M., and Jones, J.M. (2018) The effects of an additive on the release of potassium in biomass combustion. *Fuel*, 214. pp. 647-655. <https://doi.org/10.1016/j.fuel.2017.11.040>

DC, PM, and JJ designed the research. PM designed the apparatus and introduced to DC. DC carried out all experimentation and analysis and wrote the manuscript. All evaluated the results and contributed to the manuscript.

This copy has been supplied on the understanding that it is copyright material and that no quotation from the thesis may be published without proper acknowledgement.

The right of Diarmaid Seosamh Clery to be identified as Author of this work has been asserted by him in accordance with the Copyright, Designs and Patents Act 1988.

Acknowledgements

I would firstly like to thank my supervisors, Professor Jenny Jones, Professor Chris Rayner and Dr. Patrick Mason for their direction and encouragement throughout the period of this PhD.

I would also like to thank my supervisors' respective research groups. The Rayner group have been an incredible source of guidance in the laboratory – thank you Dr. Meryem Benohoud, Dr. James Wheatley, Sannia Farooque, Dr. Nikita Mexia, Muhammad Wathon, Gillian Finnerty, Nat Crompton and Harry Oates. Meryem in particular always finds the time to help others. The staff at C-Capture Ltd. were a great help with my initiation to the laboratory, namely Dr. Douglas Barnes, Dr. Gergely Jakab, Caspar Schoolderman and Dave Lawlor.

Jenny's group have provided equalled assistance. Thanks to Dr Lee Roberts, Dr Ben Dooley, Dr Bijal Gudka, Dr Leilani Darvell, Dr. Douglas Phillips, Dr. Edward Mitchell, Richard Birley and Andrew Price-Allison.

I would also like to thank the team at the PACT facilities in Sheffield for their support and collaboration throughout the project – Dr János Szuhánszki, Dr Karen Finney and Dr Muhammad Akram have provided samples and advice. The UKCCSRC and Supergen research hubs have facilitated this collaboration. The author acknowledges that the PACT facilities is funded by the Department for Business, Energy and Industrial Strategy and the EPSRC.

Thanks also to the members of staff at the University of Leeds from both the School of Chemical and Process Engineering and the School of Chemistry – Dr. Adrian Cunliffe, Karen Alves Thorne, Simon Lloyd, Simon Barrett, Dr. Mark Howard, Martin Huscroft, James Mckay, Emily Bryan-Kinns, David Haynes and Ed Woodhouse for their continued advice and support during my research time at Leeds.

My fellow students as part of the Centre for Doctoral Training in Bioenergy have been a great source of support for the duration of this integrated PhD: Luke Conibear, Andrew Dyer, Oliver Grasham, Hana Mandová, Japhet Oladipo, Kiran Parmar, Charlotte Stead and Robert White.

For financial support, I am very grateful to the EPSRC Centre for Doctoral Training in Bioenergy for the award of a postgraduate studentship, grant reference EP/L014912/1. Thanks are given to the Bio-CAP-UK project (Grant reference UKCCSRC-C1-38), a joint venture between the SUPERGEN Bioenergy Hub (Grant reference EP/P024823/1) and UKCCSRC (Grant reference EP/K000446/2). Rothamsted Research and various UK power industrial partners for the supply of biomass samples used in this project. C-Capture Ltd. for the use of their laboratories and funding of degradation vessels.

A special thank you to my new wife, Rose, and daughter, Annabelle, for distracting me from my work in the best possible way and for tolerating my grumpiness when things weren't going to plan in the lab. My mum, Siobhán, has also provided much support and advice throughout the project.

Abstract

Bioenergy with carbon capture and storage (BECCS) is expected to play an important role in mitigating the effects of climate change due to its ability, if done correctly, to remove CO₂ from the atmosphere. Many future greenhouse gas emission scenarios rely on BECCS to offset sectors that will struggle to cut emissions. The focus of this work is to examine the impact of combusting biomass on the amines used to capture CO₂ in a carbon capture plant. Biomass fuels were selected that are likely to be used by a BECCS power plant. These fuels were characterised to determine their fundamental composition and combusted under various conditions to examine the release of species volatile under combustion temperatures. Potassium is an element present in high quantities in biomass and highly volatile under combustion. A single particle combustion rig was employed to examine the release of potassium during biomass combustion and the impacts of an additive on potassium release were examined. Whilst combustion of biomass at different temperatures enabled an examination of the ashes which may encounter a carbon capture facility.

Biomass and coal ashes were used to examine the effects on the degradation of 30 wt% w/w MEA in laboratory and pilot scale experiments. Solvent samples were analysed by ¹H nuclear magnetic resonance (NMR) and gas chromatography mass spectrometry (GC-MS) for the formation degradation products. This work characterised degradation products previously identified in literature and a degradation product that had not been previously identified, which is present in significant quantities. The analysis of laboratory and pilot scale results in this thesis suggest that carbon capture solvents are likely to encounter high quantities of potassium from biomass combustion. However the degradation of MEA, and thus the associated regeneration cost, may be less when carbon capture is used with biomass flue gases rather than coal. The important findings of this work provides initial evidence for the installation of post-combustion carbon capture technologies working well with gases produced from biomass combustion.

Table of Contents

Acknowledgements	ii
Abstract	iv
Table of Contents	v
List of Tables	xi
List of Figures	xiii
Abbreviations	xviii
Chapter 1 The role of BECCS	1
1.1 Introduction	1
1.2 Climate change.....	1
1.2.1 The greenhouse effect	1
1.2.2 Global emissions and policies	3
1.2.3 UK emissions and policies	7
1.2.4 Governmental support for low carbon technologies	10
1.3 Carbon Capture and Storage (CCS) technologies	11
1.3.1 CO ₂ Capture	11
1.3.1.1 Carbon dioxide separation technologies	13
1.3.1.2 Next generation capture technologies	15
1.3.2 CO ₂ Transport	16
1.3.3 CO ₂ Utilisation	16
1.3.4 CO ₂ Storage.....	18
1.4 Bioenergy with Carbon Capture and Storage (BECCS)	19
1.4.1 Biomass for power generation	19
1.4.2 Biomass combustion with carbon capture.....	20
1.4.3 Barriers facing the implementation of BECCS	21
1.4.4 Alternative methods of Greenhouse Gas Removal (GGR)	25
1.4.4.1 Afforestation	25
1.4.4.2 Direct Air Capture and Carbon Storage (DACCS).....	26
1.4.4.3 Other Greenhouse Gas Removal (GGR) technologies.....	26
1.5 Conclusions	27

Chapter 2	Aims and objectives of thesis.....	29
2.1	Context.....	29
2.2	Aims and objectives.....	29
2.3	Structure of thesis.....	31
Chapter 3	Literature review on biomass combustion, carbon capture and amine degradation.....	32
3.1	Introduction.....	32
3.2	Solid fuels.....	32
3.2.1	Types of solid biomass.....	32
3.2.1.1	Woody biomass.....	33
3.2.1.2	Waste wood.....	33
3.2.1.3	Herbaceous and fruit biomass.....	34
3.2.2	Biomass formation and structure.....	35
3.2.3	Coal formation and structure.....	36
3.3	The combustion of solid fuels.....	36
3.3.1	Large-scale combustion of biomass.....	37
3.3.2	Drying and ignition.....	38
3.3.3	Volatile combustion.....	38
3.3.4	Char combustion.....	39
3.4	The fate of ash from biomass combustion.....	40
3.4.1	Ash formation.....	40
3.4.2	Ash deposition.....	41
3.4.2.1	Slag formation.....	42
3.4.2.2	Fouling.....	43
3.4.3	Flue gas treatment technologies.....	44
3.4.3.1	Cyclone separators.....	45
3.4.3.2	Fabric filters.....	45
3.4.3.3	Electrostatic Precipitators (ESPs).....	45
3.4.3.4	NO _x and SO _x control technologies.....	45
3.5	Additives to mitigate K release.....	45
3.5.1	The fate of K in biomass combustion.....	46
3.5.2	Aluminosilicate additives.....	47
3.5.3	Other additives.....	49
3.6	Chemistry of carbon capture with monoethanolamine (MEA).....	50

3.6.1	Introduction to amines for carbon capture	50
3.6.2	Hydration of carbon dioxide	52
3.6.3	Carbamate formation through a zwitterion mechanism	52
3.6.4	Bicarbonate formation through base-catalysed hydration of CO ₂	54
3.6.5	Reaction pathways effect on rate and capacity	55
3.6.6	Amine regeneration	56
3.7	The degradation of MEA in carbon capture.....	57
3.7.1	Introduction	57
3.7.1.1	Flue gas impurities	57
3.7.1.2	Elemental accumulation in MEA solvents	58
3.7.2	Thermal degradation	59
3.7.3	Oxidative degradation	61
3.7.3.1	Primary oxidative degradation products	61
3.7.3.2	Secondary oxidative degradation products	62
3.7.3.3	Heat Stable Salts (HSS) in MEA solvents	64
3.7.4	Pilot-scale degradation	66
3.7.5	Previous use of ¹ H NMR spectroscopy for MEA speciation and degradation	66
3.7.6	The release of amine products to the atmosphere	67
3.8	Conclusions	68
Chapter 4 The laboratory-scale release of potassium in biomass combustion and the effects of an additive.....		69
4.1	Introduction	69
4.2	Experimental methodology	69
4.2.1	Fuel selection and preparation	69
4.2.2	Fuel characterisation	70
4.2.3	Biomass and coal ash compositions	72
4.2.4	Potassium released in the combustion of single particles	73
4.2.5	Biomass ashing experiments	77
4.3	Results	81
4.3.1	Gas phase potassium release profiles of biomass fuels with additive.....	81
4.3.2	Particle surface temperature profile for olive cake	83
4.3.3	Potassium held in the solid phase.....	84
4.4	Analysis and Discussion	87

4.4.1	Release of K during the stages of combustion from single particles	87
4.4.1.1	Normalised K release signal per molar quantity of K.....	90
4.4.2	Ashing experiments.....	93
4.5	Conclusions	96
Chapter 5 Experimental work on the impact of biomass ash and K salts on the capture performance and degradation of MEA.....		98
5.1	Introduction	98
5.2	Experimental methodology and results	99
5.2.1	CO ₂ absorption analysis with ¹ H NMR spectroscopy	99
5.2.2	CO ₂ absorption analysis with vapour-liquid equilibrium apparatus	101
5.2.3	Thermal degradation procedure and results	103
5.2.3.1	Thermal MEA degradation product analysis	104
5.2.3.2	Presence of leached metals in thermally degraded MEA solvents..	109
5.2.4	Oxidative MEA degradation procedure and results	110
5.2.4.1	Oxidative MEA degradation analysis with ¹ H NMR spectroscopy	112
5.2.4.2	Purification of oxidative MEA degradation products	118
5.2.4.3	Identification of unknown oxidation product with ¹ H NMR spectroscopy.....	118
5.2.4.4	Synthesis of (hydroxyethyl)imidazole-N-oxide (HEINO).....	121
5.2.4.5	Impacts of potassium chloride, biomass ash and coal ash on oxidative degradation with ¹ H NMR spectroscopy.....	125
5.2.4.6	Validation of the known oxidative degradation product formation with GC-MS	127
5.2.4.7	Presence of Heat Stable Salts (HSS) in oxidative MEA solvents ...	130
5.2.4.8	Presence of leached metals in oxidative MEA solvents.....	131
5.3	Analysis and discussion	132
5.3.1	CO ₂ absorption	132
5.3.2	Thermal Degradation.....	133
5.3.3	Oxidative Degradation	133
5.4	Conclusions	135
Chapter 6 Pilot-scale fate of potassium		137
6.1	Introduction	137
6.2	Experimental Methodology.....	138
6.2.1	Fuel feedstocks.....	138

6.2.2	250kW pilot-scale combustion rig	139
6.2.3	Ash collection from pilot combustion rig	141
6.2.4	Pilot-scale post-combustion carbon capture facility	142
6.3	Results	144
6.3.1	Composition of ashes from particle removal locations	144
6.3.2	Elemental accumulation in pilot-scale MEA solvents	149
6.3.3	Degradation products in pilot-scale MEA solvents	150
6.3.4	Heat stable salts (HSS) in pilot-scale MEA solvents	152
6.4	Analysis and Discussion	152
6.4.1	Ashes from particle removal technologies	152
6.4.2	Quantities of K escaping removal	154
6.4.3	K in solvents	155
6.5	Conclusions	155
Chapter 7	Overall conclusions	158
7.1	Overarching key findings	158
7.2	Relevance to industrial applications of BECCS	159
7.3	Concluding remarks	159
7.4	Future research	160
7.4.1	Combustion	160
7.4.2	Amine degradation	160
Chapter 8	Experimental Details	161
8.1	Introduction	161
8.2	Biomass combustion experimental details	161
8.2.1	Fuel selection	161
8.2.2	Sample preparation	162
8.2.2.1	Retsch SM300 cutting mill	162
8.2.2.2	SPEX 6770 Freezer mill	163
8.2.2.3	SPECAC 15.011 laboratory manual hydraulic press	164
8.2.2.4	Hand drill	164
8.2.3	Fuel characterisation	164
8.2.3.1	Proximate analysis	165
8.2.3.2	Ultimate analysis	165
8.2.3.3	Inorganic content	167
8.2.4	Single Particle Combustion (SPC) rig	168

8.2.5	Laboratory ash preparations	169
8.3	Amine degradation experimental	171
8.3.1	General experimental	171
8.3.2	Spectroscopy and chromatography procedures	172
8.3.2.1	Nuclear Magnetic Resonance (NMR) spectroscopy	172
8.3.2.2	High Resolution Mass Spectrometry (HRMS).....	173
8.3.2.3	Infrared (IR) spectroscopy	174
8.3.2.4	GC-MS degradation product analysis	175
8.3.2.5	Ion Chromatography (IC).....	177
8.3.3	CO ₂ absorption procedures.....	178
8.3.3.1	CO ₂ absorption procedure for VLE measurements.....	178
8.3.4	Degradation procedures.....	179
8.3.4.1	Thermal degradation procedure and NMR spectra	179
8.3.4.2	Oxidative degradation procedure	181
8.3.5	Purification of oxidative degradation products	182
8.3.5.1	Distillation.....	182
8.3.5.2	Preparative High Performance Liquid Chromatography (HPLC)...	183
8.3.5.3	Thin-Layer Chromatography (TLC)	183
8.3.6	Synthesis of imidazole-N-oxide	184
	References	185
	Appendix 1 Integrated NMR values respective to DSS peak for oxidative degradation products, and CO₂ loadings.	201

List of Tables

Table 1.1 UK Carbon budgets and performance (BEIS, 2017a).....	8
Table 3.1 Emission limit values (mg/Nm ³) from Directive 2010/75/EU for combustion plant rated at larger than 300MW thermal input	44
Table 3.2 Primary, secondary and tertiary amine structures.....	51
Table 3.3 Major elemental accumulation from pilot MEA testing (Thompson et al., 2017).....	59
Table 3.4 Concentration of HSS form pilot testing (Thompson et al., 2017).....	65
Table 4.1 Fuel composition data (averages from duplicate runs with the standard deviation, S.D., values given for the largest value).....	72
Table 4.2 Chemical analysis of major elements present in biomass ashes and coal ash used as an additive.	73
Table 5.1 Typical NMR chemical shifts for the carboxylation of MEA	101
Table 5.2 CO ₂ absorption capacity experiments of virgin MEA with potassium salts on the VLE at 40°C	103
Table 5.3 Ash composition data for ashes used in thermal degradations of MEA .	104
Table 5.4 Typical NMR chemical shifts for thermal degradation products of MEA in D ₂ O.....	106
Table 5.5 Metals measured in the thermal degradation of MEA	109
Table 5.6 Ash composition data for ashes used in oxidative degradations of MEA	112
Table 5.7 NMR data for oxidative degradation products.....	116
Table 5.8 Chemical shifts of possible heteroaromatic compounds (Pretsch et al., 2009).....	120
Table 5.9 Heteroaromatic compounds that could match the data collected on the unknown oxidative product and reasons for exclusion	121
Table 5.10 List of attempted reactions to synthesis N-oxide.....	123
Table 5.11 Metals present in the oxidative degradation of MEA	132
Table 6.1 Fuel and ash composition analysis for the raw biomass and coal fuels used, from (Finney et al., 2018).	139
Table 6.2 Quantities of ash collected by the three ash collection locations adapted from (Al-Qayim, 2017)	145

Table 6.3 Ash composition analysis for heavy fly ashes	147
Table 6.4 Ash composition analysis for fly ashes collected at the cyclone	148
Table 6.5 Ash composition analysis for fly ashes collected at the candle filter	149
Table 6.6 Elemental accumulation analysis by ICP-OES for MEA solvents from the PACT facility trials.	150
Table 8.1 Theoretical and measured ash contents of the biomass with additive blends	170
Table 8.2 Total pressures calculated for various degradation experiment temperatures	180

List of Figures

Figure 1.1 Radiative forcing estimates for 2011 relative to 1750 (IPCC, 2014a)	2
Figure 1.2 World primary energy demand predictions in Millions of tonnes of oil equivalent (Mtoe) by fuel based on the implementation of current policy intentions (IEA, 2017).....	4
Figure 1.3 Globally averaged greenhouse gas concentrations (IPCC, 2014b).	5
Figure 1.4 Global CO ₂ emissions reductions forecast by energy source, based comparison of current policy vs. new policies that limit CO ₂ concentrations to 450ppm (IEA, 2017).	6
Figure 1.5 Observed global temperature change relative to 1850-1900 averages and predicted future projections for different pathways (IPCC, 2018).....	6
Figure 1.6 Electricity generation in the UK by fuel type (BEIS, 2018b)	9
Figure 1.7 Renewable electricity generation (BEIS, 2018a).....	9
Figure 1.8 Carbon Capture Process Flowsheet Diagram from (CO2CRC, 2018)	13
Figure 1.9 BEIS assessment of future carbon values (BEIS, 2017b)	23
Figure 3.1 Structures of coumaryl, coniferyl and sinapyl alcohols.....	35
Figure 3.2 A typical fluidised bed biomass power station schematic.	37
Figure 3.3 Main reaction mechanisms in the formation of ash from biomass combustion, from (Loo and Koppejan, 2008).	40
Figure 3.4 Transformation of ash material from biomass (Bryers, 1996)	42
Figure 3.5 K ₂ O-SiO ₂ -Al ₂ O ₃ ternary diagram with solidus temperatures from (Öhman and Nordin, 2000).	48
Figure 3.6 K ₂ O-SiO ₂ -CaO ternary diagram with solidus temperatures from (Öhman and Nordin, 2000).	50
Figure 3.7 The zwitterionic carbamate formation mechanism.....	53
Figure 3.8 Reaction of CO ₂ with amine to form bicarbonate	54
Figure 3.9 Absorption capacity of 76 amines against their pKa (Puxty et al., 2009)	56
Figure 3.10 Absorption rate of 76 amines against their pKa (Puxty et al., 2009)....	56
Figure 3.11 2-oxazolidone formation from MEA carbamate.....	60
Figure 3.12 HEEDA formation from 2-oxazolidinone	60
Figure 3.13 HEIA formation from HEEDA.....	60
Figure 3.14 Primary oxidative degradation products	61

Figure 3.15 Formation of secondary oxidative degradation products, HEF and HEA	62
Figure 3.16 Suggested formation of HEI from formaldehyde, oxalic acid and ammonia by (Vevelstad et al., 2013).....	62
Figure 3.17 Suggested formation of HEGly from (Da Silva et al., 2012) and HEPO from (Vevelstad et al., 2014).....	63
Figure 3.18 Formation of BHEOX from oxalic acid and MEA (Supap et al., 2011)	64
Figure 3.19 The role of hydrochloric acid (HCl) in MEA degradation to a MEA- chloride heat stable salt (HSS).	65
Figure 3.20 Formic acid in MEA degradation to a MEA-formic acid heat stable salt (HSS).....	66
Figure 3.21 Formation of nitramines and nitrosamines from DEA	67
Figure 4.1 Example SPC output of 3 repeated runs for olive pellets weighing 42.5 mg (run 1), 35.9 mg (run 2) and 23.6mg (run 3).	75
Figure 4.2 Stages of biomass combustion on SPC.....	76
Figure 4.3 Example output for SPC photo-detection (Mason, Darvell, et al., 2016)	77
Figure 4.4 Carbon in ash weight percentage for the different biomass types with temperature.	78
Figure 4.5 Ash content with temperature for (a) wood (b) wheat straw and (c) olive cake.....	80
Figure 4.6 Potassium release profiles for biomass pellets with 0/5/15/25 wt% additive for (a) 31 ± 6 mg of wood (b) 35 ± 7 mg of wheat straw and (c) 35 ± 7 mg of olive cake. Profiles are averages of a minimum of three test runs. Labels refer to: (i) Volatile combustion; (ii) Char combustion; (iii) 'Ash cooking'	81
Figure 4.7 Mean surface temperature of olive pellets derived from thermal imaging analysis	84
Figure 4.8 Residual potassium oxide (K_2O) in biomass ash with additive at increasing temperatures for (a) wood (b) wheat straw and (c) olive cake.	86
Figure 4.9 Quantities of K released during (a) volatile combustion (b) char combustion (plotted on a logarithmic scale) and (c) the 'ash-cooking' stages.	89

Figure 4.10 Potassium release per molar K in the biomass pellets with 0/5/15/25 wt% additive for (a) 31 ± 6 mg of wood (b) 35 ± 7 mg of wheat straw and (c) 35 ± 7 mg of olive cake. Profiles are averages of a minimum of three tests runs. Labels refer to (ii) Char combustion; (iii) ‘Ash cooking’	91
Figure 4.11 Relationship between the percentage of additive and (a) the total K release (b) total K release per mole of K.....	92
Figure 4.12 Potassium in biomass ash relative to initial content for (a) wood (b) wheat straw and (c) olive cake.	95
Figure 5.1 ^1H NMR stacked spectra for the carboxylation of 30% w/w MEA (with species assignment)	100
Figure 5.2 VLE equipment schematic.....	102
Figure 5.3 Thermal degradation products	104
Figure 5.4 ^1H NMR spectra of the pure thermal degradation products in D_2O	105
Figure 5.5 Product formation of a) OZD b) HEIA and c) HEEDA in the thermal degradation of MEA alone, MEA with coal ash #1, PACT wood ash and KCl.	108
Figure 5.6 Open-batch oxidative degradation set-up	110
Figure 5.7 Example ^1H stacked spectra following the oxidative degradation of MEA over 21 days	113
Figure 5.8 Major oxidative degradation products	114
Figure 5.9 Aromatic region of NMR spectra for oxidative degradation of MEA in the presence of olive ash	115
Figure 5.10 Equilibrium of HEI and protonated HEI	117
Figure 5.11 Stacked ^1H NMR of HEI with varied pH	117
Figure 5.12 Oxidation of HEI to (hydroxyethyl)imidazole-N-oxide (HEINO).....	122
Figure 5.13 Synthesis of (hydroxyethyl)imidazole-N-oxide (HEINO)	124
Figure 5.14 Formation of m-chloro-benzoic acid as a by-product from the oxidation of HEI with <i>m</i> CPBA, and resultant salt formation.....	125
Figure 5.15 Formation of N-(2-Hydroxyethyl)imidazole (HEI) during the sparging of 30 wt% MEA with compressed air at 40°C	126
Figure 5.16 Formation of HEINO during the sparging of 30 wt% MEA with compressed air at 40°C	127

Figure 5.17 Formation of N-(2-hydroxyethyl)formamide (HEF) during the sparging of 30 wt% MEA with compressed air at 40°C.	127
Figure 5.18 Comparison of measurement techniques analysing the formation of HEI in the oxidative degradation of MEA through sparging with compressed air at 40°C.....	129
Figure 5.19 Comparison of measurement techniques analysing the formation of HEINO in the oxidative degradation of MEA through sparging with compressed air at 40°C.....	129
Figure 5.20 Comparison of measurement techniques analysing the formation of HEF in the oxidative degradation of MEA through sparging with compressed air at 40°C.....	130
Figure 5.21 Formation of HSS's under oxidative degradation conditions	131
Figure 5.22 Correlation of potassium in solvent with potassium in ash	134
Figure 5.23 The combined integration of NMR peaks of HEI, HEF and HEINO, for a cumulative plot of the major degradation products	135
Figure 6.1 Dimensions of down-fired furnace from (Xing, 2016), with interchangeable burners located at (0,0).....	140
Figure 6.2 PACT pilot-scale combustion facility and ash sampling locations, adapted from (Finney et al., 2018).....	142
Figure 6.3 Schematic of the pilot-scale carbon capture plant at PACT, adapted from (Akram et al. 2016)	143
Figure 6.4 Elemental oxide analysis of heavy fly ash collected at location 1.....	147
Figure 6.5 Elemental oxide analysis of fly ash collected at location 2	148
Figure 6.6 Elemental oxide analysis of fly ash collected at location 3	149
Figure 6.7 Degradation product quantities in pilot-scale MEA samples measured with GC-MS	151
Figure 6.8 Trend comparison of extrapolated HEINO formed under pilot scale experiments compared to the laboratory MEA oxidation	151
Figure 6.9 HSS quantities measured in pilot-scale MEA samples.....	152
Figure 6.10 Biomass ash flow at PACT facilities	154
Figure 8.1 Biomass fuel samples used by this work; a) North American white wood pellet; b) UK wheat straw; c) olive cake.	161
Figure 8.2 Retsch SM300 Cutting Mill.....	162
Figure 8.3 SPEX 6770 freezer mill	163

Figure 8.4 SPECAC 15.011 laboratory manual hydraulic press.....	164
Figure 8.5 CE Instrument Flash EA 112 Series elemental analyser	166
Figure 8.6 Varian AA240FS atomic absorption spectrophotometer.....	167
Figure 8.7 Single Particle Combustion Rig	168
Figure 8.8 Bruker Avance III HD-400 NMR spectrometer	172
Figure 8.9 Structure of 4,4-dimethyl-4-silapentane-1-sulfonic acid.....	172
Figure 8.10 Bruker maxis impact spectrometer	173
Figure 8.11 Bruker Alpha FT-IR spectrometer.....	174
Figure 8.12 Perkin Elmer Clarus GC-MS with autosampler	175
Figure 8.13 Example GC-MS chromatogram of thermally degraded MEA solvent	176
Figure 8.14 Example GC-MS chromatogram of MEA solvent degraded through oxidation.....	176
Figure 8.15 Dionex ICS-900 ion chromatography system.....	177
Figure 8.16 Vapour-liquid equilibrium (VLE) apparatus at C-Capture Ltd.	178
Figure 8.17 Vapour pressure of MEA against temperature	179
Figure 8.18 Oxidative degradation apparatus set-up.....	181
Figure 8.19 Distillation apparatus set-up	182
Figure 8.20 Agilent 1260 Mass Directed Preparative HPLC.....	183
Figure 8.21 Thin-layer chromatography (TLC) of degradation products in 20 % MeOH, 80% DCM and 5 % Triethylamine.....	184

Abbreviations

AAS	Atomic Absorption Spectroscopy
AFOLU	Agriculture Forestry and Other Land Use
BECCS	Bio-energy Carbon Capture and Storage
BEIS	Department of Business, Energy and Industrial Strategy
BHEOX	N,N'-Bis(2-hydroxyethyl)oxalamide
CaL	Calcium Looping Technology
CCC	Committee on Climate Change
CCGT	Combined Cycle Gas Turbines
CCS	Carbon Capture and Storage
CCU	Carbon Capture and Utilisation
CCUS	Carbon Capture Utilisation and Storage
CDR	Carbon Dioxide Removal
CFB	Circulating Fluidised Bed
CfDs	Contracts for Difference
CLC	Chemical Looping Combustion
CO _{2e}	Carbon dioxide equivalent
DAC	Direct Air Capture
DACCS	Direct Air Capture and Storage
daf	Dry Ash Free
DCM	Dichloromethane
DEA	Diethanolamine
DECC	Department of Energy and Climate Change
DSS	4,4-Dimethyl-4-silpentane-1-sulfonic acid
EMR	Electricity Market Reform
EOR	Enhanced Oil Recovery
ESP	Electrostatic Precipitator
ETI	Energy Technologies Institute
EU	European Union
FB	Fixed Bed Reactor
FC	Fixed Carbon
FGD	Flue Gas Desulphurisation
GC-MS	Gas Chromatography Mass Spectrometry

GHG	Greenhouse Gas
Gt	Gigatonnes
GWP	Global Warming Potential
HEA	N-(2-Hydroxyethyl)acetamide
HEEDA	N-(2-Hydroxyethyl)ethylenediamine
HEF	N-(2-Hydroxyethyl)formamide
HEGly	N-(2-Hydroxyethyl)glycine
HEI	N-(2-Hydroxyethyl)imidazole
HEIA	1-(2-Hydroxyethyl)-2-imidazolidone
HEINO	N-(2-Hydroxyethyl)imidazole-N-oxide
HEPO	4-(2-Hydroxyethyl)piperazin-2-one
HPLC	High Performance Liquid Chromatography
HSS	Heat Stable Salt
IC	Ion Chromatography
ICP-OES	Inductively Coupled Plasma – Optical Emission Spectroscopy
IEA	International Energy Agency
IEAGHG	International Energy Agency Greenhouse Gas R & D Programme
IGCC	Integrated Gasification Combined Cycle
INDC	Intended National Determined Contributions
IPCC	Intergovernmental Panel on Climate Change
IR	Infrared
LCA	Life Cycle Assessment
LC-MS	Liquid Chromatography Mass Spectrometry
LCPD	Large Combustion Plant Directive
mCPBA	<i>meta</i> -Chloroperoxybenzoic acid
MDEA	Methyldiethanolamine
MEA	Monoethanolamine
Mha	Mega hectare
Mt	Mega tonnes
MtOe	Million Tonnes of Oil Equivalent
MWh	Megawatt Hour
NET	Negative Emission Technology
NERC	Natural Environment Research Council
NMR	Nuclear Magnetic Resonance
OFGEM	Office for Gas and Energy Market

OZD	2-Oxazolidone
PACT	Pilot Scale Advanced Capture Technology Facilities
PCC	Post-combustion capture
PF	Pulverised Fuel
PM	Particulate Matter
RF	Radiative Forcing
ROCs	Renewable Obligation Certificates
TGA	Thermogravimetric Analyser
TLC	Thin Layer Chromatography
TRL	Technology Readiness Level
SEM	Scanning Electron Microscopy
SPC	Single Particle Combustion
SRC	Short Rotation Coppice
SRF	Short Rotation Forestry
UKCCSRC	UK Carbon Capture and Storage Research Centre
UNFCCC	United Nations Framework on Climate Change Committee
VLE	Vapour-Liquid Equilibrium

Chapter 1

The role of BECCS

1.1 Introduction

It is now generally accepted amongst the public and scientists that the human race is having an undesirable impact on the temperature of our planet. We are already seeing changes to our climate as extreme weather scenarios increase across the globe; sea levels continue to rise and irreversible changes to oceans and ecosystems are being observed (IPCC, 2018a). This chapter will give an overview of the current climate situation, including the role of carbon dioxide in global warming, relevant policy, targets and technologies available to assist in minimising the warming of the planet. A detailed overview of carbon capture and storage (CCS), bioenergy with carbon capture and storage (BECCS) and other greenhouse gas removal (GGR) technologies is provided.

1.2 Climate change

1.2.1 The greenhouse effect

The slow increase in global temperature since the industrial revolution of the 18th century is closely linked with the rise in anthropogenic emissions (IPCC, 2018a). These emissions contain gases, known as greenhouse gases (GHGs), which prevent infrared (IR) radiation from the sun leaving the Earth's atmosphere, resulting in a warming effect similar to that experienced by a greenhouse – hence the name.

The two double bonds of carbon dioxide (CO₂) give the gas a strong IR absorption at 2349cm⁻¹ and 667 cm⁻¹. This absorbance has been identified by climate scientists as a primary contributor to man-made global warming by affecting the incoming and outgoing radiative energy from the planet's atmosphere, known as radiative forcing (RF). Carbon dioxide (CO₂) is one of several greenhouse gases (GHGs) that has this warming effect along with water vapour (H₂O), methane (CH₄), nitrous oxide (N₂O), Ozone (O₃) and fluorinated gases. Different molecules have differing RF values

depending on how much energy is let in to the planet’s atmosphere minus the amount of energy being released. Figure 1.1 shows the estimated radiative forcing of GHGs and other radiative agents, whereby a large RF value is seen for CO₂ compared to other GHGs. The effect from GHGs and other radiative agents, such as aerosols, solar radiation and albedo, are combined to give the overall radiative forcing exerted on the planet’s atmosphere.

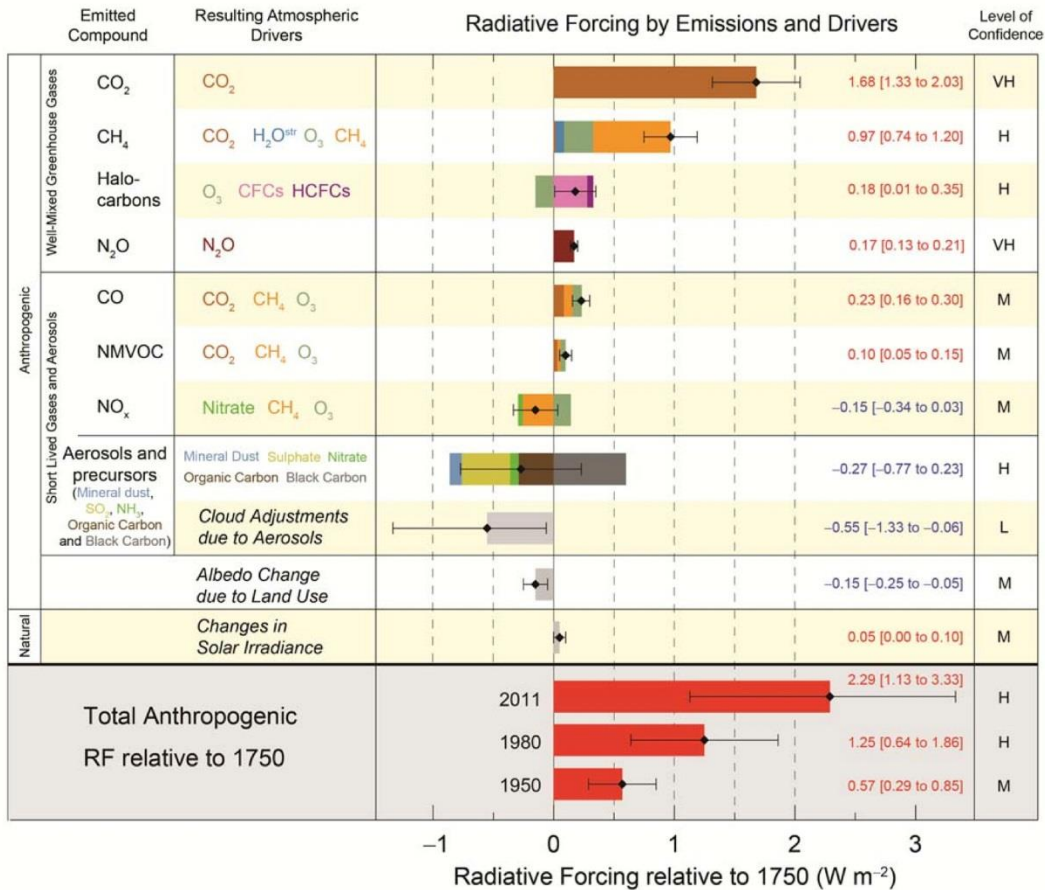


Figure 1.1 Radiative forcing estimates for 2011 relative to 1750 (IPCC, 2014a)

Another measure used to compare the impacts of GHGs in the atmosphere is global warming potential (GWP). It is calculated as the averaged radiative forcing impacts of particular GHGs relative to CO₂ and is integrated over a period of time. Carbon dioxide is the reference gas for this measure and thus has a GWP equal to 1. Some molecules, such as methane and nitrous oxide, have higher GWP values than carbon dioxide on a molar basis, 34 and 298 over 100 years, respectively. However the larger concentrations and longer lifetime of CO₂ (200 times more concentrated than methane) in the atmosphere make its contribution to the greenhouse effect larger and hence its removal more beneficial (Lashof and Ahuja, 1990). Thus, large global

efforts are being taken to reduce anthropogenic emissions of CO₂ from large scale processes.

An alternative to reducing emissions is to actively remove greenhouse gases from the atmosphere – a process known and referred to throughout this thesis as greenhouse gas removal (GGR), but also known by many other terms including: negative emission technologies (NET) and carbon dioxide removal (CDR). These technologies provide the opportunity to offset current GHG emissions and remove CO₂ already emitted into the atmosphere, thus providing the potential to undo some of the harmful emissions that have already occurred. However care must be taken to ensure that these GGR technologies are permanently removing and storing the GHGs out of the atmosphere – which can come with a considerable cost.

1.2.2 Global emissions and policies

Global energy demand has consistently risen over the past 30 years and is predicted to continue in the short-term future due to global population growth and the development of emerging economies such as China and the Middle East. Figure 1.2 shows the expected reliance of this growth on fossil fuels if current intentions for climate policy are implemented. This reliance is largely due to the dependence on fossil fuels by many industries such as petrochemicals, shipping and aviation. Emissions from fossil fuel combustion and cement production has increased 65% above their 1990 level by 2014 (Fuss et al., 2014). Such a large use of fossil fuels will result in continued growth of anthropogenic CO₂ emissions if mitigation technologies are not used.

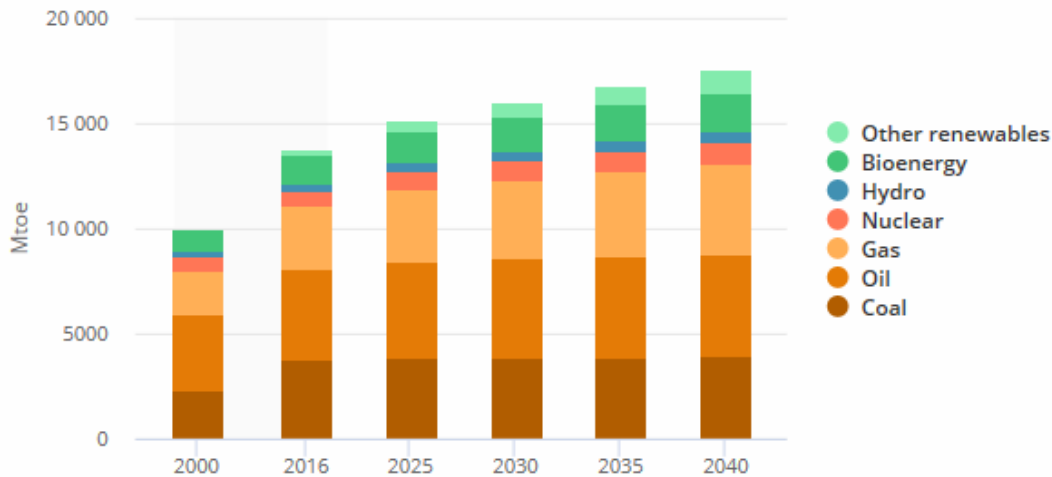


Figure 1.2 World primary energy demand predictions in Millions of tonnes of oil equivalent (Mtoe) by fuel based on the implementation of current policy intentions (IEA, 2017).

An awareness of this situation has led to growing political pressure in recent decades to prevent the irreversible effects of climate change. This resulted in 196 state parties within the United Nations Framework Convention on Climate Change (UNFCCC) agreeing to legally binding global climate targets in 2015 - known as “the Paris Agreement”. The agreement involved all parties submitting an Intended Nationally Determined Contributions (INDCs) which outlined how each signatory is planning to meet emission reduction targets, in line with the agreement's long-term goal to keep the increase in global temperature rise to well below 2°C above pre-industrial levels and if possible, keep below 1.5°C increase. The agreement has been ratified by 182 of the 196 UNFCCC parties and it came into force in November 2016 (UNFCCC, 2017). However, it has been identified that the current INDCs in place would result in a best-case outcome of around 3°C temperature increase (UNEP, 2017), identifying the need for updated policies. Also, U.S. President Donald Trump announced in 2017 that he intends to withdraw the USA from the Paris Agreement.

In order to achieve the climate targets of limiting global temperature rise to 1.5°C or 2°C the Intergovernmental Panel on Climate Change’s (IPCC) fifth report estimated that stabilising CO₂ atmospheric concentrations at 430 or 450 ppm, respectively, would likely be adequate. Concentrations of CO₂ in the atmosphere have risen from approximately 280ppm over the 1750-1900 period, to approximately 310ppm in the

1950s and 400ppm in 2013. This accelerating rate of increase is illustrated in Figure 1.3, thus CO₂ concentrations of 450ppm are likely to occur in the short-term future without dramatic reductions in carbon emissions (IPCC, 2014b).

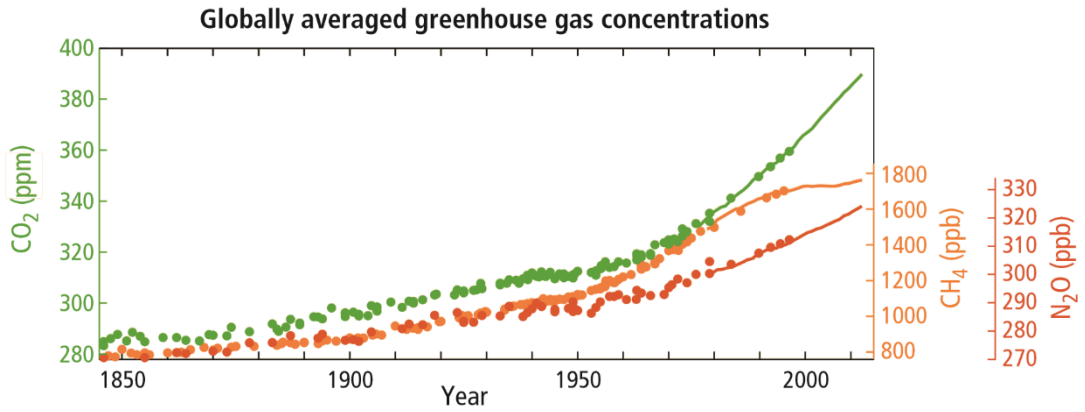


Figure 1.3 Globally averaged greenhouse gas concentrations (IPCC, 2014b).

Figure 1.4 gives a recent projection from the International Energy Agency (IEA) on how energy production is expected to adapt to meet the Paris Agreement. There is currently a gap between the intentions of current climate policy, top line on Figure 1.4, which is expected to let CO₂ emissions grow, and what is needed to meet the 450 ppm goal, bottom line on Figure 1.4. Renewable energy technologies such as solar and wind are seen to provide considerable reductions in carbon dioxide emissions, along with large improvements in end-use efficiency. Carbon capture and storage (CCS) can be seen to make up a large (near 20%) proportion of these global emission cuts which highlights the need for deployment in the near future if global targets are to be met.

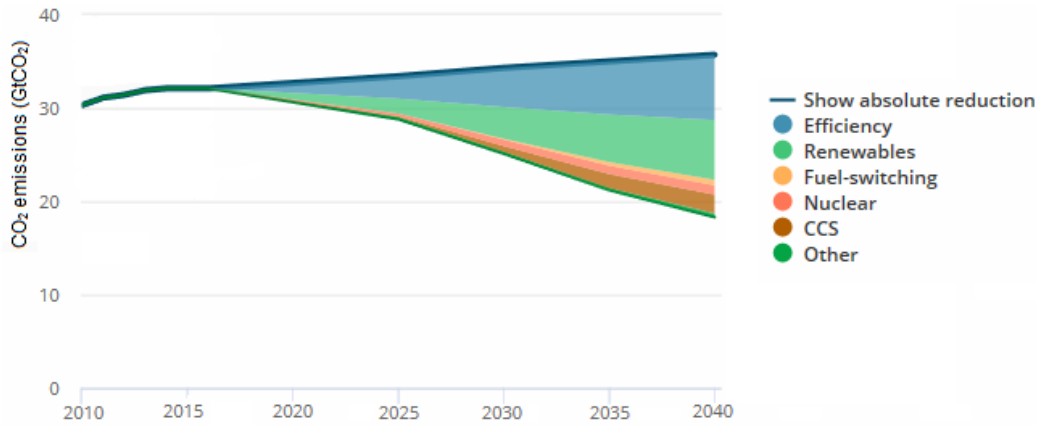


Figure 1.4 Global CO₂ emissions reductions forecast by energy source, based comparison of current policy vs. new policies that limit CO₂ concentrations to 450ppm (IEA, 2017).

In order to limit global warming to 1.5°C in line with the Paris Agreement, a recent report by the IPCC discussed the possible options. It suggested that large reductions in CO₂ emissions are needed before 2030. Figure 1.5 illustrates how reaching net-zero carbon emissions before 2050 (in blue) provides the highest probability of hitting the 1.5°C warming target, compared to reaching net-zero later (grey). However the radiative forcing impacts of non-CO₂ forcing agents (methane, nitrous oxide, aerosols and others) cannot be neglected in order to meet the target, with the purple area showing the pathway if no reductions in non-CO₂ RF occur.

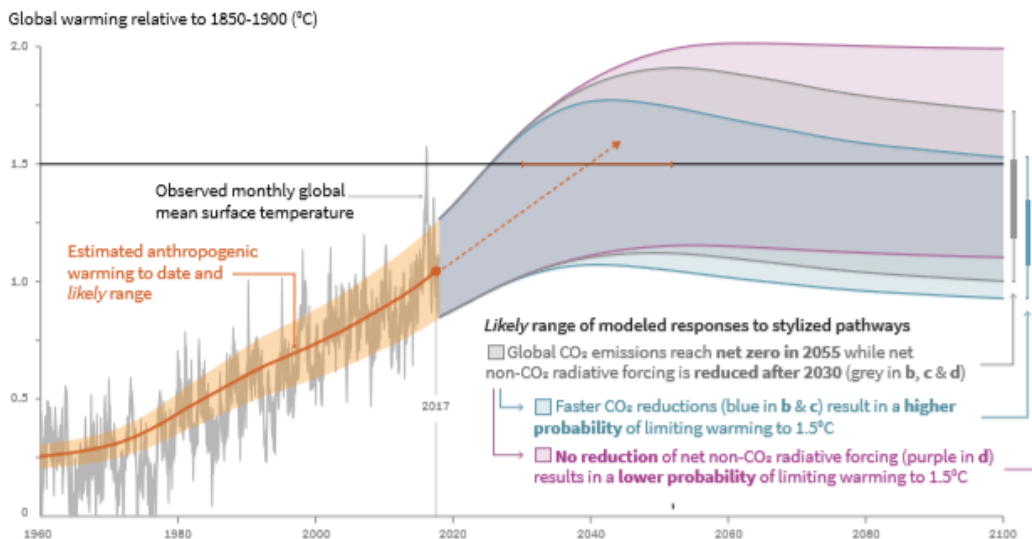


Figure 1.5 Observed global temperature change relative to 1850-1900 averages and predicted future projections for different pathways (IPCC, 2018).

However even with such reductions, global greenhouse gas removal (GGR) technologies will be required to offset carbon emissions remaining from industries such as aviation and agriculture. GGR requirements are estimated to be in the cumulative region of 810 GtCO₂ by 2100, likely requiring significant land area for bioenergy crop growth (UNEP, 2017). However, there is currently no international market to incentivise the deployment of GGR technologies. Such a market could help Paris Agreement signatories to meet net-zero targets in the most globally efficient way.

1.2.3 UK emissions and policies

The UK voted to leave the European Union in June 2016. Until the UK leaves the EU it must follow its INDC which aims for at least a 40% reduction in GHG emissions by 2030 relative to 1990 levels. The UK has recently confirmed commitment to the Paris Agreement upon leaving the EU through recent legislation to reach net zero emissions by 2050 (BEIS, 2019).

In terms of existing UK policy, in 2008 the UK passed the Climate Change Act, committing itself to a stepped percentage reduction in GHG emissions by 2050. The timing of this UK policy closely followed the ratification of the Kyoto Protocol in 2005 - an international treaty that commits state parties to reducing GHG emissions. The Climate Change Act remains as the UK's main policy for emissions reduction that aims to reduce emissions by at least 34% by 2020 and 80% by 2050, compared to 1990 levels.

In 2011, the UK Government initiated the Carbon Plan which outlines how it plans to meet the targets of the 2008 Climate Change Act. The Plan sets out 5 yearly carbon budgets, seen in Table 1.1 (reductions are in comparison to 1990 levels). Note that the 57% reduction in emissions by 2030 is significantly higher than the 40% agreed by the Paris Agreement. This explains why in 2016 the Committee on Climate Change advised that the Climate Change Act already exceeds the emissions reduction targets set by the Paris Agreement and thus no further emission reduction commitments needed to be set. However the CCC did identify that the UK should have a strategy in place to support the development GGR technologies if the UK is to achieve net zero emissions by 2050 (Committee on Climate Change, 2016).

Table 1.1 UK Carbon budgets and performance (BEIS, 2017a)

Carbon Budget:	1st	2nd	3rd	4th	5th
	2008-12	2013-17	2018-22	2023-27	2028-32
Emissions budget (Mt)	3,018	2,782	2,544	1,950	1,725
Budget reduction (%)	-25%	-31%	-37%	-51%	-57%
Projected cumulative emissions (Mt)	2,982	2,650	2,453	2,066	1,892
	Measured	Estimate	Estimate	Estimate	Estimate
Result vs. Budget (Mt)	-36	-132	-91	+116	+167
Result vs. Budget (%)	-1.2%	-4.7%	-3.6%	-6.0%	-9.7%
Cumulative surplus (Mt)		+132	+223	+107	-60

In 2017, the UK government published the ‘Clean Growth Strategy’ which stated that although the first two carbon budgets have been met, the UK is not in a strong position to meet the fourth and fifth budgets, illustrated in Table 1.1. Emissions from the power sector are highest contributor to reductions in UK carbon dioxide emissions, accounting for 75% of reductions since 2012 (Committee on Climate Change, 2018b). This has been driven by the closure of many coal fired plants or conversion to biomass in the case of Drax power station and increases in renewables which is expected to continue as seen in Figure 1.6. The use of gas is predicted to fall however it continues to be a responsive fuel for when renewable energy is naturally low due to low wind, sun or rain. This change has enabled UK emissions to drop since 1990, but has masked a lack of reductions in sectors such as waste, transport, industry, buildings and agriculture (Committee on Climate Change, 2018b).

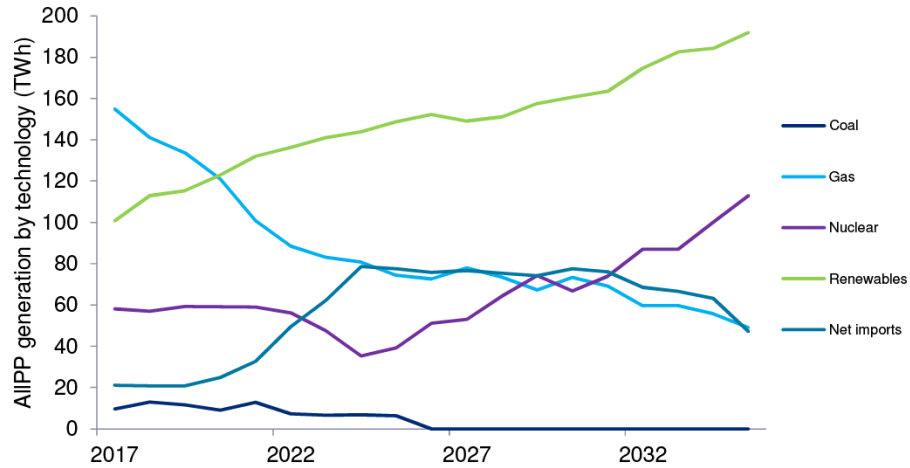


Figure 1.6 Electricity generation in the UK by fuel type (BEIS, 2018b)

The current division of this renewable energy generation is shown in Figure 1.7. As renewables start to replace fossil fuel energy generation in the coming years, the considerable proportions of bioenergy that contribute to this renewables sector can be observed. Onshore and offshore wind made up 63% of renewable generation in the first quarter of 2018, due to increased capacity and higher wind speeds. Whilst bioenergy reliably contributes ~25% to renewable generation from biomass, landfill gas, sewage gas, biodegradable municipal solid waste, anaerobic digestion and co-firing.

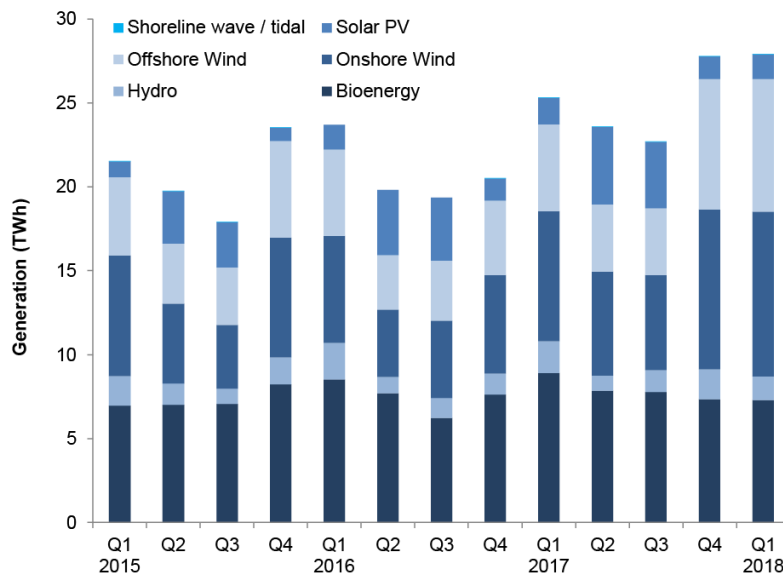


Figure 1.7 Renewable electricity generation (BEIS, 2018a)

In the Clean Growth Strategy of 2017 the government announced that it intends to enable the UK to be a global leader for carbon capture, utilisation and storage

(CCUS) technology so that large-scale deployment can occur during the 2030s. However, it identified that if this is to occur the costs of CCUS need to reduce sufficiently. BEIS will fund up to £100 million to assist the UK in CCUS innovation and deployment with £20 million going to a CCUS demonstration programme. The strategy agrees with the CCC 2016 report on the UK's need to develop GGR technologies and expressed a desire for UK to be well placed in order to exploit global demand for GGR. In April 2017 the government funded an £8.6 million research programme into GGR technologies (NERC, 2017).

In 2018 a Royal Society report reinforced the UK's urgency to implement GGR technologies soon in order to enable the acceleration of these in the following decades. As the scale of GGR required to counterbalance the emissions remaining after UK decarbonisation is approximately 130 MtCO₂ per year by 2050 (The Royal Society, 2018).

1.2.4 Governmental support for low carbon technologies

Contracts for Difference (CfD) is the government's main mechanism for providing financial support for the introduction of low carbon technologies, such as biomass, into the UK energy sector. CfD replaces the Renewable Obligation (RO) scheme which continues to pay power generators for each MWh of renewable electricity generated. The scheme will continue to pay generators already issued with Renewable Obligation Certificates (ROCs), however is no longer open to new applicants.

The CfD for renewable energy is the first key mechanism of Electricity Market Reform policy as part of the Energy Act of 2013. The CfD is a contract between a low carbon electricity generator and a government-owned company, Low Carbon Contracts Company (LCCC). This contract guarantees that a low carbon generator is paid the difference between the average market price for electricity and a fixed 'strike price' which is technology specific depending on the cost of investing in the particular low carbon technology. It provides certainty to electricity generators in the profits that can be expected from low carbon electricity generation, however if the market price of electricity exceeds the strike price the generator must pay back anything above the strike price.

The second key part of the Electricity Market Reform policy, the Capacity Market, aims to ensure that electricity is supplied to consumers at the lowest possible cost.

With the generation of power in the UK currently undergoing a large reform due to the replacement of constant output coal plants with intermittent renewable technologies, the coordination of meeting demand requirements with varying supply becomes challenging. The Capacity Market provides payments to encourage investment in new power generation technologies or to keep existing generators operational. Energy providers compete in an auction for a ‘Capacity Market Agreement’. Successful bidders are then obliged to maintain power generation facilities for times of peak demand and are provided with monthly payments for this service.

1.3 Carbon Capture and Storage (CCS) technologies

Carbon capture is a technology that provides the ability to catch approximately 85-95% of the carbon dioxide from mixed gas streams . This creates a nearly pure supply of carbon dioxide which is then transported to a geological site for permanent storage and thus removed from the atmosphere. A review of the global role of CCS in meeting climate targets identified that models estimate a cumulative range of 600-3050 GtCO₂ will require capturing by 2100 (Koelbl et al., 2014). However a recent report by the IEA reviewed current progress on CCS and deemed the progress to be behind what is need to meet climate targets (International Energy Agency, 2016). An overview of the capture options, transport and storage of carbon dioxide are given in this section.

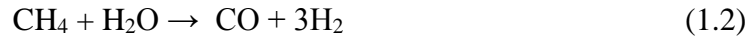
1.3.1 CO₂ Capture

Three main methods exist for capturing carbon dioxide from solid fuel combustion: pre-combustion, post-combustion capture and oxyfuel combustion. These methods will be briefly described along with the suite of technologies available for the separation of carbon dioxide from gas streams.

Pre-combustion capture

Pre-combustion capture involves converting a hydrocarbon fuel into a mixture of hydrogen and carbon dioxide as in equations (1.1)-(1.3) below. This is achieved by gasification for solid fuels, where the fuel is partially oxidised in the presence of steam at elevated temperatures and pressures to create a syngas. The syngas is mostly comprised mostly of hydrogen gas and carbon monoxide formed via

equation (1.1) and the conversion of small amounts of methane through equation (1.2) due to the presence of steam (IPCC, 2005). Carbon dioxide generated via the water shift equation (1.3) is separated for storage using absorption.



Gasification has an associated energy cost however the hydrogen generated can be used for combustion without GHG emissions in large or small scale applications such as power stations, trains or domestic appliances. A hydrogen fuelled economy would have environmental benefits as the oxidation of H₂ releases energy, with water as the only by-product (IPCC, 2005). However switching to a hydrogen fuelled economy would require costly adaptations to our current energy system, it is being explored as an alternative to natural gas for heating and vehicle fuelling in the UK (BEIS, 2017a).

Post-combustion capture (PCC)

Post-combustion capture (PCC) separates carbon dioxide from the flue gas stream of a combustion plant and has the potential to be retrofitted to existing coal, biomass or gas fired power stations. The post combustion carbon capture process is in simple terms formed of an absorber tank, where the flue gas encounters a solvent that reacts with CO₂ present in the gas stream. Absorber tanks are typically held at 40°C, hence flue gases require cooling prior to processing. The CO₂ free flue gas is then released from the absorber to atmosphere at close to atmospheric temperatures. A desorber/stripper tank is held at high temperatures (120-140°C) to release the CO₂ and recover the solvent, as illustrated in Figure 1.8. PCC using MEA is arguably one of the lead technologies for BECCS implementation, therefore this research aims to examine the effects of biomass flue gas contaminants on MEA for carbon capture.

2014, it uses Shell's CANSOLV amine solvent (IEAGHG, 2015). Petra Nova, the world's largest operating post-combustion CO₂ capture system operating on a slipstream from a coal burning power plant in Texas, US which uses KS-1, an amine solvent developed by Mitsubishi and Kansai Electric Power (IEAGHG, 2007). Both of these commercial solvent technologies contain proprietary blends of amines (Heldebrant et al., 2017). Recent years have seen the development of solvents which are less toxic (Vega et al., 2014; Vevelstad et al., 2017), faster absorbing (Puxty et al., 2009) and less degradable (Freeman et al., 2009) resulting in lower energy requirements. However, MEA remains the benchmark solvent to which other solvents are compared.

Adsorption

Adsorption is the adhesion of molecules of a gas, in this case CO₂ to a solid sorbent. Commonly used sorbents for CCS purposes includes zeolites, metal organic frameworks (MOFs), activated carbon or calcium oxides. However some sorbents are susceptible to low CO₂ selectivity, such that smaller molecule gases or impurities such as N₂ can also penetrate and fill adsorbent pores, thus decreasing the number of available active sites and decreasing efficiency (Aaron and Tsouris, 2005). The CO₂ is usually released by pressure or temperature swing adsorption (PSA/TSA). PSA/TSA are mature technologies for CO₂ release that have been used for industrial applications, whilst adsorbents prove a promising technology for processes not suited to solvent absorption, with a current TRL of 5 (Bui et al., 2018).

Chemical looping combustion (CLC)

Chemical looping combustion (CLC) is a form of oxyfuel combustion which utilises two fluidized bed (FB) systems side-by-side, a reducer and an oxidiser. CLC has been demonstrated on the megawatt scale and can be used for solid fuels such as biomass. The process uses a metal oxide, commonly a transition metal such as FeO, MnO or CuO, as an oxygen carrier to supply oxygen for combustion. The metal oxide undergoes a phase change to release the oxygen for combustion in the reducer, to generate a flue gas similar to oxy-fuel combustion and composed of CO₂ and H₂O. The H₂O is then condensed out to make a near pure stream of CO₂ for sequestration. The reduced metal oxygen carrier is separated from the flue gas by a cyclone and transferred to the oxidiser. The metal is oxidised again using oxygen from air, before the regenerated metal oxide is returned to the reducer (Boot-

Handford et al., 2014). The benefits of the CLC process include low energy penalty and cost due to a removed need for CO₂ and air separation equipment however requires regeneration of the oxygen carrier (IPCC, 2005).

Calcium looping separation (CaL)

Calcium looping (CaL) works in a similar way to the CLC process, but uses CaO as a carrier for the removal of CO₂ from flue gases post-combustion. Calcium looping uses two reactors, firstly a carbonator, where CaO reacts with CO₂ to make CaCO₃, and then the calciner, where high temperatures are used to release CO₂ and regenerate the CaO. Degradation of the CaO can be significant, however the degraded sorbent can be used to decarbonise industrial processes such as cement making (Fennell, 2015). The input sorbent also has benefits of being able to use limestone as a cheap and readily available form of sorbent (Bui et al., 2018).

1.3.1.2 Next generation capture technologies

Membrane separation

Membranes can be used to selectively separate gases. They can be applied as a pre-combustion capture method by separating H₂ from a synthesis gas as an alternative to steam reforming. Alternatively membranes can also be used to separate O₂ from air for oxyfuel combustion, or separate CO₂ from flue gases for post-combustion capture processes. There is a wide range of membrane technologies available for gas separation with permeability of the membrane being a key property for the selectivity of H₂, O₂ and CO₂. Some membrane technologies, such as porous inorganic membranes, currently do not have selectivity high enough for carbon capture applications (IPCC, 2005). There are currently no commercial examples of membrane processes for CO₂ capture and thus is given a TRL of 3 or 4. (Bui et al., 2018).

Ionic liquids

Ionic liquids (ILs) are substances completely composed entirely of ions and with a melting point below 100°C. ILs have very low vapour pressures and high conductivity. The main promise of ILs is their adaptability, as it is possible to customise the cation and anion choices to adapt the solvent characteristics (such as polarity, density, viscosity and stability) for the desired application .

ILs have shown reasonable absorption capacity in laboratory studies, TRL 3, and further potential benefits due to their stability and low volatility which avoids solvent losses from evaporation and degradation (Bui et al., 2018). However, their high viscosity leads to poor gas uptake kinetics, which combined with high costs makes their scale-up currently undesirable (Li et al., 2013).

Other CO₂ separation technologies

The technologies available for carbon dioxide separation and capture is constantly evolving given the current urgency for reductions in emissions to atmosphere. Such as, electrical desorption, hydrate based separation and redox technologies. These technologies provide promise for future deployment, however due to their currently low level of readiness for large-scale deployment they are not discussed in this work.

1.3.2 CO₂ Transport

Carbon dioxide captured by any of the methods reviewed must then be transported to a utilisation or permanent storage site. The transport of large amounts of CO₂ is already operational for enhanced oil recovery (EOR) applications, thus the technology could be used for CO₂ captured from industrial carbon capture processes. However in the UK an infrastructure does not yet exist for the large quantities of CO₂ that would require transportation from these applications. Demand for such an infrastructure is likely to be low initially due to the low number of carbon capture sites, hence a pipe network which links the largest point source emitters makes economic sense. The Europipe project examined how best to link Europe's largest CO₂ emitters for storage (Neele et al., 2013). The shipping of CO₂ is an alternative well established transport option to pipelines and requires lower infrastructure costs but limited volumes of gas (Element Energy, 2018).

1.3.3 CO₂ Utilisation

The costs associated with the storage of CO₂ has raised recent interest in the potential of adding value to the carbon capture process by utilising the CO₂ rather than storing it, widely known as carbon capture and utilisation (CCU). CCU is already applied in the food and drink sector, primarily in beverage carbonation. Such CO₂ utilisation projects have a high readiness level of 9 as they are in commercial operation (Bui et al., 2018). The implementation of CCU may improve public

acceptance of carbon capture technology as the CO₂ is reused rather than being disposed of as a waste product.

More than 250 technologies are currently in development worldwide aiming to utilise CO₂ in various ways (Scott, 2015). A recent study by Ecofys and Imperial College London assessed the potential for CCU in the UK. Which identified the most promising applications of CCU technologies for the UK market as (ECOFYS, 2018):

Carbonate mineralisation (Carbonation) is the reacting of CO₂ with Ca/MgO/Si to form a solid carbonate mineral structure which are stable over long time scales and therefore can be used as construction materials.

Concrete curing is carbonation using CO₂ to produce solid calcium carbonate (CaCO₃) which can replace traditional energy intensive steam concrete curing resulting in bound CO₂ being permanently sequestered.

Novel cements attempt to develop cements which use CO₂ as an ingredient, thus locking the CO₂ in the cement as a solid carbonate.

Horticulture can use industrial CO₂ used to enrich the growing environment of crops, however 80% is usually vented to atmosphere leaving just 20% of the CO₂ being temporarily stored in the crop (ECOFYS, 2018):.

Polymer production uses catalytic transformation of CO₂ into polycarbonates, and then polymers such as polyurethane. The CO₂ is temporarily stored in the material (up to 50% by weight) for the lifetime of the product.

Synthetic methane/methanol can be produced through the hydrogenation of CO₂, either through a catalytic or biological processes. However H₂ would need to be renewable, and CO₂ would be released when the methane is combusted.

Some CCU technologies that are commercially extracting carbon dioxide from the atmosphere are not effective at permanently storing the greenhouse gas out of the atmosphere, such as production of liquid biofuels from DAC. When the biofuel is combusted the carbon dioxide, initially removed from the atmosphere, will simply be re-emitted into the atmosphere and hence must not be considered a greenhouse gas removal (GGR) technology.

Mineral carbonation is a popular option for CO₂ usage as this method is both highly developed and permanent (IPCC, 2005). Carbon 8 has two plants that treat thermal

wastes with CO₂ to produce an aggregate. By utilising waste products such as fly ash from the energy industry the company is able to charge for the disposal of these products as a source of income (Scott, 2015).

However, the major technical challenge facing the implementation of carbon dioxide utilisation is the scale of carbon dioxide emissions. Global anthropogenic CO₂ emissions is approximately 32 GtCO₂ per annum, whereas the current global usage of CO₂ is of the order of ~200MtCO₂ per annum (Bui et al., 2018). The production of fuels from CO₂ may increase this, however these fuels would re-emit CO₂ to the atmosphere.

On a UK scale, it is estimated that the total size of the UK market for CO₂ in 2016 was 400-500 ktCO₂/yr whereas Drax power station alone emits 12 MtCO₂ per year (Drax Group Plc, 2017). This makes it unlikely that CCU will only contribute very small amounts towards the mitigation of climate change, with the potential to storage less than 1% of the UK and global CO₂ emissions. However it likely to remain present alongside CCS as a method to decarbonise the chemical industry (Peters et al., 2011; Markewitz et al., 2012).

Carbon dioxide enhanced oil recovery (CO₂-EOR) is also a mature form of CO₂ utilisation technology which enhances the quantities of oil extracted from depleted reservoirs. The technology can be implemented with the intention of permanently storing the carbon dioxide in the reservoir, known as carbon capture and storage with enhanced oil recovery (CCS-EOR). Thus providing a financial incentive for CO₂ storage, however this comes with the significant drawback of generating oil which will re-emit CO₂ into the atmosphere if it is not captured during processing.

1.3.4 CO₂ Storage

The capture of carbon dioxide from any technology to produce a near pure stream of CO₂ requires permanent storage of the gas in order to have a mitigation effect on the climate. This storage can be in any form that permanently retains the CO₂ out of the atmosphere, including the utilisation methods described above, however this section will examine the geological storage options for CO₂ that cannot be utilised.

The UK has access to substantial potential CO₂ storage sites beneath the North Sea. Depleted oil and gas fields and saline aquifers can provide 1-20 GtCO₂ of storage capacity (Energy Technologies Institute, 2016), adequate for UK storage

requirement. While global CO₂ sedimentary storage capacity is estimated to be 3360 GtCO₂ (IEA, 2013), ample for the cumulative 600-3050 GtCO₂ estimated to require storing by 2100 (Koelbl et al., 2014). Leakage must be monitored for the lifetime of the storage but it is trusted that CO₂ can be safely store by this method for more than a thousand years (IPCC, 2005).

1.4 Bioenergy with Carbon Capture and Storage (BECCS)

As identified in section 1.2, even with large reductions in CO₂ in the next 12 years it is likely that a combination of greenhouse gas removal (GGR) technologies will be needed in order to meet limit global warming to 1.5°C. BECCS is a leading GGR technology which can be used to offset unavoidable carbon emissions remaining from industries such as aviation and agriculture. The IPCC recently identified that BECCS will likely be required to globally remove 0–8 GtCO₂ per annum by 2050 if no temperature overshoot of the 1.5°C global warming target specified in Paris is to be achieved (IPCC, 2018b).

This section will give an overview of biomass for power generation, BECCS and other technologies available for the removal of carbon dioxide from the atmosphere. Also included is an overview of the major barriers facing the implementation of GGR technologies and ways to overcome these challenges.

1.4.1 Biomass for power generation

With the phase out of all coal-fired power stations within the UK by 2025, biomass combustion has become an important technology to act as a comparable substitute for solid fuel power generation. Drax power station is currently the UK's largest power plant and point source emitter of CO₂ in the UK. The plant has switched three of its generating units to burn compressed wood pellets instead of coal in recent years.

The term 'biomass' covers a wide variety of organic matter which can be used to generate useful energy. Some examples include: trees, dedicated crops, trimmings, organic waste and peat. The combustion of these biomass will result in a similar amount of carbon dioxide released as coal, however biomass combustion is close to 'carbon neutral' due to the carbon dioxide that is absorbed by the plant during growing. Based on this, international accounting of CO₂ emissions does not

currently include biogenic emissions from biomass combustion at UK power stations (Committee on Climate Change, 2018a). This is an important gap that exists in current international reporting, as CO₂ is being released into the atmosphere and countries that are exporting biomass are not required to account for the use of that biomass. Changes in land carbon stocks are reported in EU Land use, Land-use change and Forestry (LULUCF) regulation, however this doesn't account for what the exported biomass is used for, such as combustion or construction. Currently, international accounting also doesn't contain sustainability criteria to monitor risks to carbon stocks (Committee on Climate Change, 2018a). Under the current UN Framework Convention on Climate Change (UNFCCC) reporting, a BECCS power station would give carbon-credit to the country capturing and storing the carbon, rather than the country exporting the biomass (The Royal Society, 2018).

1.4.2 Biomass combustion with carbon capture

Using bioenergy with carbon capture and storage (BECCS) has the ability to create negative carbon dioxide emissions. Carbon dioxide from the air is absorbed by biomass during photosynthesis and the carbon dioxide released in biomass combustion can be captured during processing for long term storage. The term 'BECCS' covers the capture and storage of CO₂ from any bioenergy type but is typically thought of as the application of CCS to biomass combustion for large scale electricity generation. Estimates for the time taken for a BECCS plant to be effective at removing CO₂ from the atmosphere vary between 1 and 50 years, mostly dependant of the land used for the biomass growth (Fajardy and Mac Dowell, 2017).

Biofuels and large scale electricity generation using biomass provide the biggest BECCS potential for CO₂ removal. Leading options for BECCS from power generation are post-combustion carbon capture on fluidised bed (FB) or pulverised fuel (PF) biomass combustion plants, or biomass integrated gasification combined cycle (BIGCC) as a pre-combustion capture option. Biofuel options with the largest potential for GGR are bioethanol production, using hydrolysis and fermentation, or biodiesel based on Fischer-Tropsch synthesis (IEAGHG, 2011). Biofuels are the only currently operational methods of BECCS with three bioethanol fermentation plants in the US being coupled with CO₂-EOR. However the 10 GtCO₂/yr requirement of carbon dioxide removal by 2050 to meet climate targets cannot be met by the small scale application of BECCS to biofuels (Kemper, 2015). BECCS is

required to be applied to large scale power generation, either gasification or combustion, in order to meet the required GGR target (IEAGHG, 2011).

In terms of GGR in the UK, BECCS has the potential to provide 50 MtCO₂/year (The Royal Society, 2018). Drax could provide half of that (25 MtCO₂/year) if fitted with CCS, while assuming it continues to import 50% of biomass. The additional GGR coming from BECCS with perennial energy crops, UK bio-waste, waste straw and forest trimmings in the UK. Although the land used for the growth of such biomass would be replacing existing farmland which may compete with the production of food, whereas the development of an ocean based biomass for BECCS would be overcome this competition for land.

Drax power station has shown interest in CCS and BECCS technology. It was one of the investors involved in a successful bid to secure £1 billion of funding from the UK Government to complete a front-end engineering design (FEED) study examining the set up of an oxy-fuelled coal plant, called the White Rose Project. However funding for the project was cut in 2015, shortly after Drax announced its withdrawal of investment (Cozier, 2016). It would have been the first large-scale CCS project in the UK. In 2017 Drax announced plans to partner up with a University of Leeds spin-off company, C-Capture Ltd., to trial their post-combustion technology as a pilot-scale demonstration of BECCS (Drax Group Plc, 2018).

1.4.3 Barriers facing the implementation of BECCS

BECCS and more generally meeting climate targets are topics that have many cross cutting challenges to overcome in the coming decades. These include social, legislative, economic and technical challenges. Expert elicitation of BECCS supply chains identified the quantities of bioenergy deployment, societal support and governance structures as the largest challenges (Vaughan and Gough, 2016).

Sustainable production of biomass

The sustainable use of biomass and land-use changes are important challenges facing the successful uptake of BECCS technology. The use of unsustainable biomass, that cannot be replaced at the rate of consumption, can result in positive carbon emissions (Brack, 2017; Röder et al., 2014). Therefore, it is important that BECCS projects are assessed on the overall carbon emissions generated during its lifecycle, as consideration of specific conditions such as the transport of biomass,

type of fertiliser and length of rotation can result in differing levels of carbon dioxide removal or even positive emissions (Fajardy and Mac Dowell, 2017; Röder et al., 2019).

Land use is an important consideration in the large-scale application of BECCS as large amounts (2600 Mha) of land would be required globally to meet global GGR targets (The Royal Society, 2018). Direct and indirect land use change can significantly inhibit the amount of carbon dioxide removed from the atmosphere by BECCS through poor management of bioenergy crop production (Vaughan et al., 2018). Land use changes are a key factor in the viability of BECCS projects and importantly could compete with production of food, a problem that DACCS could provide a solution to.

Water used for biomass growth is another significant consideration in some parts of the world with lower availability, where it could compete with water required for food production. Agriculture is responsible for up to 90% of water usage in some part of the world, which could lead to future water scarcity as populations continue to grow (Fajardy and Mac Dowell, 2017). However with intelligent use of BECCS supply chains including land and water usage, BECCS can be deployed to meet GGR and energy generation objectives whilst satisfying resource efficiency (Fajardy et al., 2018).

Energy cost

The energy used for the carbon capture process, adds approximately an additional 20% to the energy requirements of a combustion plant. This and the initial capital costs of CCS infrastructure continue to be a major barrier facing the implementation of CCS. It is estimated that a 500MW biomass post-combustion carbon capture plant would cost approximately £1.3 billion in capital expenditure with £58 million per year for operating costs (Wood Group, 2018). There is currently no financial incentive in place, outside of the US, for the capture and storage of CO₂ or the removal of GHGs from the atmosphere. Within the US, the 45Q provides tax credits for companies capturing and storing carbon dioxide emissions. However outside of the US there is no current financial incentives for power plant operators to invest in the high capital and operational costs associated with a CCS plant. Although the environmental benefits are obvious for removing CO₂ from the atmosphere, a high carbon price is needed to make it economically viable for businesses.

An option to remove this barrier would be to provide a credit system for the removal and storage of carbon from the atmosphere. The UK's current carbon price is set through a combination of a carbon price floor, £18/tCO₂ until 2021, and the European Union Emissions Trading System (EU ETS). However Brexit could impact the UK's participation in the EU ETS and the UK government have indicated that carbon prices will rise to £40-120 by 2030, illustrated in Figure 1.9, which may be sufficient for GGR deployment.

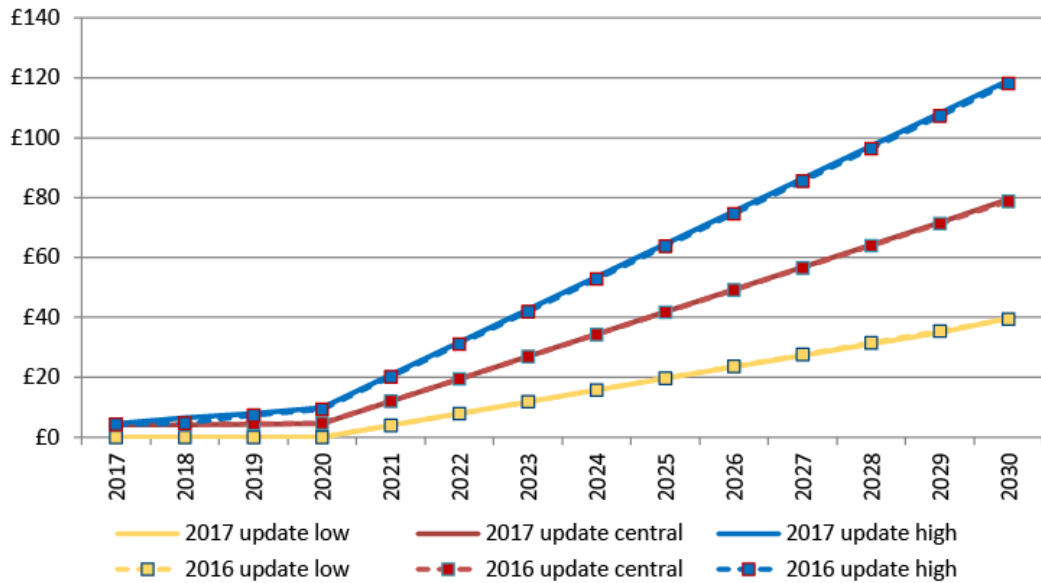


Figure 1.9 BEIS assessment of future carbon values (BEIS, 2017b)

The removal of carbon dioxide from the atmosphere is likely to require incentivisation by governments and is expected to be very expensive, especially if large quantities of DACCS are required towards the end of the century. BECCS is one of the lower cost technologies that can be implemented now to avoid large amounts of expensive GGR at a later date.

Nutrient cycles

The large-scale growing of biomass in one part of the world for biomass power in other parts of the world, currently white wood in North America for biomass combustion in the UK, will result in large movements of key biomass growth nutrients (such as nitrate and phosphate). The environmental impact of the moving large quantities of nutrients may result in depleted land but is not fully understood.

Leakage

The risk of CO₂ leakage from a geologic storage site remains low however can range from 0.00001% to 1% dependant on the location (IPCC, 2005). Although this is manageable with careful site monitoring, it is an issue that will benefit from social engagement with civil society.

Biodiversity

Large-scale implementation of BECCS or afforestation for carbon dioxide removal would be expected to have significant impacts on conservation biodiversity (Heck et al., 2018). This impact will vary dramatically depending on the location of biomass growth, but may prove to be a significant issue if large areas suitable for biomass growth are protected due to biodiversity concerns.

Technical feasibility

Since both biomass combustion and CCS are individually operating in full-scale commercial plants already, the technical readiness of this form of BECCS is significantly ahead of some of the alternative forms. The main technical challenge will be combining these two separate technologies for use in tandem. This work begins to examine on a laboratory and pilot scale what the impact of this combination may have on two of the biggest challenges facing the individual technologies; boiler slagging and amine degradation. But many other technical challenges may arise that were not expected and may require further scientific investigation or optimisation. For most other forms of BECCS further scale-up work is required to increase technology readiness.

Social barriers

Societal opposition or support could significantly restrict or accelerate the deployment of BECCS (Anderson and Peters, 2016), or influence the location and size of biomass resources and CO₂ storage sites. Society is likely to have reactions to the afforestation of biomass for BECCS, thus making public engagements to explain the available options for carbon dioxide removal highly important. Local communities may show concern for the storage sites being located close to inhabited areas.

The creation of jobs and industries can have a dramatic effect of public perceptions of technology implementation. Especially in areas with high unemployment such as

Teesside, UK with the movement of many iron and steel-making plants to countries with cheaper raw materials. BECCS would provide employment opportunities in power generation, chemical engineering and leakage monitoring which may prove societally popular.

1.4.4 Alternative methods of Greenhouse Gas Removal (GGR)

A collection of GGR technologies will be needed in order to meet the global requirements of 810 GtCO₂ cumulatively removed by 2100. Alternatives such as afforestation and geoengineering can provide cheaper forms of carbon dioxide removal compared to BECCS, but have other disadvantages. Direct air capture (DAC) provides the potential to remove large amounts of CO₂ without large land requirements, however it is currently expensive due to the energy required to extract CO₂ from the low concentrations present in atmospheric air. This section provides a brief overview of the advantages and disadvantages of these alternative GGR technologies and their expected role in the future.

In 2018 the Royal Society published a scenario which they considered to be feasible for the deployment of GGR technologies, globally and nationally, to keep warming below 1.5°C. The UK is expected to contribute 130 MtCO₂ per year by 2050. In general, both the global and national GGR requirements are predicted by scenario models to be made up of approximately 50% by a combination of BECCS and DACCS, 15% by forestation and the rest by a mix of biochar, enhanced weathering, soil carbon sequestration and building materials (The Royal Society, 2018).

1.4.4.1 Afforestation

Afforestation is the process of planting trees or sowing seeds to create new trees. This process increases the amount of existing forestry and thus the amount of carbon stored in biomass reserves. Large scale forestation would be one of the cheapest GGR methods and is already an established activity, thus could be rapidly increased immediately.

Whilst there is not vast amounts of arable land in the UK (approx. 6 Mha) available as there is in some other parts of the world, it has been estimated that there is 1.5 Mha of low quality, non-agricultural land available suitable for GGR (Lovett et al., 2014). Currently, total UK woodland covers an area of 3.2 Mha. Optimisation of forests for carbon sequestration requires approximately trees of approximately 10-20

years age, after which they do not absorb significant amounts of CO₂. The harvesting of forestry can enable new growth and further carbon storage whilst providing wood for the construction, biofuels or BECCS industries.

1.4.4.2 Direct Air Capture and Carbon Storage (DACCS)

Often referred to as Direct Air Capture (DAC) which is the capture of carbon dioxide from ambient air with typical CO₂ concentrations of approximately 400ppm. If DAC is to be used as a GGR technology the CO₂ must be permanently removed and stored in some form, hence DACCS. DACCS will likely be required to make up the difference between the amount of GGR required to meet net-zero and the amount that other technologies can optimally remove.

Climeworks have recently implemented their amine absorption technology, similar to traditional CCS held on a porous material for large surface area. The demonstration DACCS project is being implemented on a geothermal power plant in Iceland, removing 50 tCO₂/year (Gutknecht et al., 2018). While Carbon Engineering uses potassium hydroxide (KOH) and calcium hydroxide (CaOH) for their 1 MtCO₂/year DAC units to react with CO₂ from the atmosphere in a two-step process (Keith et al., 2018).

Due to the DACCS process and low concentrations of CO₂ in the atmosphere, a large energy input is required. This energy requirement is likely to reduce as the process is further engineered and optimised, however the energy input currently makes DACCS uneconomic without a high carbon price. Current estimates for the cost of carbon dioxide removal using DACCS are on the order of \$1000 per tCO₂, however the technology has only recently begun demonstration with a TRL of 7 (Bui et al., 2018). Recent UK pathways expect DACCS contributions to be in the region of 25 MtCO₂/year GGR by 2050 (The Royal Society, 2018), which would require a large development of the technology.

1.4.4.3 Other Greenhouse Gas Removal (GGR) technologies

There is an array of other technologies that can provide carbon dioxide removal capacity for contribution to meeting climate targets. Including enhanced weathering, biochar, soil carbon sequestration and low carbon concrete. A brief description of these technologies is provided below however they are not discussed in detail by this work due to the low global CO₂ removal potential of these technologies compared to BECCS (The Royal Society, 2018).

Enhanced terrestrial weathering - the spreading of milled silicate rocks spread on land which chemically react to absorb carbon dioxide.

Soil carbon sequestration - the adaptation of agricultural practices to increase the content of carbon stored in soil.

Biochar – The pyrolysis of biomass to create a char which can be spread on soils to stably store carbon.

Ocean fertilisation or alkalinity – The increasing of ocean photosynthesis or pH to increase the absorbance of carbon dioxide

Low-carbon concrete – The adaptation of concrete manufacture to incorporate the storage of carbon dioxide.

1.5 Conclusions

This chapter has shown the commitment of the UK and other nations to reduce the quantities of greenhouse gases emitted to the atmosphere in order to limit the impacts on global warming. Reviews by the Intergovernmental Committee on Climate Change such as their ‘Special report on the impacts of global warming of 1.5 °C’ have identified the urgency for these emission reductions to all GHGs and the likely requirement for carbon dioxide removal technologies such as afforestation, BECCS and DACCS.

Various CCS and GGR technologies available have been outlined. Biomass combustion combined with post-combustion carbon capture shows promise for deployment due to its readiness level compared to other BECCS options. The lack of financial incentives for carbon dioxide removal is identified a major barrier facing the implementation of GGR technologies. However a forecast for how this may change with a rising carbon price in the future is described. The main social, environmental and technical challenges facing BECCS are also described. This chapter has identified key considerations on the implementation of GGR, beyond the technical challenges, and has identified the scales of GGR technologies being relied upon in the second half of this century if we are to safely avoid dangerous amounts of climate change.

Sustainability of the large amounts of biomass required for BECCS is one of the most important challenges. Since the quantities of carbon dioxide removal needed

from BECCS is likely to be in the range of 0-8 GtCO₂ every year by 2050, this will put a large demand on land required for the growth of bioenergy crops and will require thorough monitoring in order to achieve effective CO₂ removal. The most sustainable approach will likely be an international one, with biomass being grown in the most suitable parts of the world to avoid water shortages and negative impacts from changing land use.

This chapter highlights that BECCS and DAC will be required in large quantities during this century, near the limits of their feasible deployment, however both technologies have not currently been demonstrated in the UK. Rapid development of these technologies will be required in order to meet the scales required for meeting climate targets. The need for commercial scale-up and the development of a transport and storage network is clear.

Chapter 2

Aims and objectives of thesis

2.1 Context

This project aims to address a gap in the current research and improve academic understanding of applying carbon capture processes to flue gases derived from biomass combustion. As identified in the previous chapter, CCS has the potential to be applied to a vast array of industrial practises in order to cut carbon emissions. It is likely to be used in many countries around the world to meet future carbon reduction targets. BECCS has recently been trialled in the UK on a pilot-scale however it is yet to be implemented on a large scale. Therefore the experimental work in this thesis aims to contribute to our understanding of how successfully CCS can be applied to biomass flue gases for use within our future energy mix.

2.2 Aims and objectives

Having identified the main technical barriers facing the application of CCS to bioenergy, the aims of the research presented in this thesis are described. Four particular challenges are selected as relevant to the large scale implementation of BECCS for power generation, resulting in this thesis having the following main aims:

Aim 1 - To improve our current understanding of the fate of potassium from the combustion of white wood, wheat straw and olive cake.

Objectives:

- Proximate and ultimate analysis of biomass for fuel composition data.
- Single particle combustion (SPC) experiments of biomass pellets to investigate the release of potassium.
- Single particle combustion (SPC) experiments of biomass pellets with the addition of 0/5/15/25 wt% additive to investigate the mitigation of potassium release.

- Ashes to be generated at a range of temperatures to investigate potassium remaining in solid phase.
- Ashes to be generated at a range of temperatures with the addition of 0/5/15/25 wt% additive to investigate the mitigation of potassium release.
- Atomic absorption spectroscopy (AAS) of biomass ashes for inorganic content.

Aim 2 - To assess the impact of biomass ash, potassium salts and coal ashes on the CO₂ absorption and degradation of monoethanolamine (MEA).

Objectives:

- Vapour-liquid equilibrium (VLE) analysis of 30 wt% w/w MEA with and without the addition of potassium salts to measure impacts on CO₂ absorption capacity.
- Laboratory thermal degradations of 30 wt% w/w MEA with and without the addition of potassium salts, biomass ash and coal ash.
- Laboratory oxidative degradations of 30 wt% w/w MEA with and without the addition of potassium salts, biomass ashes and coal ashes.
- Measuring of degradation product formation using nuclear magnetic resonance (NMR) and gas chromatography-mass spectroscopy (GC-MS).
- Inductively coupled plasma - optical emission spectrometry (ICP-OES) to measure quantities of elements leached into amine solvents.

Aim 3 - To identify the key degradation products formed in the degradation of monoethanolamine (MEA) and characterise any degradation products not previously identified in literature.

Objectives:

- Characterisation of thermal and oxidative degradation products previously identified in literature using nuclear magnetic resonance (NMR).
- Identification of significant products not yet identified in literature.
- Preparation of unknown degradation product to confirm presence in degraded amine samples.

Aim 4 - To track the inorganics and amine degradation from a pilot-scale biomass combustion and carbon capture facility.

Objectives:

- Pilot-scale operation of carbon capture plant using 30 wt% w/w MEA with flue gases from biomass and coal combustion.
- Analysis of ashes from different locations in the combustion plant to enable the tracking of elemental species through the flue gas using inductively coupled plasma - optical emission spectrometry (ICP-OES).
- Measuring of MEA degradation products formed in MEA solvents used carbon capture in each case using nuclear magnetic resonance (NMR) and gas chromatography-mass spectroscopy (GC-MS).
- Inductively coupled plasma - optical emission spectrometry (ICP-OES) to measure quantities of elements leached into amine solvents.

2.3 Structure of thesis

Each chapter of this thesis addresses a specific part of the thesis aims described above. **Chapter 3** summarises the background literature relevant to the biomass combustion, chemistry of carbon dioxide capture and amine degradation. **Chapter 4** presents the results on the fate of potassium from biomass combustion in line with aim 1. **Chapter 5** contains the results and analysis from the laboratory degradations of MEA along with characterisation of degradation products for aims 2 and 3. **Chapter 6** is the analysis of ashes and MEA solvents from the UKCCSRC's PACT facilities to provide a comparison of CCS applied to biomass and coal combustion from aim 4. **Chapter 7** brings together the conclusions from all preceding chapters to give an overview of the project conclusions in relation to the project aims. **Chapter 8** provides the experimental details for the laboratory experiments described in chapters 4 and 5.

Chapter 3

Literature review on biomass combustion, carbon capture and amine degradation

3.1 Introduction

This chapter is a literature review of the existing research relevant to this project. It includes a detailed look at biomass and coal fuel composition, differences in decomposition during combustion and ash residue compositions which will contact carbon capture processes. The review then moves on to the fate of ash from combustion, ash deposition and additives that can be used to prevent the slagging and fouling of boiler surfaces. The chapter finishes with a detailed review of the chemistry of carbon dioxide capture with amines, their degradation and further impacts on carbon capture efficiency. Experimental work on these topics is discussed in the subsequent chapters.

3.2 Solid fuels

3.2.1 Types of solid biomass

The term “biomass” covers a large variety of materials derived from living organisms, including by-products such as animal waste, sewage sludge and used coffee grinds. The biomass feedstocks used for various energy applications depends on resource quantity, availability and process suitability. For large scale combustion the biomass feedstock options are mostly limited to wood and herbaceous crops such as wheat straw.

Woody biomass is currently preferred for large scale power applications due to forestry trimmings and residues being by-products with low moisture and alkali metal content. However a recent study on the optimal biomass to be used for BECCS found woody biomass didn't perform well on water usage and carbon dioxide removal due to the slow growth. Thus suggesting that herbaceous biomass such as miscanthus and switchgrass were the most sustainable forms of biomass for global biomass supply to BECCS power stations in the future (Fajardy and Mac

Dowell, 2017). Within the UK, short rotation coppice (SRC) species such as willow are expected to be a major part of the national bioenergy mix (Aylott et al., 2008).

3.2.1.1 Woody biomass

Woody biomass for combustion purposes is predominantly obtained from trees, bushes or crops. Dedicated crops or forestry can be used to make combustion fuels, however by-products such as trimmings and residues from commercial forestry is preferable to avoid direct implications on forest ecosystems and carbon stores (The Royal Society, 2018). Commercial forestry is a well-established industry which has been built for many years on the demands of wood for construction and furniture. Sustainable forestry requires the removal of no more biomass in a harvest than will be replenished by the time of the next harvest, and must not lessen the yields of subsequent harvests. Hence fast growing trees are preferred such as fir, pine and spruce (40-80 years for harvest cycles) or short rotation forestry (SRF) tree species such as ash, alder, birch, eucalyptus, poplar and sycamore (10-20 years for harvest cycles) (Thornley et al., 2008).

Short-rotation coppice (SRC) is a recognised method of harvesting tree species by cutting plants back to the stump to enable regrowth for future harvest. Harvest cycles typically last less than 5 years however, as with any grown biomass, SRC requires dedicated land for growing as it is not a by-product which puts it into competition with food unless grown on degraded land rather than agricultural (Tilman et al., 2009).

Wood pellets can be a more convenient form of woody biomass than wood chips or logs. It can make possible the transportation and handling of a homogenous biomass sample, with low moisture and high energy density. Pellets can be made from many forms of herbaceous or waste biomass, but white wood pellets are the most commonly used biomass for energy generation with high production in North America and Canada. In 2017 Drax sourced 4 million tonnes of biomass feedstock from the US and 1.6 million tonnes from Canada (Ofgem, 2018). These pellets were mostly made from sawmill residues, low grade round wood, branches and thinnings.

3.2.1.2 Waste wood

Waste wood is generated from a range of backgrounds such as undesired wood materials from the construction industry, old furniture and municipal solid waste. Waste wood can often be treated with undesired chemicals such as paints and

varnishes or contain hard to remove metals from destruction. British Standard PAS 111 defines the different grades of waste wood as:

- Grade A is defined as “clean” recycled wood, suitable for use as animal bedding, horticultural mulch or biomass pellets.
- Grade B is not clean enough for use in animal products (i.e. Grade A) but can be used as a feedstock for manufacture of wood panel products such as chipboard and fibreboard.
- Grade C is the class of recycled wood suited to use as a biomass fuel for the generation of electricity and/or heat.
- Grade D requires disposal at hazardous waste disposal facilities.

3.2.1.3 Herbaceous and fruit biomass

Herbaceous biomass are non-woody biomass such as grasses, straws and by-products from agricultural crops such as sugar cane. Grasses can be grown with short rotation (2/3 years) but will be in competition with agricultural land that could be used for food or farming unless grown on degraded land. The fast growth of SRC results in a large uptake of plant nutrients such as N, P and K – this can result in the depletion of these soil nutrients for future biomass growth if unmonitored. Crops such as miscanthus show promise for use in future BECCS scenarios due to their quick growth, absorbance of CO₂ and low water footprint (Fajardy and Mac Dowell, 2017).

Fruit biomass are predominately the by-products of seeds grown for food production such as olives, nuts and palm kernels. Europe is the largest producer of olive oil in the world with 95% of the world’s olive trees being grown in the Mediterranean region. 10 million tonnes of olive were harvested in Europe in 2016 (Eurostat, 2018). This results in significant proportion of olive being left as a residue from olive oil production in the form of stones and fibres, which are suitable for combustion as a renewable fuel. However, the United Kingdom’s exit from the European Union might make olive a less likely fuel for use by UK power generators, but interest will continue in Europe.

3.2.2 Biomass formation and structure

Plant matter is made with a complicated structure of three major compounds: cellulose, hemicellulose and lignin. The percentage of which varies depending on the type of biomass. Due to these major components it is commonly known as lignocellulosic biomass.

Woody biomass, from the outside, begins with bark which is made up of the phloem, phellem, rhytidome layers and a xylem core. The rhytidome layer is the dead layer of cells that sits on the outside on the bark to provide protection to the tree; the phellem layer is an impermeable layer that sits behind the rhytidome. The phloem layer sits behind the phellem layer which transports key growth nutrients around the plant (Pereira, 2007). The xylem core sits inside of this and transports water – this core makes up the majority of the woody biomass structure.

Xylem wood uses cellulose as the main component to provide a woody structure. Cellulose is a long chain, linear polymer which is made up of 5-10 thousands glucose monomers. The polymers form rigid strands due to hydrogen bonding between the adjacent sides of the chain, creating microfibrils (Mohan et al., 2006).

Hemicellulose is a polysaccharide similar to cellulose, however hemicellulose contains a variety of sugar monomers other than glucose, such as xylose and mannose. Hemicellulose consists of shorter chains with random structure and hence low strength. Hemicellulose connects to the rigid strands of cellulose through hydrogen bonds and to the binding lignin through covalent bonds (Chen, 2014). Lignin covers a range of complex organic polymers which provide binding strength to the cellulose strands. Lignin from biomass varies dependant of the biomass type but the major monolignols usually present are coumaryl, coniferyl and sinapyl aromatic alcohols (Zhang et al., 2011).

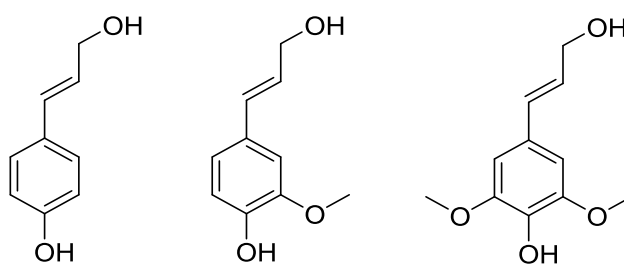


Figure 3.1 Structures of coumaryl, coniferyl and sinapyl alcohols.

3.2.3 Coal formation and structure

Coal remains the largest source of electricity generation worldwide, accounting for approximately 35% of all power (IEA, 2017). Under current policy intentions, coal is set to continue as the largest source of power towards 2050. However if policy shifts towards a 'sustainable development scenario' biomass combustion has the potential to replace a significant proportion of this (IEA, 2017) as a solid fuel with similar characteristics to coal.

Coal is a complex polymeric matrix of fused benzene rings and polycyclic aromatic hydrocarbons formed from degradation of organic plant matter over millions of years through a process called coalification. As a basic overview, plant matter on the earth surface is partially decomposed into peat in wetlands where water obstructs the presence of oxygen to form anaerobic conditions (Keddy, 2010). The peat is then gradually buried underneath soil where it was compressed and subject to high temperatures as it descends deeper. As the coalification process continues the peat is progressively converted into lignite, sub-bituminous coal, bituminous coal and finally, anthracite (Miller, 2005) with the type of plant matter, depth, temperature, acidity and water content of decay conditions impacting the quality of the coal types. As coalification progresses the carbon content of the coal increases whilst moisture, volatiles, hydrogen and oxygen contents decrease. Nitrogen and sulphur are present in the forms of amines, pyridines or pyrroles and sulphide, disulphide, mercaptan or cyclic sulphide, respectively (Kubacki, 2007).

3.3 The combustion of solid fuels

A particle of solid fuel placed in a high temperature environment will undergo three main processes as it combusts: moisture loss, devolatilisation and char combustion. These stages remain the same for both biomass and coal solid fuel combustion. This section will firstly introduce how biomass is combusted in large-scale applications and continue with a detailed description of what happens to biomass particles during the different stages of combustion.

3.3.1 Large-scale combustion of biomass

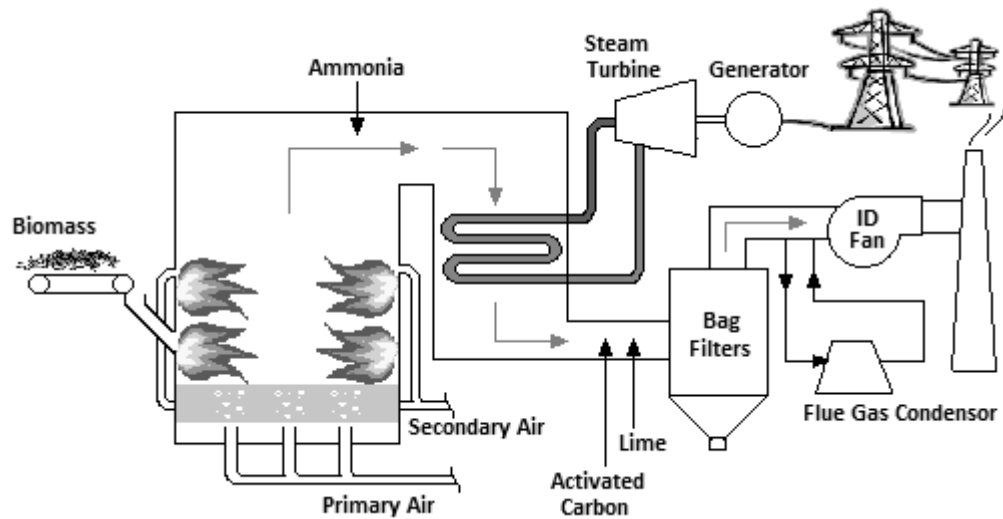


Figure 3.2 A typical fluidised bed biomass power station schematic.

Due to coal and biomass both being solid fuels, their combustion within a power station is similar. Figure 3.2 illustrates how the biomass is combusted using a typical fluidised bed (FB) furnace to generate high pressure steam and the associated post-combustion treatments for biomass combustion. FB combustion uses solid particles to create a fluid-like bed which holds a solid fuel in the combustion zone of a boiler. FB technology allows for flexibility in terms of fuel particle size (Loo and Koppejan, 2008), whilst allowing any heavy bottom ash particles from combustion to drop through the fluid bed for collection.

Although large scale facilities burning biomass can use either pulverized fuel (PF) or fluidised bed (FB) boilers, this project will focus on the combustion from a PF scenario as it is applicable to the current largest scale combustion of biomass in the UK at Drax power station (Drax Group Plc, 2016). PF combustion involves the solid fuel being milled down to a small particle size (typically $<400\mu\text{m}$) so that the fuel is light enough to be entrained into an air stream providing primary combustion air into the boiler burners. In PF boilers the flame temperatures are relatively high ($1200\text{-}1600^{\circ}\text{C}$) and particles are heated rapidly. Residence times in the combustion chamber are short, typically less than two seconds, but should allow for the complete combustion of biomass particles in order to obtain the most efficient output of thermal energy. During combustion, part of the particle will pass into the flue gas as volatile matter and incombustible components will remain in the solid phase as ash. Some of the smaller size ash particles are dispersed in with the flue

gases after combustion, where temperatures remain high which can result in further combustion of incompletely combusted particles.

Prior to PF combustion, solid fuels are milled down to small particle sizes for gas entrainment. Biomass is more difficult to mill than coal. Milling processes that are used to mill coal to $<50\mu\text{m}$ are only effective at milling woody biomass to $<3\text{mm}$ (Loo and Koppejan, 2008). Biomass also typically has higher volatile content than coal, approximately 80-90%, which will result in rapid volatile combustion in the furnace. Secondary and tertiary air is often used to attempt to oxidise incompletely burned particles from the primary combustion zone (Nussbaumer, 2003).

Achieving the maximum thermal output with minimal input energy is an important balance for the consideration of milling processes – as biomass with smaller particle sizes can obtain quicker burn-out and hence higher thermal efficiencies, however this will require larger input energy from mills.

3.3.2 Drying and ignition

The first stage of combustion involves the release of moisture from the solid fuel particle. In this time moisture is evaporated as the particle begins to heat up prior to ignition of the first volatile flame. This time period is often measured and referred to as ‘ignition delay’. It is logical that higher moisture content fuels such as biomass will take longer for this stage which undesirably results in longer residence times being required for particles in boilers (Loo and Koppejan, 2008). Heat is transferred to the centre of the fuel particle by conduction through the solid matter and furnace temperatures are typically lower for high moisture biomass (Klass, 1998).

3.3.3 Volatile combustion

After the adequate drying of the biomass particle, the second stage of combustion is the devolatilisation of organic matter from the particle, resulting in the production of a visible flame (Mason et al., 2015). As the temperature of the particle starts to rise, the chemical components of the fuel begin to break down further and release volatile compounds. This release of volatiles from particle surfaces prevents the penetration of oxygen, resulting in a pyrolysis like environment inside the particle (Loo and Koppejan, 2008). Pyrolysis is effective at breaking up the long polymeric chains and functional groups associated with cellulose and hemicellulose in biomass to further produce volatile matter and char. This process begins when the outer surface of the

particle reaches pyrolysis temperatures, approximately 200°C, when char is then progressively formed towards the centre of the particle. Hemicellulose is the first part of biomass to decompose within the 200-260°C temperature range, to form formaldehyde, acetic acid, CO, H₂, furfural and furan. Cellulose is next to decompose in the 240-350°C range, to produce hydroxyl-acetaldehyde, acetol, furfural and CO as volatiles. Lignin is the last part of the major biomass components to decompose at temperatures of 280-500°C. Lignin produces mostly char from devolatilisation but also volatile aromatics are released with phenols, CO, hydrocarbons, formic acid, acetic acids, methanol and higher fatty acids (Desideri and Fantozzi, 2014).

The volatiles released during pyrolysis ignite when reacted with oxygen producing flaming combustion. The high proportion of volatiles in biomass (up to 80%) results in a large amount of the total heat output coming from the volatile combustion stage, differing to coal which is predominantly char combustion (Jenkins et al., 1998).

3.3.4 Char combustion

Char combustion occurs after the visible burning of volatile organic matter around the particle. When the devolatilisation is complete, oxygen is able to pass the surface of the particle and oxidise the char matter that remains after volatile combustion. This process occurs typically at temperatures of 400-1000°C. Char combustion is typically the slowest stage of combustion and therefore the rate determining step in the overall combustion process. Biomass chars are usually porous compared to coal particles, thus enabling the rapid diffusion of oxygen through the particle for oxidation (Loo and Koppejan, 2008). The oxidised carbon products (CO and CO₂) are then desorbed and diffuse out of the particle.

Char “burn-out” marks the end of char combustion, when all combustible matter has been removed from the particle, and only ash remains. It requires the complete reaction of carbon in the char with oxygen diffused in the particle. In the time after char burn-out, a biomass particle can remain in a high temperature environment either within the furnace or in the stages of flue gas treatment. Ashes held at high temperatures can undergo further reactions resulting in the later release of inorganic components.

3.4 The fate of ash from biomass combustion

The fate of ash from combustion can have important impacts on post-combustion processes such as heat transfer, SO_x , NO_x and CO_2 removal. Ash compositions, and temperature, play a major role in the likelihood of ash deposition occurring in combustion plant. Thus this section will provide an overview of how ash is formed and what components are found to impact the different types of ash deposition. The section finishes with an overview of the most commonly used flue gas treatment technologies that are used to remove ashes and harmful species from flue gases prior to release to the atmosphere.

3.4.1 Ash formation

In combustion, some inorganic matter that is typically considered to be ash-forming compounds (such as SiO_2 , CaO , MgO and Zn) are oxidised and volatilised into the gas phase. These gas phase inorganics often form small particulates in the boundary layer of the combusting char particles due to nucleation and will grow to form a large proportion of fine particulates ($<2.5\mu\text{m}$) by coagulation, agglomeration and condensation as illustrated in Figure 3.3.

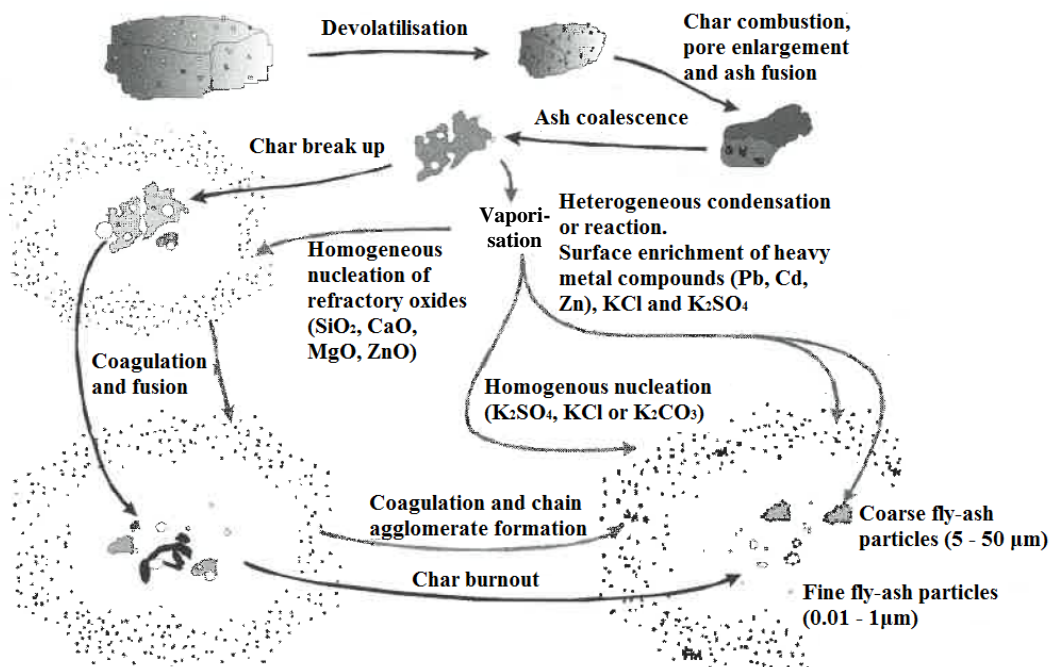


Figure 3.3 Main reaction mechanisms in the formation of ash from biomass combustion, from (Loo and Koppejan, 2008).

Non-volatile ash components remain in the solid phase ash residue particle which may begin to melt and coalesce inside the char particle. Ashes formed through this mechanism are typically larger than ashes formed from volatilised ash compounds, and thus this makes up the majority of bottom ash or coarse fly ash ($>2.5\mu\text{m}$) entrained in the flue gas (Loo and Koppejan, 2008).

Some elements with higher volatility (such as K, S, Cl, Cd and Pb) will manage to pass through the boundary layer into the outer furnace conditions remaining in the gas phase. For high concentration inorganic vapours, such as K, homogeneous nucleation can occur as the flue gas is cooled resulting in the new formation of fine particles (van Lith et al., 2008).

3.4.2 Ash deposition

Typical biomass ash is comprised of Na, Mg, Al, Si, P, Cl, K, Ca, Ti, Mn, Fe, and S. The exact composition of these is dependent on the type of biomass and combustion conditions. Alkali compounds, K and Na, are found to be high in biomass ashes which can cause problems from ash deposition due to the low melting points of compounds such as potassium-silicates ($\text{K}_2\text{O-SiO}_2$) which encourages the agglomeration of sand/ash particles, deposition and sintering of ash on boiler equipment (Bryers, 1996). Sintering and alkali chlorides (KCl and NaCl) are known to have corrosive effects on the materials used for furnace equipment, thus resulting in damaged equipment that will need repair.

Ash deposition occurs as a result of combustion ashes melting under the high temperatures of FB ($<900^\circ\text{C}$) or PF furnace ($<1600^\circ\text{C}$). This can result in molten ash sticking to the surface of the boiler or water tubes which can dramatically effect boiler efficiency. As ashes pass through post-combustion apparatus, some molten particles will inevitably deposit on equipment surfaces, fly ash is known to have a few different forms of deposition onto boiler surfaces:

- Impact inertia – When ash particles with a diameter larger than $10\mu\text{m}$ have a large inertial momentum, the particle will impact a surface. Depending on the ash viscosity and composition, and the roughness/composition of the material contacted, the particle may stick to the contacted surface (Plaza, 2013).

- Condensation – Surfaces such as heat exchangers or boiler tubes can act to condense volatile inorganic species which cause fouling problems (Shao et al., 2012).
- Thermophoresis – Temperature gradients within the boiler can result in a transportation of submicron particles to cool surfaces where the sticky particles may remain (Shao et al., 2012; Baxter, 1993).
- Diffusion – as a result of the movement of submicron particles in accordance with the Brownian motion of particles (Aho and Silvennoinen, 2004; Bryers, 1996).

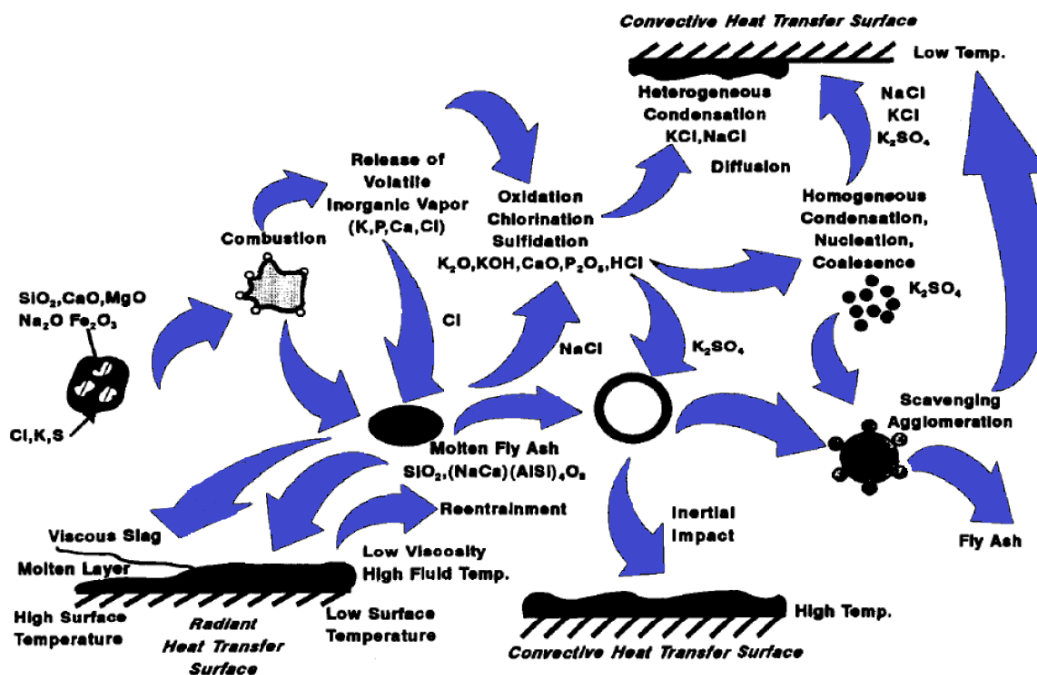


Figure 3.4 Transformation of ash material from biomass (Bryers, 1996)

Bryers illustrated the different transformations the ash components can undergo in Figure 3.4, dependant on the combustion environment. K, Na, Ca, Cl species can volatilise in combustion, but may then condense or nucleate onto fly ashes. These species could also be absorbed by Si-minerals present in molten fly ashes in the flue gas or molten slag layer on boiler surfaces. The surface on which the ash is deposited determines its classification of deposition, in the case of slagging and fouling.

3.4.2.1 Slag formation

Slagging is the higher temperature ash deposition that occurs within the boiler combustion zone, where surfaces are subjected to high radiant heat transfer. The

composition and formation of slag in different regions of the furnace can vary dramatically depending upon the temperatures, absorption rates, gas flow and composition of the ash (Bryers, 1996).

Slag deposits are formed from the impact of molten ash particles from combustion on boiler surfaces. Upon collision with the surface much of the heat from the ash is lost to the surface, resulting in solidification of the ash and often sintering. Sintered deposits are particles fused through heat and pressure, at temperatures below melting. The slag deposits often consist of a powdery inner layer covered by molten ash layer as they grow in size. Alkali compounds, such as potassium silicates which are present in high quantities in biomass fuels compared to coal, are known to worsen this sintering and deposition process due to their low melting points.

The ratio of base to acid ($R_{b/a}$) quantities of the fuel ash provides a useful indicator of slagging potential (equation 3.1). As the ratio value increases, the ash becomes more basic resulting a tendency for lower ash melting temperatures, and hence increased potential for slagging (Darvell et al., 2010; Bryers, 1996). This enables the prediction of which biomass fuels are likely to cause the largest slagging problems.

$$R_{b/a} = (Fe_2O_3 + CaO + MgO + K_2O + Na_2O) / (SiO_2 + TiO_2 + Al_2O_3) \quad (3.1)$$

3.4.2.2 Fouling

Fouling is the deposition of ashes on surfaces through non-radiant convective heat exchange parts of the boiler i.e. areas outside of the combustion flame radiation zone. Fouling usually occurs from the condensation of previously volatilised species from combustion. Alkali metal compounds, once condensed, often react with gaseous SO_x in the flue gas resulting in large quantities of sulphates in the deposited ashes (Loo and Koppejan, 2008). Fouling usually effects equipment in lower temperature zones, such as heat exchangers/economisers. A study that aimed to investigate fouling of super-heaters identified potassium as the primary element of concern for fouling by biomass combustion (Baxter et al., 1998). Deposition rates for fouling are typically lower than slagging, due to predominantly being a condensation mechanism however this can result in denser deposits that are hard to remove from boiler tubes (Loo and Koppejan, 2008).

Fouling on boiler tubes can cause problems further than decreased efficiencies, namely corrosion. The presence of chlorine, commonly found in straws and grasses,

is particularly harmful in fouling scenarios as it often results in the formation of KCl, NaCl or HCl which catalyses the corrosion of the surfaces (Nielsen et al., 2000).

3.4.3 Flue gas treatment technologies

Many methods are employed in large scale biomass power stations to treat and adapt the composition of flue gases for performance and environmental purposes. From an environmental perspective, UK power plants must comply with all relevant environmental legislation. This includes the requirements of the Industrial Emissions Directive (Directive 2010/75/EU) which superseded the Large Combustion Plant Directive (LCPD) in 2016. This legislation imposes an obligation on industrial emitters to lower emissions through an integrated ‘best available technology’ approach for pollutants such as PM, NO_x and SO_x. Hence, this usually consists of flue gas treatment technologies for the removal of PM, SO_x and NO_x from flue gas streams prior to release into the atmosphere. The emission limit values for combustion plants under this regulation are summarised in Table 3.1 for combustion plant with greater thermal capacity than 300MW.

Table 3.1 Emission limit values (mg/Nm³) from Directive 2010/75/EU for combustion plant rated at larger than 300MW thermal input

	Biomass/Coal
NO _x (mg/Nm ³)	200
SO ₂ (mg/Nm ³)	200
PM (mg/Nm ³)	30

For particles removal, fabric filters and electrostatic precipitators (ESPs) are the most commonly used technologies due to their high removal efficiencies of greater than 99%. These technologies are also beneficial to the carbon capture process as impurities within flue gas streams can result in the contamination of capture solvents (Adams, 2010). Wet scrubbers and cyclones can also be used but with reduced efficiencies. ESPs have typically been the most common form of PM removal technology for UK coal-fired power stations.

3.4.3.1 Cyclone separators

Cyclones and multicyclones utilize gravity and centrifugal forces to get particles to contact the cyclone body wall and then slide down the wall into a collection hopper.

3.4.3.2 Fabric filters

Fabric filters control particle emissions by using a physical barrier with appropriately sized gaps to allow flue gases to pass through the filter, whilst trapping dust in the filter. Fabric woven with specially designed fibres is used to remove solids from flue gas streams (Sánchez et al., 2007).

3.4.3.3 Electrostatic Precipitators (ESPs)

Electrostatic precipitators (ESPs) use ionisation to charge fly ash particles before being passed through an electric field. The charged ash particles are attracted to an electrode, resulting in the slow build-up of ash on the electrode surfaces. The electrodes are periodically cleaned through vibration as the accumulation of particles reduces the ESPs efficiency.

3.4.3.4 NO_x and SO_x control technologies

These pollutant removal technologies are shown in the example power station schematic in Figure 3.2, with the injection of ammonia and lime for selective catalytic reduction (SCR) and flue gas desulphurisation (FGD) respectively.

3.5 Additives to mitigate K release

Additives in this case refer to the minerals or chemicals added to the biomass combustion environment to avoid ash related operational problems. They are often used in biomass power generation to adapt the chemistry of combustion and ash formation in order to reduce impacts of slagging and fouling on the thermal efficiencies of a power plant. Additives abate the harmful effects from the formation of potassium species by four main methods; chemical reaction, physical adsorption, increasing ash melting temperatures or limiting ash sintering (Wang et al., 2012).

This study will examine the effects of using a chemical adsorption additive (coal fly ash) on the release of potassium from different biomass. Coal fly ash is an aluminosilicate-based additive ($Al_xSi_yO_z$) which is an effective additive for power generation uses. Many studies (Steenari and Karlfeldt Fedje, 2010; H. Wu et al.,

2013; Öhman and Nordin, 2000) have proven that coal ash additives high in Al or Si are effective at capturing potassium during biomass combustion, with the side-effect of increasing chloride release. However there is some evidence of important impacts on the flue gas composition from the use of additives, namely increased SO₂ levels, reduced CO and increased ash deposition, but less KCl and K₂SO₄ present (H. Wu et al., 2013) and a less sintered deposit.

Whilst the mechanism of action for aluminosilicate additives is known, the efficacy when used with different biomass types (and with varying contents of potassium and other inorganics) has been less studied. In addition, limited research has been published around the quantities of additives required to see the desired effects. However, some studies have found evidence of threshold ratios of additive to biomass ash, whereby further increasing the quantity of additive above this threshold value has been found to show no improvements in potassium capture (Damoe et al., 2012; H. Wu et al., 2013).

3.5.1 The fate of K in biomass combustion

Potassium bound to organic structures within biomass such as hemicellulose (<10%) usually decompose during the low temperatures of volatile combustion (200-500°C) (Yu and Zhang, 2001; Jensen and Frandsen, 2000; Olsson et al., 1997; Olsson et al., 1998) resulting in the potential release of potassium into the gas phase. The release is likely to occur in the form of potassium ions (K⁺) in the gas which combines to form KCl (g) if the biomass K:Cl ratio is low, or as KOH (g) for higher K:Cl ratios (Akbar et al., 2010). The remaining potassium plays a key role in char formation and some is released during the char combustion stage at temperatures above 600°C (Jones et al., 2007; Mason, Jones, et al., 2016; Yu and Zhang, 2008; Jensen and Frandsen, 2000; Olsson et al., 1997).

Potassium is highly mobile in living biomass and is mostly present as hydrated K⁺ ions in solution within the xylem cells. However, during drying these ions precipitate as inorganic potassium salts (e.g. KCl, KNO₃) which make up more than 90% of the total potassium in raw biomass (Loo and Koppejan, 2008). Since these species are soluble, the majority of potassium in biomass are extractable by water washing (Saddawi et al., 2012). This, together with possible remobilization during plant senescence, accounts for the variability of potassium within different biomass. KNO₃ is known to dissociate at temperatures above 400°C, whereas KCl is found to

almost completely evaporate at temperatures between 780-950°C (Bridgwater and Boocock, 2013). Under the high temperatures of combustion, much of the inorganic and organic forms of potassium found in raw biomass are volatilised which can result in undesirable deposition and corrosion effects as they condense out on boiler surfaces, or result in ash deposition after rejoining with solid phase ash particles (Knudsen et al., 2004).

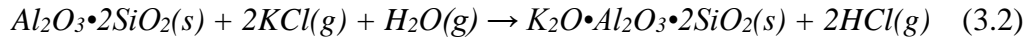
Work by Van Lith et al. suggested that any potassium that is not vaporised during the volatile combustion stage is most likely held in the solid phase as K_2CO_3 and KCl . The carbonates decompose in the higher temperatures of char combustion ($>850^\circ C$), which may result in the formation of potassium in the gas phase, which again can react with water or chloride to form KOH or KCl respectively (van Lith et al., 2008). Any potassium that remains in the solid phase after complete combustion will have typically reacted with other inorganic elements present in the ash to form minerals such as K_2CaSiO_4 and $KAlSi_3O_8$ (Vassilev et al., 2014). Indeed, silicates have been shown to help 'fix' the potassium in the ash as potassium silicates (Jensen and Frandsen, 2000).

3.5.2 Aluminosilicate additives

Aluminosilicate (Al-Si) additives are found to be effective as a chemical adsorption type of additive that reacts with volatile potassium species to form potassium aluminosilicates. Chemical adsorption and reactions are closely related to the mass/molar ratios between the problematic elements in the biomass ash and the effective additives (Wang et al., 2012). Limited research has been published around the quantities of these additives required to see these desired effects. Therefore this study will use increasing amounts of additive to investigate the effects on potassium held in the solid ash phase at varied temperatures. It is expected that the results will fit with previous studies which have found additives to reduce the release of potassium from biomass heated at a fixed temperature (Wang et al., 2012).

Much research has been completed examining the effects of using aluminosilicate additives with large scale biomass combustion. These have supported the effectiveness of coal fly ash at reduce quantities of KCl , K_2SO_4 and KOH in the flue gas from wood combustion in a 800 MW suspension-fired boiler. Evidence for reducing ash sintering has been detected with frequent shedding of ash deposits (H. Wu et al., 2013).

Coal fly ash is an aluminosilicate based additive which is a commonly used type of additive for biomass power generation due to its availability and cost as a waste product. It is believed that aluminosilicates react with the potassium chloride to create potassium-aluminum silicate (mineral) and hydrogen chloride as in equation 3.2 – which is governed by chemical kinetics and mass transfer constraints (Coda et al., 2001). It is worth noting that the increased HCl production would need to be removed from the flue gas as it can cause acidification.



The ternary diagram in Figure 3.5 illustrates how the reaction of potassium species with Al to produce K-Al-Silicates is preferable to K-Silicates. The use of Al-Si additives results in a change in the ternary diagram positioning, from the top of the diagram where solidus temperatures are low (600-900°C) towards the bottom-right corner, representing Al content, where solidus temperatures are much higher (<1000°C). Al-Si additives enable this shift as they react with volatile K species to form K_2O - SiO_2 - Al_2O_3 minerals.

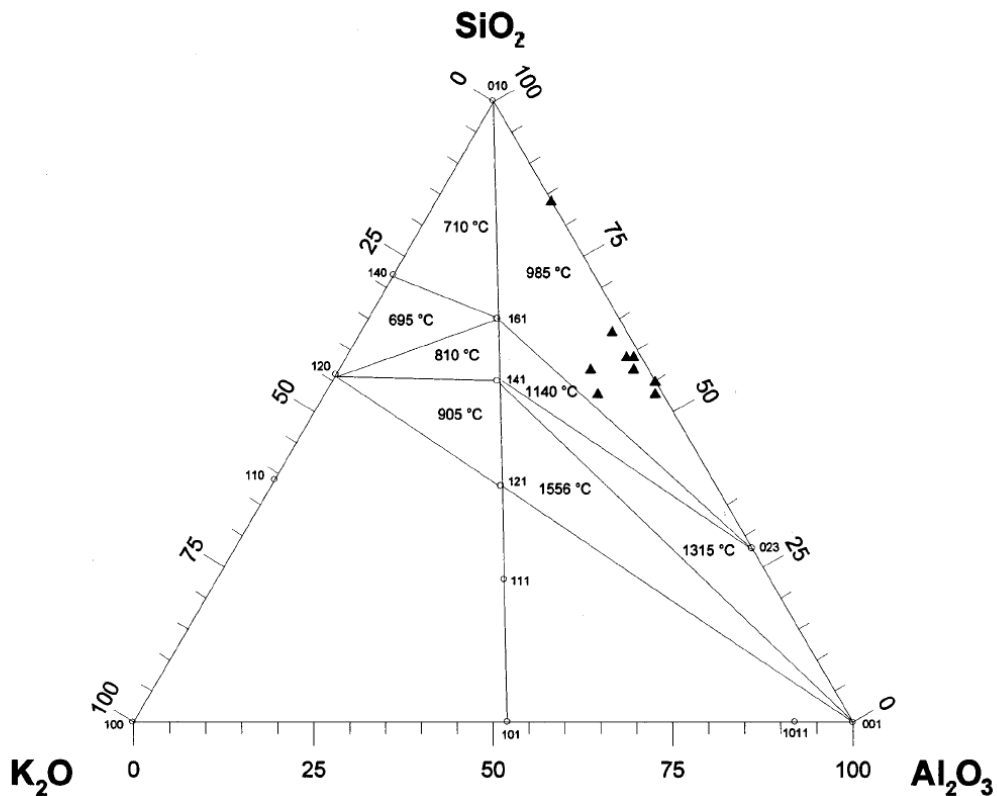


Figure 3.5 K_2O - SiO_2 - Al_2O_3 ternary diagram with solidus temperatures from (Öhman and Nordin, 2000).

The generation of coal fly ash in 2015 for the US and China was approximately 130 million tonnes and 580 million tonnes respectively, with roughly half that being utilised (Yao et al., 2015). Drax currently produces an average of average 700,000 tonnes of ash every year, the majority is sold to the construction industry for utilisation with the remainder being sent for landfill at the power station's adjacent Barlow Mound ash disposal site (Drax Group Plc, 2019b).

Kaolin mineral, $\text{Al}_2\text{Si}_2\text{O}_5(\text{OH})_4$, is another commonly used example of an aluminosilicate which has been found to be effective as a potassium sorbent during the combustion of wood. Kaolin was found to concentrate in fly ashes from large scale combustion, due to its small particle size, and hence does not impact bottom ash composition (Davidsson et al., 2007; Steenari and Karlfeldt Fedje, 2010). However, coal ash is often preferred for use over kaolin due to its availability and low cost as a waste product from power generation.

3.5.3 Other additives

Calcium, phosphorus and sulphur based additives can also be used to absorb volatile potassium species into solid phase compounds. Calcium based additives are effective in a similar way to aluminosilicate based additives by reacting with potassium silicates to form calcium potassium silicates, which have relatively higher melting temperatures. The ternary diagram in Figure 3.6 illustrates the K_2O - SiO_2 - CaO relationship that results from the use of a Ca additive. It can be seen that with high Si content, solidus temperatures can be $<700^\circ\text{C}$ but with higher proportions of CaO this changes to $800\text{-}1000^\circ\text{C}$.

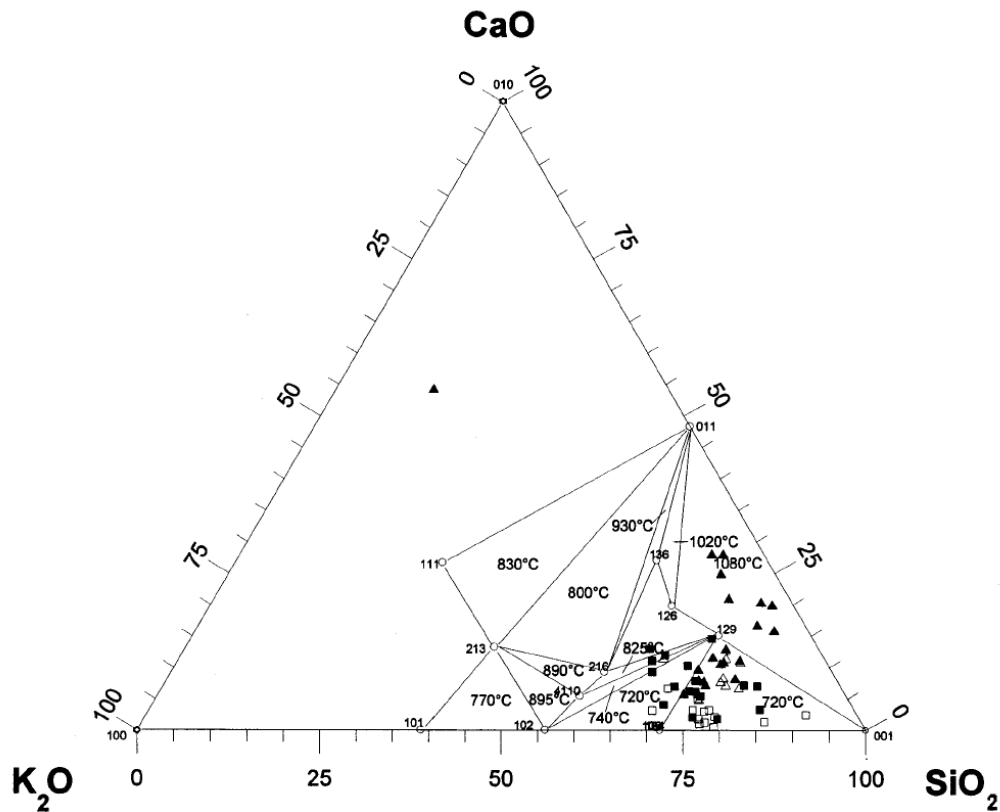


Figure 3.6 K₂O-SiO₂-CaO ternary diagram with solidus temperatures from (Öhman and Nordin, 2000).

Phosphorus based additives react with the potassium to create potassium phosphates, that may also further react with CaO. The result is that less potassium is available to form the low-melting temperature potassium silicates (Wang et al., 2012).

Sulphur based additives react with potassium chloride to create potassium sulphate and hydrogen chloride. The potassium sulphate has a much higher melting temperature than KCl, thus making it less problematic (Wang et al., 2012). However the sulphation of KCl can result in the release of HCl into the flue gas which may need treatment before atmospheric release but can reduce Cl related corrosion.

3.6 Chemistry of carbon capture with monoethanolamine (MEA)

3.6.1 Introduction to amines for carbon capture

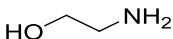
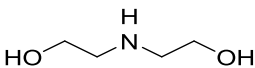
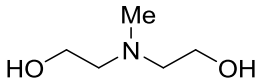
Amines have been used for many years to remove carbon dioxide and hydrogen sulphide from natural gas – in a process known as gas sweetening. Most carbon capture systems used now are based on the same chemical absorption technology with amine based solvents, due to their high reactivity and absorbance capacity.

Amines are a reasonably cheap solvent and can be produced from the reaction of ethylene oxide (C₂H₄O) with ammonia (NH₃) to create a mixture of MEA and DEA (Goetze et al., 1970). Other amines are produced by different methods. Existing literature tends to use monoethanolamine (MEA) as a base case scenario for the comparison of alternative solvents. This project continues this examination of MEA degradation, by assessing the impacts of biomass flue gas impurities.

As mentioned in Chapter 1, amine degradation is a unexpectedly significant operating cost associated with carbon dioxide removal due to amine reclamation. Understanding the chemistry of amine degradation is important for forecasting how efficient the combination of carbon dioxide capture with various gas streams might be. To understand the chemistry of degradation, it is essential to firstly understand the chemistry of carbon dioxide capture with MEA. From this an understanding of the role of the cyclical CO₂ capture and release process plays in the degradation of amine solvents.

Amines are organic chemicals containing a basic nitrogen atom. The most well understood solvents for post-combustion carbon capture are alkanol-amines such as monoethanolamine (MEA), diethanolamine (DEA) and methyldiethanolamine (MDEA). MEA has one carbon containing group attached to the nitrogen atom of the amine molecule, whereas DEA has two carbon-containing groups attached and MDEA has three. All of the amine molecules include an alcohol (O-H) group as seen in Table 3.2, which reduces volatility and improves solubility in water.

Table 3.2 Primary, secondary and tertiary amine structures

Primary amine	Secondary amine	Tertiary amine
MEA	DEA	MDEA
		

Nitrogen is the most reactive atom in the amine molecule, due to its basic lone pair of electrons which react with the acidic and electrophilic CO₂ gas. By altering the structure of the amine molecule around the nitrogen atom, the reaction pathways for carbon dioxide absorption are changed. For example, with a methyl group to make an amine without an NH (MDEA instead of DEA in Table 3.2), a tertiary amine is formed which favours the bicarbonate mechanism, a slower mechanism described

later. This is the same for sterically hindered amines whereby a bulky substituent group is attached to the nitrogen to limit its reactivity. Primary and secondary amines can react with CO₂ to form different products (carbamate or bicarbonate) whereas tertiary amines don't have an NH and hence can only react via the bicarbonate pathway discussed in more detail below.

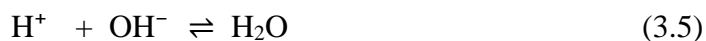
The range of amines available for use as a carbon capture solvent, make the selection of a solvent for a CCS plant a compromise of CO₂ absorption capacity and rate, cyclic capacity, energy requirements, degradation and corrosion rates, volatility and toxicity.

3.6.2 Hydration of carbon dioxide

The interaction of carbon dioxide with water is of the utmost importance for the earth's atmosphere and is hence a well-researched area. Dissolved CO₂ can reversibly react with the water (H₂O) or hydroxide (OH⁻) to create carbonic acid (H₂CO₃) and bicarbonate ion (HCO₃⁻) respectively, as seen in equations (3.3) and (3.4). The bicarbonate ion can react further to form carbonate (CO₃²⁻) though this occurs in less significant quantities. Equations (3.5)-(3.8) show the types of protonation that can follow these initial reactions (Wang et al., 2009).



Many of these species undergo instantaneous protonation reactions which are reversible but should be considered. This includes the protonation of the amine as in equation (3.8)



3.6.3 Carbamate formation through a zwitterion mechanism

The lone pair of electrons on the amine nitrogen atom are electron rich and are thus attracted the electrophilic carbon atom of the carbon dioxide. These carbon and

nitrogen atoms form a bond, which forces one of the CO₂ double bonds with oxygen to be broken, resulting in a net negative charge on this oxygen.

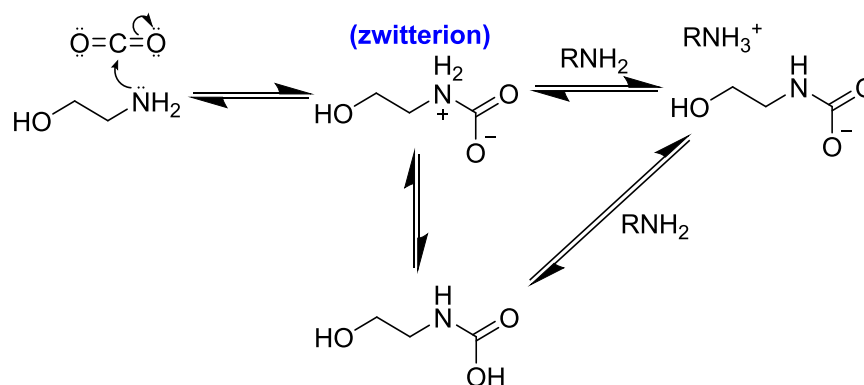


Figure 3.7 The zwitterionic carbamate formation mechanism

The *zwitterion mechanism* has been found to be the most prominent form of carbamate formation, whereby the amine reacts with CO₂ to form a zwitterionic molecule shown in Figure 3.7. This zwitterion protonates a base (usually another amine) to leave a carbamate (McCann et al., 2009). This results in an undesired 1:2 ratio of CO₂ to amine on a stoichiometric basis:



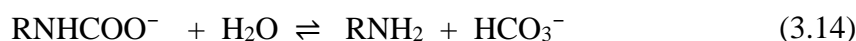
The *termolecular reaction* of CO₂ with an amine and a base is another possible mechanism identified for carbamate formation. However for a termolecular reaction to occur the relevant reacting molecules (amine, CO₂ and water) are required to collide at the same place and time, thus making the statistical likelihood of occurrence rather unlikely. For that reason it is realistically believed that these reactions are only likely to occur as a combination of lower order reactions rather than any termolecular interactions. However the overall mechanism is described as:



The reaction of amine with CO₂ to form a carbamic acid which is then deprotonated to leave a carbamate is deemed more realistic. However this mechanism alone is not seen to give an accurate kinetic representation of carbamate formation for an aqueous solution with carbonate species (McCann et al., 2009).



The carbamate reversion reaction whereby a carbamate formed via the zwitterion mechanism reacts with a water molecule is important to consider, resulting in a reversion back to an amine molecule and a bicarbonate, as in equation (3.14).



Also to consider is the deprotonation of a protonated amine molecule by a hydroxide ion, as in equation (3.15).



It is important to note that two molecules of MEA are used to capture each molecule of CO₂ as this limits the amount of CO₂ captured to 50% the amount of MEA. Primary and secondary amines typically have fast kinetics (speed of chemical reaction), however they have a reduced CO₂ load capacity and a high regeneration cost due to the high ‘heat of absorption’ of carbamates (Puxty et al., 2009). MDEA or other tertiary amines have a higher load capacity but slower kinetics. Therefore the solvents used for carbon capture are usually a mixture of amines with complementary reaction characteristics.

3.6.4 Bicarbonate formation through base-catalysed hydration of CO₂

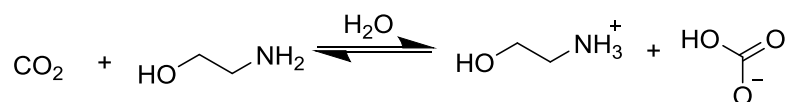


Figure 3.8 Reaction of CO₂ with amine to form bicarbonate

Bicarbonate salts can also be created via the base-catalysed hydration of carbon dioxide, however this is unlikely due to the low equilibrium constants for H₂CO₃, and hence is more likely to be termolecular. This is more commonly found in tertiary amines where carbon dioxide first reacts with H₂O or hydroxide (OH⁻) in the aqueous solution to form carbonic acid (H₂CO₃) or a bicarbonate ion (HCO₃⁻) respectively, equation (3.3) and (3.4). The formed carbonic acid then almost immediately reacts with the amine via Brønstedt-Lowry’s acid-base theory - the amine is protonated leaving a bicarbonate ion (Barth et al., 1981).



In line with Le Chatelier's principle, a solution with a higher pH will favour more deprotonation of the carbonic acid and will therefore encourage this reaction. However this bicarbonate formation mechanism is believed to be slow due to the relatively small amounts of carbonic acid being present as most is dissolved CO₂.

3.6.5 Reaction pathways effect on rate and capacity

As discussed previously, the carbamate and bicarbonate pathways are the mechanisms by which amines can absorb CO₂. In general the acid-base nature of this reaction would lead us to think the strength of the base (pKa) will have a strong influence on the amine capacity – however this is also dependent on the reaction pathway through which the amine reacts (Puxty et al., 2009). The strength of an acid or base can be measured as the logarithmic acid dissociation constant, pKa, whereby a stronger base will have higher pKa value and be more susceptible to gaining a proton. The reverse reaction is also important and is unfavourable with high pKa.

Figure 3.9 is a plot of capacity of the various amines tested with respect to their pKa from (Puxty et al., 2009). The plotted lines illustrates theoretical model predictions of capacity depending on amine pKa, for solely the carbamate pathway (dotted line) and the bicarbonate pathway (dashed line). The primary and secondary amines are not seen to show much effect from pKa and it is believed that this is due to the carbamate equilibrium constant for each amine which effects the pKa value (Puxty et al., 2009). However it can be seen that the capacity of tertiary amines (which must use the bicarbonate pathway) is highly dependent on pKa.

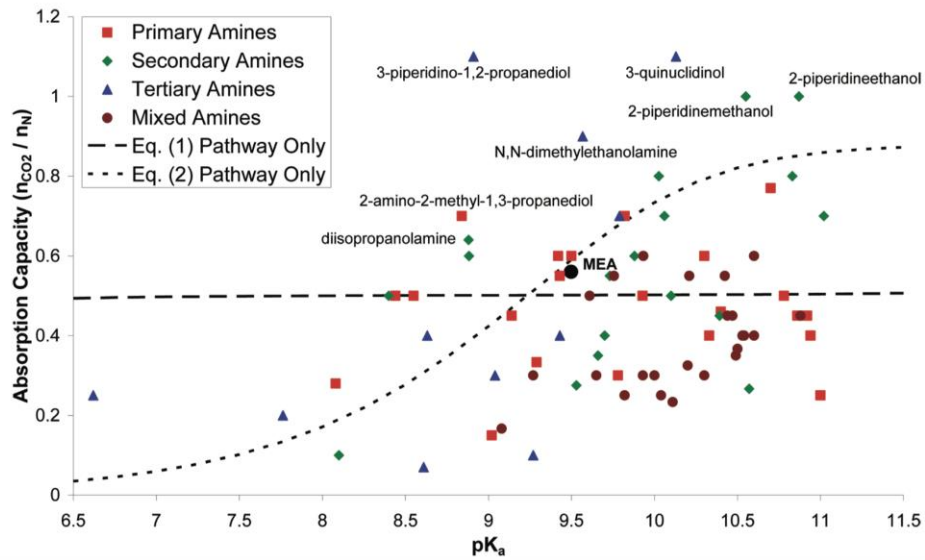


Figure 3.9 Absorption capacity of 76 amines against their pKa (Puxty et al., 2009)

Figure 3.10 shows the dependence of the absorption rate on pKa, as stronger bases become protonated fastest. Tertiary amines are seen to show slower rates due to bicarbonate pathway kinetics. The carbamate pathway is kinetically faster than the bicarbonate pathway, therefore primary and secondary amines are usually found to have faster reaction rates than tertiary.

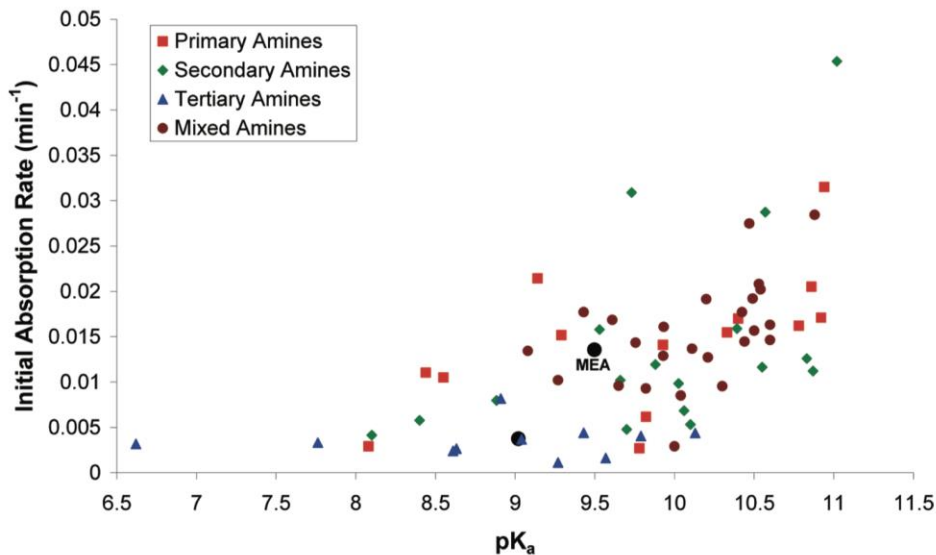


Figure 3.10 Absorption rate of 76 amines against their pKa (Puxty et al., 2009).

3.6.6 Amine regeneration

It is important to note that the regeneration of amine generally requires a lot of heat (Rao & Rubin 2002). The reaction of amines with CO₂ is exothermic (releases heat)

however energy is then required for the endothermic (requires heat) reaction of decarboxylation. The amine solvent that has reacted is heated to approximately 120 °C in order release the CO₂ and regenerate the aqueous amine solution.

There is an energy cost associated with this regeneration process due to the heating requirements. The costs associated with solvent regeneration can vary dramatically depending on the solvent and it's rate of degradation (Abanades et al., 2004). An understanding of the degradation of MEA and other solvents over extended periods of capture is essential for the comparison of these costs. As a solvent degrades a solvent reclaiming process becomes necessary, whereby a solvent can be cleaned of degradation products, heat stable salts (HSSs) and other impurities by solvent distillation (Dumée et al., 2012).

3.7 The degradation of MEA in carbon capture

3.7.1 Introduction

The carbon capture process subjects solvents to varied conditions including: high temperatures, cool temperatures, varying pH, variations of flue gas temperatures, composition and impurities from ash and corrosion. These differing conditions can lead to the degradation of amine solvents to form a variety of degradation products. The formation of these products results in higher viscosity and less amine molecules being available to react with CO₂, which will lead to a reduction in absorption capacity unless the solvent is reclaimed which will lead to increased running costs and some solvent loss. This section will break down the different elements that can end up in the carbon capture system and the different types of amine degradation products that can be formed.

3.7.1.1 Flue gas impurities

The flue gas from an air fired solid fuel combustion process will be mostly comprised of nitrogen, oxygen, moisture and carbon dioxide as the main gases present from combustion. However the flue gas from a solid fuel combustion facility will also contain a lot of other components that are not necessarily desired during the combustion process but are innate. These are called flue gas impurities and include volatile and solid phase species such as NO_x, SO_x, CO, acid gases and PM.

The European Commission's Large Combustion Plant Directive (LCPD, 2001/80/EC) was the main driver for many existing power stations with capacity greater than 50MW to be fitted with pollutant removal devices for SO_x, NO_x, and PM. The Industrial Emissions Directive (2010/75/EU) superseded the LCPD in 2016 and aims to implement the best available technologies for pollutant removal, provided the cost of installation doesn't outweigh the benefits. Such technologies are beneficial to the carbon capture processes as they clean impurities from flue gas streams, preventing contamination of capture solvents.

However, even with improvements to flue gas treatment and particulate removal devices, it is expected that traces of volatile metals and fine particulates from the flue gas will accumulate within carbon capture plants (Thompson et al., 2017). This has already been well documented in literature and recently demonstrated on the world's first industrial scale carbon capture facility, Boundary Dam, where fly ash related problems caused the majority of major outages, resulting in the plant initially operating at 40% capacity (Estevan Mercury, 2017). Fouling and amine degradation were the lead problems caused by fly-ash, resulting in a cost twice as big as expected for maintenance of the amine-based solvent, resulting in a legal battle between Sask Power and Shell Cansolv (CBC News, 2018). Typically, amine degradation has been estimated to account for 10% of the operating costs associated with carbon capture (Vega et al., 2014).

3.7.1.2 Elemental accumulation in MEA solvents

Although metals that accumulate in the carbon capture solvents are typically small, as illustrated in Table 3.3 for pilot-scale coal-combustion, they can still be enough to catalyse amine degradation reactions (Chandan et al., 2014; Huang et al., 2014) resulting in increased costs for amine regeneration. Metals have typically high catalytic activity, so low quantities can have significant impacts on degradation. Previous work on metal accumulation in carbon capture plants has focussed on metals known to be volatile from coal combustion and equipment corrosion as CCS was predominately developed as a technology to remove carbon emissions associated with coal. This research has identified trace metals such as Mercury (Hg), Arsenic (As) and Selenium (Se) had the potential to reach the CO₂ capture process (Azzi et al., 2013). Many countries are still planning continued coal use, whereas the UK is currently phasing out the combustion of coal. Therefore the examination of

elements present in high quantities in biomass, such as K, Ca and Mg are of high importance along with metals with high catalytic activity which may leached into MEA solvents from combustion ashes or corrosion of stainless steel reactors – Cr, Fe, Ni, Cu and Mn.

Table 3.3 Major elemental accumulation from pilot MEA testing (Thompson et al., 2017)

Element	UKy-CAER (mg/L)	NCCC (mg/kg)	CSIRO (mg/kg)
Cr	29.3	45.9	4.2
Fe	265.3	137.2	199.0
Ni	28.0	28.8	4.6
Cu	34.0	<LOD	3.5
Mg		15.3	6.2
Al		4.1	
Mn		5.6	2.1

3.7.2 Thermal degradation

Under capture conditions, solvents are exposed to a cycle of different conditions. To investigate the individual causes of degradation from the specific conditions, laboratory experiments used in the literature are broken down into thermal and oxidative studies. Thermal degradation of the MEA molecule is found to create by-products such as ethylenediamines (known as diamines or dimers). It is suggested that these diamine by-products may also have corrosive effects on equipment used for carbon capture and storage (Sexton and Rochelle, 2006).

Both primary and secondary amines begin thermal degradation with the closing of a carbamate ring. It was suggested by Polderman (1955) that the carbamate molecule cyclises to form 2-oxazolidone (OZD) as in Figure 3.11. Oxazolidone is an organic compound containing a 5-membered ring with both nitrogen and oxygen present. It has a CAS number of 497-25-6 and is available for purchase however due to its instability only small quantities are reported in degradation experiments.

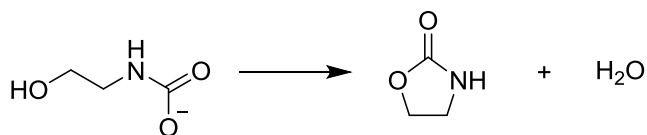


Figure 3.11 2-oxazolidone formation from MEA carbamate

OZD molecules are sensitive to nucleophilic reactions and are therefore often react with another amine molecule to form a dimer such as N-(2-hydroxyethyl)-ethylenediamine, abbreviated as HEEDA (H. Lepaumier et al., 2009). HEEDA has a CAS number of 111-41-1 and is available for purchase. It is a liquid at room temperature with boiling point of 239 °C.

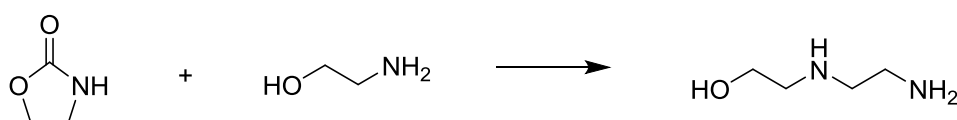


Figure 3.12 HEEDA formation from 2-oxazolidinone

HEEDA can cyclise to form 1-(2-hydroxyethyl)-2-imidazolidone, known as HEIA, which is the major product from thermal degradation. Literature on the thermal degradation of MEA doesn't find the formation of HEIA to be affected by coal fly ashes (Davis and Rochelle, 2009). However HEIA is found to significantly contribute to degradation at pilot-scale facilities (Thompson et al., 2017). It has a CAS number of 3699-54-5 and is available for purchase. It is a liquid at room temperature with a boiling point of 185 °C.

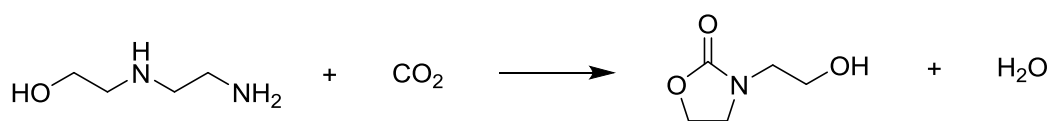


Figure 3.13 HEIA formation from HEEDA

Experiments using solvent samples stored in stainless steel batch reactors under high temperatures is one of the most effective methods for replication of thermal degradation conditions within the laboratory. The analysis of thermally degraded samples using gas chromatography mass spectrometry (GC-MS), liquid chromatography mass spectrometry (LC-MS) and ion chromatography (IC) has enabled the identification and quantification of key thermal degradation products.

3.7.3 Oxidative degradation

Oxidative degradation describes the degradation of solvents in the presence of oxygen, mostly applicable to the conditions of the absorber sump and cross heat-exchanger where the solvent is rich in dissolved oxygen and exposed to high temperatures (Monteiro et al., 2018). The degradation is found to be affected by flue gas conditions such as the concentration of O₂, CO₂, SO₂, NO₂ and coal fly ash (Vevelstad et al., 2013; Da Silva et al., 2012; Uyanga and Idem, 2007). Typical oxygen concentrations in flue gases from a coal fired power station are 3-4%, compared to 12-15% from gas turbines (Global CCS Institute, 2012). Oxidation can occur at two active sites of the MEA molecule, the amine or the alcohol. The initial oxidation of MEA is found to mostly lead to the formation of ammonia, aldehydes and carboxylic acids (acetate, glycolate, formate and oxalate) as the primary degradation products shown in Figure 3.14.

3.7.3.1 Primary oxidative degradation products

Ammonia, methylamine, formaldehyde and acetaldehyde are the initial products formed from the oxidation of MEA. Carboxylic acids, such as formic, acetic, glycolic and oxalic have been previously identified and reaction pathways have been suggested (Strazisar et al., 2003; Rooney et al., 1998). Ammonia is likely formed from the oxidation or fragmentation of the MEA molecule, whereas the acids are oxidized fragments of the MEA molecule such as aldehydes (Da Silva et al., 2012; Helene Lepaumier et al., 2009).

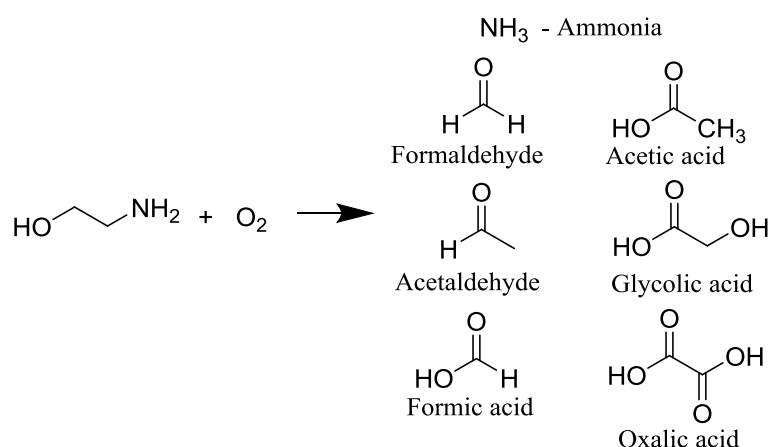


Figure 3.14 Primary oxidative degradation products

Figure 3.14 shows the initial oxidative degradation products that are believed to be formed as the first stage of degradation. These products are reactive species that react further to generate more stable, secondary degradation products.

3.7.3.2 Secondary oxidative degradation products

These primary degradation products are found to degrade further to form secondary degradation compounds from reaction with oxygen, MEA, aldehydes or ammonia. The major secondary oxidative degradation products are N-(2-hydroxyethyl)formamide (HEF), N-(2-hydroxyethyl)acetamide (HEA) and N-(2-hydroxyethyl)imidazole (HEI), which are more stable than primary degradation products and thus are detectable through various analysis techniques. The mechanisms by which these secondary products could be formed are not well understood, though mechanisms have been suggested in literature shown below in Figure 3.15 (da Silva et al., 2012; Lepaumier et al., 2011a; Strazisar et al., 2003).

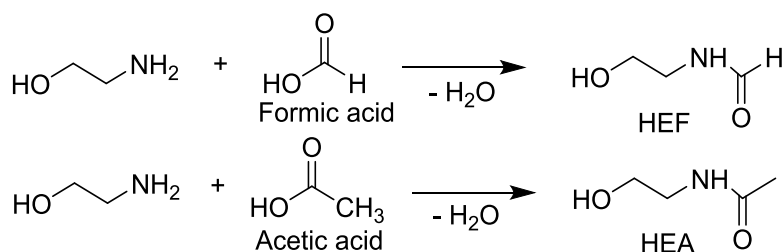


Figure 3.15 Formation of secondary oxidative degradation products, HEF and HEA

HEI is the most abundantly observed degradation product from the oxidation of MEA. HEI has been reportedly formed from glyoxal, formaldehyde, MEA and ammonia by (Vevelstad et al., 2013). It has a CAS number of 1615-14-1 and is available for purchase. It is a solid at room temperature, with a melting point of 38 °C.

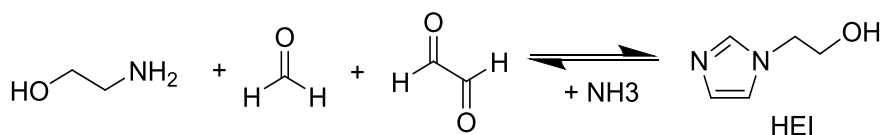


Figure 3.16 Suggested formation of HEI from formaldehyde, oxalic acid and ammonia by (Vevelstad et al., 2013).

Significant amounts of N-(2-hydroxyethyl)glycine, HeGly, has also been detected through LC-MS from laboratory oxidative degradations. It has a CAS number of 5835-28-9 and is available to purchase. HeGly is believed to be the result of a reaction between MEA and a primary degradation product, however it is not known which primary product or the mechanism for this reaction. HEGLy is suggested to be playing a role in the formation of 4-(2-hydroxyethyl)piperazin-2-one, HEPO, as illustrated in Figure 3.17 with N-(2-hydroxyethyl)-2-[(2-hydroxyethyl)amino]-acetamide, HEHEAA, as an intermediate product.

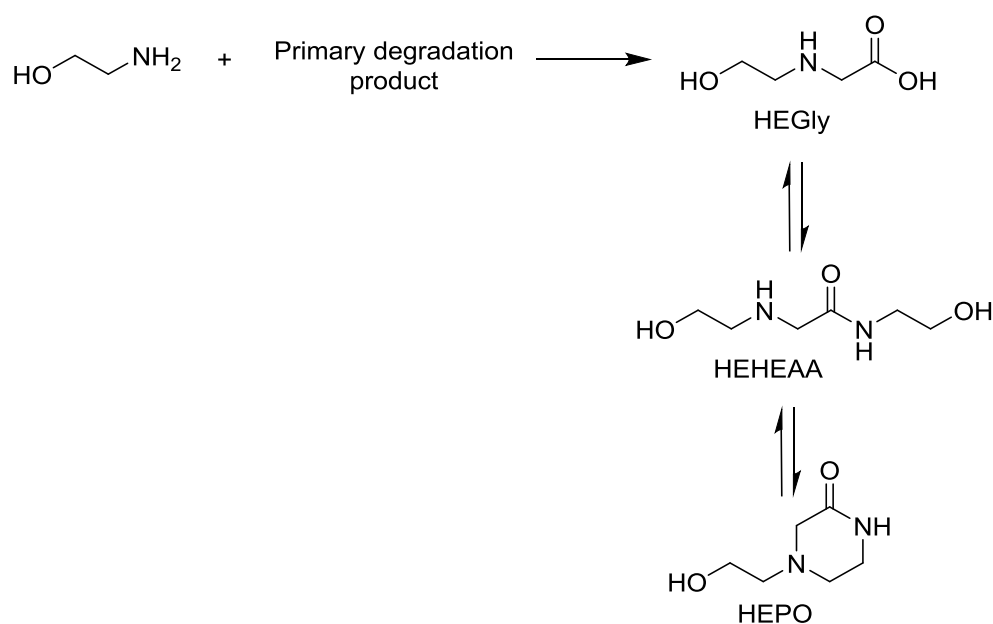


Figure 3.17 Suggested formation of HEGLy from (Da Silva et al., 2012) and HEPO from (Vewelstad et al., 2014)

Mixing MEA with oxalic acid has been found result in the formation of N,N'-bis(2-hydroxyethyl)oxalamide, BHEOX. A suggested mechanism for its formation is provided in Figure 3.18. The presence of BHEOX has been confirmed as present by other studies as a molecule with a mass of 176 (Chandan et al., 2014; Da Silva et al., 2012). Concentrations of this compound were found to be very low but coal fly ash appeared to slightly catalyse its formation (Chandan et al., 2014).

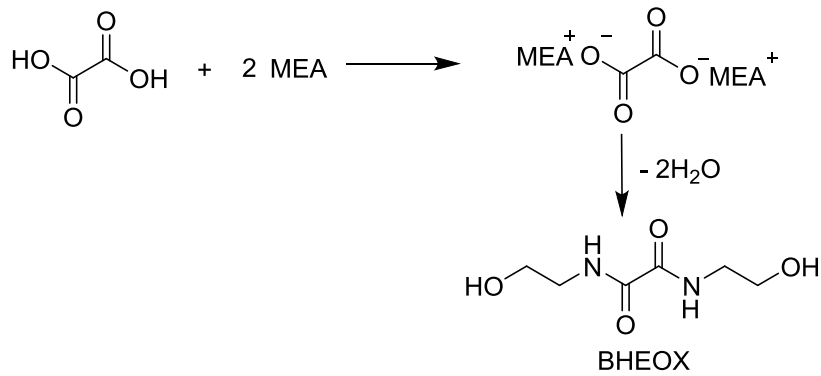


Figure 3.18 Formation of BHEOX from oxalic acid and MEA (Supap et al., 2011)

Some metals such as copper, chromium, nickel and iron have been found to speed up this degradative process of MEA. These metals are often found in the metal alloys or corrosion inhibitors used by amine absorber columns. However, inhibitors such as ethylenediaminetetracetic acid (EDTA) can be used to effectively reduce the degradation caused by oxidation, by approximately 90% (Sexton and Rochelle, 2009).

3.7.3.3 Heat Stable Salts (HSS) in MEA solvents

The major HSS observed at pilot carbon capture facilities are listed in Table 3.4. From this it can be seen that formate, sulphate and oxalate are the main salt species of concern at a carbon capture facility. These salts are stable under high temperatures, hence called heat stable salts (HSS). Thus making them very undesirable for the regeneration of amine as they require neutralisation by a base alkali metal base such as potassium hydroxide or sodium hydroxide (Rooney, 1999). This releases the amine for the absorption of CO₂, but leaves the heat stable anions or neutralised species still requiring removal from the solvent (Dumée et al., 2012).

Table 3.4 Concentration of HSS form pilot testing (Thompson et al., 2017)

HSS	UKy-CAER (mg/L)	NCCC (mg/kg)	CSIRO (mg/kg)
Chloride	89	21.2	167
Nitrite	< 1ppm	2.3	108
Nitrate	1009	19.3	1510
Sulphate	3350	1010	2400
Acetate	884		
Formate	7588	1820	11,800
Glycolate	619		
Oxalate	3643	393	3100

Acidic gases present in flue gases are also of concern for amine degradation. Volatile pollutants such as NO_x, SO₂, hydrogen chloride (HCl) and hydrogen fluoride (HF) can react with the basic amines to form undesired stable salts. As illustrated in Figure 3.19, the reaction of a free MEA molecule with hydrochloric acid (HCl) to form a salt that does not separate when heated. Due to this unrenderable nature of these salts they will accumulate within the solvent until removed by reclaiming. Resulting in decreased CO₂ absorption capacity of the solvent (Supap et al., 2011).

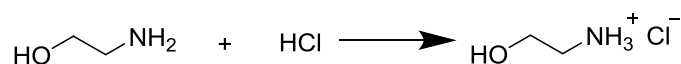


Figure 3.19 The role of hydrochloric acid (HCl) in MEA degradation to a MEA-chloride heat stable salt (HSS).

The accumulation of these flue gas derived anion salts includes sulphate, nitrate, nitrite and chloride, often form due to the presence of SO₂, NO_x and fly ash in flue gas streams. For high sulphur fuels like coal, high concentrations of SO₂ are common in flue gases and are highly soluble MEA solvents resulting in sulphate being the main HSS species observed (Thompson et al., 2017). Nitrite, NO₂⁻, and nitrate, NO₃⁻, are formed from the reaction of O₂ with ammonia and hydroxyl radicals as the primary oxidant, converting ammonia into nitrite and then on to nitrate (Huang et al., 2008).

The acids formed by the oxidation of MEA such as formic and acetic acid, exist in equilibrium between the MEA salts, as in Figure 3.20, and amides (HEF and HEA). Oxidative degradation of MEA can also result in the formation of salt anions such as

glycolate and oxalate. Glycolic acid is observed to favour the formation of a HSS instead of its amide which is unstable and hydrolyses back to glycolate. While oxalic acid mostly decomposes to formic acid (Supap et al., 2011). Formate is the major oxidative HSS observed at pilot carbon capture facilities, as illustrated in Table 3.4, due to high quantities of formic acid produced through oxidative MEA degradation (Chandan et al., 2014).

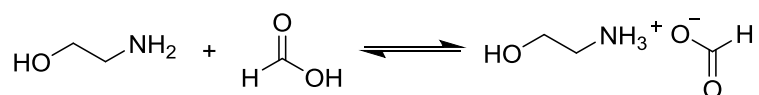


Figure 3.20 Formic acid in MEA degradation to a MEA-formic acid heat stable salt (HSS).

3.7.4 Pilot-scale degradation

Oxidative degradation products, (HEI, HEGly, HEF and HEA) are found to be the dominant degradation products found in MEA samples from pilot facilities. This suggests that degradation within a full scale CO₂ capture plant is largely oxidative, with the exception of HEIA as a significant contribution from thermal degradation. N-(2-hydroxyethyl)-glycine (HeGly) is found to be one of the major products seen from the degradation of MEA at a pilot-scale CO₂ capture facility (Da Silva et al., 2012).

HEPO from Figure 3.17 is also found to be present in significant quantities in the pilot plants. This product is not seen in the laboratory oxidative experiments, except for at high temperatures and is thus likely formed as a result of the varied, cyclical processes the solvent is exposed to in a pilot facility. HEPO has a CAS number of 23936-04-1 but is not readily available for purchase.

3.7.5 Previous use of ¹H NMR spectroscopy for MEA speciation and degradation

Literature on MEA degradation has predominately used non-exact forms of product identification such as gas chromatography-mass spectrometry (GC-MS) and liquid chromatography-mass spectrometry (LC-MS). This work uses ¹H NMR spectroscopy as a highly accurate analysis technique to confirm the presence of previously suggested products, and interrogate the presence of other products yet to

be identified by literature. Existing chromatography methods will be used to validate findings from NMR spectroscopy.

Existing NMR literature has focused heavily on MEA absorption rather than degradation. The author is only aware of two studies that use NMR spectroscopy to examine the degradation of MEA. The first study to use NMR spectroscopy for MEA degradation was successful in identifying 3 of the major degradation products: N-(2-hydroxyethyl) imidazole (HEI), 2-oxazolidone (OZD), N-(2-hydroxyethyl) formamide (HEF). However, this study also found unassigned ^1H and ^{13}C NMR peaks and these were not identified or quantified in the work (Ciftja et al., 2012). The second study evaluated the use of NMR to track degradation and identified N-acetyethanolamine (HEA) to have an observable chemical shift at 2.0ppm and HES at 2.45ppm through the purchase of standards. The quantification of these peaks correlated linearly with the formation of heat stable salts, suggesting NMR is a viable option for rapid tracking of HSS formation (Reynolds et al., 2015).

3.7.6 The release of amine products to the atmosphere

The release of amine solvents and their degradation products into the atmosphere is known to result in the formation of products such as amides, aldehydes and nitrosamines which are highly carcinogenic. The main route for such release is through volatile amine species being present in flue gases as they exit the absorber column. Figure 3.21 illustrates how the release of amine species into the air can lead to the formation of nitramines (from NO_2) or nitrosamines (from NO) - products with known carcinogenic effects (MacDowell et al., 2010).

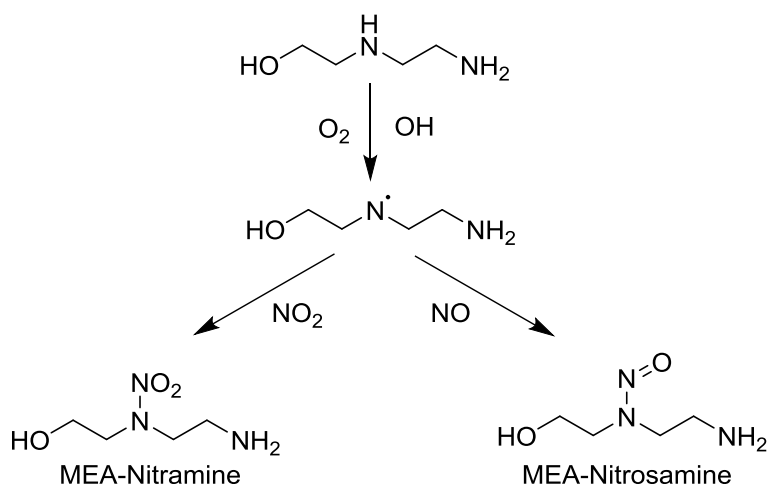


Figure 3.21 Formation of nitramines and nitrosamines from DEA

The release of MEA to atmosphere has shown impacts on the toxicity of nearby freshwater ecosystems and terrestrial ecosystems (Veltman et al., 2010), while this literature study didn't find evidence of environmental impacts from formaldehyde, acetaldehyde, and ammonia as key volatile oxidative degradation products. Toxicity of carbon capture solvents remains a key consideration for the selection of solvents, it is therefore of vital importance to monitor solvent emissions and minimise volatility.

3.8 Conclusions

The combustion of solid fuels for power generation will result in the creation of a flue gas composed of N₂, O₂, H₂O, CO₂, NO_x, SO_x, CO and PM. The type of fuel being combusted will have a significant impact on flue gas composition. Biomass is a fundamentally different fuel to coal and its composition can vary dramatically depending on the type of biomass used, however it is a likely replacement for many coal combustion plants and will follow the same combustion processes as a solid fuel.

Differences in the fuel composition will have significant impacts on combustion and the resulting flue gases that are encountered by carbon capture processes. Potassium is an element observed to be in high concentrations with biomass compared to coal and is observed to be volatilised during combustion, since much carbon capture literature to date has focussed on coal combustion the effects of potassium on amines has not yet been examined. Coal ashes are observed to catalyse the oxidative degradation of MEA, however biomass ashes have not yet been examined.

Chapter 4

The laboratory-scale release of potassium in biomass combustion and the effects of an additive

4.1 Introduction

This chapter focuses on the fate of potassium (K) during laboratory-scale combustion of biomass and the effects of an aluminosilicate additive upon it. As identified in Chapter 3, such additives have shown some success in mitigating slagging and fouling problems in boilers and furnaces, and the mobility of potassium in combustion systems is one of the key factors dictating ash behaviour. To investigate this, two laboratory scale experimental methods were used to detect: (i) the release of K from the combustion of single particles of biomass, and (ii) the amounts of solid phase K remaining in biomass ashes at different temperatures.

The chapter starts with the experimental data gathered on the composition of the biomass fuels and the additive used by this work and why they were selected. Following this is an experimental methodology section detailing the apparatus set-up and procedures for the flame emission spectroscopy and ash generation experiments with various quantities of additive (5, 15 and 25 wt% of the raw biomass). The results of these experiments are presented, together with a discussion of what this means for the fate of ash and K in large-scale facilities.

4.2 Experimental methodology

4.2.1 Fuel selection and preparation

Three types of biomass were selected for this investigation, typical of the biomass types that are used in large-scale power generation. The biomass selected were a North American white wood pellet, a UK wheat straw and a European olive cake. It can be seen from the images in chapter 8 that the softwood fuel was supplied in pellet form, whereas the olive residue was a powder and the wheat straw was in a bale. These raw fuels were initially milled using a Retsch SM300 cutting mill detailed in chapter 8 to reduce the particle size of all biomass types to <5 mm.

Samples of each biomass were further milled to $<90 \mu\text{m}$ using an SPEX 6770 freezer mill (detailed in chapter 8) which cools samples to cryogenic temperatures before pulverising samples by magnetically shuttling a steel impactor. This size of sample was used for the ultimate analysis and making of pellets for the single particle combustion experiments, which are both detailed in this chapter. The coal ash used as an additive in this work was provided by a UK power station and required no preparation as it was already $<90 \mu\text{m}$.

The 5 mm diameter pellets used for the single particle combustion (SPC) experiments were made using a SPECAC hand press and SPECAC 5 mm diameter pellet die loaded with 20–60 mg of the biomass and additive blends. Holes were drilled in the centre of the pellets with a hand drill and 0.8 mm diameter drill bit for the attachment to the single particle combustion rig.

4.2.2 Fuel characterisation

Characterisation of the fuels used for this project allows for the interpretation of the fundamental compositional differences which could explain the differing behaviours observed during experimental work. Characterisation of fuels were completed in accordance with the European Standard methods for the proximate and ultimate analysis of the raw fuels and additive.

The proximate analysis provides an overview of the main components of the fuel in terms of moisture, volatiles, fixed carbon and ash contents. Moisture content is defined as the mass of water held within the “as received” fuel that is removable through oven drying at 105°C for a prolonged period (up to 3 hours). Volatile matter is taken to be the mass loss of a small sample (approximately 1g) when rapidly heated upon placement in a 900°C furnace for 7 minutes in a crucible with a loose-fitting lid. Volatile matter on a dry basis is adjusted to account for moisture content. ‘Fixed carbon’ is the quantity of material remaining in the sample after the release of volatiles and excluding ash. This is considered to be predominantly non-volatile organic compounds. Ash is the solid residue remaining after the complete combustion of all carbon and volatile compounds present in the biomass. Ash is measured as the mass remaining after heating a small sample (approximately 1g) in air with a furnace to fix the temperature at 250°C for 1 hour and then 550°C for a further two hours to obtain complete combustion. All fuels were characterized using a Carbolite AAF 1100 furnace and Carbolite moisture oven in accordance with the

European Standard methods (EN 18134-1:2015, EN 18122:2015, EN 18123:2015). All samples were run in duplicate and fixed carbon content was calculated by mass difference.

Ultimate analysis provides an overview of the elemental composition of the biomass fuels used. For raw lignocellulosic biomass these main elemental components are carbon (C), hydrogen (H) and oxygen (O). Nitrogen (N) and sulphur (S) are present in much smaller quantities but are measured due to the oxide gases (NO_x and SO_x) that they form during combustion. These were carried out using a CE Instruments Flash EA 1112 Series elemental analyser for C, H, N, S values, with O calculated by difference after accounting for the ash and moisture contents. These analysers combust the sample at 900°C to produce CO₂, H₂O, NO₂ and SO₂. These gases then pass through a gas-chromatography column which separates the gases so that the relative percentages of each gas can be detected using a thermal conductivity detector (TCD). The absolute masses of C, H (adjusted for moisture), N and S in the original sample can then be calculated.

Samples were run in duplicate in accordance with EN 16948. Weighed samples (2-4mg) of the <90 µm sample were added into small tin capsules which were folded to remove any air. Calibration standard materials were used to calibrate the equipment prior to the running of samples. The calibration standards used for the raw biomass fuels were:

- Atropine (C = 70.56%, H = 8.00%, and N = 4.79%).
- Methionine (C = 40.22%, H = 7.46%, N = 9.43% and S = 21.52%).
- Cystine (C = 29.95%, H = 5.09%, N = 11.59% and S = 26.67%).
- Sulphanilamide (C = 41.85%, H = 4.68%, N = 16.26% and S = 18.62%).
- 2,5-bis(5-tert-butyl-benzoxazol-2-yl)thiophene (C = 72.56%, H = 6.11%, N=6.49% and S=7.40%).

Ash samples were also run using this method to analyse the quantities of unburned carbon in some ash samples (carbon-in-ash). Additional calibration standards were used for these experiments due to the lower wt% of carbon present in the samples. For these samples, soil (C = 2.29% and N = 0.21%) and sediment (C = 6.72%, N = 0.50% and S = 0.92%) standards were used to compliment the calibration of the analyser. Results of the proximate and ultimate analysis of the fuels and coal ash are

presented in Table 4.1. Wheat straw and olive cake are both high in ash and chlorine content relative to the wood pellets.

Table 4.1 Fuel composition data (averages from duplicate runs with the standard deviation, S.D., values given for the largest value)

Content	Basis	Units	Wheat straw	Wood pellets	Olive cake	Coal ash	S.D.
Moisture	a.r.	wt%	10.4	7.3	6.8	0.4	0.6
Volatiles	a.r.	wt%	78.6	83.3	73.9	2.3	0.3
Ash	a.r.	wt%	5.1	0.8	8.1	96.9	0.6
Fixed carbon*	a.r.	wt%	5.9	8.5	11.3	0.4	0.6
Elemental analysis							
C	daf	wt%	48.5	52.8	55.2	84.4	0.45
H	daf	wt%	7.3	6.7	6.9	3.1	0.03
N	daf	wt%	0.5	0.2	3.1	<0.1	0.04
S	daf	wt%	0.05	0.02	0.14	9.7	0.01
Cl	daf	wt%	0.08	<0.01	0.28	0.32	0.01
O*	daf	wt%	43.6	40.3	34.4	2.5	0.45

* by difference

4.2.3 Biomass and coal ash compositions

Many of the inorganics found in biomass are essential nutrients for plant growth. Inorganics typically remain in the solid ash phase through combustion but they can have an impact upon combustion processes. Measuring the inorganic content of fuels can be completed by various experimental methods such as wet chemical analysis, x-ray fluorescence spectroscopy (XRF) or energy dispersive x-ray spectroscopy (EDX). These techniques can be applied to raw fuels or combustion ashes as the majority of inorganics are not combustible and hence will remain in the solid residue. Inorganics (Na, Mg, Al, K, Ca, Mn, Fe) were measured in this project using atomic absorption spectroscopy (AAS) on ashes digested in accordance with EN 16967:2015. However, ashes produced for analysis may lose some inorganics that are volatile at combustion temperatures, such as potassium (Xing et al., 2016).

Ashes of the various biomass types used in this project were generated at 550°C in large sample size (10–100 g) in a muffle furnace with a large inert stainless-steel tray in accordance with EN 18122. Due to the low ash content of white wood pellets (0.8 wt%), large quantities of raw fuel required combustion.

Biomass and coal ashes were digested and analysed for major elements using atomic absorption spectroscopy (AAS) in accordance with EN 16967 (experimental details in chapter 8). Digested samples were analysed in duplicate and a coal ash reference material was used to validate and normalise the data gathered from this ash analysis technique, which was found to measure potassium with an accuracy of 0.18%. Table 4.2 reveals the high K and Ca content present in the ash of the three biomass types, and the high Al and Si content of the coal ash. Wheat straw is particularly high in silica and olive cake is very high in potassium (35 wt% K₂O in the ash).

Table 4.2 Chemical analysis of major elements present in biomass ashes and coal ash used as an additive.

Parameter	Wheat straw (wt%)	Wood pellets (wt%)	Olive cake (wt%)	Coal ash (wt%)
SiO ₂	66.2	16.6	11.2	58.2
Al ₂ O ₃	0.2	2.5	1.2	20.8
Fe ₂ O ₃	0.3	2.1	0.9	9.3
CaO	9.2	29.3	10.3	2.9
MgO	1.7	5.9	3.0	1.4
Na ₂ O	0.2	2.2	0.6	2.3
K ₂ O	11.0	10.0	34.8	1.7
MnO	0.1	2.1	<0.1	<0.1

4.2.4 Potassium released in the combustion of single particles

Small pellets of biomass were combusted to measure the release of potassium using the single particle combustion (SPC) detailed in (Mason et al., 2015) and chapter 8. This rig was designed and constructed by Dr. Patrick Mason who provided the training for the experimental work of this project. The 5mm diameter pellets were made using a SPECAC hand press and die. The effects of coal ash additive on the potassium release was assessed by adding a measured amount of additive (5 wt%, 15

wt% and 25 wt%) to the biomass pellets before pressing. Note that a 5% mix of additive and raw biomass has ash ratios (on a mass basis) of 1:1, 1:0.16 and 1:1.6 for wheat straw, wood pellets and olive cake, respectively for ash produced at 550°C. This would dramatically increase the amount of ash generated by biomass power stations. The quantities of additive used were selected to exaggerate the effects seen in experimentation, lower quantities of approximately 1-2 wt% additive would be required for mitigation stoichiometry of wood pellets in power generation applications. However for this study higher percentages were required to achieve stoichiometry with the higher ash and potassium content of the other biomass. Each pellet was repeated three times.

The SPC apparatus used enabled the study of K-release under relatively high heating rates (~ 85 °C/second) and temperatures. The rig uses a stainless-steel needle to suspend a particle above a methane burner which is used to ignite the particle. Whereas some other SPC rigs in literature have used radiant heating elements to combust individual biomass particles (Flower and Gibbins, 2009). Based on the principles of atomic emission spectroscopy (and assuming a steady temperature of the flame $\sim 1600\text{K}$) a photodetector with an optical band-pass filter is used to measure the relative intensity of the strong electronic spectral emissions around 766nm. This wavelength is characteristic of potassium and the detector signal then indicates the relative concentration of potassium atoms in an excited state present in the flame above the particle. A second photodetector with an optical band-pass filter of 750 nm was used to measure background wavelengths emissions not specifically associated with potassium e.g. soot (Mason, Jones, et al., 2016). An average of the three runs was taken for each sample and smoothed over 12 data points to remove noise from the recorded signal. Figure 4.1 illustrates this smoothing and averaging, whereby the impact of pellet mass on burnout time can be observed.

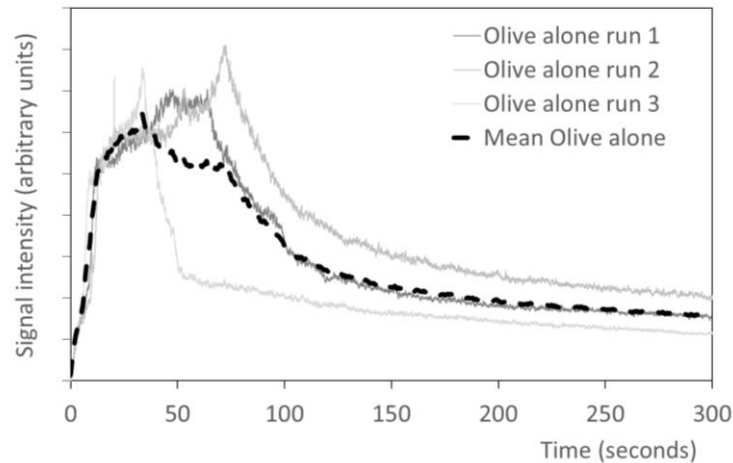


Figure 4.1 Example SPC output of 3 repeated runs for olive pellets weighing 42.5 mg (run 1), 35.9 mg (run 2) and 23.6mg (run 3).

When the biomass particle is placed in a high temperature environment it will undergo three main processes as it combusts: moisture loss, devolatilisation and char combustion. These stages can be observed to slightly overlap when analysing a combusting particle, however, the stages of combustion can generally be identified as:

- 1. Ignition delay** – time in which moisture evaporates from the particle and particle heats up before ignition produces a visible flame.
- 2. Volatile combustion** – time in which the particle is predominantly devolatilising organic matter and producing a visible flame.
- 3. Char combustion** – time in which the particle is predominantly oxidising the matter that remains after volatile combustion.
- 4. Char burn-out** – time at which all combustible matter has been removed from the particle and only ash remains.
- 5. Ash cooking** – Ash held at high temperatures can undergo further reactions resulting in the release of inorganic components.

A high-speed thermal imaging camera (FLIR A655sc) was used to measure particle surface temperatures concurrent with K-release for the olive cake experiments. Particle temperatures rise rapidly during combustion to a final temperature of approximately 1100°C - similar to the highest temperatures applied in the complementary study detailed in the next section. This experimentation is most applicable to fluidised bed conditions due to similar temperatures and physical mixing limitations associated with pulverised fuel combustion. A high-speed video

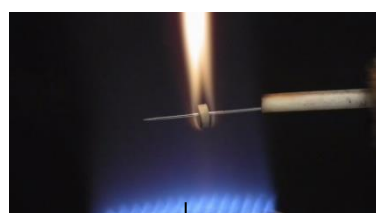
camera (FujiFilm Finepix HS10 camera) was used to insure a consistent integrity of the biomass pellets was maintained and to interrogate the combustion events further. Previous literature has used such video analysis for the comparison of biomass and coal combustion and burnout times (Riaza et al., 2017). An example of the video analysis seen is given in Figure 4.2.



Start – Water-cooled jacket withdrawn.



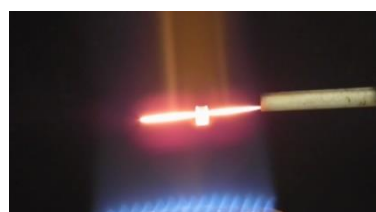
Ignition – Within a second of the jacket being withdrawn the pellet shows the first signs of combustion.



Start of volatile combustion – A bright flame appears above the pellet where vapour phase combustion occurs.



End of volatile combustion – The bright flame above the pellet disappears.



Char combustion – The particle glows as the solid phase combustion occurs.

Figure 4.2 Stages of biomass combustion on SPC

An example of the photodetector signal from the single particle combustion rig is provided in Figure 4.3. The potassium release profiles change for the different stages of combustion as can be observed in in Figure 4.2. The 750nm detector is seen to fall to zero after the volatile combustion stage due to the lack of subsequent black-body radiation from the soot. Char combustion of the single biomass particle reveals

a continual increase in potassium release until just before char burnout. After this, the melting ash particle continues to be heated and slowly releases some potassium depending on the ash content of the particle.

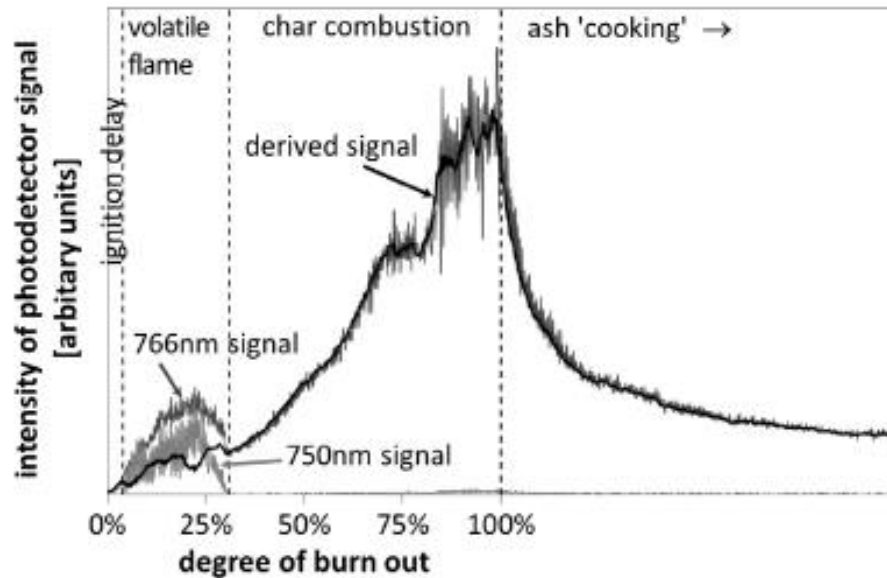


Figure 4.3 Example output for SPC photo-detection (Mason, Darvell, et al., 2016)

4.2.5 Biomass ashing experiments

Experiments were also undertaken at lower heating rates by preparing ashes with percentage blends of coal ash as an additive to the raw biomass. Ash samples were generated at 550°C for 5 hours in accordance with the European Standard method for the determination of ash (EN 18122) in a Carbolite AAF 1100 furnace. Samples were weighed before and after ashing. The ashes prepared at 550°C were then heated in platinum crucibles at three different temperatures, namely 850°C, 1000°C and 1150°C, for 1 hour. The additive was mixed with the raw biomass in varying amounts (5 wt%, 15 wt% and 25 wt%) on an as-received basis as an exaggeration of the quantities required in power generation for experimental clarity.

Carbon analysis of these ashes found the carbon contents to be low – between 1 and 9 wt% for the biomass ashes produced at 550°C. Figure 4.4 shows the change in carbon-in-ash for the biomass ashes prepared at different temperatures. The results show significant carbon is retained in the ashes at lower temperatures which is gradually lost with increasing temperature. However, carbon in wheat straw ashes at temperatures above 550°C were found to be negligible. The presence of a coal ash

additive was found to decrease the carbon-in-ash below that expected by dilution per equation (4.1), suggesting that the presence of the additive improves the completeness of combustion (data provided in Table 8.1).

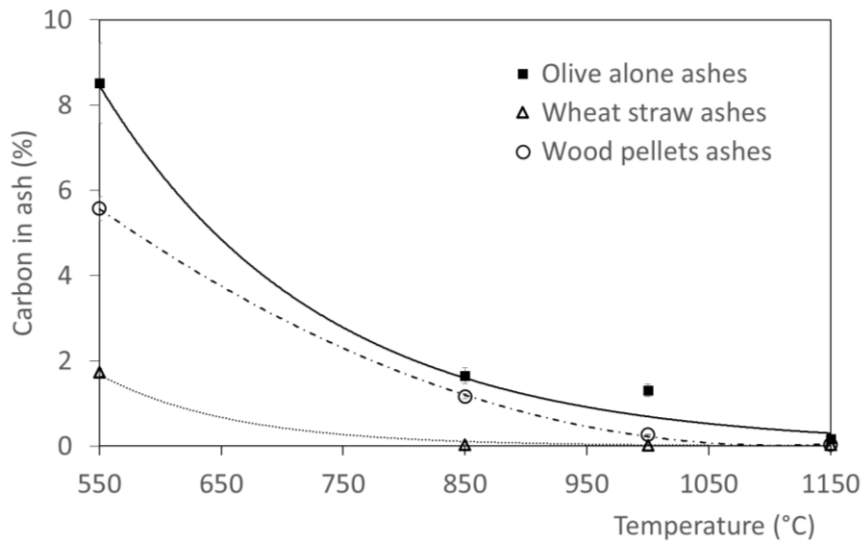


Figure 4.4 Carbon in ash weight percentage for the different biomass types with temperature.

The primary method used for analysis of the inorganics in the generated ash samples was atomic absorption spectroscopy (AAS). Ashes were digested in accordance with EN 16967 and as described in chapter 8, with elemental concentrations measured by a Varian AA240FS spectrometer. Digested samples were analysed in duplicate and a coal ash reference material was used to validate the data gathered from this ash analysis technique, which was found to measure potassium with an accuracy of 0.18%.

Data acquired from the atomic absorption spectrometer for the measurement of potassium retained in the ash was recorded in parts per million present in the digested solutions. This is used to calculate an inferred potassium oxide (K_2O) weight percentage in the ash detailed in Chapter 8. An average of the duplicates was taken prior to accounting for the ash dilution effects of the additive. The blending of additive with biomass prior to ash generation will result in a dilution effect on the biomass ash being prepared since the additive is of high ash content – 96 wt% on an as received basis. Data processing is further complicated by the decreasing ash yield with higher temperatures. This is shown in Figure 4.5. This difference in the ash content at higher temperatures is noted in EN 18122:

“Difference in the ash content determined at a higher temperature, 815 °C, according to ISO 1171, compared to 550 °C is explained by the decomposition of carbonates forming CO₂, by losses of volatile inorganic compounds and further oxidation of inorganic compounds.”

Higher quantities of additive were found to result in lower levels of mass loss during combustion in line with previous thermogravimetric analysis (Höfer and Kaltschmitt, 2016). Thus, the ash contents of the additive and of the biomass samples were measured separately at elevated temperatures in order to gauge the equivalent mass of the biomass ash in accordance with equation (4.1). This was used to calculate the ratios of biomass ash to additive for the experiments with the biomass-additive blends; it assumes that the ash content of the biomass and additive is unchanged when mixed together before ashing. Table 8.1 provides the raw laboratory data used as inputs into equation (4.1) for the mass calculation of biomass ashes alone from additive blends.

$$(Biomass\ blend\ ash\ mass)_T = (Biomass\ ash\ mass)_T + (Additive\ ash\ mass)_T \quad (4.1)$$

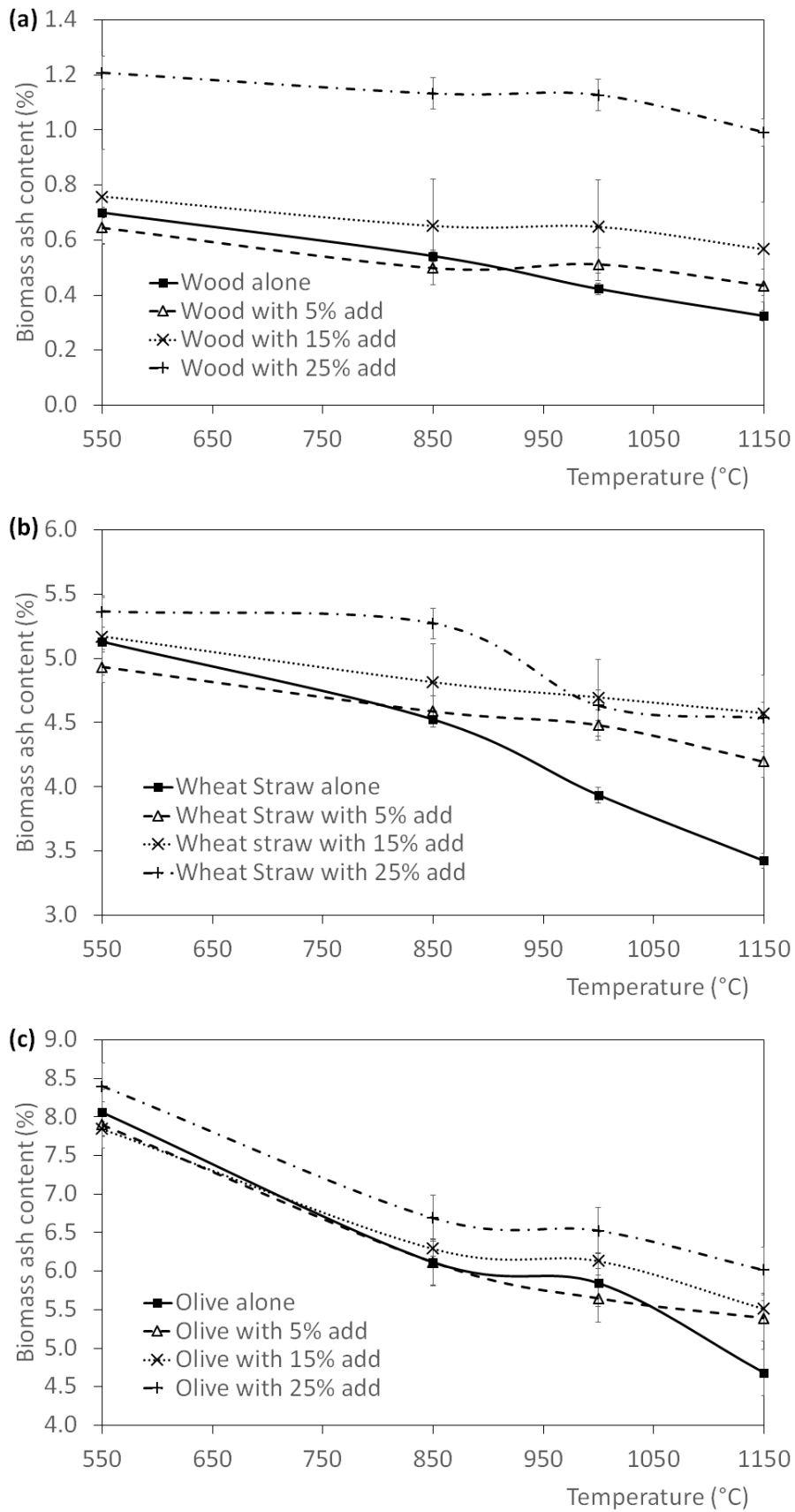


Figure 4.5 Ash content with temperature for (a) wood (b) wheat straw and (c) olive cake.

4.3 Results

4.3.1 Gas phase potassium release profiles of biomass fuels with additive

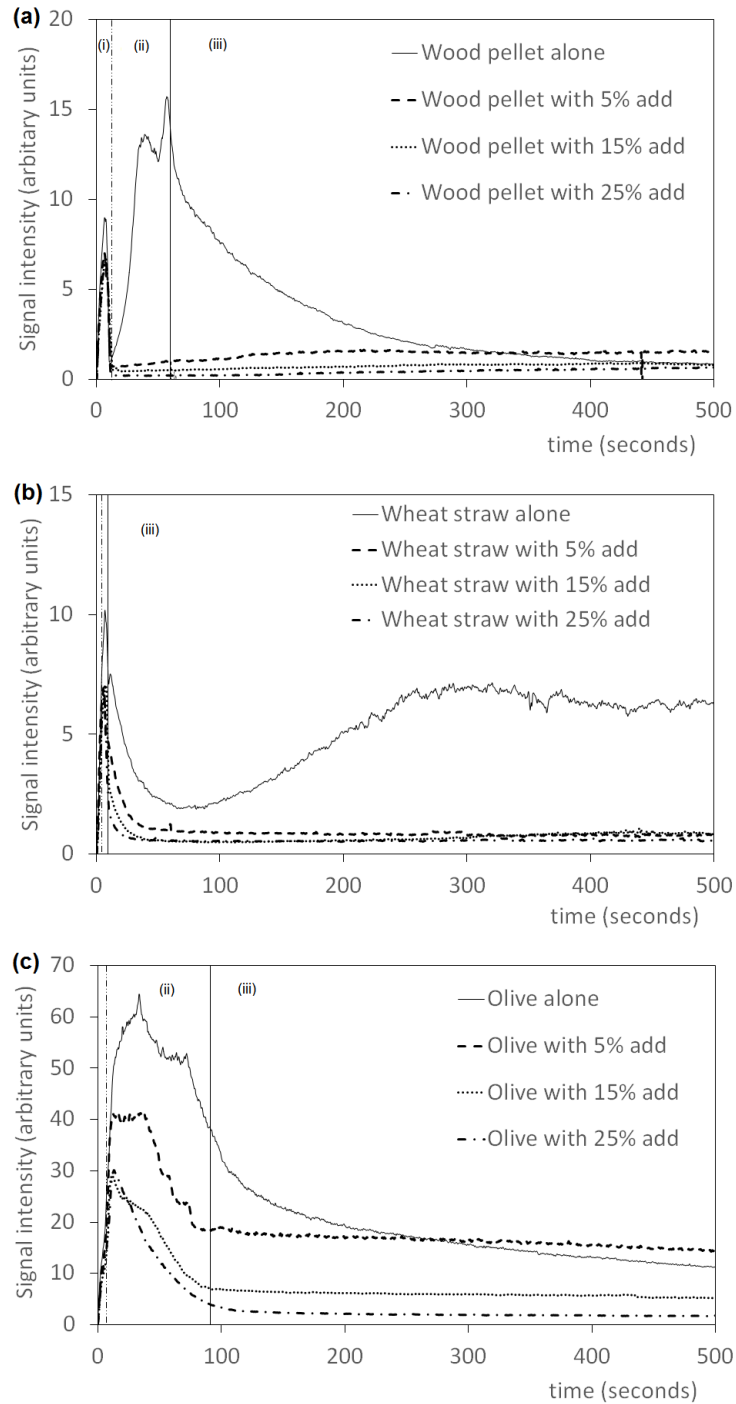


Figure 4.6 Potassium release profiles for biomass pellets with 0/5/15/25 wt% additive for (a) 31 ± 6 mg of wood (b) 35 ± 7 mg of wheat straw and (c) 35 ± 7 mg of olive cake. Profiles are averages of a minimum of three test runs. Labels refer to: (i) Volatile combustion; (ii) Char combustion; (iii) ‘Ash cooking’.

The potassium release (K-release) profiles for the three biomass fuels, each with varying amounts of additive are shown in Figure 4.6. The combustion phases were clearly identified from the visual inspection of the images from the high-speed video camera. Photodetector recordings were made for a period of 8 minutes and 20 seconds (500 s) in order to examine the potassium release behaviour of the remaining ash particle during the continued high temperatures after char burn-out – denoted “ash cooking”. Different combustion technologies have different residence times and fate of ash particles, therefore the length of time that particles are exposed to high temperatures can vary.

Examination of the K-release profile for the wood pellet, Figure 4.6(a), shows a short but rapid release during volatile combustion, followed by a slower increase in the potassium release rate until a peak that marks the end of char combustion. The K-release then slowly decreases during the “ash cooking” stage. This profile is very similar to the characteristic profiles for woody biomass found in previous work using this method (Mason, Darvell, et al., 2016). Addition of the additive has a clear effect. Potassium release during the volatile combustion stage shows a small reduction, the rate of potassium evolving during the char combustion stage reduces very significantly, and is, in fact, reduced almost to zero at high additive loadings. Similarly, there is no K-release during “ash cooking” except for a small fraction with the 5 wt% additive blend.

The K-release profiles for the wheat straw pellets are shown in Figure 4.6(b). The profile of the raw fuel is very different to that observed for the white wood; there is a rapid release of K during volatile combustion, but the profile during char combustion is quite different, and K-release increases slowly until peaking near the end of char combustion. The wheat straw pellets have a notably longer release of potassium after char burn-out which is seen to increase to a later peak during an “ash cooking” phase of the experiments. The “ash cooking” stage sees some disintegration of the ash residue, but it is not complete, and thus evolution of K during this stage indicates some transformation of minerals under high temperature conditions with the parallel evaporation of potassium salts. The profile also suggests that there are significant quantities of potassium in ash after the char burn-out. Interestingly, this part of the profile is almost completely absent when additive is mixed with the wheat straw and there is a slight reduction in the peak potassium release observed during the volatile and char combustion stage. Thus, the higher

amounts of additive can be seen to prevent potassium release after char burn-out and maintain this low release rate during the “ash cooking” stage, which could be very important within a biomass boiler: Ash deposits that are more stable will release less potassium even if they are held at high temperatures.

Olive cake has the highest potassium content of all three fuels, and shows the largest K-release profile of the raw biomass as presented in Figure 4.6(c). The profile shows overlapping peaks for K-release from volatile combustion and char combustion, but the profile is dominated by K-release during char combustion. Increasing amounts of the additive dramatically decrease the potassium release rate, particularly during this char combustion stage. After the peak in potassium release rate associated with combustion, a characteristic slow decrease in release rate is seen during the “ash cooking” phase. Interestingly, K-release from the pellets with additive during this stage seems to plateau at lower signal intensity for the 15 and 25 wt% additive blends. This implies that the additive is fixing potassium in the ash, which is then released only very slowly at high temperature, compared to behaviour of the raw fuel ash.

4.3.2 Particle surface temperature profile for olive cake

Thermal imaging analysis using a high-speed thermal imaging camera (FLIR A655sc) of the olive cake pellets during the combustion experiments revealed a sharp rise in pellet temperature occurs during devolatilisation up to approximately 850-900°C, as illustrated in Figure 4.7. The char combustion stage is identified by the exothermic reaction causing the temperature to rise further (particularly evident in the results for olive cake alone). The equilibrium temperature of approximately 1000°C among the pellets (which decreases slightly with additive addition) continues into the “ash cooking” phase. While thermal imaging was only used for the olive pellet experiments, these results, coupled with previous work (Mason, Jones, et al., 2016), indicate that the samples heat rapidly during volatile combustion and reach a final temperature of approximately 1100 °C during the char combustion stage i.e. temperatures are similar to the highest temperatures applied in the complementary study detailed in the next section.

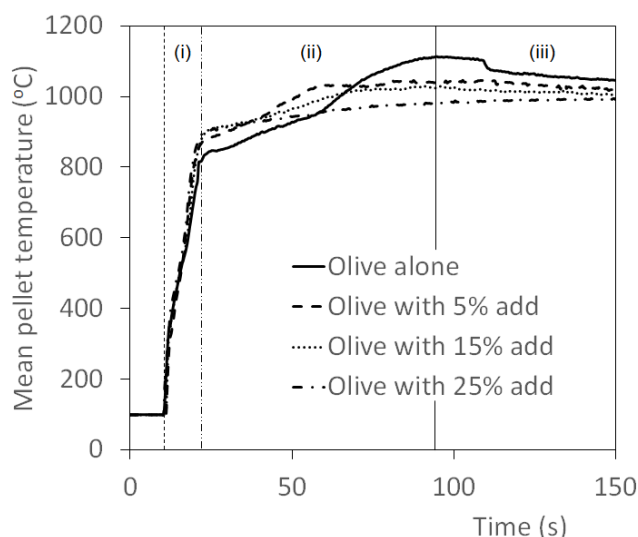


Figure 4.7 Mean surface temperature of olive pellets derived from thermal imaging analysis

4.3.3 Potassium held in the solid phase

The results of AAS analysis on the residual potassium retained in the ashes generated at different temperatures are shown in Figure 4.8 (a) to (c) for the wood, wheat straw and olive cake, respectively. In general, the amount of potassium (given as wt% K_2O) retained in the raw biomass ashes formed between 550-1150°C remains quite constant, although there appears to be some difference at the highest temperature studied. These amounts are $\sim 10 \pm 1\%$ for wood, $\sim 12 \pm 0.1\%$ for the straw and $36 \pm 2.5\%$ for olive. The slight variation in potassium percentages measured for the 550°C ashes across the biomass types is possibly due to the small amounts (<10%) of organically associated potassium lost at low temperatures (<500°C) (Yu and Zhang, 2001; Jensen and Frandsen, 2000; Olsson et al., 1997; Olsson et al., 1998) combined with the slight inhomogeneity in potassium concentrations throughout the fuels. If we assume there is no interaction between the ashes at 550°C then, for all fuels, an indication of the errors in the method of analysis is approximately $\pm 2\%$ of potassium oxide content.

At any given temperature, when additive is present, the fraction of potassium retained in the ash is always higher than in the raw biomass cases. However, trends are quite complex and it does not always follow that higher additive equates to higher fixation of potassium in the ash. For example, the optimum concentration of additive for fixing potassium in white wood pellet ash (and possibly wheat straw) appears to be 5 wt%, while 15 or 25% is better for the olive pellet. This can be

related to the K:(Si+Al) ratios of the raw biomass fuels and the formation of potassium aluminosilicates ($K_2O-SiO_2-Al_2O_3$) which help fix potassium in the ash (Wang et al., 2012). For example, wood pellets have an atomic K:(Si+Al) in the order of 1:1 whereas olive cake has a notably high potassium content (K:(Si+Al) = 3:1) and wheat straw has a low potassium content relative to combined aluminum and silica (K:(Si+Al) =1:3). Thus, it is sensible that higher levels of additive are needed to fix potassium in olive ash. For the wheat straw and olive cake ashes, the fraction of K fixed in the ash is seen to peak at 1000°C, suggesting significant release of K above this temperature which may impact the additive's effectiveness at temperatures within a PF boiler (<1600°C).

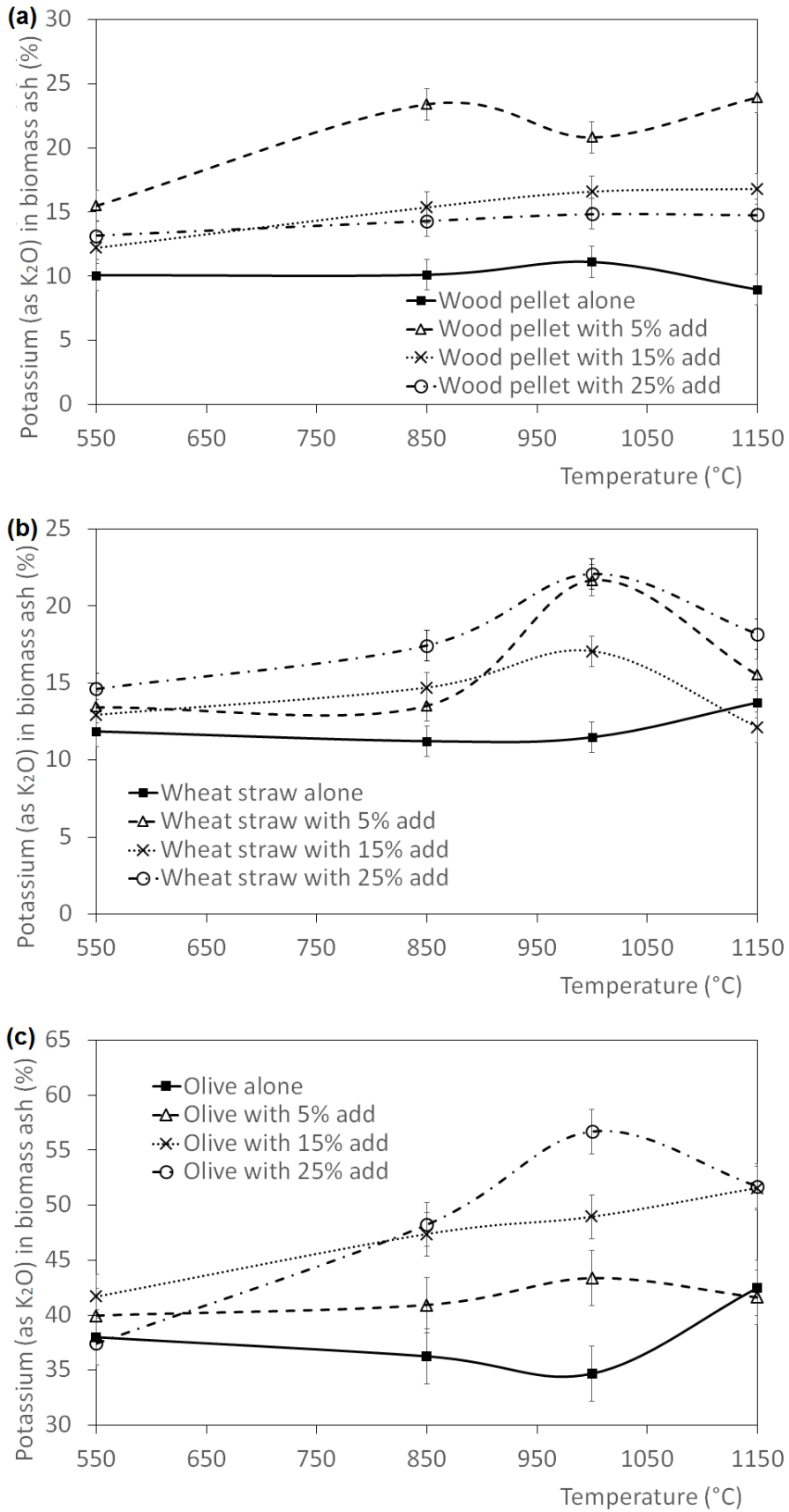


Figure 4.8 Residual potassium oxide (K₂O) in biomass ash with additive at increasing temperatures for (a) wood (b) wheat straw and (c) olive cake.

4.4 Analysis and Discussion

The addition of the coal ash additive to the raw biomass shows a clear reduction in the potassium released from all the biomass pellets. This section starts with an analysis of the quantities of potassium released during the different stages of combustion from the single particle combustion rig, and finishes with comparisons of the K measured in biomass ashes at higher temperatures compared to initial contents of K in the raw fuel.

The difference in the emission profiles can be interpreted in terms of the K:Cl ratios and the K:(Si+Al) ratios: high chlorine and/or low (Si+Al) facilitates the release of KCl or KOH to the gas phase, while high (Si+Al) helps to fix K in the solid phase. Further to this, it is important to note the additive ash to biomass ash ratios to enable a comparison of the K:(Si+Al) ratios between the biomass types. A 5 wt% mix of additive and raw biomass has an ash ratio of 1:1, 1:0.16 and 1:1.6 for wheat straw, wood pellets and olive cake, respectively, for ashes produced at 550°C. Also considered in this section is a comparison of the K release for each fuel relative to the amount of K starting in the raw fuel to assess trends.

4.4.1 Release of K during the stages of combustion from single particles

Figure 4.9 (a)-(c) provides a semi-quantitative comparison of the release of K during volatile combustion, char combustion and “ash cooking” for each of the three biomass studied. These relative release totals are obtained by integrating the area under the rate release profiles in each of the three stages and for each of the biomass fuels. Figure 4.9 (a) shows that the K-release during volatile combustion is less sensitive to the addition of the additive. K-release in this region may be more related to physical effects, mainly the entrainment of rapidly evolving volatiles. The impact of the additive is more apparent in Figure 4.9 (b) and (c) which illustrate the reduction in K-release rates with increasing additive present during the char combustion and “ash cooking” stages. Wood pellets were found to show a dramatic reduction in potassium release during the char combustion phase (Figure 4.9 (b)), whereas this reduction is more prominent in the “ash cooking” phase of combustion for wheat straw (Figure 4.9 (c)). This could be an important effect for the combustion of biomass in a boiler since ash deposits on furnace surfaces will be more stable with the use of an additive and may prevent the release or evaporation of vapour phase potassium at high temperatures.

The potassium release profiles demonstrate potassium is released over the volatile and char combustion stages as reported previously (Mason, Darvell, et al., 2016). Where the chlorine content is relatively high (relative to potassium content) the potassium is largely released in the form of KCl due to its high volatility at temperatures between 700°C and 800°C (Knudsen et al., 2004; Olsson et al., 1997; Jensen and Frandsen, 2000). For low chlorine fuels, KOH becomes the main species evaporated during combustion. However, potassium release is also seen as the ash is “cooked” by the high temperature gases from the methane-air flame. The type of fuel, and therefore, ash composition, does have an impact on the level of potassium release over these three stages. The high chlorine content of wheat straw and olive (see Table 4.1) promotes K release during combustion, but there is no obvious relationship between the observed level of emission and Cl content. However, the increased release of potassium during the “ash cooking” of the raw wheat straw compared to the raw olive and wood pellets may be explained by the high Si and low Al content of this fuel. For example, K-oxides are known to associate with Si species (e.g. K_2OSiO_2) and begin to melt at temperatures of approximately 1000°C (Jensen and Frandsen, 2000; Knudsen et al., 2004; Wang et al., 2012), which could then lead to K-release in the “ash cooking” stage. In contrast, the slightly higher Al contents of olive and wood pellets may result in the formation of potassium feldspars with higher melting points (Öhman and Nordin, 2000). This could explain the mitigating effects of the additive to wheat straw in the “ash cooking” phase as the additional Al provided by the additive would lead to the formation of K feldspars rather than K-silicates.

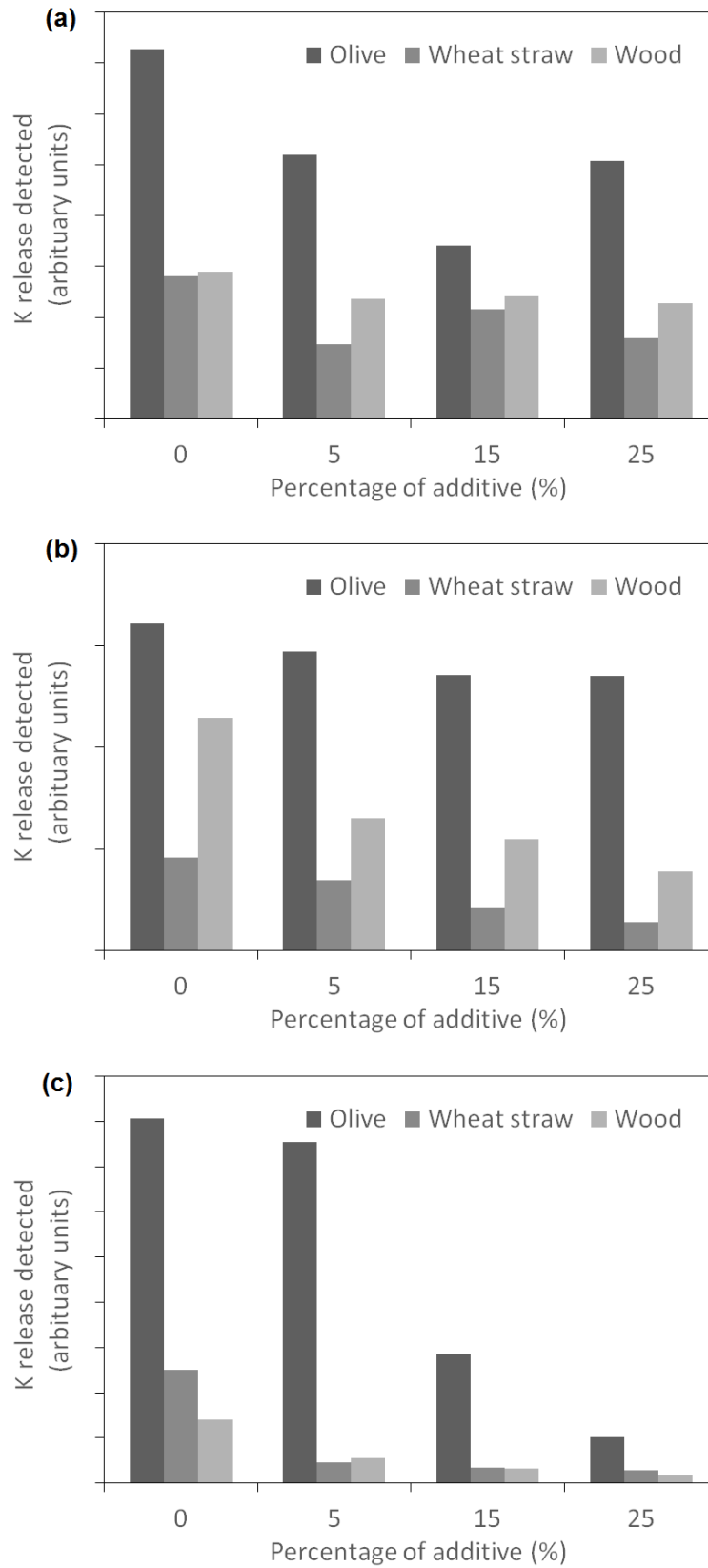


Figure 4.9 Quantities of K released during (a) volatile combustion (b) char combustion (plotted on a logarithmic scale) and (c) the 'ash-cooking' stages.

4.4.1.1 Normalised K release signal per molar quantity of K

Figure 4.10 illustrates the normalised release signal intensity per molar quantity of potassium in the biomass pellets. This analysis of the results reveals a similar maximum in intensity/per mol K for wheat straw and olive (Figure 4.10 (b) and (c)). However, perhaps surprisingly, Figure 4.10 (a) shows a much higher maximum intensity/mol K for the wood pellets, nearly ten times larger than the other biomass. This indicates that although the wood contains the smallest quantities of potassium in the raw biomass, it is highly mobile under the high heating rates of this experiment. The wood pellets contain the lowest chlorine content of the three fuels studied, and so it can be assumed that the majority of K released during combustion is from the evaporation of KOH. In contrast, both wheat straw and olive residue have an excess of chlorine compared to potassium, so it can be assumed that much of the K released in combustion is from the evaporation of KCl. Crystalline KOH melts at a much lower temperature than KCl (405°C compared to 769°C), meaning KOH is more mobile under combustion conditions. While the boiling points are more similar (1326°C compared to 1406°C for KOH and KCl respectively) there is, approximately, a threefold difference in vapour pressure at the particle temperature (based on data from Rodrigues and Silva Fernandes, 2007; Gurvich et al., 1997) and thus the evaporation rate of KOH will be greater than that of KCl. Since evaporation will be competing with reactions that help fix K in the ash (e.g. formation of potassium silicates), this may begin to explain the high mobility of K into the vapour phase in the case of the wood pellets. With the addition of the additive it is clear that the ash-fixing reactions with potassium begin to dominate, and far less evaporation of potassium occurs during combustion.

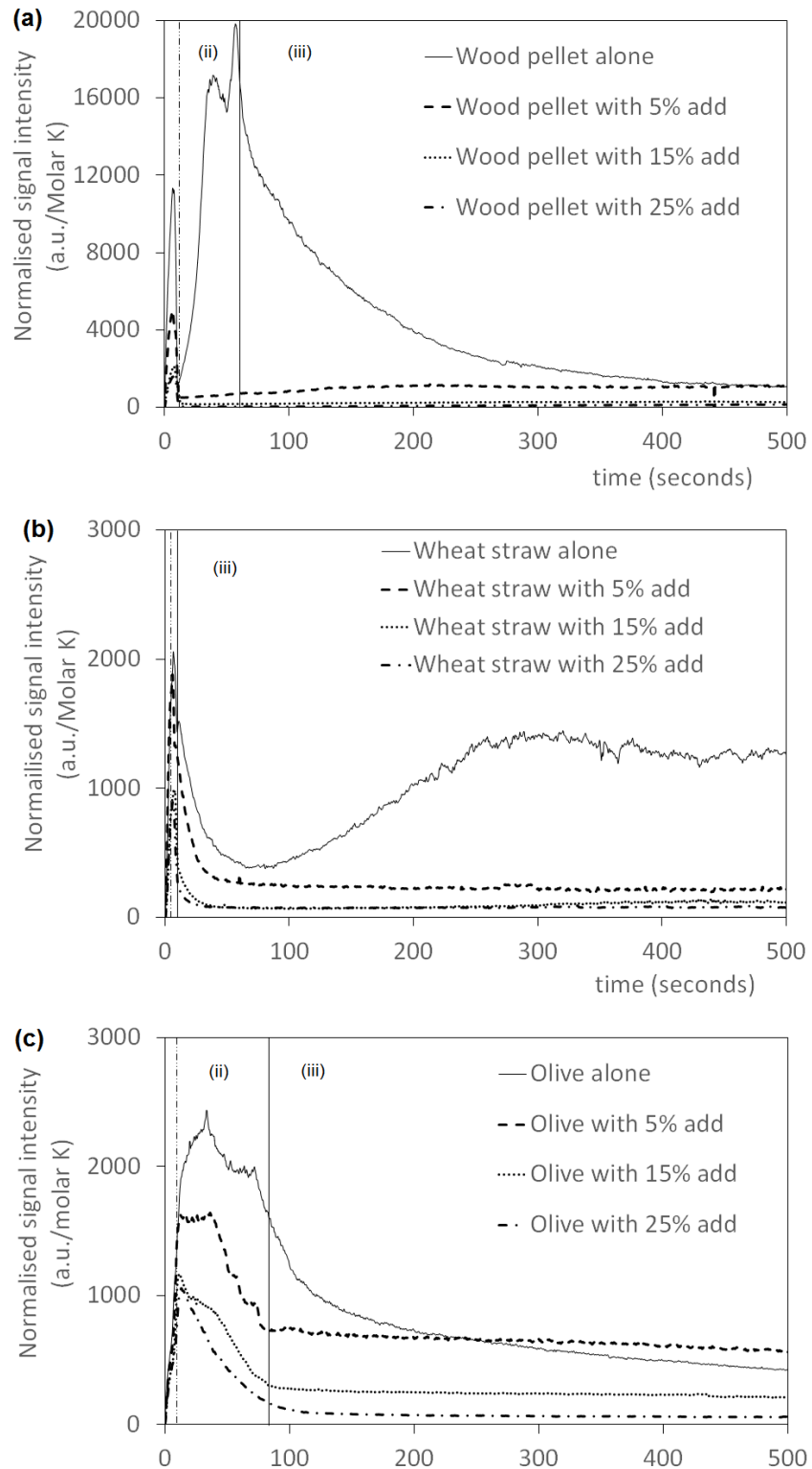


Figure 4.10 Potassium release per molar K in the biomass pellets with 0/5/15/25 wt% additive for (a) 31 ± 6 mg of wood (b) 35 ± 7 mg of wheat straw and (c) 35 ± 7 mg of olive cake. Profiles are averages of a minimum of three tests runs. Labels refer to (ii) Char combustion; (iii) ‘Ash cooking’.

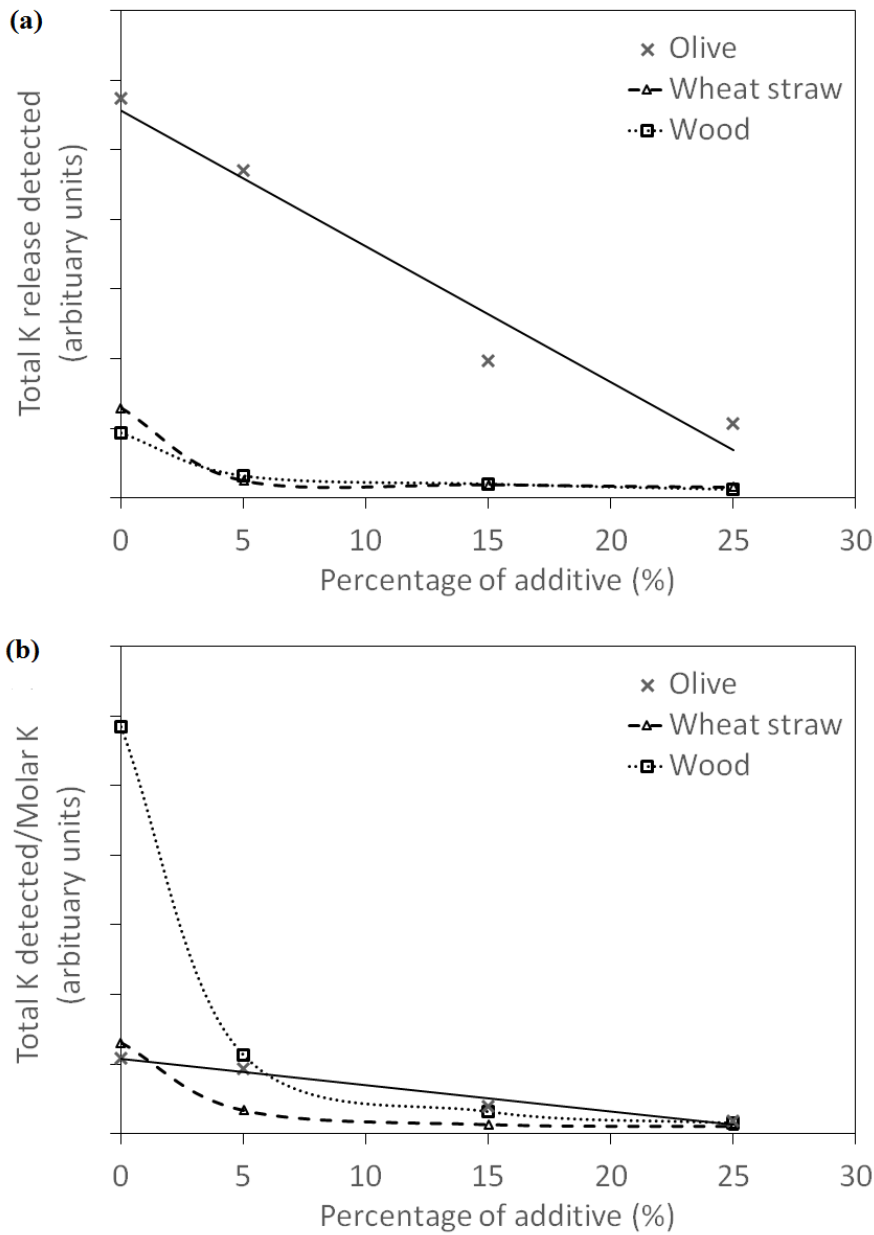


Figure 4.11 Relationship between the percentage of additive and (a) the total K release (b) total K release per mole of K.

This work has identified how the aluminosilicate additive affects the potassium release profiles of three different biomass types. As shown in Figure 4.11 (a), using increasing proportions of additive in biomass combustion results in an overall decrease in the quantities of potassium released to the gas phase across the three fuels tested in this study. The additive shows a linear reduction in the fraction of potassium released for the highest potassium content fuel, olive cake, whereas the fuels with lower potassium content are found to show little change from larger

proportions of additive. This indicates that there is a threshold quantity of potassium that may be captured by a quantity of additive. Figure 4.11 (b) shows how the normalised release signal (per molar quantities of K) is affected by the additive for each of the biomass. The results for olive show a rather linear effect of the additive on this normalised signal whereas wheat straw and wood pellets show large reductions from raw biomass signals, likely due to the smaller quantities of potassium in those fuels.

4.4.2 Ashing experiments

The data in Figure 4.5 and Figure 4.8 were used to calculate the relative quantities of potassium in the biomass ash compared to the initial content, and this is presented in Figure 4.12 (a-c). This figure helps identify trends in the fractions of potassium retained in the ash. Initial potassium contents for Figure 4.12 were taken from the biomass with 25 wt% additive at 550°C for the truest representation of initial K content, since little potassium is expected to be released at temperatures <550°C. For the raw fuels, there is evidence of potassium evolving when the ash is “cooked” at temperatures >550°C and large decreases in K-contents are seen for all fuels at the highest temperature studied (1150°C). Note that this temperature is comparable to the top temperature experienced by the fuels in the flame studies, although residence times are much longer in the ashing experiments. From these ashing experiments the amount of potassium released can be quantified: Wood ash, evolves up to 80% of K at elevated temperature, wheat straw 50% and olive 40%. Note also that the absolute K content is very different between these three biomass, as listed in Table 4.2.

It can be seen from Figure 4.12 that very little potassium is released from wheat straw without additive between 850°C and 1150°C. This suggests, contrary to the wheat straw flame studies, that little potassium is released during the “ash cooking” phase of combustion. This may be explained by the low heating rate combustion of these experiments which results in a release of K during lower temperature “ash cooking”, or the differences in the experimental configurations used by the two studies (i.e. there is a kinetic effect being observed in the flame studies): In the flame studies, evaporation of melted ash components such as potassium silicates will be accelerated through the dynamic flow of hot gas around the heated particle. However, Figure 4.12 also demonstrates the fixation of K in ash by the additive and

a change in the ease of evaporation of K at elevated temperatures. For the wood ash, 70-100% of K is retained in the ash in the presence of additive; for the wheat straw, this figure is 60-80% and for the olive pellets it is 70-100%.

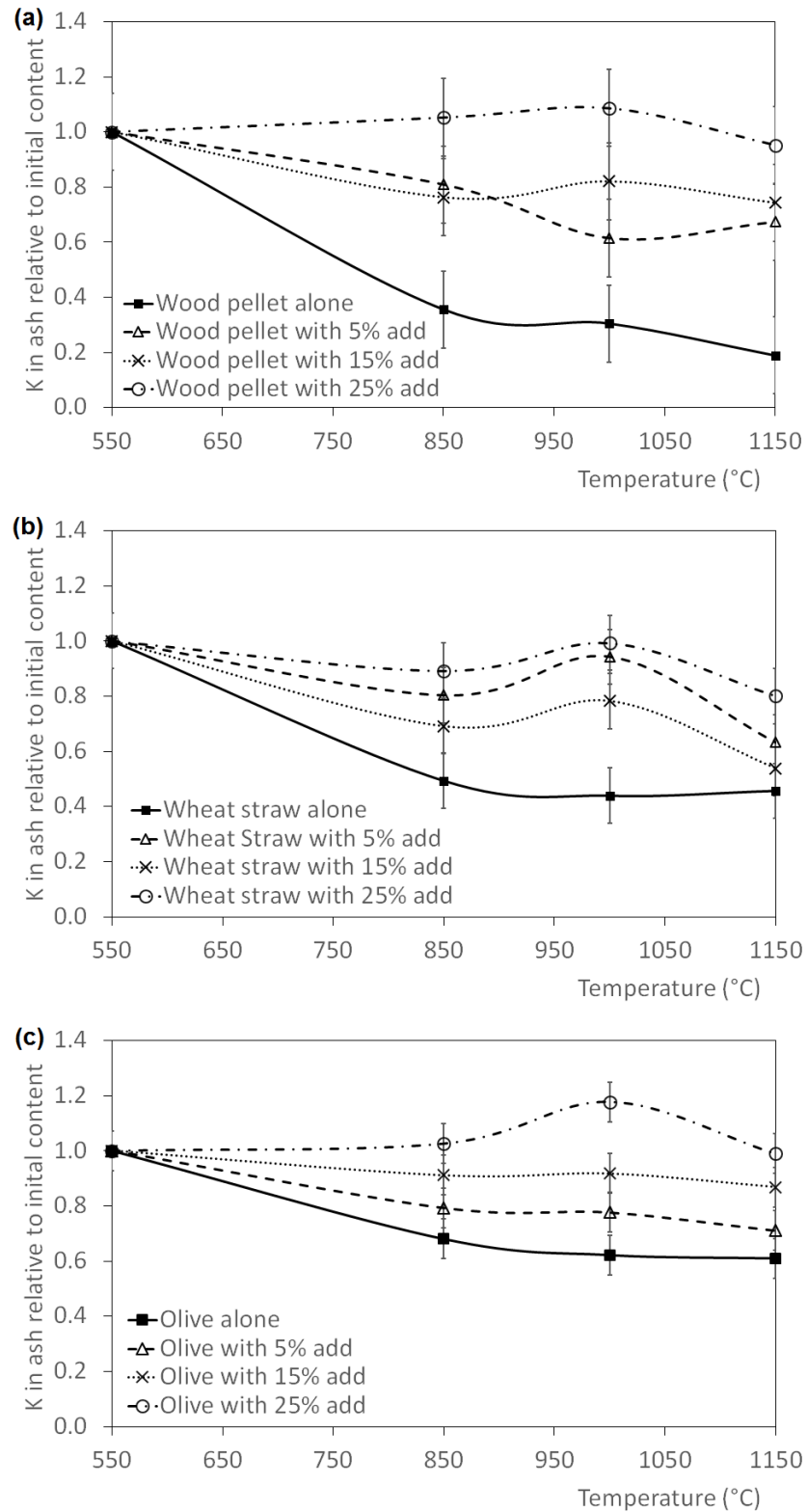


Figure 4.12 Potassium in biomass ash relative to initial content for (a) wood (b) wheat straw and (c) olive cake.

4.5 Conclusions

The use of biomass as a solid fuel for power generation can result in slagging and fouling problems associated with the high potassium content of some biomass types. This can result in undesirable increases in operating costs and time off-line for power stations. Understanding the effects of additives on the fate of potassium during the combustion process is, therefore, of high importance for power plant operators but also will have implications for the operation of carbon capture facilities (discussed in Chapter 6).

Two experimental methods were used in this laboratory scale study to analyse the fate of potassium from the combustion of biomass. Firstly, a flame emission spectroscopy technique was used to evaluate the differences in the gas-phase potassium release profiles during the combustion of 5 mm diameter pellets of different biomass suspended in a methane-air flame. Secondly, the same biomass fuels were combusted in a furnace at low heating rates to analyse the quantities of potassium remaining in the biomass ashes after combustion at different temperatures, with various quantities of a coal ash additive.

During combustion, potassium is released over three stages: volatile combustion (a sharp peak in the emission profile), char combustion (a broader peak) and “ash cooking” (a very broad peak over an extended period after the end of combustion). The relative importance of each of these stages depends on the biomass type and the other inorganics present in the fuel.

For the softwood currently being used in large-scale biomass combustion applications, a high potassium release rate was seen when compared to the other biomass. This shows that the potassium in the wood is in a more mobile state. This could be due to a higher proportion of KOH in a low chlorine fuel. Differing diffusion rates within the particle structure will also affect mobility (Mason et al., 2017). The addition of the aluminosilicate additive results in a clear reduction in the potassium released from all the biomass pellets, particularly during the char-oxidation and “ash cooking” stages, and the level of additive required is related to the amount of K in the biomass.

For wheat straw, there is a rapid release of K (probably as KCl) as the particle heats and burns, and then a slow release of K from the ash. This slow release has

important implications for boiler slagging if ash deposits are kept at high temperatures since the ash composition (and hence sintering properties) will change with time. Also revealed was the effectiveness of an aluminosilicate additive in biomass combustion for mitigating the release of potassium throughout the different stages of combustion, including the “ash cooking” phase in the case of wheat straw. The effects of different quantities (5, 15 and 25 wt%) of additive on the potassium release profiles show that optimisation is necessary for the reduction of K release from each biomass; wood and wheat straw require lower amounts of additive than olive residue, presumably because the potassium content of the olive cake was so much higher.

When the results are normalised for the amount of potassium in the fuel, it is clear that a large fraction of potassium enters the gas phase during the volatile and char combustion of the softwood. Olive residue releases a lower fraction of potassium during the volatile and char combustion stages, indicating that more potassium is fixed in the ash. In contrast, wheat straw shows a release of potassium during combustion, and then, after a period of “ash cooking”, a substantial gradual release with continued exposure to hot combustion gases.

Ashes generated at temperatures ranging from 550-1150°C were analysed by atomic absorption spectroscopy to identify the quantities of potassium lost at temperatures in this range and to quantify the effects of the coal ash additive. These were found to support the case for increased potassium being retained within the biomass ash if aluminosilicate additives are used. Again, wood pellets were seen to release a high proportion of K. In the absence of additive, the loss of K at the elevated temperature is 80% for wood pellets, 50% for wheat straw and 40% for olive. In the presence of additive, 70-100% of K is retained in the wood ash, 60-80% in the wheat straw ash, and 70-100% in the olive cake ash.

The two experimental techniques revealed differing results in terms of optimal quantities of additive related to the difference in time-temperature histories. However this work demonstrates that the use of an aluminosilicate additive reduces the proportion of K released into the gas-phase by retaining it in a solid-phase mineral ash. This can help to mitigate fouling in PF boilers by reducing the potential for deposits being stimulated by condensing potassium.

Chapter 5

Experimental work on the impact of biomass ash and K salts on the capture performance and degradation of MEA

5.1 Introduction

It is clear from the literature in chapter 3 that fly ash from coal combustion can escape particle removal technologies and deposit in carbon capture processes. This is observed to have large impacts on the reclamation rate required for an amine carbon capture solvent, thus having relatable impacts on the operating expenditure for a carbon capture plant. This chapter aims to investigate the impact of biomass combustion ashes on the degradation of MEA and solubility of CO₂ in MEA solutions.

The chapter starts with an initial description of the key chemical species associated with the absorption of CO₂ into an MEA solution and the associated NMR peaks observed. This is complemented with an examination of the impacts of potassium species on the CO₂ absorption rate and capacity of 30% MEA using vapour-liquid equilibrium (VLE) apparatus. As potassium is particularly abundant in biomass and is volatile under combustion conditions it is expected that significant quantities of potassium will deposit in carbon capture solvents, thus an examination of effects of potassium species on amine performance is important.

While the VLE apparatus can be used to assess the impacts of potassium on capture performance, the large solvent sample size required for VLE experiments made its use for the analysis of degraded samples undesirable. Only small quantities of thermally degraded MEA solvent are possible to replicate in laboratory conditions making it preferable to analyse samples by nuclear magnetic resonance (NMR), gas chromatography mass spectrometry (GC-MS) and ion chromatography (IC).

The assignment of ¹H NMR peaks and quantification of the degradation products is then provided. The thermal degradation products are presented in order of their formation; 2-oxazolidione (OZD), N-(2-hydroxyethyl)ethylenediamine (HEEDA) and 1-(2-hydroxyethyl)-2-imidazolidone (HEIA) as described in chapter 3. Oxidative degradation products are divided into subgroups for clarity; primary

products, secondary products and heat stable salts. Primary degradation products are the products such as ammonia, aldehydes and carboxylic acids that are initially formed from the degradation of the amine. Mechanisms remain unclear but it has been suggested that electron abstraction from the lone pair on the nitrogen or hydrogen abstraction from the nitrogen, α -carbon or β -carbon is the current general understanding (Goff and Rochelle, 2006; Sexton and Rochelle, 2006).

Secondary degradation compounds are formed from the reaction of oxygen/MEA/aldehydes/ammonia with primary degradation products to form stable degradation products such as N-(2-hydroxyethyl)formamide (HEF), N-(2-hydroxyethyl)acetamide (HEA) and N-(2-hydroxyethyl)imidazole (HEI). The mechanisms by which these secondary products are formed are also not well understood, with various mechanisms suggested in literature (Strazisar et al., 2003; Lepaumier et al., 2011; Da Silva et al., 2012). These are the main degradation products visible through ^1H NMR analysis, for which NMR data is presented in this chapter.

Quantitative NMR analysis of oxidative MEA degradation in the presence of potassium and various ashes from combustion (olive, white wood and two types of coal ash) enables comparison between the rates of degradation across the different cases.

5.2 Experimental methodology and results

5.2.1 CO₂ absorption analysis with ^1H NMR spectroscopy

There is currently very limited literature which uses NMR spectroscopy for the examination of amine degradation. However there is a large amount of literature using NMR spectroscopy for the analysis of MEA speciation. In 2014 Perinu et al. provided a review of NMR spectroscopy applied to amine capture systems, highlighting the dependability of ^1H and ^{13}C NMR as a fast and reliable method for the quantitative analyse of many common species associated with the absorption of CO₂ by MEA solutions. This includes the identification and quantification of MEA, carbamate, protonated MEA and oxidative degradation products. ^1H NMR analysis of changes to the chemical shifts of MEA allows for the tracking of CO₂ loadings for MEA samples (Wheatley, 2017), which was used in the degradation experiments described in this chapter.

Initial experiments on the absorption of CO₂ by MEA solvents were complete by sparging CO₂ through a 250ml quantity of 30% w/w MEA in a 500ml round bottom flask. The samples were sparged with CO₂ at 0.3L/min for 90 minutes, with 0.5 ml aliquots taken to track the carboxylation. 75 μL of D₂O was added to these 0.5 ml aliquots in an NMR tube to provide a lock frequency for the NMR spectrometer. 13 mg of 4,4-dimethyl-4-silapentane-1-sulfonic acid (DSS) was premixed in 10 ml of D₂O for the addition of approximately 0.1 mg per NMR tube which enabled quantification via integration.

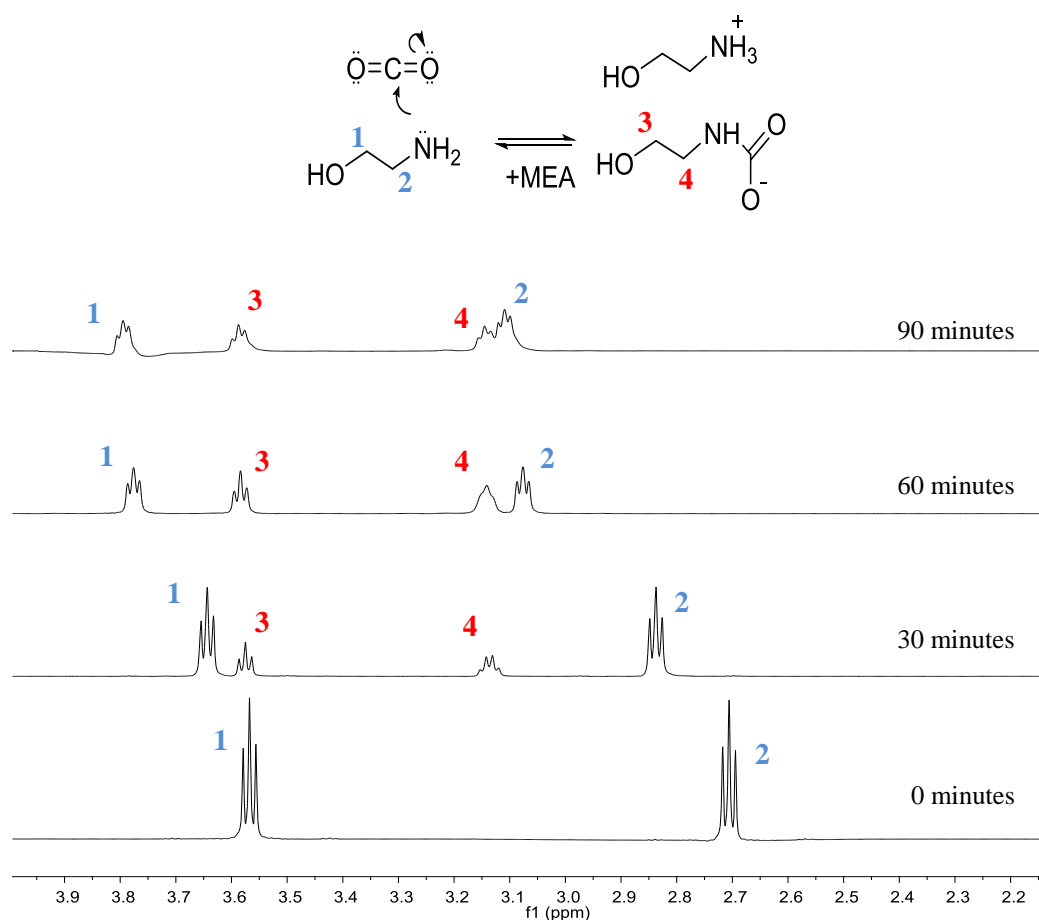
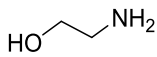
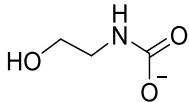


Figure 5.1 ¹H NMR stacked spectra for the carboxylation of 30% w/w MEA (with species assignment)

The stacked NMR plot with increasing amounts of carboxylated MEA (Figure 5.1) illustrates how the chemical shifts of MEA in water arise at 3.57 ppm and 2.71 ppm. With increasing quantities of CO₂ added to the 30% w/w MEA sample, the MEA peaks are seen to move further downfield and the carbamate peaks are seen to increase as a triplet at 3.57 ppm and a doublet of triplets at 3.15 ppm. MEA peaks move further downfield as MEA reacts with CO₂ to form the carbamate and a

protonated base, however the rate of proton exchange between the free base and the protonated base is considerably faster than the time taken for ^1H NMR measurements, hence the peaks seen are a combination of the two forms (Wheatley, 2017). (As more CO_2 is absorbed by the solvent, more and more protonated MEA is formed, thus explaining the movement of the peaks seen for MEA.) The NMR data associated with the identification and quantification of MEA, carbamate and bicarbonate are provided in Table 5.1.

Table 5.1 Typical NMR chemical shifts for the carboxylation of MEA

Compound	^1H NMR Data (D_2O)	^{13}C NMR Data
	3.57 (t, 2H, $^3J_{\text{HH}} = 5.5$ Hz, O- CH_2)	57.7 (HO- CH_2)
	2.71 (t, 2H, $^3J_{\text{HH}} = 5.5$ Hz, N- CH_2)	41.2 (N- CH_2)
	-	164.3 (C=O)
	3.58 (t, 2H, $^3J_{\text{HH}} = 5.5$ Hz, O- CH_2)	61.1 (HO- CH_2)
	3.15 (dt, 2H, $^3J_{\text{HH}} = 5.5, 5.0$ Hz, N- CH_2)	43.1 (N- CH_2)
	n/a	160.6

5.2.2 CO_2 absorption analysis with vapour-liquid equilibrium apparatus

Measures of the absorption capacity and rate of 30% w/w MEA were made using the vapour-liquid equilibrium (VLE) vessel, illustrated in Figure 5.2 and pictured in chapter 8. The equipment enables the measurement of molar quantities of CO_2 absorbed by a defined volume of solvent through the ideal gas equation as in literature with similar VLE apparatus (Aronu et al., 2011; Dang and Rochelle, 2003; Ma'mun et al., 2006). A precise experimental methodology was generated for experiments using this equipment which included a step-by-step guide on the experimental set-up procedures in order to minimise any possible effects of changes in experimental conditions. Molar quantities of KCl were added to virgin MEA samples to assess the impacts of the most abundant form of potassium on the absorption capacity and rates of MEA. KOH was identified in chapter 4 as a volatile K species in the flue gas for a low chlorine fuel such as wood pellets. KOH is not stable at flue gas temperatures and is thus likely to react with CO_2 in the flue gas to

form K_2CO_3 and water (Blomberg, 2006). If K_2CO_3 manages to stay in the flue gas to encounter aqueous MEA solvents, the MEA would expectedly react with K_2CO_3 to form MEA carbamate and K_2O . K_2O is the form of potassium in ash and will thus be examined through the addition of ashes, while KCl has been found in numerous slag deposits and thus is examined separately. Experiments were carried out with a CO_2 partial pressure of 14%, similar to that of a solid fuel combustion plant.

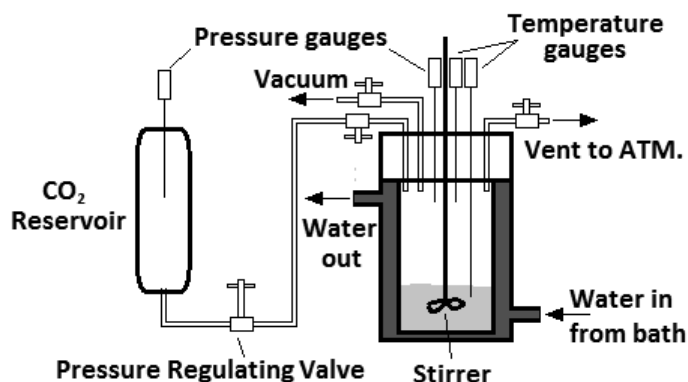


Figure 5.2 VLE equipment schematic

The vapour-liquid equilibrium (VLE) apparatus was designed and assembled by C-Capture Ltd. and consists of a jacketed reactor (Parr Instrument Company), with mechanical stirrer with incorporated gas supply (Parr Instrument Company), water/oil heater unit (Grant Instruments) and a CO_2 storage reservoir. Measuring probes on the equipment are used to measure the pressure and temperature change within the vessel as CO_2 is absorbed by the solvent. The CO_2 reservoir and pressure regulating valve are used to maintain a constant partial pressure of CO_2 within the reactor vessel throughout experiments. An electrical signal reading from the pressure gauge is fed back to the data acquisition software (Labview) during the experiments so that the amount of CO_2 removed from the burette can be measured. Data processing for these VLE experiments was complete using an Excel macro developed by Gergley Jakab, an employee at C-Capture Ltd.

KCl is the most abundant form of potassium present in flue gases from biomass combustion and thus it is important to study its effect on the performance of MEA absorption of CO_2 . The impacts of KCl on the capacity of 30% w/w MEA is presented in Table 5.2 (results presented are averages from three repeats), where the results from the VLE apparatus found KCl to slightly decrease the capacity of the MEA solvent. This result is found to be repeatable for experiments with virgin MEA

and stripped MEA carried out at both 40°C and room temperature. The findings suggest that very high proportions of potassium present in the biomass flue gas may have small impacts on MEA performance, though such large quantities are unlikely to be encountered. This analysis does not account for any effects on MEA degradation which may contribute to decreased capture performance of MEA over time.

Table 5.2 CO₂ absorption capacity experiments of virgin MEA with potassium salts on the VLE at 40°C

Solvent	Capacity (mol/L)	S.D. (+/-)	Rate (mmol/s)	S.D. (+/-)
Fresh MEA alone	2.24	0.03	1.34	0.01
0.5M KCl	2.23	0.01	1.28	0.03
1.0M KCl	2.21	0.01	1.31	0.01
1.5M KCl	2.20	0.01	1.32	0.01

5.2.3 Thermal degradation procedure and results

Thermal degradation experiments were carried out using stainless steel batch reactors stored under heated conditions, which is the most established method for examining the effects of thermal degradation within the laboratory (Davis and Rochelle, 2009; Lepaumier et al., 2011). To investigate the impact of biomass ash and potassium chloride on the thermal degradation of MEA in the presence of CO₂, a ~150 mL batch of 30 wt % MEA solution was sparged with CO₂ at a rate of 0.3 L/min for 120 minutes to obtain a loading of 0.5 mole of CO₂ per mole of amine, which was confirmed with NMR spectroscopy. 20 mL samples of the loaded solution was poured into a 2-inch diameter 304 stainless steel cylinders, which were then sealed and kept in a Memmert oven (model 600) for 6 weeks at 135 °C.

The compositional data for the white wood and coal ashes added to the MEA solvent being exposed to the thermal degradation experiments are provided in Table 5.3. In line with previous literature the effect of ash on thermal degradation was investigated by adding 3.4 g of ash per kilogram of MEA solution (Da Silva et al., 2012), equating to 68 mg of ash in the 20mL MEA samples used in these thermal degradation experiments. The ashes used were:

- A white wood ash prepared using laboratory ovens at 550 °C from chapter 4 (named ‘white wood ash’).
- A coal ash provided by a UK power station (named ‘coal ash #1’).

To examine the effect of KCl on thermal MEA degradation 30 mM KCl (99% purchased from Alfa Aesar) was added to the amine solvent, equating to 45 mg in the 20mL samples used in these experiments as an exaggeration of the highest quantities of KCl that are likely to deposit in a capture solvent.

Table 5.3 Ash composition data for ashes used in thermal degradations of MEA

Content	Basis	Units	White wood ash	Coal ash #1
Al₂O₃	in ash	%	2.5	20.8
Fe₂O₃	in ash	%	2.1	9.3
CaO	in ash	%	29.3	2.9
MgO	in ash	%	5.9	1.9
Na₂O	in ash	%	2.2	2.3
K₂O	in ash	%	10.0	1.7
SiO₂	in ash	%	16.6	58.2

5.2.3.1 Thermal MEA degradation product analysis

Following the identification of the key ¹H NMR peaks associated with the reaction of CO₂ with monoethanolamine, ¹H NMR spectroscopy was further used to track the degradation of aqueous MEA under temperatures similar to that of a stripper column. After the 6 week degradation at 135 °C, 0.5 ml of the degraded solvent was added to an NMR tube along with 75 μL of D₂O to provide a lock frequency for the NMR spectrometer analysis and approximately 0.1 mg of 4,4-dimethyl-4-silapentane-1-sulfonic acid (DSS) for quantification of the degradation products through integration.

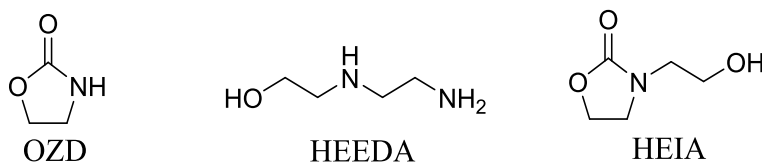


Figure 5.3 Thermal degradation products

OZD (497-25-6), HEEDA (111-41-1) and HEIA (3699-54-5) were all purchased from Sigma Aldrich and 100 mg of each were placed in 0.5 ml of D₂O in order to obtain a clean NMR spectra for each product.

The NMR spectra for the main products from the thermal degradation of MEA (aged at 135 °C for 6 weeks) are presented in Figure 5.4, which illustrates that the chemical shifts of the associated product are primarily observed in the 2.5 – 4.6ppm region of the NMR spectra. The presence of HEIA, the most abundant thermal degradation product, is clearly observed in the sample from after the 6 week degradation, while OZD and HEEDA are smaller so require closer analysis.

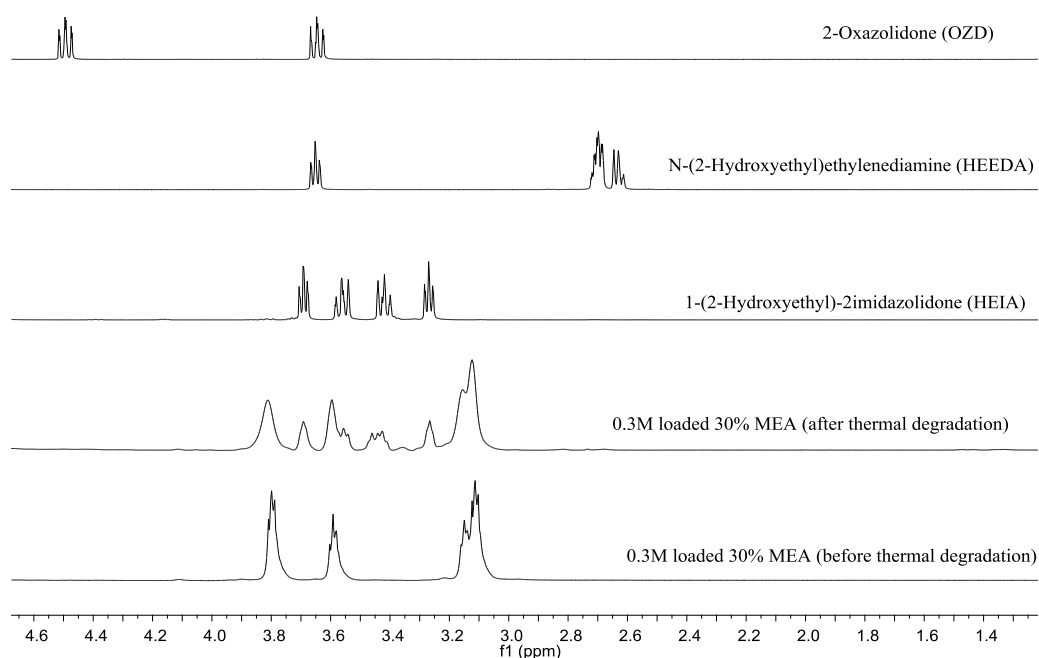
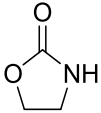
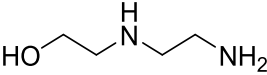
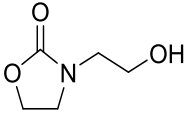


Figure 5.4 ¹H NMR spectra of the pure thermal degradation products in D₂O

The main thermal degradation compounds reported in previous work were also detected in this study. The NMR data for the associated identification and quantification of 2-oxazolidinone (OZD), N-(2-hydroxyethyl)ethylenediamine (HEEDA), and N-(2-hydroxyethyl)-2-imidazolidinone (HEIA) are provided in Table 5.4.

Table 5.4 Typical NMR chemical shifts for thermal degradation products of MEA in D₂O

Compound	¹ H NMR Data (D ₂ O)	¹³ C NMR Data (D ₂ O)
 2-Oxazolidinone	-	162.7 (C=O)
	4.49 (t, 1H, ³ J _{HH} = 8.5 Hz, O-CH ₂)	66.1 (O-CH ₂)
	3.65 (t, 1H, ³ J _{HH} = 8.5 Hz, N-CH ₂)	40.5 (N-CH ₂)
 N-(2-Hydroxyethyl) ethylenediamine	3.65 (t, 2H, ³ J _{HH} = 5.5 Hz, HO-CH ₂)	60.4 (HO-CH ₂)
	2.70 (dt, 4H, ³ J _{HH} = 4.8, 5.5 Hz, HN-CH ₂)	50.6 (HN-CH ₂)
	2.63 (t, 2H, ³ J _{HH} = 4.8 Hz, HN ₂ -CH ₂)	49.9 (HN-CH ₂) 40.0 (H ₂ N-CH ₂)
 N-(2-Hydroxyethyl) imidazolidinone	-	164.9 (C=O)
	3.70 (t, 2H, ³ J _{HH} = 5.5 Hz, HO-CH ₂)	58.9 (HO-CH)
	3.56 (t, 2H, ³ J _{HH} = 8.0 Hz, O-CH ₂)	45.4 (O-CH ₂)
	3.43 (t, 2H, ³ J _{HH} = 8.0 Hz, N-CH ₂)	45.2 (N-CH ₂)
	3.27 (t, 2H, ³ J _{HH} = 5.5 Hz, N-CH ₂)	38.1 (N-CH ₂)

A complementary analysis of the thermal degradation products was completed using gas chromatography mass spectrometry (GC-MS). Analyses were complete using a Perkin Elmer Clarus 580 gas chromatograph equipped with an autosampler and Perkin Elmer Clarus 560 mass spectrometer detailed in chapter 8. 1 ml of the thermally degraded solvents was placed in the 2ml borosilicate glass vials before being covered with aluminium crimp seals and loaded in to the GC-MS autosampler. Calibration standards were made for each of the degradation products to enable peak identification and calibration curves of known thermal degradation products; OZD, HEEDA and HEIA. The times for the associated elution of HEEDA, OZD and HEIA were 12.3 minutes, 21.2 minutes and 34.4 minutes respectively, which were confirmed with doped sample runs. Chromatograms are provided in chapter 8 which enabled quantification of the product formation across the cases examined, with and without the addition of ashes and KCl.

Figure 5.5 shows the extent of degradation observed for the thermal degradation experiments of 30 wt% MEA (0.5M CO₂ loading) at 135°C after 6 weeks. No significant impact was seen from the addition of potassium chloride, white wood ash or coal ash to the formation of OZD, HEEDA and HEIA. The results show slightly higher levels of HEEDA and HEIA for all cases when compared to the base case of 30 wt% MEA alone however no significant differences are seen in order to suggest the degradation is accelerated by the ashes or KCl.

Quantification of GC-MS experiments were based of the calibration of the equipment with known percentages of each degradation product. Whereas NMR quantities were calculated by integrating the product chemical shifts compared to the known quantities of DSS in each NMR sample. From this is can be seen that approximately 14% of HEIA is present in the solvent which equates to nearly half of the original 30% MEA w/w. This finding is confirmed by the measures with GC-MS. Some slight differences are seen between the analysis techniques for OZD and HEIA – likely due to slight variations in the methodology associated with gas chromatography. Whilst the significant difference in quantities of HEEDA are detected between the two analysis techniques. NMR spectra are observed to consistently measure quantities of the degradation products across the cases, whereas GC-MS shows larger variations in measurement.

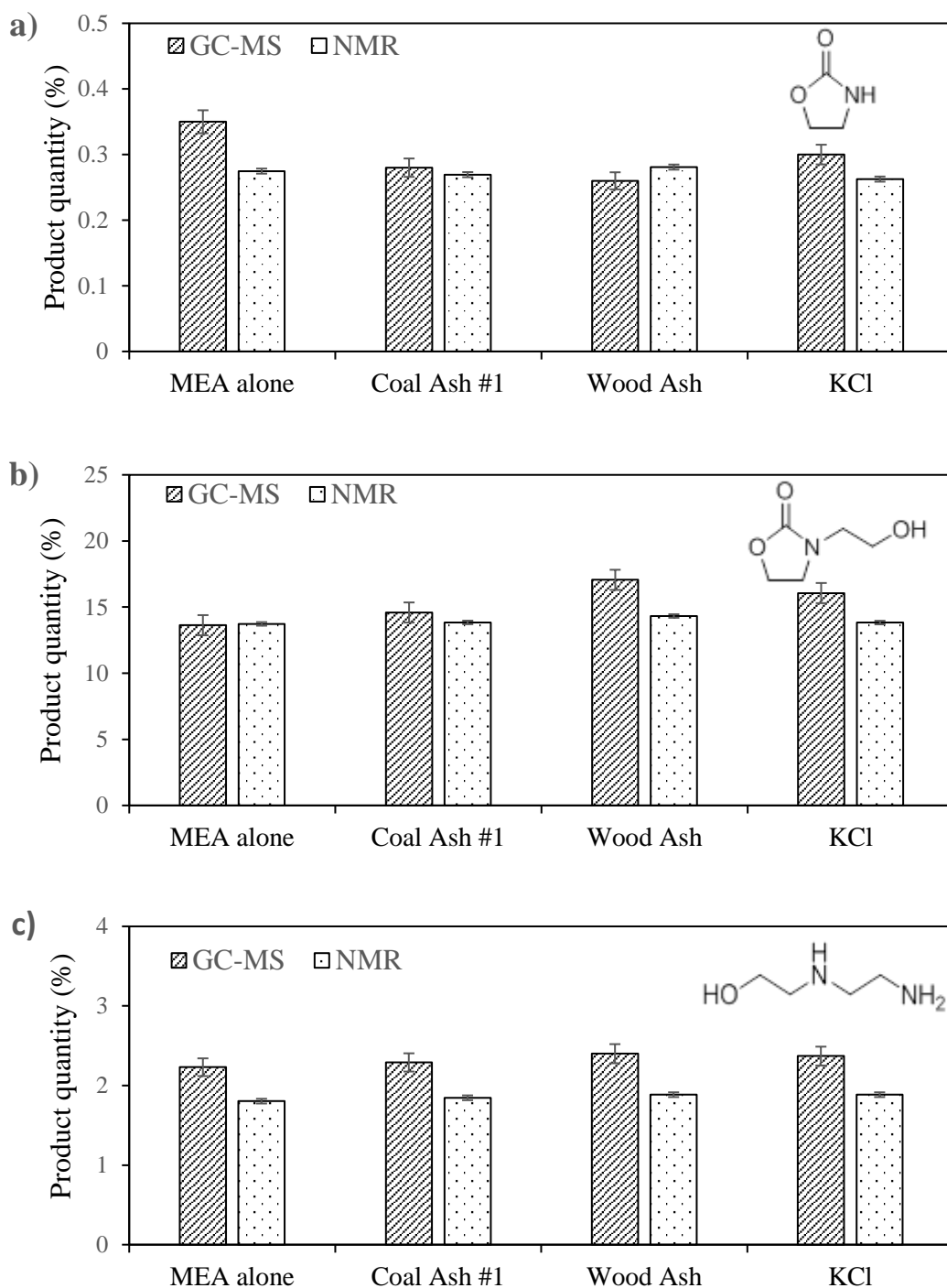


Figure 5.5 Product formation of a) OZD b) HEIA and c) HEEDA in the thermal degradation of MEA alone, MEA with coal ash #1, PACT wood ash and KCl.

5.2.3.2 Presence of leached metals in thermally degraded MEA solvents

The samples of 30% w/w MEA that were subjected to the thermal degradation conditions described previous were analysed by inductively coupled plasma - optical emission spectrometry (ICP-OES) to measure the quantities of elements that had leached into the MEA solution. This enables an analysis of the key elements that could affect the degradation. A Thermo Fisher iCAP 7400 Radial ICP-OES was used to measure concentrations of Al, Mg, Ca, Mn, Pb, Ni, Cu, Cr, K, Na, Fe and Si as the key constituents of biomass and coal ashes. The equipment was operated by Stephen Reid from the School of Earth and Environment at the University of Leeds.

Measures of the metals present in solution from the thermal degradation of MEA (aged at 135 °C for 6 weeks) in the presence of ash or KCl are presented in Table 5.5. Metals could have leached from the ashes added to the solvent or from corrosion of the stainless steel degradation vessels.

Table 5.5 Metals measured in the thermal degradation of MEA

	MEA alone	KCl	Coal ash #1	Wood ash
	(mg/L)	(mg/L)	(mg/L)	(mg/L)
Al	10.42	10.58	10.42	10.44
Mg	0.50	1.19	<LOQ	0.18
Ca	<LOQ	<LOQ	3.14	20.81
Mn	2.43	2.25	10.23	9.40
Pb	2.00	2.47	2.34	6.34
Ni	<LOQ	<LOQ	<LOQ	<LOQ
Cu	26.17	28.19	50.95	26.37
Cr	0.10	0.12	0.27	0.45
K	1.09	1038.70	9.72	292.48
Na	45.14	40.70	51.96	87.25
Fe	147.02	181.25	162.46	169.35
Si	6.81	4.76	19.45	28.13

The quantities of potassium found in solution correlate well with the quantities measured in ash composition data provided in earlier in this chapter. Very low amounts of potassium are seen for the MEA alone case and the addition of coal ash. Whereas significant quantities are seen for the addition of KCl and wood ash.

Iron is the element of second highest concentration, surprisingly the highest amounts are measured in the KCl case – perhaps due to corrosivity of chloride (Song et al., 2017) on the stainless steel reactor vessels. The reactor vessels were made of stainless steel 304 which is mostly comprised from 70% Fe, 20% Cr and 10% Ni with small contributions from Mn, Si, C, Ph, S and N. Higher amounts of Cr were also measured in the presence of KCl compared to the base case but higher quantities are seen when the ashes are added, likely due to these both containing Cr.

The addition of wood ash to the MEA solvent leads to the highest quantities of Na, Ca, and Cr whilst Cu is higher for the coal case, matching typical comparisons for ashes from each fuel (Finney et al., 2018). Mn is highest for both ash cases but slightly higher for the coal ash case which is the only value that doesn't match ash compositional data which would usually be higher for biomass.

5.2.4 Oxidative MEA degradation procedure and results

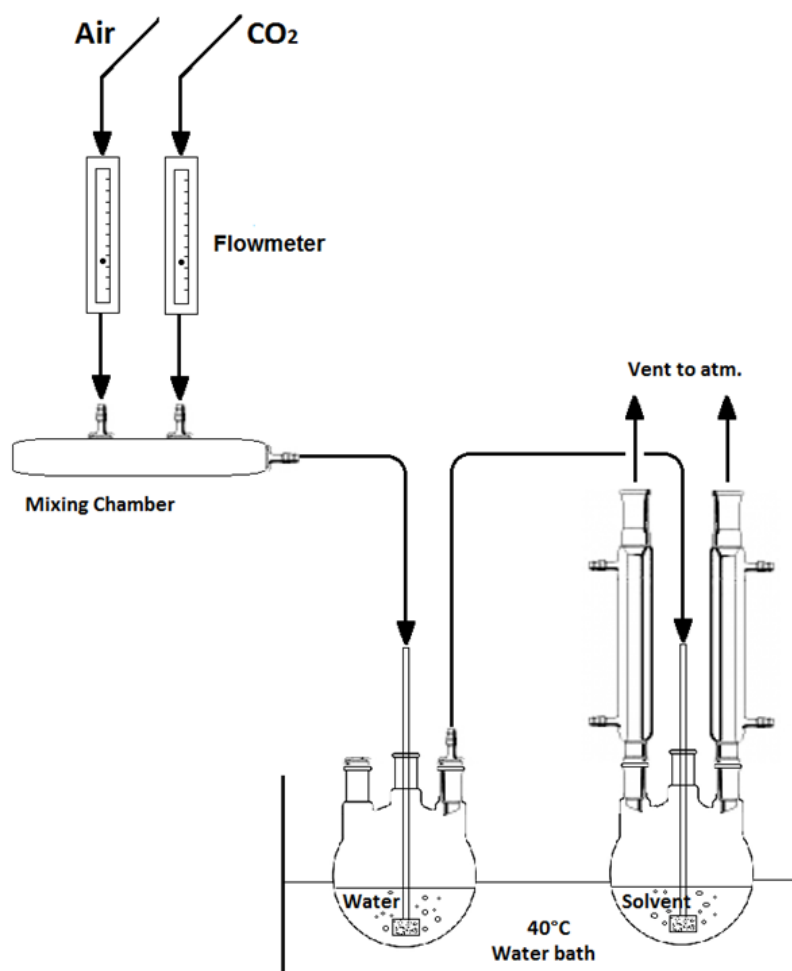


Figure 5.6 Open-batch oxidative degradation set-up

To investigate the impact of biomass ash and potassium salts on the oxidative degradation of MEA, an apparatus set-up similar to previous MEA oxidation experiments was used (Da Silva et al., 2012): A 250mL batch of 30 wt % MEA solution was located in a 500mL open batch round bottom flask held at 40°C as illustrated in Figure 5.6, with a thin layer of paraffin oil on top of the water bath to prevent evaporation. The solution was initially loaded fully ($\alpha = 0.5$ mole of CO₂ per mole of amine) by sparging 0.3 L/min of CO₂ through the solvent for 2 hours. This was followed by a sparging of compressed air at 0.15 L/min for 21 days, with periodic (every 3 days) CO₂ sparging (0.3 L/min for 30 minutes) to maintain high carbamate levels deemed essential to the oxidative degradation process (Da Silva et al., 2012). CO₂ loading of the amine being degraded was tracked using NMR spectroscopy which is provided in Appendix 1, generally 3 days of air sparging resulted in loading of 0.5 mole of CO₂ per mole of amine dropping to 0.3 mole of CO₂ per mole of amine. 5 ml aliquots were taken every 3 days in order to track the degradation.

The compressed air was first sparged through water to saturate the air and minimize any moisture losses in the solvent reactor which would affect the measured MEA concentrations in solution. Volumes of solvent were measured before and after experiments, however no significant water losses were seen throughout the degradation experiments. Oxidative degradation experiments in the laboratory used ashes collected from the candle filter from the same pilot scale trials that 30% MEA solvents were sampled in chapter 6.

The compositional data for the ashes added to the oxidative degradation experiments are provided in Table 5.6. In line with previous literature the effect of ash on oxidative degradation was investigated by adding 3.4 g of ash per kilogram of MEA solution, equating to 0.85 g of ash in the 500mL round bottom flasks used in these experiments. The ashes used were:

- A white wood ash collected from the candle filter at the UKCCSRC's PACT combustion and carbon capture facilities (named 'PACT wood ash').
- A coal ash collected from the candle filter at the UKCCSRC's PACT combustion and carbon capture facilities (named 'PACT coal ash').
- An olive residue ash - the same ash prepared using laboratory ovens at 550 °C from chapter 4 (named 'olive ash').

- A coal ash used as the additive for the experiments in chapter 4 (named ‘coal ash #1’), and used in the thermal degradation experiments.

To examine the effect of KCl on oxidative MEA degradation 23 mM KCl (99% purchased from Alfa Aesar) was added to the amine solvent, equating to 0.43 g in the 500mL round bottom flasks used in these experiments as an exaggeration of the highest quantities of KCl that are likely to deposit in a capture solvent.

Table 5.6 Ash composition data for ashes used in oxidative degradations of MEA

Content	Basis	Units	PACT wood ash	PACT coal ash	Olive ash	Coal ash #1
Al ₂ O ₃	in ash	%	4.1	19.9	1.2	20.8
Fe ₂ O ₃	in ash	%	4.7	14.3	0.9	9.3
CaO	in ash	%	18.3	19.3	10.3	2.9
MgO	in ash	%	3.8	3.4	3.0	1.9
Na ₂ O	in ash	%	3.9	4.2	0.6	2.3
K ₂ O	in ash	%	21.0	1.7	34.8	1.7
SiO ₂	in ash	%	7.6	5.7	11.2	58.2

5.2.4.1 Oxidative MEA degradation analysis with ¹H NMR spectroscopy

As described in chapter 3, the first stage of MEA degradation involves the fragmentation and oxidation of amines to carboxylic acids, such as formic, acetic and glycolic acid, or volatile species, such as formaldehyde, acetaldehyde or ammonia. It is hence important to measure the formation of such species. Formaldehyde, acetaldehyde and ammonia could not be directly measured due to their reactivity and low concentrations, while the chemical shifts associated with formic, acetic and glycolic acids are provided in this chapter.

¹H NMR spectroscopy was used to identify and quantify the products formed during the oxidative degradation of aqueous MEA. Gas chromatography mass spectrometry (GC-MS) was used to validate the findings of NMR spectroscopy with equipment specifications described in chapter 8. From the 5 ml aliquots that were taken every 3 days, 0.5 ml was added to an NMR tube along with 75 μL of D₂O to provide a lock

frequency for the NMR spectrometer analysis. 1 ml of the degraded solvents was used for GC-MS analysis with a 5:1 split.

Figure 5.7 illustrates how product peaks are seen to grow in the aromatic region (6.5-9ppm) of the NMR spectra over the experimental period. To quantify the results obtained, spectral peaks were integrated relative to the area of the standard peak of 4,4-dimethyl-4-silapentane-1-sulfonic acid (DSS) with a chemical shift $\delta = 0.00$ using MestReNova software.

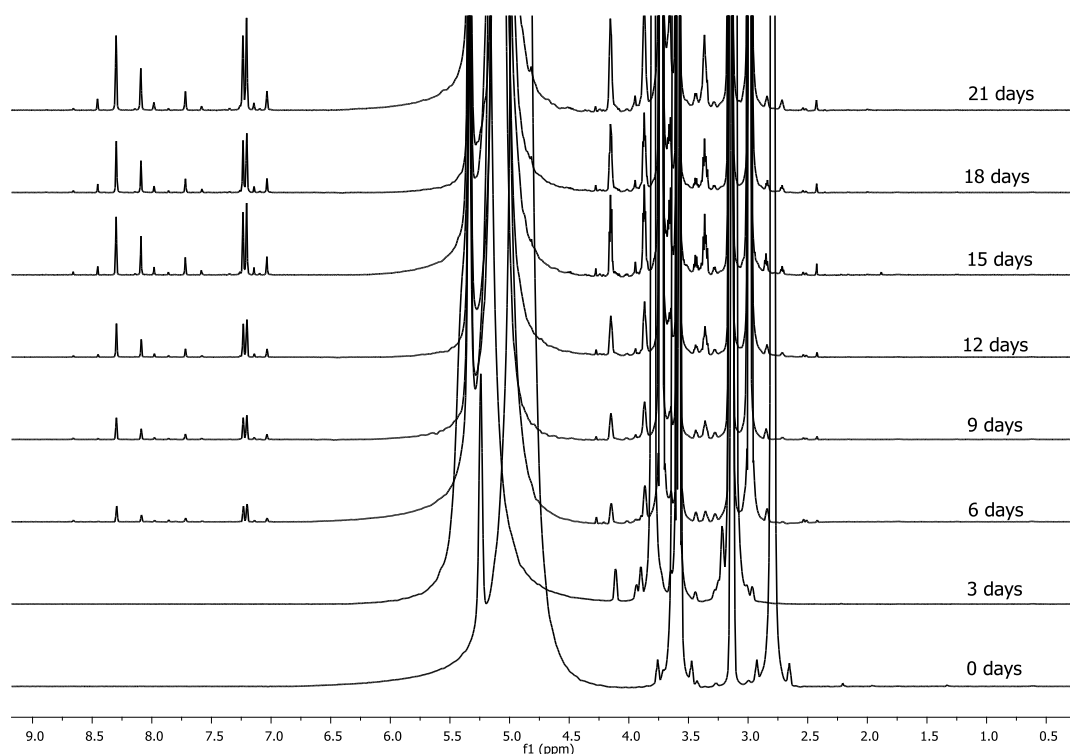


Figure 5.7 Example ¹H stacked spectra following the oxidative degradation of MEA over 21 days

It can be seen in Figure 5.7 that as the oxidative degradation experiment elapsed, the formation of new ¹H NMR peaks is seen to occur. The new NMR peaks were assigned to the associated degradation product by comparison with NMR spectra of the pure products in D₂O. Approximately 100mg of each purchased degradation product was weighed into 0.5ml of D₂O to obtain a NMR spectra for each pure product. Samples of the degraded solvent were also spiked with the purchased degradation products to confirm these chemical shifts.

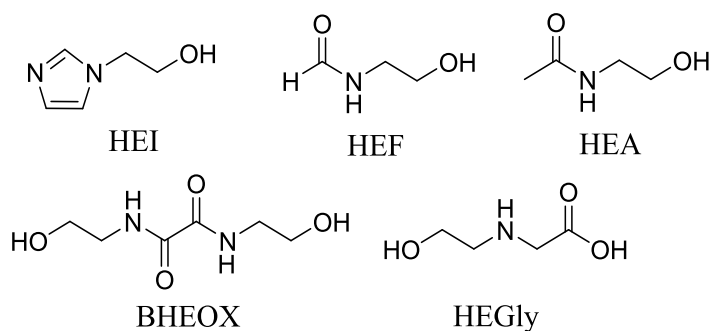


Figure 5.8 Major oxidative degradation products

The main oxidative degradation compounds reported in Figure 5.8 from previous work were also detected in this study: 2-oxazolidinone (OZD), formic acid, N-(2-hydroxyethyl)formamide (HEF) and N-(2-hydroxyethyl)imidazole (HEI) (Da Silva et al., 2012). HEI (1615-14-1), HEF (693-06-1), HEA (142-26-7) HES (18190-44-8) and BHEOX (1871-89-2) were all purchased from Sigma Aldrich. HEPO (23936-04-1) and HEGly (5835-28-9) were not purchased due the small quantities found by previous literature in oxidative degradation (Da Silva et al., 2012). NMR spectra data is not yet available in literature for HEPO or HEGly (5835-28-9). Degraded oxidative MEA samples were also individually spiked with each degradation product to confirm the suspected chemical shifts under sample conditions, where factors such as pH can influence shift measurements.

Only one study has previously used ^1H NMR analysis for the identification of MEA degradation products (Ciftja et al., 2012), which found peaks associated with the oxidative degradation of MEA to be isolated in the aromatic region of NMR spectra, nearly identical to that seen in Figure 5.7. This literature study assigned the chemical shifts of the oxidative degradation products in this region, HEI and HEF. However these chemical shifts appear to have been incorrectly assigned in the existing literature. Ciftja et al. assigned the aromatic peaks for HEI as 7.22 ppm, 7.24 ppm and 8.31 ppm, whereas shifts obtained for pure HEI and spiked MEA samples in this work observes shifts at 7.05 ppm, 7.19 ppm and 7.69 ppm. HEF is also incorrectly assigned as 8.48 ppm in the literature, whereas this study confirms a peak at 8.09 ppm.

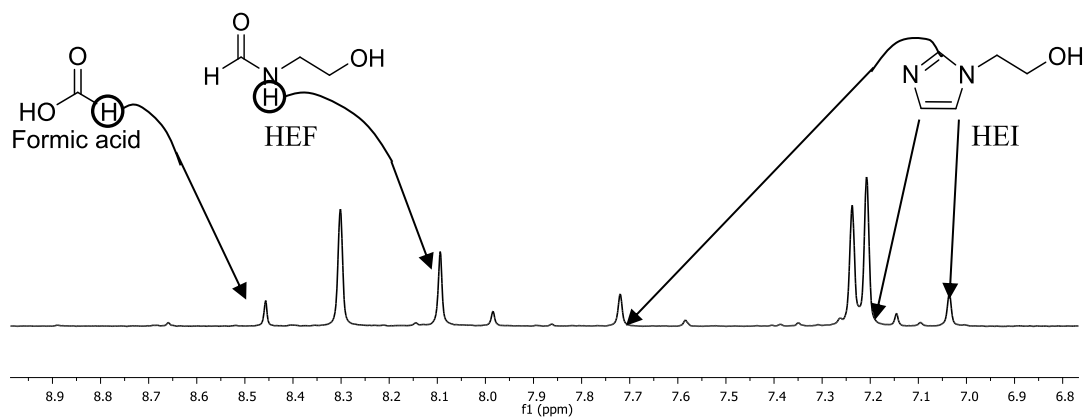
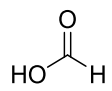
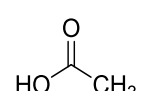
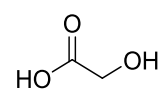
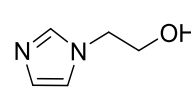
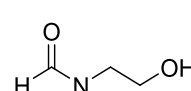
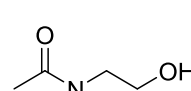
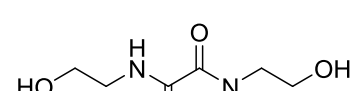


Figure 5.9 Aromatic region of NMR spectra for oxidative degradation of MEA in the presence of olive ash

Figure 5.9 illustrates the corrected assigning of peaks in the aromatic region of NMR spectra, this leaves the peaks at 7.22 ppm, 7.24 ppm and 8.31 ppm as associated with a significant unknown compound and requiring identification. Attempts to isolate this product are described in the following section. The NMR data for the major primary and secondary oxidative degradation compounds detectable by NMR are provided in provided in Table 5.7.

Table 5.7 NMR data for oxidative degradation products

Compound	¹ H NMR Data (D ₂ O)	¹³ C NMR Data
 Formic acid	8.44 (1H, s, CH)	165.5 (C=O)
 Acetic acid	2.08 (3H, s, CH ₃)	176.5 (C=O) 20.3 (CH ₃)
 Glycolic acid	4.21 (2H, s, CH ₂)	176.2 59.2
 HEI	7.69 (s, 1H, C-H)	138.3 (C=N)
	7.19 (d, 2H, ³ J _{HH} = 0.8 Hz, C-H)	127.7 (C=C)
	7.05 (d, 2H, ³ J _{HH} = 0.8 Hz, C-H)	120.2 (C=C)
	4.12 (t, 2H, ³ J _{HH} = 5.6 Hz, O-CH ₂)	60.8 (O-CH ₂)
	3.85 (t, 2H, ³ J _{HH} = 5.6 Hz, N-CH ₂)	48.9 (N-CH ₂)
 HEF	8.09 (s, 1H, N-H)	164.5 (C=O)
	3.67 (t, 2H, ³ J _{HH} = 5.6 Hz, O-CH ₂)	59.8 (O-CH ₂)
	3.37 (t, 2H, ³ J _{HH} = 5.2 Hz, N-CH ₂)	40.1 (N-CH ₂)
 HEA	8.00 (s, 1H, N-H)	174.5 (C=O)
	3.65 (t, 2H, ³ J _{HH} = 5.6 Hz, O-CH ₂)	59.9 (O-CH ₂)
	3.32 (t, 2H, ³ J _{HH} = 5.6 Hz, N-CH ₂)	41.5 (N-CH ₂)
	2.00 (s, 1H, C-CH ₃)	21.8 (C-CH ₃)
 BHEOX		161.1 (C=O)
	3.72 (t, 2H, ³ J _{HH} = 5.6 Hz, O-CH ₂)	59.7 (O-CH ₂)
	3.45 (t, 2H, ³ J _{HH} = 5.6 Hz, N-CH ₂)	41.6 (N-CH ₂)

However, as seen with the carboxylation of MEA, the pH of the solvent samples used for NMR can influence the observed chemical shifts for a molecule. The impact of pH on one of the major oxidative degradation products, HEI, is shown in

Figure 5.11. This movement in peaks is due to the same effects that pH has on observed peaks for MEA. pHs were varied using deuterium chloride (DCl) and sodium deuterioxide (NaOD). HEI is basic when alone in D₂O, the addition of DCl leads to the protonation of HEI as in Figure 5.10, however the rate of proton exchange between the free base and the protonated base is considerably faster than the time taken for ¹H NMR measurements, hence the peaks seen are a combination of the two forms.

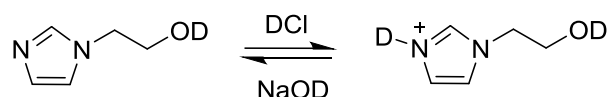


Figure 5.10 Equilibrium of HEI and protonated HEI

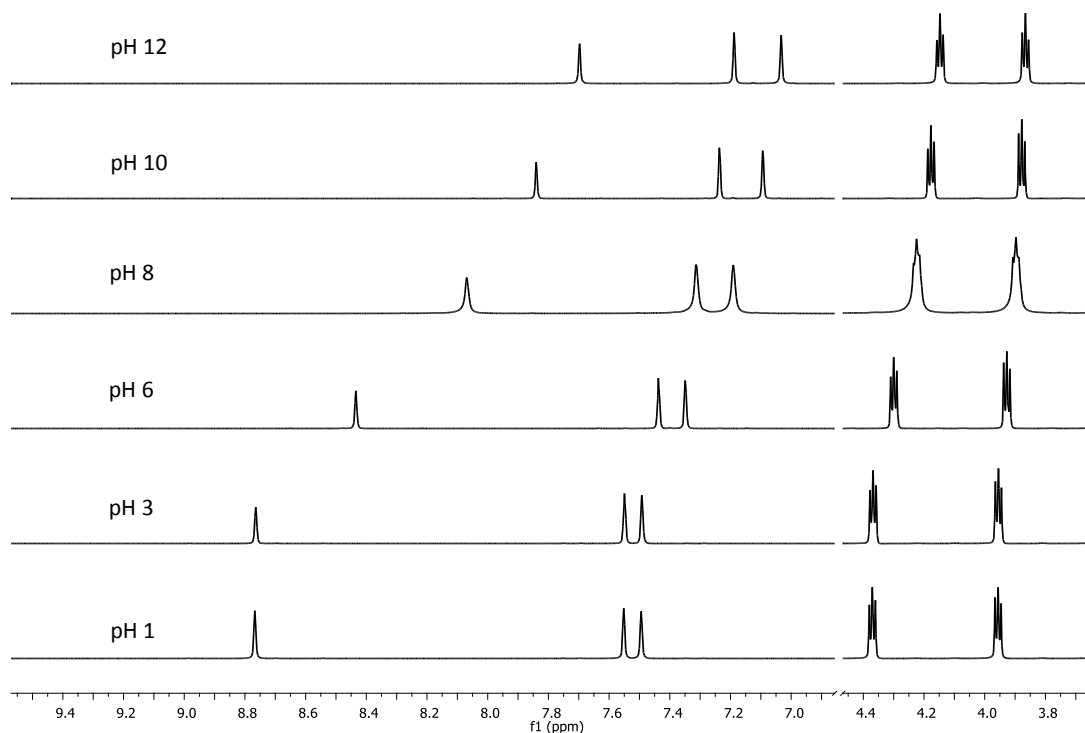


Figure 5.11 Stacked ¹H NMR of HEI with varied pH

Since HEI is basic in water, contact with CO₂ (which is acidic) will result in a neutralisation reaction and thus movement of the chemical shifts observed by ¹H NMR in a similar way to MEA carboxylation in Figure 5.1. Bubbling of the distillation residue (containing no MEA or H₂O) with CO₂ resulted in a movement of the observed chemical shifts for HEI as in Figure 5.11 but none of the other

oxidative degradation products showed similar effect on chemical shifts, including the unknown product.

5.2.4.2 Purification of oxidative MEA degradation products

In order to characterise the unknown degradation product peaks observed with ^1H NMR spectroscopy, attempts were made to isolate the compound from the degraded MEA samples. The degradation products were firstly concentrated by distillation under vacuum (details provided in chapter 8) to evaporate H_2O and excess MEA from the sample.

Attempts were made to separate the unknown product from the distillation residue using several methods of purification summarised below:

- Liquid-liquid extraction (LLE) with different organic layers tested - ethyl acetate, chloroform and diethyl ether.
- Preparative high performance liquid chromatography (HPLC) with a mobile phase of gradiented acetonitrile (5 to 50%) in water with 0.1% formic acid.
- Thin-layer chromatography (TLC) with mobile phase of 20% MeOH in DCM + 5% triethylamine (TEA).

Liquid-liquid extraction using ethyl acetate and prep HPLC were not effective at separating the unknown compound from other degradation products. Experimental details of the purification methods are provided in chapter 8.

The most effective form of separation was thin-layer chromatography (TLC). However, the product was not visible under 254 nm UV light illustrated in chapter 8, suggesting the compound doesn't contain a chromophore that absorbs light of this wavelength. Full glass preparative TLC was scraped in sections to confirm the location of the unknown product. This method effectively separated the compound with confirmation through NMR spectroscopy, with a relative r_f value of ~ 0.1 .

5.2.4.3 Identification of unknown oxidation product with ^1H NMR spectroscopy

Much of the previous literature identifying MEA degradation products has used GC-MS coupled with mass spectra database software to match measured mass spectra of known compounds, often supported with elemental analysis and standards run on GC-MS but no NMR data. As mentioned in the previous section, the use of NMR analysis by this work revealed the presence of significant quantities of a degradation

compound that had been incorrectly identified by literature. The compound was observed to have ^1H NMR chemical shifts at 7.22 ppm, 7.24 ppm and 8.31 ppm in D_2O – characteristic of aromatic compounds, but incorrectly assigned to HEI with the associated ^{13}C NMR shifts at 119.6 ppm, 120.9 ppm and 128.3 ppm (Ciftja et al., 2012).

Two-dimensional nuclear magnetic resonance (2D NMR) spectroscopy is a set of NMR methods that can be used to identify which proton shifts correlate with each other proton or carbon shifts. 2D NMR analysis techniques were used in this work:

- Correlation spectroscopy (COSY) with ^1H along both axes.
- Heteronuclear multiple-bond correlation spectroscopy (HMBC).
- Heteronuclear multiple-quantum correlation spectroscopy (HMQC)

These techniques were used to confirm that the ^1H and ^{13}C peaks corresponded to the unknown degradation product. The corrected ^1H and ^{13}C data for HEI were also identified. The chemical shifts for the unknown correspond closely with those found for HEI and thus suggest that the unknown compound is likely an imidazole.

Given that the ^1H and ^{13}C NMR data strongly suggest the unknown compound to be an imidazole, a detailed examination of the possible compound structures was considered. An imidazole is a cyclic compound consisting of a five-membered ring with three carbon atoms and two nitrogen atoms. However it must be considered that the positioning of the nitrogen atoms in the ring may be different to an imidazole. For example, the nitrogen atoms may be next to each other in the ring to form a pyrazole or 1,2-diazole which would result in different chemical shifts as presented in Table 5.8.

Table 5.8 Chemical shifts of possible heteroaromatic compounds (Pretsch et al., 2009)

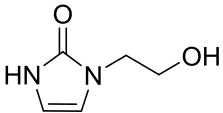
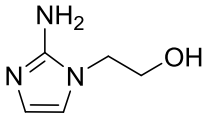
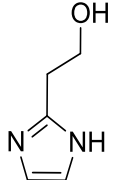
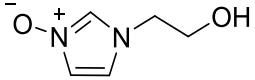
Compound		¹ H shift	¹³ C shift
Imidazole		a – 7.70	a – 136.2
		b – 7.13	b – 122.3
		c – 7.13	c – 122.3
Oxazole		a – 7.95	a – 150.6
		b – 7.09	b – 125.4
		c – 7.69	c – 138.1
Pyrazole		a – 7.55	a – 133.3
		b – 6.25	b – 104.7
		c – 7.55	c – 133.3
Isoxazole		a – 8.15	a – 150.0
		b – 6.28	b – 100.5
		c – 8.39	c – 158.9
1,2,3-Triazole		b – 7.75	b – 130.4
		c – 7.75	c – 130.4
1,2,5-Oxadiazole		b – 8.19	
		c – 8.19	
1,2,4-Triazole		b – 8.27	b – 147.9
		c – 8.27	c – 147.9

Liquid chromatography mass spectrometry (LC-MS) found the unknown compound to be difficult to separate from other degradation compounds, however mass spectroscopy data obtained from liquid chromatography detected masses of 112, 128, 144 and 146 to be present in the degradation product mix.

Since the shifts measured through both the ¹H and ¹³C NMR data do not appear to match other heteroaromatic options in Table 5.8, it is likely that the unknown

compound is an imidazole with an attached ethanol plus an oxygen or amine to make a compound with M+1 of 129. Table 5.9 lists the considered compounds that could fit this description along with reasons why they can be discounted as not matching the product being observed. Through a process of elimination, an N-oxide compound appears to have the only suitable combination of MS, ^1H and ^{13}C NMR data.

Table 5.9 Heteroaromatic compounds that could match the data collected on the unknown oxidative product and reasons for exclusion

Compound	Reason for exclusion
	^1H imidazole alkene shifts from literature of 6.14 ppm and 6.28 ppm (Kakeshpour et al., 2017). ^{13}C would show a peak in the 160-170ppm region
	^{13}C would show a peak in the 150ppm region and peak at 6.8ppm for ^1H imidazole alkene shifts (Mancini et al., 1996).
	^1H would show NH in the 2ppm region and alkenes would appear as one peak ~7 ppm due to symmetry of molecule (Langat et al., 2006). ^{13}C would show a peak in the 135-140 ppm region (Lebuis et al., 1993).
	None, ^1H and ^{13}C in correct region (Jasinski et al., 2007) and limited effect of pH on observed NMR shifts.

5.2.4.4 Synthesis of (hydroxyethyl)imidazole-N-oxide (HEINO)

In order to confirm the correct assignment of the suspected degradation compound the desired N-oxide was synthesised. The similarity of the suspected compound to HEI made a logical starting material for further reaction. The free nitrogen of the imidazole will contain two free electrons making it susceptible to reaction, in this case the aim is to oxidise the nitrogen to the N-oxide (Figure 5.12).

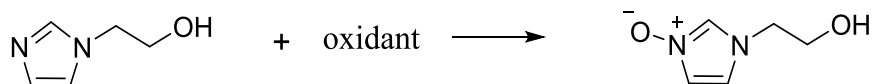


Figure 5.12 Oxidation of HEI to (hydroxyethyl)imidazole-N-oxide (HEINO)

Attempts were first made to oxidise HEI with H_2O_2 based on previous synthesis of 1-methylimidazole 3-N-oxide from the oxidation of 1-methyl imidazole under such conditions (Lin et al., 2005). Further attempts were made with different oxidants such as; meta-chloroperoxybenzoic acid (*m*CPBA), tert-butyl hydroperoxide (TBHP) and catalysed with vanadyl acetylacetonate ($\text{VO}_{(\text{acac})}$) in various solvents and conditions which are summarised in Table 5.10.

Table 5.10 List of attempted reactions to synthesis N-oxide

Reaction Number	Oxidant	Molar eq.	Solvent	Temp	Conversion from HEI
1	H ₂ O ₂	1:1.2	THF	r.t.	0 %
2	H ₂ O ₂	1:1.2	H ₂ O	r.t.	0 %
3	H ₂ O ₂	1:1.2	H ₂ O	80 °C	0 %
4	Compressed air	n/a	H ₂ O	r.t.	0 %
5	mCPBA	1:3	H ₂ O	r.t.	0 %
6	TBHP	1:3	DCM	r.t.	0 %
7	TBHP (VO(acac) ₂ cat.)	1:3:1	DCM	r.t.	0 %
8	TBHP	1:3	DCM	40 °C	0 %
9	TBHP (VO(acac) ₂ cat.)	1:3:0.5	DCM	r.t.	0 %
10	mCPBA	1:1	DCM	r.t.	11 %
11	mCPBA (and K ₂ CO ₃)	1:2:2	DCM	r.t.	0 %
12	mCPBA (and TEA)	1:2:2	DCM	r.t.	5 %
13	mCPBA	1:1.2	DCM	r.t.	11 %
14	mCPBA (and K ₂ CO ₃)	1:1.2:1	DCM	r.t.	0 %
15	mCPBA (and TEA)	1:1.2:1	DCM	r.t.	0 %
16	H ₂ O ₂	1:1.2	H ₂ O	r.t.	0 %
17	mCPBA	1:1.2	DCM	r.t.	26 %
18	mCPBA	1:2	EtOH	r.t.	18 %
19	mCPBA	1:2	EtOAc	r.t.	22 %
20	mCPBA	1:3	EtOAc	r.t.	28 %
21	mCPBA (and K ₂ CO ₃)	1:3:3	EtOAc	r.t.	0 %
22	mCPBA added stepwise	1:3	EtOAc	r.t.	17 %

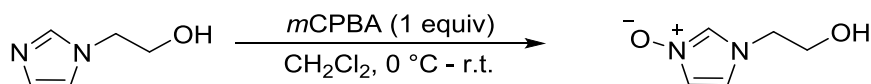


Figure 5.13 Synthesis of (hydroxyethyl)imidazole-N-oxide (HEINO)

The successful synthesis of N-(2-hydroxyethyl)imidazole-N-oxide, abbreviated as HEINO, was carried out via oxidation of N-(2-hydroxyethyl)imidazole using 1.2-3.0 equivalents of *m*CPBA (Figure 5.13). Dichloromethane was employed as the solvent system. The N-oxide was obtained in a yield of 20% following column chromatography for purification, with 20% MeOH in DCM as the mobile phase. The product was found to match the desired unknown degradation compound with ^1H and ^{13}C NMR data. Accurate mass found the desired mass of 128.0656 compared to the calculated mass of 128.0665. Infrared spectroscopy found a peak at 1307 cm^{-1} , matching that previous measured for an N-oxide imidazole (Murray, 2016).

Attempts were made to improve the yield of the desired N-oxide by using a base (TEA and K_2CO_3) to minimize presence of the benzoic acid by-product formed as part of the oxidation reaction as shown in Figure 5.14. As the imidazole cannot be oxidised once it is protonated thus making 50% the maximum possible yield. However these attempts to improve the reaction yield were unsuccessful as seen in Table 5.10.

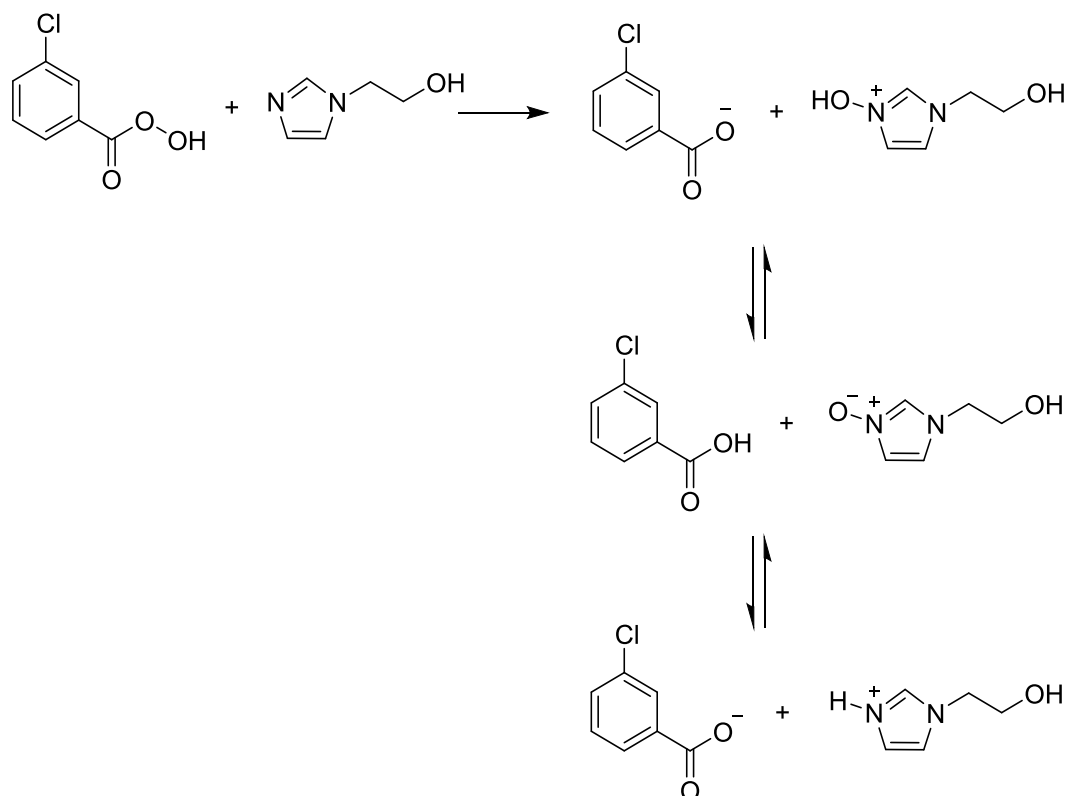


Figure 5.14 Formation of *m*-chloro-benzoic acid as a by-product from the oxidation of HEI with *m*CPBA, and resultant salt formation.

5.2.4.5 Impacts of potassium chloride, biomass ash and coal ash on oxidative degradation with ^1H NMR spectroscopy

Following the identification of the unknown NMR peaks, the quantities of these oxidative degradation products were plotted over the period of the laboratory degradations. This section provides a comparison of the quantities of key secondary oxidative degradation products (HEI, HEINO and HEF) in the presence of different flue gas contaminants. This enables an examination of the differing impacts on MEA degradation observed in the presence of ashes from biomass combustion rather than coal. Potassium chloride is again examined for effects on degradation due to its known high quantities in biomass flue gas and expected deposition in carbon capture solvents.

Figure 5.15 demonstrates the influence that a particular fuel combustion ash can have on the formation of HEI during oxidative degradation. The ‘PACT coal ash’ is seen to result in a significant increase in the formation of HEI over the 3 week period. Approximately three times greater than the quantities of HEI observed for all other cases including a ‘coal ash #1’ sourced from a UK power station. The addition

of olive ash and KCl do not appear to effect on the formation of HEI whilst the 'PACT wood ash' appears to show slightly lower levels of HEI than the other cases.

Interestingly Figure 5.16 illustrates that both types of coal ash appear to dramatically catalyse the formation of the newly identified HEINO (with chemical shifts at 7.22 and 7.24ppm). 'Olive ash' also appears to catalyse the formation of this product whilst relatively small quantities of the HEINO are seen for MEA alone, with KCl or 'PACT wood ash'.

N-(2-hydroxyethyl)-formamide (HEF) does not appear to be affected much from the addition of any ashes or KCl as seen in Figure 5.17. The only noticeable difference between the cases is slightly lower quantities of HEF for the oxidative degradation of MEA in the presence of 'PACT wood ash'.

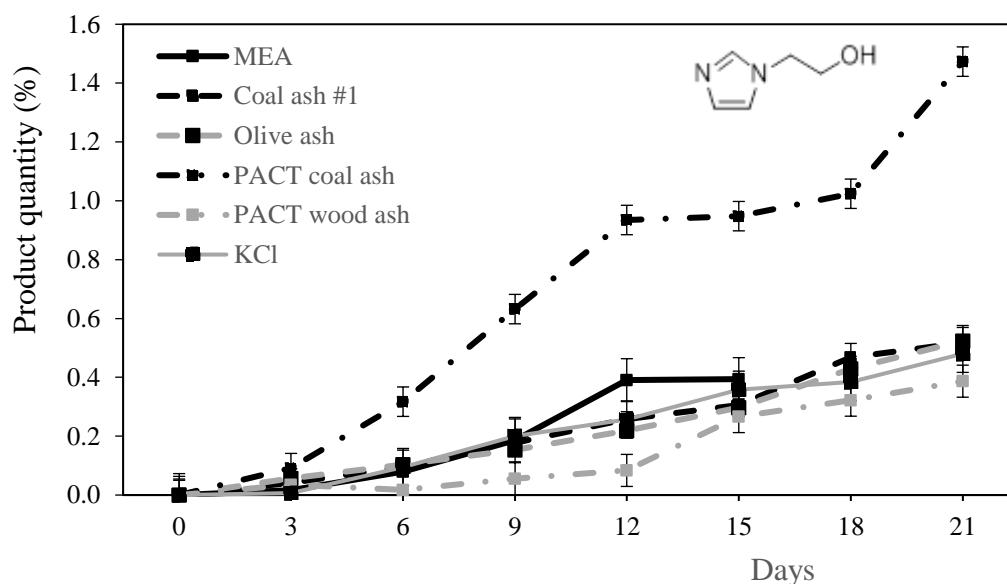


Figure 5.15 Formation of N-(2-Hydroxyethyl)imidazole (HEI) during the sparging of 30 wt% MEA with compressed air at 40°C.

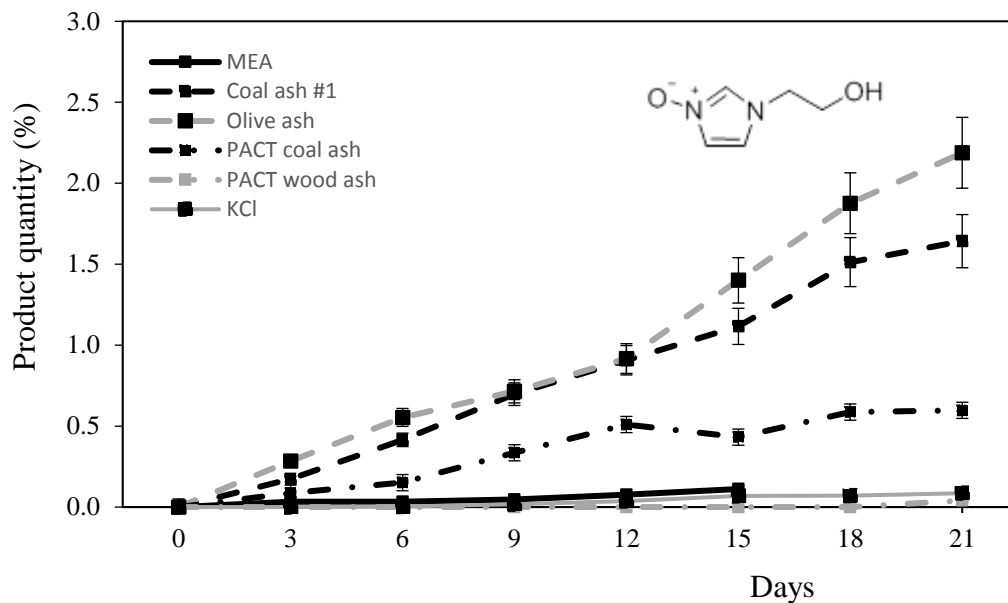


Figure 5.16 Formation of HEINO during the sparging of 30 wt% MEA with compressed air at 40°C.

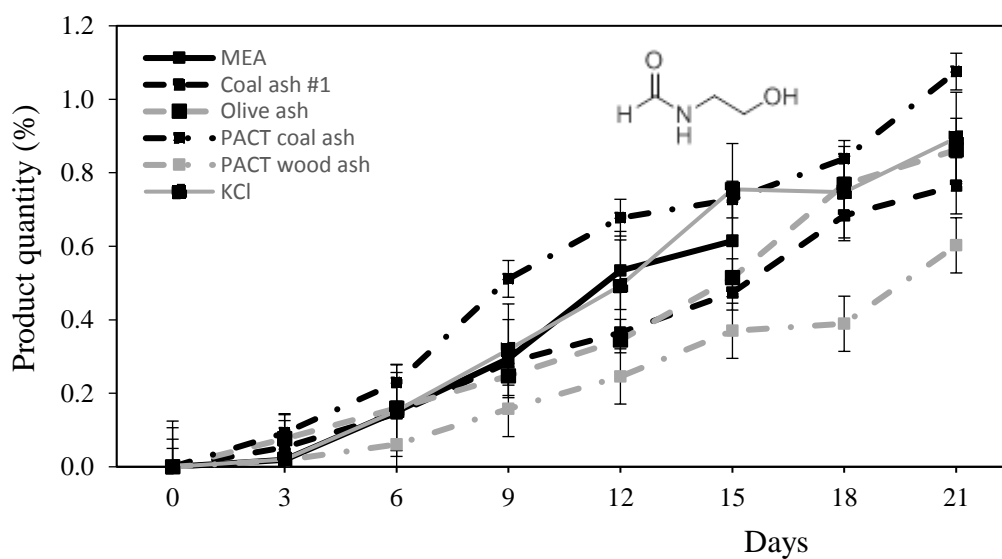


Figure 5.17 Formation of N-(2-hydroxyethyl)formamide (HEF) during the sparging of 30 wt% MEA with compressed air at 40°C.

5.2.4.6 Validation of the known oxidative degradation product formation with GC-MS

Gas chromatography mass spectrometry (GC-MS) was used under the same conditions described previously for the thermal degradation samples. The purchased oxidative degradation products from literature were used to calibrate the device for their quantification. An example chromatogram is provided in chapter 8. The

retention times for the associated elution of HEF, OZD and HEI were 17.3 minutes, 20.4 minutes and 24.6 minutes respectively, which were confirmed with spiked sample runs. The small quantities of HEINO synthesised in this work meant that it was not calibrated for GC-MS analysis.

Figure 5.18 illustrates an important difference in the quantities of HEI measured by the two measurement techniques. NMR detected fairly equal amounts of HEI in the oxidative degradation cases except for the addition of 'PACT coal ash' which is seen to result in a significant increase in HEI formation. However the GC-MS measurements appear to detect high levels of HEI also for the 'Olive ash' and 'Coal ash #1'. These are not supported by the quantification of HEI using NMR.

Interestingly Figure 5.19 shows that NMR spectroscopy detects higher levels of HEINO for the 'Olive ash', 'Coal ash #1' and 'PACT coal ash' cases. This graph compares the quantities of HEINO measured with NMR against the quantities of HEI detected with GC-MS. The correlation between these two measures would suggest that HEINO in the liquid samples may be detected by the GC-MS as HEI, this could be caused by the reduction of HEINO to HEI under the high temperature chromatography conditions.

Whereas the comparison of GC-MS and NMR quantities of HEF in Figure 5.20 show good correlation between the two measurement techniques. From this it is confirmed that slightly higher quantities of HEF are formed in the presence of 'PACT coal ash' and slightly lower quantities of HEF are observed in the presence of 'PACT wood ash', when compared to the other cases.

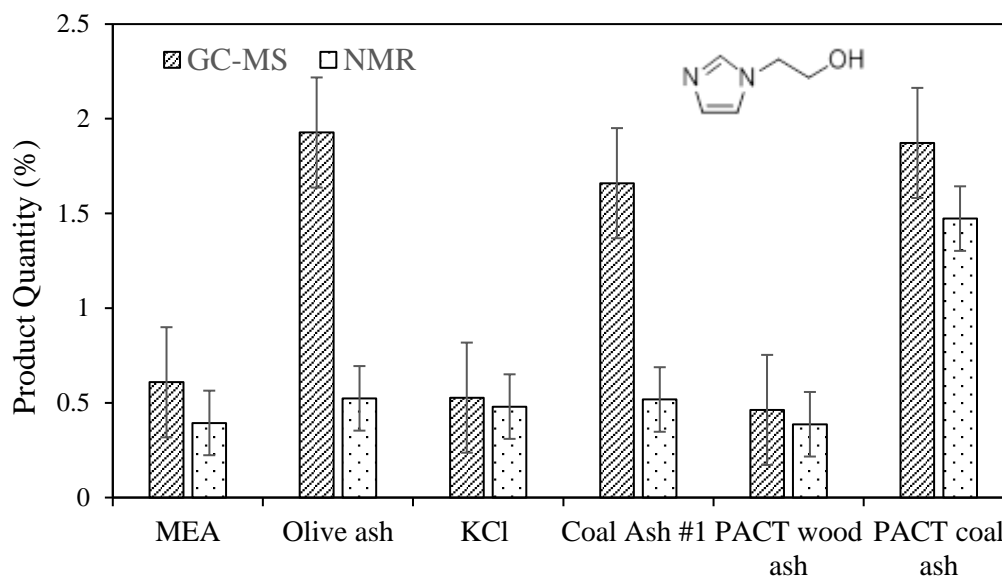


Figure 5.18 Comparison of measurement techniques analysing the formation of HEI in the oxidative degradation of MEA through sparging with compressed air at 40°C.

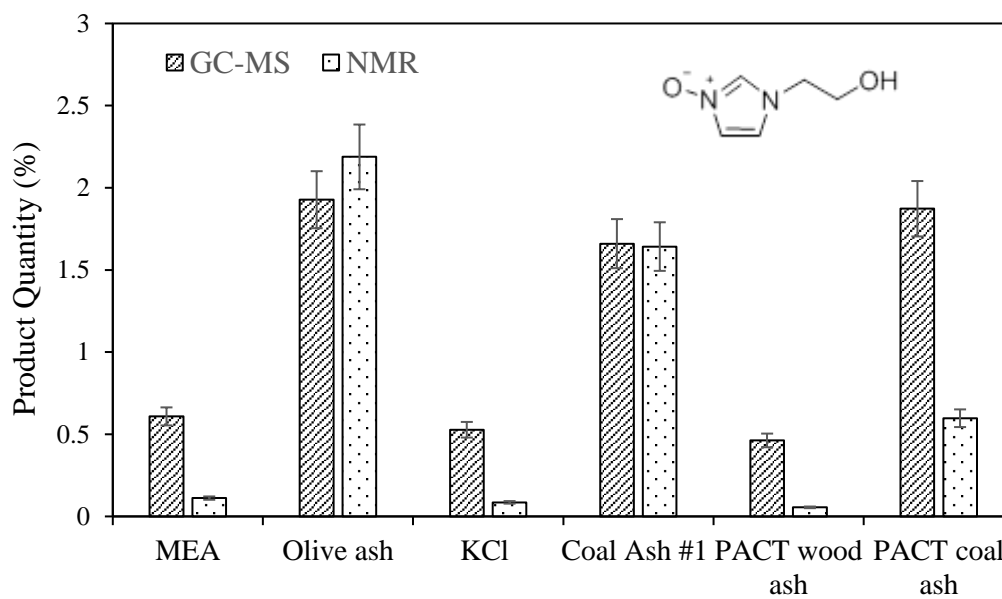


Figure 5.19 Comparison of measurement techniques analysing the formation of HEINO in the oxidative degradation of MEA through sparging with compressed air at 40°C.

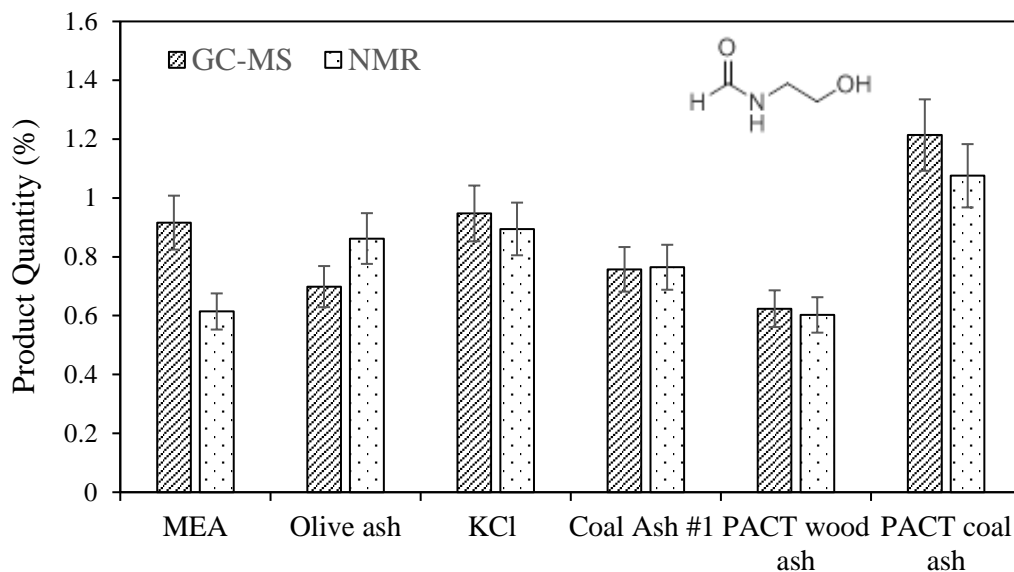


Figure 5.20 Comparison of measurement techniques analysing the formation of HEF in the oxidative degradation of MEA through sparging with compressed air at 40°C.

5.2.4.7 Presence of Heat Stable Salts (HSS) in oxidative MEA solvents

Heat stable salts can be formed through interaction with flue gas impurities or primary MEA oxidation products. Chapter 3 identified that sulphate, nitrate, nitrite and chloride anion salts are often formed due to the presence of SO₂, NO_x and fly ash in flue gas streams. Sulphate is formed from the oxidation of SO₂ in flue gases (Thompson et al., 2017), while nitrite and nitrate are formed from the oxidation of ammonia (Huang et al., 2008).

Organic acids formed from the oxidation of MEA such as formic and acetic exist in equilibrium between the MEA salts (formate and acetate), and can form amides (HEF and HEA), which can be tracked through proton and carbon NMR spectroscopy. Formate is the main oxidative HSS observed at pilot carbon capture facilities due to high quantities of formic acid from oxidation - which was identified using ¹H NMR spectroscopy. However inorganic salts such as sulphate (SO₄²⁻), nitrate (NO₃⁻) and nitrite (NO₂⁻) required the use of ion chromatography (IC) for quantification (Vevelstad et al., 2012). Formate, acetate and glycolate, could not be monitored by IC due to the co-elution of peaks.

The measurements of HSS was carried out using a Dionex ICS-900 ion chromatography system (detailed in chapter 8) with an eluent of 5 mM NaOH and

was calibrated for nitrite, nitrate, sulphate and oxalate using purchased standards for IC. As seen in Figure 5.21 the highest quantities of nitrite were measured in oxidative degradations in the presence of both types of coal ashes but especially the ‘Coal ash #1’ sourced from a UK power station. Both coal ashes also appeared to show slightly higher formation of oxalate and nitrate. However, surprisingly the ‘PACT wood ash’ from the candle filter at the UKCCSRC’s PACT facilities produced significantly higher quantities of sulphate than any other case, likely due to high quantities of sulphur in the ash.

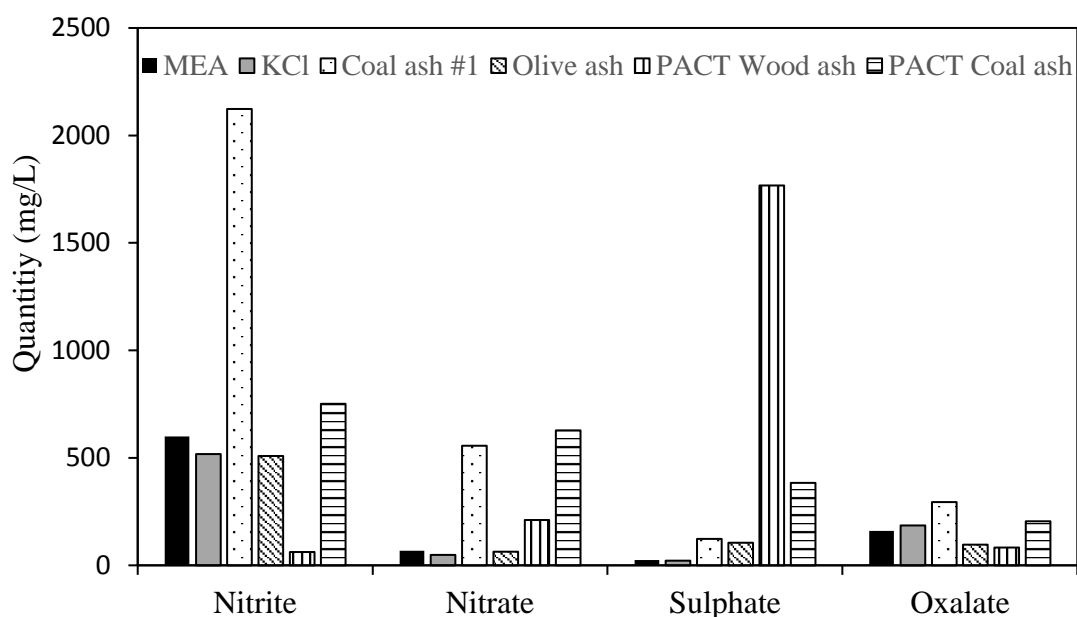


Figure 5.21 Formation of HSS's under oxidative degradation conditions

5.2.4.8 Presence of leached metals in oxidative MEA solvents

The samples of 30% w/w MEA that were subjected to the oxidative conditions described previous were again analysed by inductively coupled plasma - optical emission spectrometry (ICP-OES) to measure the concentrations of Al, Mg, Ca, Mn, Pb, Ni, Cu, Cr, K, Na, Fe and Si present in the solvent. A Thermo Fisher iCAP 7400 Radial ICP-OES was used for the measurements and was operated by Stephen Reid from the School of Earth and Environment at the University of Leeds.

The quantities of K, Na and Mg found in solution from ICP-OES measurements correlate with the quantities measured in ash composition data provided in section 5.2.4. Very low amounts of potassium are seen in the case of both coal ash and for the MEA alone degradation, whereas significant quantities are seen in all biomass cases. It follows that more potassium is seen in the olive ash case as there is larger

amounts of potassium in this ash compared to wood ash, thus suggesting a similar amount of potassium is in a water soluble state for both biomass ashes.

High quantities of Na were measured in both coal ash cases compared to MEA, KCl and olive. However the highest quantities of Na are measured in the wood ash case. Ca, Cu, Cr, Mn and Pb are also seen to be significantly higher for the white wood case. However Mg is higher for both coal cases.

Table 5.11 Metals present in the oxidative degradation of MEA

	MEA alone (mg/L)	Olive ash (mg/L)	KCl (mg/L)	Coal ash #1 (mg/L)	PACT wood ash (mg/L)	PACT coal ash (mg/L)
Al	10.08	10.42	10.37	10.27	10.12	10.25
Mg	<LOD	<LOD	<LOD	2.12	0.92	4.97
Ca	<LOQ	28.70	<LOQ	2.07	45.76	9.18
Mn	1.19	22.42	1.37	15.65	25.14	10.25
Cu	<LOQ	0.07	<LOQ	0.01	0.19	0.06
Cr	<LOD	0.41	<LOQ	0.04	1.07	0.17
K	0.90	738.80	1089.85	3.02	511.84	10.15
Na	27.08	19.64	22.61	47.56	110.34	61.96
Fe	0.21	3.13	0.14	4.25	9.34	20.01
Si	7.16	16.52	9.39	2.28	2.27	1.40

5.3 Analysis and discussion

5.3.1 CO₂ absorption

This work has used ¹H NMR for the analysis of CO₂ absorption into MEA, providing the basis for a rapid method of monitoring CO₂ loading and quantities of base available for further reaction. CO₂ absorption studies using the vapour-liquid equilibrium (VLE) apparatus found the addition of potassium salts to have little or no detectable effect on the capacity of 30% w/w MEA. This is important as potassium is a dominant species present in many types of biomass that could be combusted in a BECCS power station. Since potassium is volatile under combustion temperature and mostly forms KCl in the flue gas it is crucial that KCl does not have impacts on the performance of an amine capture solvent. These results confirm that

the quantities of KCl likely to encounter a carbon capture plant would not affect the ability of 30 wt% MEA to capture CO₂.

5.3.2 Thermal Degradation

This work used NMR spectroscopy and GC-MS to identify the presence of key thermal degradation products and quantify their presence in samples of 30 wt% MEA degraded at 135 °C for 6 weeks in sealed stainless steel vessels. Samples were loaded with CO₂ prior to the degradations and were mixed with either KCl, biomass ash, coal ash, or nothing. The findings of the thermal degradation experiments suggest that ashes, coal or biomass, and KCl have little impact of the formation of degradation products under thermal conditions. This is supported by other literature on thermal degradation (Huang et al., 2014). These experiments were carried out at 135 °C to accelerate the conditions seen in a reboiler at which the main thermal degradation products are formed. The principal mechanism supposed for the thermal degradation of MEA suggests that the main stable degradation product is HEIA formed from HEEDA which is unstable in the presence of CO₂ (Da Silva et al., 2012; Helene Lepaumier et al., 2009). This work also found HEIA to be the thermal degradation product present in the highest quantities at approximately 14%.

5.3.3 Oxidative Degradation

The laboratory oxidations of 30 wt% MEA in this work used NMR spectroscopy to characterise the oxidative degradation products identified previously in literature. These characterisations were compared with NMR data from literature which revealed the incorrect assignment of NMR shifts for the most abundant oxidative degradation product, HEI. Correct NMR data is provided in this work along with characterisation of the peaks previously mistaken for HEI. A new degradation product was discovered by this work, (hydroxyethyl)imidazole-N-oxide (HEINO), which is found to be present in significant quantities.

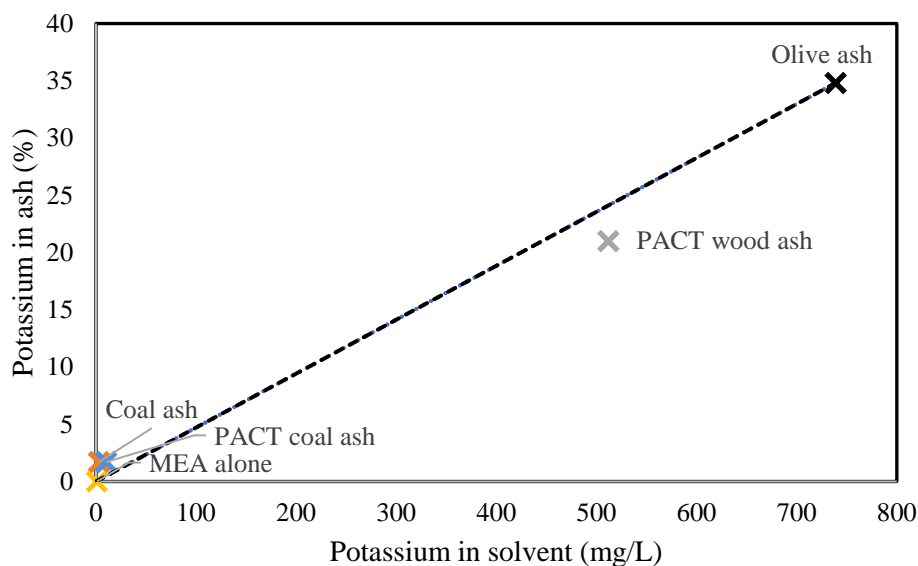


Figure 5.22 Correlation of potassium in solvent with potassium in ash

Elemental analysis of the oxidative degradation amine samples shows that higher K content ashes from the combustion of fuels such as olive residue and white wood result in a higher leaching of potassium into amine solvents, illustrated in Figure 5.22.

Results from the NMR analysis of oxidative degradation experiments suggest that ashes from coal and olive combustion can catalyse the formation of HEINO identified in this work, whereas only one of the coal ashes appears to catalyse the formation of a previously identified oxidative degradation product, HEI. The comparison of fly ashes collected from the UKCCSRC's PACT facilities shows higher rates of HEI and HEINO formation with coal ash compared to wood ash. Slower rates of HEI, HEINO and HEF formation were seen for the wood ash collected from the UKCCSRC's PACT facilities compared to all other cases.

This work has shown that the composition of an ash can influence the formation of amine degradation products. For example, the coal fly ash collected from the UKCCSRC's PACT facilities (PACT coal ash) showed a larger production of HEI than the other ashes, but lower amounts of HEINO than coal ash #1 and the olive ash. This appears to suggest that the PACT coal ash may push the degradation reactions towards the formation of HEI over HEINO. Figure 5.23 plots the total of the integrated NMR peaks at shift: 7.21ppm for the N-oxide, 7.03ppm for HEI and 8.09ppm for HEF. This comparison suggests that olive ash produces the largest total quantities of degradation products, followed by the coal ash #1 and PACT coal ash,

and that the PACT wood ash and KCl have negligible effects on the formation of imidazoles or HEF.

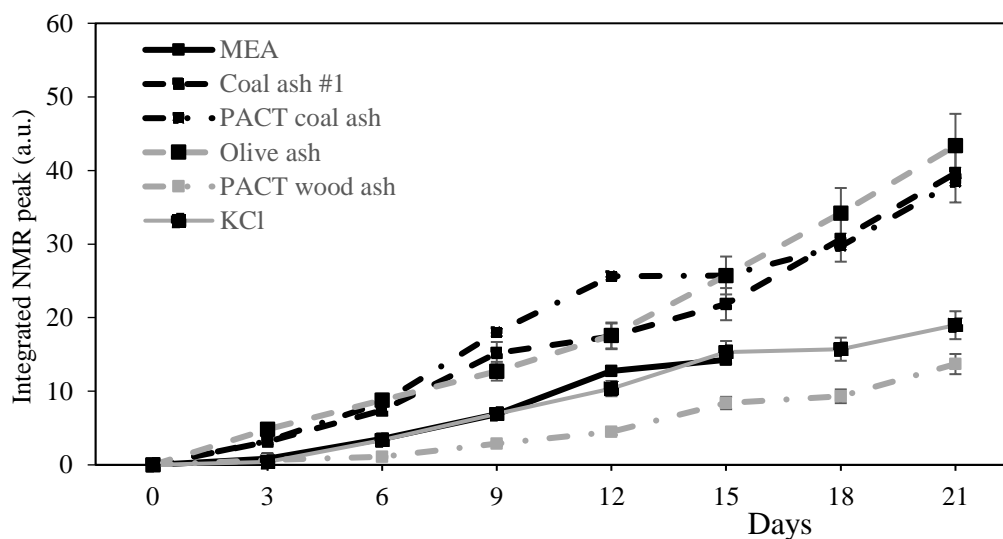


Figure 5.23 The combined integration of NMR peaks of HEI, HEF and HEINO, for a cumulative plot of the major degradation products

OZD and HEF appear less affected by the addition of ash. It has been suggested that HEA and HEF are formed through the base MEA molecule reacting with acidic oxidized MEA fragments, such as acetic acid and formic acid respectively (Da Silva et al., 2012). The formation of HEI is less understood than the other oxidative constituents, however it has been confirmed that HEI can be formed from the mixing of MEA, formaldehyde, glyoxal and ammonia which are all known products and fragments of MEA degradation (Vevelstad et al., 2013).

Catalytic effects on degradation are complex, high metal presence, such as Fe in the 'PACT wood ash' case doesn't necessarily result in the largest quantities of degradation product formation. There are no clear links between any of the individual ash components and degradation, this is likely due to combined effect from the elements present. Ca, Cu and Mn which are also high in concentration for the 'PACT wood ash' case don't appear to show catalytic degradation effects.

5.4 Conclusions

This work has demonstrated the capability of NMR spectroscopy to be applied to the carboxylation and degradation of MEA. ^1H and ^{13}C NMR analysis have been successfully used to monitor the CO_2 loadings and formation of major degradation

products (OZD, HEEDA, HEIA, HEI, HEF and formate). The chemical shifts for each of the protons and carbons associated with MEA, carbamate and the degradation products are provided.

Incorrectly assigned NMR shifts for existing degradation products have been corrected and a new degradation product has been identified, which in some cases is the most abundant degradation product. This work has examined the impact that fly ashes from biomass combustion will have on amine degradation compared to coal fly ashes. The results of laboratory testing in this study has found biomass ashes from white wood combustion to reduce the formation of the major oxidative degradation products. These findings suggest the carbon capture applied to flue gases from white wood biomass combustion may observe less amine degradation, and thus reduced regeneration costs, than coal or olive biomass plant combustion.

Mitigating degradation in a full-scale industry CCS plant would reduce the operational costs associated with running such a plant and could thus make it more attractive to investors in the power industry. Continued analysis of the products generated by oxidative degradation can enable assessment of the different reactions undertaken during MEA degradation in a carbon capture plant.

Chapter 6

Pilot-scale fate of potassium

6.1 Introduction

After combustion the gases produced are processed through a series of flue gas treatment options as outlined in Chapter 3. The fate of the flue gas impurities is of great importance to the effects seen on downstream processes such as boiler tubes or carbon capture plant. Thus an investigation of where combustion ashes and volatile species are found is very important for understanding the impacts this would have on a full-scale BECCS plant. This chapter presents experimental data and analysis from pilot scale trials of a 250kW air combustion furnace and amine carbon capture plant at the UKCCSRC's PACT (Pilot-Scale Advanced Capture Technology) facilities.

The trials consisted of combustion runs with biomass and coal as the solid fuel to enable a comparison between the two cases. This work builds on the experimental work from the laboratory in the previous two chapters, with comparison to pilot-scale results. Using the methods described in chapter 4 to analyse the inorganic content of ashes collected from the pilot-scale combustion rig enable conclusions to be drawn on the fate of inorganics at a power plant, while amine samples were analysed using the spectroscopy techniques described in chapter 5 to measure the quantities of degradation products formed for the biomass and coal case.

Published work (Finney et al., 2018) on metal aerosols at the PACT facilities used the exact fuels and experimental apparatus described in this chapter. This previous work assessed the differences in metal aerosols found in the vapour phase flue gas from biomass and coal. The results suggest that K was the only metal aerosol to be found in significantly higher concentrations for the biomass case than in coal. Only K, Ca, Na, Mg and Fe showed any significant amounts of aerosol in the flue for biomass. Na and transition metals were found in slightly lower concentrations in biomass flue gases. Many other heavy metals were found to be present at much lower concentrations for the biomass case, including Fe which the authors suggested could result in less solvent degradation.

We observed in chapter 4 that K is volatile under the high temperatures of combustion. This enables it to pass through the particle boundary layer during combustion and into the furnace environment as gaseous K^+ which is highly unstable and mostly likely to react to form KCl or KOH (van Lith et al., 2008). As flue gases are cooled some of these potassium compounds can be converted through homogeneous gas-phase reactions into K_2SO_4 which become highly supersaturated and likely results in homogeneous nucleation to form new particles. This chapter will use samples of ash and amines from the pilot facility to examine if gaseous forms of K are mostly collected by particle removal technologies, or accumulate in carbon capture solvents

6.2 Experimental Methodology

6.2.1 Fuel feedstocks

Two fuels typically used for power generation were combusted at the pilot-scale facility. A North American Grade A white wood pellet and a bituminous coal, from the El Cerrejon region in Columbia. The proximate, ultimate and ash oxides analyses for the fuels are provided in Table 6.1, which were completed in line with the International Standard methods for the determination of moisture, volatiles and ash for the biomass (EN 14774-3:2009, EN 15148:2009 and EN 14775:2009); and the coal (ISO 11722:2013, ISO 562:2010 and ISO 1171:2010). Ultimate contents were determined using an EA1112 elemental analyser in accordance with EN 16948. The elemental oxides in ash were analysed with inductively coupled plasma optical emission spectrometry (ICP-OES) after digestion by an accredited analytical laboratory - SOCOTEC UK Limited.

Table 6.1 Fuel and ash composition analysis for the raw biomass and coal fuels used, from (Finney et al., 2018).

Content	Basis	Units	Biomass	Coal
Moisture	a.r.	wt%	6.7	7.6
Volatiles	dry	wt%	83.7	38.4
Ash	dry	wt%	0.7	3.1
Fixed carbon*	dry	wt%	15.6	58.4
Elemental				
C	a.r.	wt%	48.44	69.44
H	a.r.	wt%	6.34	4.55
N	a.r.	wt%	0.15	1.32
S	a.r.	wt%	<0.02	0.07
Cl	a.r.	wt%	< 0.01	0.03
O	a.r.	wt%	37.69	15.15
Oxides in ash				
Al₂O₃	in ash	%	1.9	16.6
Fe₂O₃	in ash	%	1.3	10.8
CaO	in ash	%	27.0	14.4
MgO	in ash	%	5.5	1.9
Na₂O	in ash	%	1.3	1.9
K₂O	in ash	%	10.1	1.6
SiO₂	in ash	%	13.6	39.9

The white wood pellets used are typical of the biomass currently used for biomass power generation in the UK. As seen in Table 6.1 the biomass is low in ash and fixed carbon content compared to the coal, but high in volatiles. The coal has a higher carbon content than biomass and is high in Al, Si and Fe content – all of which are typical for coal. Fe is of particular importance due to its known catalysis of oxidative degradation of amine solvents (Sexton and Rochelle, 2009) along with Cu and V. In contrast, the biomass ash contains high K and Ca content – typical of most biomass types as identified in chapter 4.

6.2.2 250kW pilot-scale combustion rig

The 250 kW pilot-scale combustion facility is part of the UKCCSRC PACT facilities, located near Sheffield, UK. The facility holds a down-fired PF furnace capable of operating in air-firing conditions or oxyfuel conditions. Interchangeable

burners and feeding systems are used for the firing of coal and biomass solid fuel combustion and natural gas is used for preheating the furnace (Szuhánszki, 2014). Fuel is supplied through a hopper, seen in Figure 6.2, prior to being mixing with primary air and transported to the furnace. A screw feeder is used to provide measured quantities of fuel from the hopper based on the rotation speed of the screw. Fuel from the screw feeder is dropped onto a vibrating plate to create a more uniform fuel feed prior to being dropped into the primary air line through a venturi feeder. The rig was operated and monitored by Dr. János Szuhánszki of the University of Sheffield through a local Human-Machine Interface (HMI).

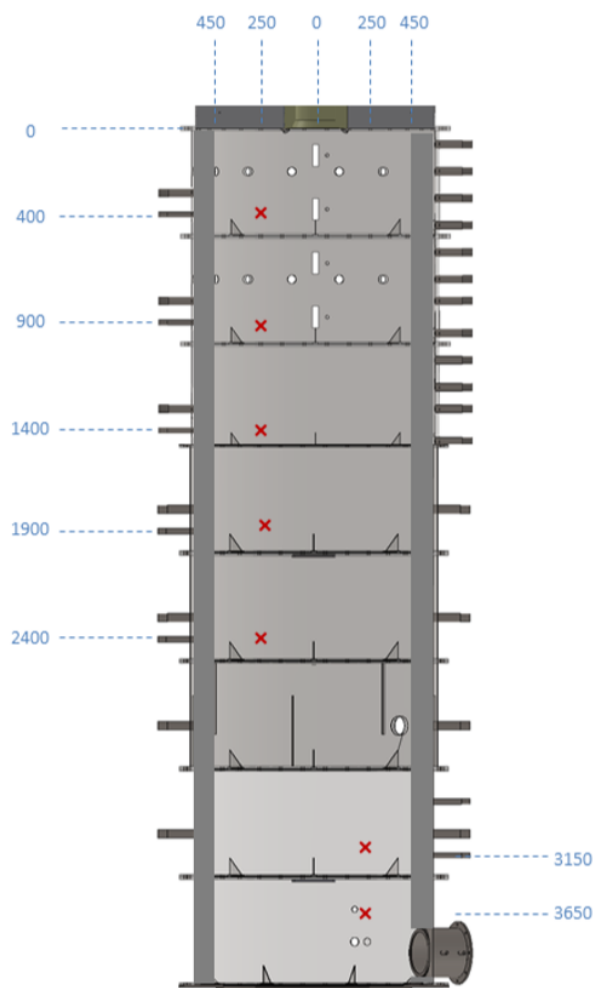


Figure 6.1 Dimensions of down-fired furnace from (Xing, 2016), with interchangeable burners located at (0,0).

The pulverized fuel is carried into the burner located at position 0,0 in Figure 6.1 in the primary air. The furnace is 4 m tall, made from 8 x 0.5m sections lined with a 100 mm thick, lightweight alumina silicate to enable rapid heating and fast steady

state conditions. A General Electric (GE) burner design was used for the combustion of biomass and a version of the Doosan Mark III burner was used for coal. Combustion air is supplied by a compressor at 6-7 bar pressure. The air supply line is fitted with 2 coalescing filters and a carbon filter to remove both oil and moisture contamination from the air supply. Secondary and tertiary air are supplied to the burners at 250 °C for further combustion. Temperatures within the furnace start at 1350 °C at top and fall to approximately 1200 °C just above the heavy fly ash collection water tray (Finney et al., 2018) at position (0,0). This is slightly higher than the highest temperatures used by the laboratory combustion experiments of chapter 4; single particle combustion experiments (1100 °C) and ashing experiments (1150 °C).

The top six furnace sections are water cooled through ports in the sections. The bottom of the rig is sealed with a water tray which collects bottom ash and slag deposits from the furnace. The furnace pressure is maintained at -1 mbar by the exhaust fan and the flue gas is drawn from the bottom section of the furnace, 4 metres below the burner (Szuhánszki, 2014).

6.2.3 Ash collection from pilot combustion rig

Pilot scale testing facilities are fitted with particulate removal equipment similar to that used by a full scale biomass combustion plant. The collection of these ashes, in combination with previous work on aerosols in the flue gas, enables the tracking of ash species through the treatment process. Figure 6.2 illustrates an overview of the combustion furnace and flue gas treatment facilities at UKCCSRC PACT facilities where the ashes were collected. Ashes were collected from three locations:

1. A collection pot located at the bottom of the furnace – Heavy fly ash.
2. A cyclone situated before heat exchangers – Coarse PM.
3. A ceramic candle filter situated after heat exchanger – Fine PM.

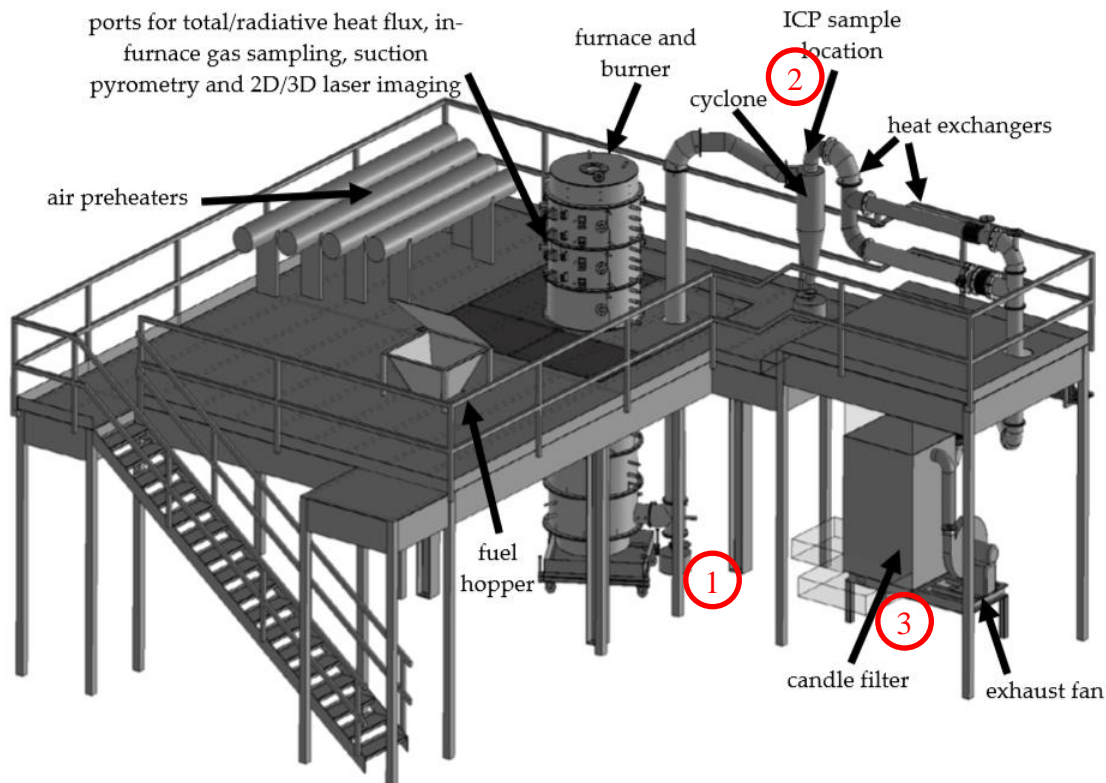


Figure 6.2 PACT pilot-scale combustion facility and ash sampling locations, adapted from (Finney et al., 2018)

Fly ash samples taken at locations 1 and 2 were collected using clean catchpots to collect ashes for a 30-45 minute period of steady state combustion. The cyclone was custom built while the candle filter is a Glosfume ceramic biomass filter unit. Fly ash samples from location 3 were collected from a large ash collection tray at the bottom of the candle filter at the end of each day, with an hour of firing provided to reach steady state conditions.

6.2.4 Pilot-scale post-combustion carbon capture facility

Figure 6.3 shows a schematic diagram of the post-combustion CO₂ capture facility at the PACT facilities, whereby the flue gas enters at the right of the diagram. The flue gas first encounters the particle removal technologies described in Section 6.2.3, before passing through the flue gas desulphurisation (FGD) system to remove SO₂. A fan is used after the FGD to pressurise the flue gas through the CO₂ absorber where the gas contacts the 30% w/w MEA solvent and the CO₂ reacts with the counter flowing solvent to be removed from the flue gas. A water wash column is

also located after the absorber for the removal of solvent droplets entrained in the CO₂ free flue gases. The plant is equipped with instrumentation for tracking the temperature at different heights within the absorber and analysing the flue gas composition at the absorber inlet, absorber outlet and water wash outlet. This data was monitored and recorded by Dr. Muhammad Akram, who operated the plant during both trials.

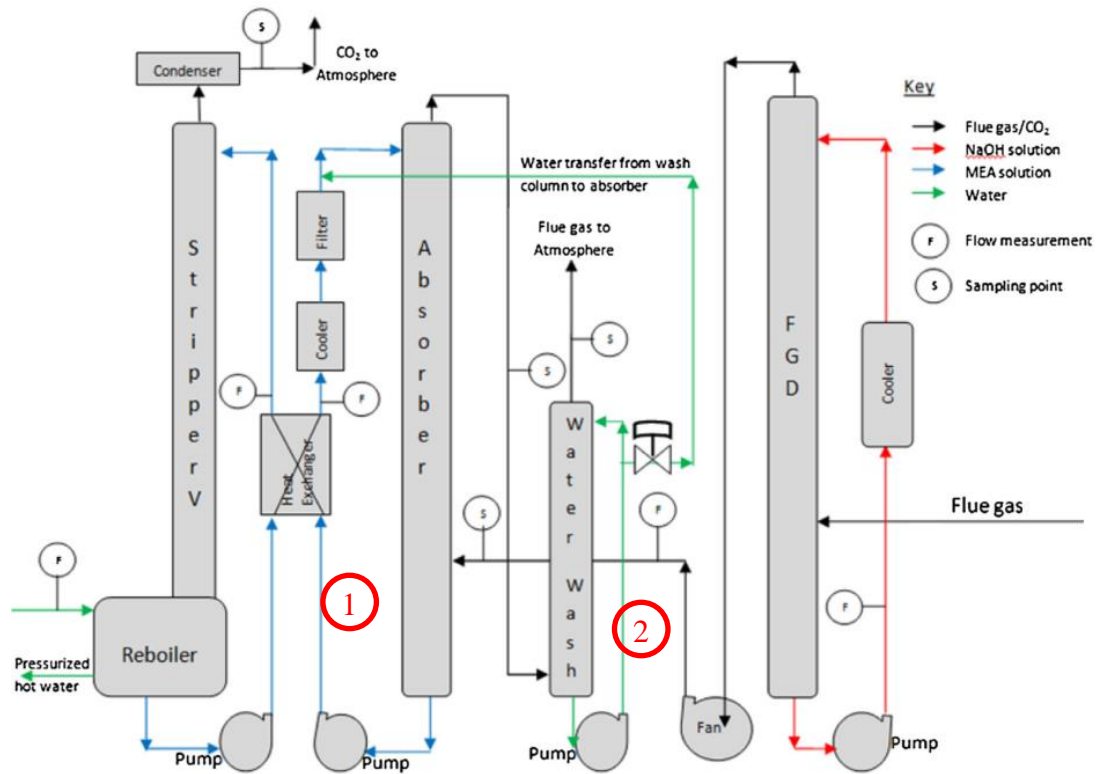


Figure 6.3 Schematic of the pilot-scale carbon capture plant at PACT, adapted from (Akram et al. 2016)

The solvent-based CO₂ capture plant at the PACT facilities is fitted with a flue gas desulphurisation (FGD) tower prior to the CO₂ capture apparatus. The FGD uses a basic (sodium hydroxide) solution to remove the acidic SO₂ from the flue gas before it encounters the CO₂ absorber where SO₂ can react with the carbon dioxide capture solvent. For the experiments in this work, FGD was used to remove SO₂ when burning coal, as it is a high sulphur fuel, but was not used for biomass as it is a lower sulphur content fuel demonstrated in Table 6.1. Instead the FGD unit was operated as a direct contact cooler (DCC) unit by using water to cool the flue gas. The FGD unit was also not operational for 1 day of the coal trial.

The CO₂ absorber used at the pilot-scale facility is 8 metres tall with an inner diameter of 30 cm. Random stainless steel packing (IMTP25) was used inside the column to disperse the solvent, aiding the adsorption process and reducing solvent foaming. This packing was also used for the stripper column which has an air-cooled condenser at the top of the column to prevent solvent loss and a reboiler at the bottom of the column.

The stripper column used by this plant is again 8 metres tall and 30cm wide. It is used to heat the rich MEA to a high enough temperature to release the captured CO₂, which exits the top of the stripper. This is achieved using a downward flowing solvent from the top of the stripper, with a reboiler producing the maximum temperatures at the bottom of the stripper. The reboiler uses pressurised hot water to heat the solvent to a maximum temperature of 120 °C. The pressure was maintained at 1.2 bara. A heat exchanger is used to cool the hot, CO₂ lean solvent from the stripper whilst heating the cool, CO₂ rich solvent from the absorber (Akram et al., 2016).

The pilot scale facilities are fitted with solvent sample removal points at two points in the process. These are located at:

1. The bottom of the absorber – rich MEA sample.
2. The bottom of the water wash – water wash sample.

Samples of rich solvent were collected at the end of each trial and fresh solvent loaded at the start of each 3 day (30 hours) trial. The solvent concentrations and CO₂ loadings were measured for each sample using ¹H NMR spectroscopy and were found to be relatively lean compared to laboratory degradation samples, with loading of 0.12 mole of CO₂ per mole of amine. GC-MS and ¹H NMR spectroscopy were used to quantify the amounts of MEA degradation products in each sample.

6.3 Results

6.3.1 Composition of ashes from particle removal locations

Analysis of the ashes collected from the three particle removal technologies in Figure 6.2 at the PACT pilot scale combustion facilities enabled for the tracking of potassium species at various points in the flue gas. The quantities of ash collected at each of the collection locations are listed in Table 6.2, which reveals larger

quantities of ashes collected by the cyclone and the candle filter for the coal case than for biomass. However the larger quantities of unaccounted for ashes (assumed to have deposited in the water tray) from the biomass case is likely due to the poor grindability of biomass. It is likely that the larger particle sizes in the furnace resulted in more of the ashes falling out of the flue gas early and ending up in the furnace water tray. This is supported by the significantly larger ash percentages accumulating at the heavy fly ash (collection location 1) for the biomass trial compared to coal.

Table 6.2 Quantities of ash collected by the three ash collection locations adapted from (Al-Qayim, 2017)

	Heavy fly ash (wt%)	Cyclone (wt%)	Candle filter (wt%)	Water tray* (wt%)
Biomass-air	2.45	29.45	13.54	54.57
Coal-air	0.51	38.64	16.24	44.61

*by difference

Ashes analysed from collection location 1 were found to have higher moisture content for the biomass trial, as seen in Table 6.3, suggesting incomplete combustion of particles as ashes still contain moisture and carbon. Significantly higher quantities of carbon in the coal ash compared to biomass is unsurprising due the higher quantities of carbon in the raw fossil fuel and the slower combustion rates (Finney et al., 2018). However the higher sulphur measurement for the biomass case is surprising and may be due to the reaction of gaseous SO_x with condensed alkali metals (Loo and Koppejan, 2008).

Elemental oxides analysis of the collected heavy fly ashes reveals an interesting result for potassium oxide (K₂O). Laboratory ash preparation of the fuels used in these trials finds approximately six times as much K₂O in biomass ash compared to coal ash (Table 6.1). However analysis of the collected heavy fly ashes reveals only two times as much K₂O for the biomass case, as seen in Figure 6.4. Unsurprisingly, SiO₂, Al₂O₃ and FeO₃ were found to be highest for the coal case. CaO and MgO were higher for the biomass case, as expected by the fuel analysis. Concentrations of Mn₃O₄, P₂O₅ and SO₃ were also found to be higher for the biomass case.

Ashes from collection location 2, the cyclone, show similar compositional measurements with nearly negligible moisture and very high ash contents shown in

Table 6.4. High carbon and low sulphur measurements for coal match previous findings for collection location 1. Elemental oxides analysis of the collected ashes, Figure 6.5, shows similar trends to the previous with high SiO_2 , Al_2O_3 and FeO_3 for coal and high CaO and MgO for biomass. Concentrations of Mn_3O_4 , P_2O_5 and SO_3 remain higher for the biomass trial and K_2O appears to be notably larger than the difference seen for heavy fly ashes – four times larger for biomass than coal.

Ashes from collection location 3, the candle filter, show higher moisture and carbon contents than location 2, given in Table 6.5. Sulphur and chlorine contributions are significant for the biomass trial at this location. K_2O is shown to be the largest major elemental oxide contributor in Figure 6.6, significantly higher than the concentrations at collection location 2 suggesting that the potassium aerosols are of a particle size small enough to pass through the cyclone but a considerable amount are captured at the ceramic filter. This is supported by the high Cl concentrations at location 2, which may cause the high sulphur content due to metals reaction with sulphur oxides. CaO and SO_3 follow as the second and third highest concentrations for the biomass ash. Whilst SiO_2 , Al_2O_3 and FeO_3 continue to be the largest contributors for coal, a rise in the concentration of CaO is observed. MgO , Mn_3O_4 and P_2O_5 continue to make notably percentage for the biomass case.

Table 6.3 Ash composition analysis for heavy fly ashes

Content	Basis	Units	Biomass	Coal
Moisture	a.r.	wt%	3.7	0.5
Ash	a.r.	wt%	93.1	93.8
Fixed carbon*	a.r.	wt%	3.2	5.7
Elemental				
C	dry	wt%	4.02	9.29
H	dry	wt%	< 0.05	0.23
N	dry	wt%	< 0.05	0.11
S	dry	wt%	0.71	0.41
Cl	dry	wt%	< 0.01	0.08

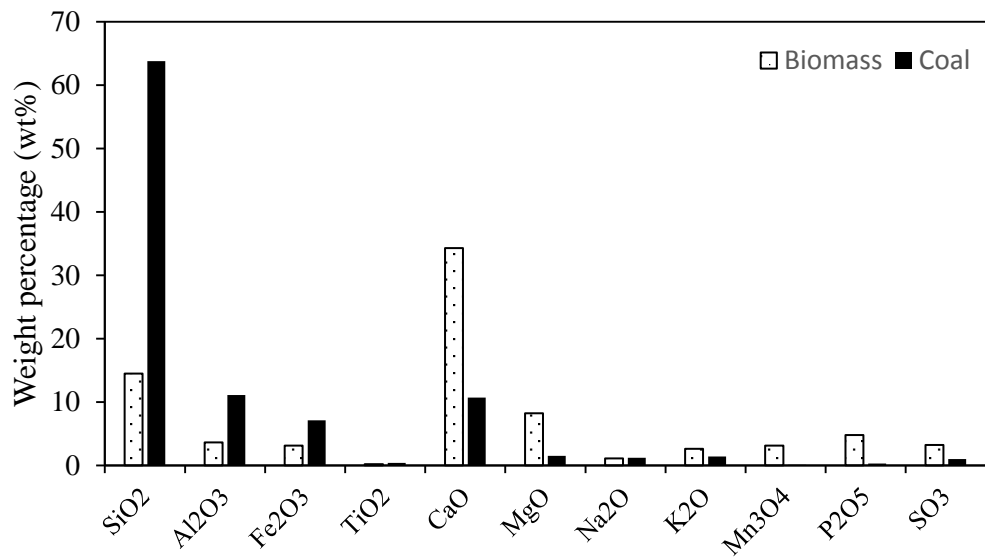


Figure 6.4 Elemental oxide analysis of heavy fly ash collected at location 1

Table 6.4 Ash composition analysis for fly ashes collected at the cyclone

Content	Basis	Units	Biomass	Coal
Moisture	a.r.	wt%	0.1	0.1
Ash	a.r.	wt%	99.9	96.4
Fixed carbon*	a.r.	wt%	0.0	3.5
Elemental:				
C	dry	wt%	0.76	1.83
H	dry	wt%	0.08	< 0.05
N	dry	wt%	< 0.05	< 0.05
S	dry	wt%	0.24	0.16
Cl	dry	wt%	0.03	0.02

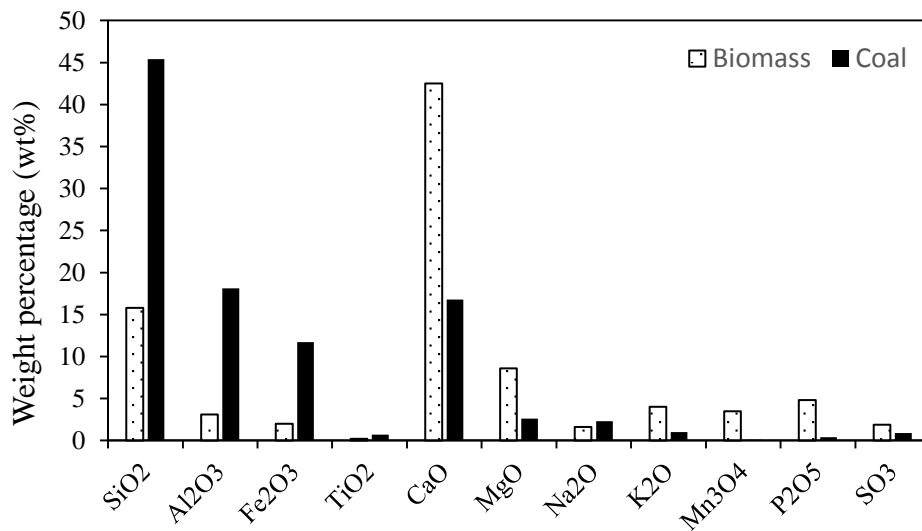


Figure 6.5 Elemental oxide analysis of fly ash collected at location 2

Table 6.5 Ash composition analysis for fly ashes collected at the candle filter

Content	Basis	Units	Biomass	Coal
Moisture	a.r.	wt%	1.8	0.6
Ash	a.r.	wt%	96.5	96.8
Fixed carbon*	a.r.	wt%	1.7	2.6
Elemental				
C	dry	wt%	2.61	1.24
H	dry	wt%	< 0.05	< 0.05
N	dry	wt%	0.05	< 0.05
S	dry	wt%	6.00	2.12
Cl	dry	wt%	0.58	0.05

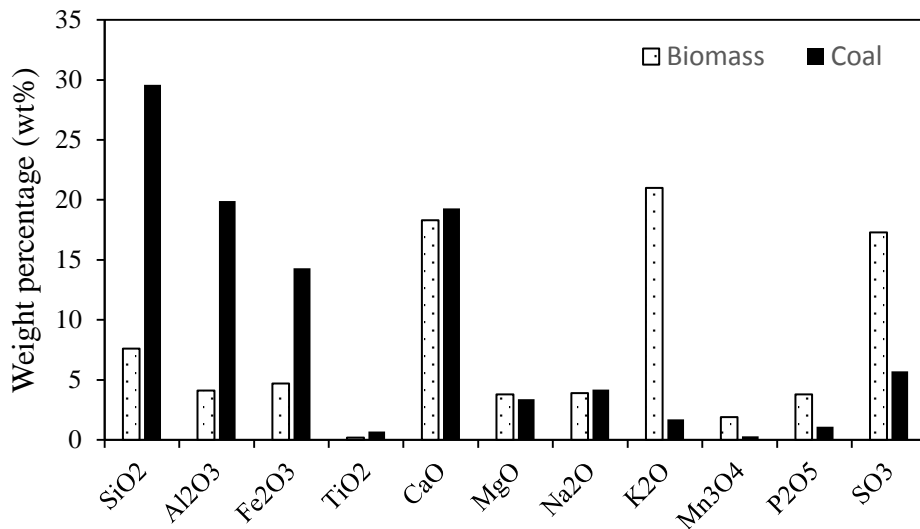


Figure 6.6 Elemental oxide analysis of fly ash collected at location 3

6.3.2 Elemental accumulation in pilot-scale MEA solvents

Solvents used for the pilot scale carbon capture process on biomass and coal flue gases at the PACT facilities were analysed for metal impurities thus enabling the tracking of ash and volatile species that escape the three particle removal technologies used in the previous section. The data for these MEA samples are presented in Table 6.6.

Table 6.6 Elemental accumulation analysis by ICP-OES for MEA solvents from the PACT facility trials.

Element	PACT Biomass (mg/L)	PACT Coal (mg/L)
Al	10.44	10.63
Mg	0.20	<LOQ
Ca	1.44	1.19
Mn	2.73	4.32
Cu	0.17	0.11
Cr	2.64	0.69
K	27.00	4.42
Na	5.73	19.20
Fe	0.58	0.81
Si	6.08	7.61

Results of the ICP-OES analysis of MEA samples from the pilot-scale facility find high quantities of K, Ca and Cr in solution from the biomass trial, compared to the coal trial. MEA samples from the coal trial were found to have more Si, Mn, Fe and Na. These findings generally correlate well with the measures of elemental oxides from ash analysis of the fuels, however the vast difference in Na for coal is unexpected. The higher Cr measurement from the biomass solvent is likely due to the higher fuel Cr content, as found in previous work (Finney et al., 2018).

6.3.3 Degradation products in pilot-scale MEA solvents

The samples of rich solvent collected at the end of each 3 day (30 hours) trial were analysed for the formation of degradation products. The quantification of degradation products was measured using ¹H NMR spectroscopy and GC-MS. ¹H NMR spectroscopy was also used to measure solvent concentrations and CO₂ loadings. Figure 6.7 illustrates the GC-MS quantification of the key oxidative degradation products described in chapter 5, significantly more HEF and HEI are formed in the coal combustion case. Whereas OZD is observed as higher for biomass and similar quantities of HEIA (the main thermal degradation product) are seen for both cases. This is discussed in Section 6.4.

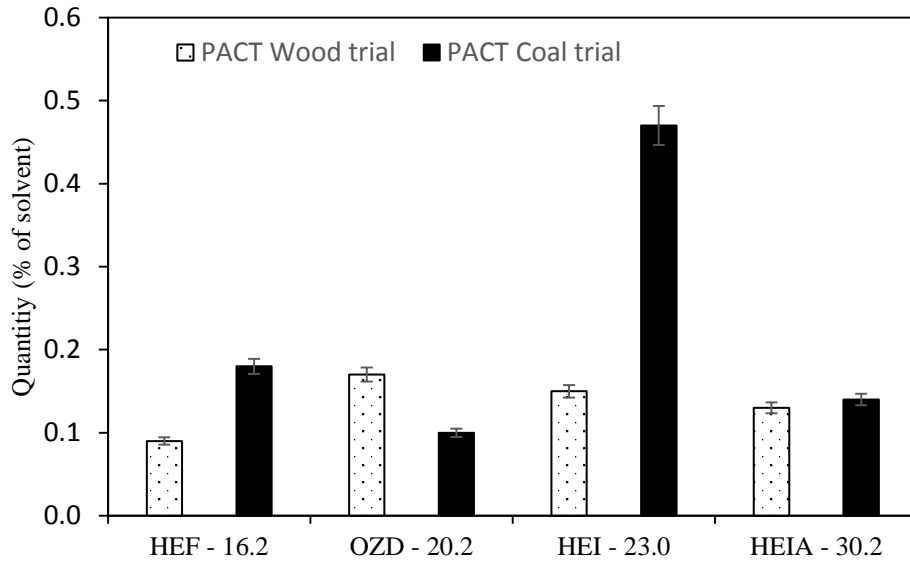


Figure 6.7 Degradation product quantities in pilot-scale MEA samples measured with GC-MS

Interestingly, NMR analysis of the pilot scale MEA samples found no HEI to be present for either case. However the N-oxide characterised in Chapter 5 was present in ratios matching that measured as HEI by the GC-MS results. As illustrated in Figure 6.8, the NMR analysis observed lower quantities of HEINO formed in the biomass test campaign compared to the coal run.

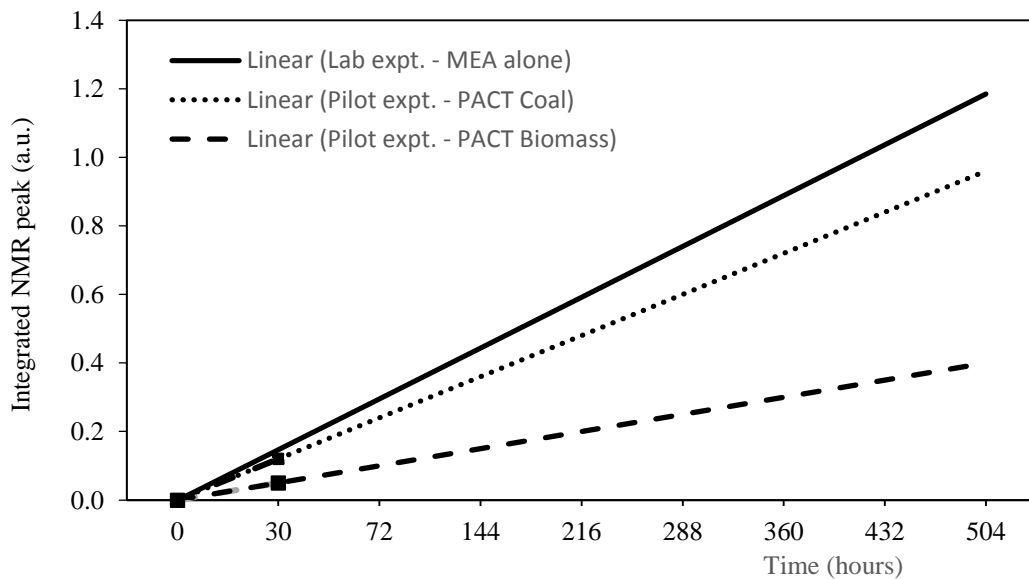


Figure 6.8 Trend comparison of extrapolated HEINO formed under pilot scale experiments compared to the laboratory MEA oxidation

6.3.4 Heat stable salts (HSS) in pilot-scale MEA solvents

Ion chromatography analysis (detailed in chapter 8) of the pilot-scale solvents also reveal higher quantities of nitrate, nitrite, sulphate and oxalate for the coal case as heat stable salts (HSS). Interestingly, all salts are found to be higher for the coal case and up to quantities more than 4 times the amount measured from the biomass trial in the case of sulphate, as seen in Figure 6.9. This is likely due to the fuel sulphur content of coal and higher concentrations of sulphur detected in the biomass ashes at all of the ash collection locations in Section 6.3.1.

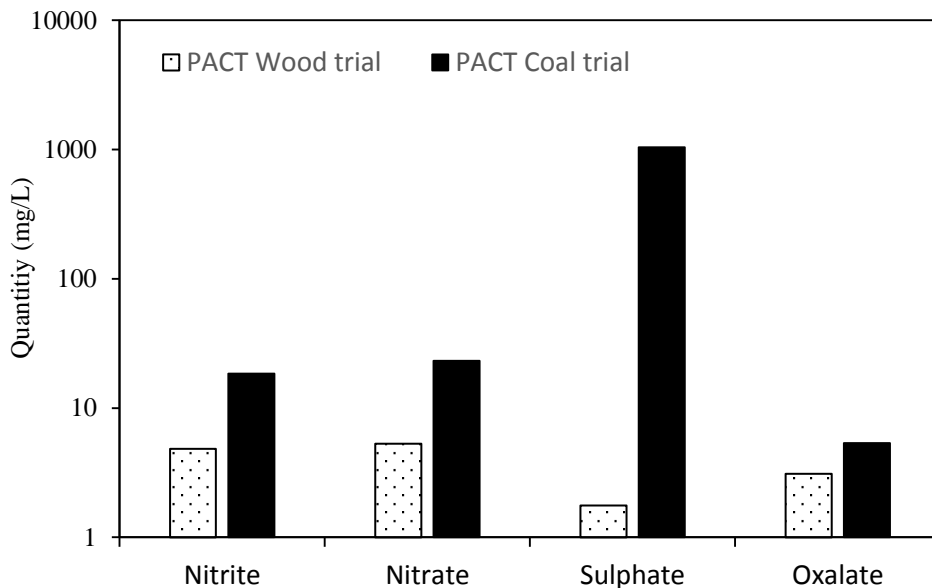


Figure 6.9 HSS quantities measured in pilot-scale MEA samples

6.4 Analysis and Discussion

6.4.1 Ashes from particle removal technologies

The analysis of ashes collected at the three particle removal locations of the pilot-scale combustion facility enables the tracking of key fuel components. The large quantities of bottom ash ending in the water tray of the pilot-scale furnace make it not possible to complete a full mass balance of the fly ash produced during combustion. However it does enable the tracking of flue gas species and compositional data on the ashes that are likely to encounter carbon capture plants.

The results presented in Section 6.3.1 reveal the impacts of the fuels combusted on the composition of ashes removed from the flue gas at the particle collection locations. The initial notable difference between the trials was the larger quantities

of unaccounted ashes for the biomass trial. However the larger quantities of ash collected at the heavy fly ash tee section (location 1) for the biomass case and the high moisture of this ash support the case that this is likely due to the better grindability of coal, which allows for the smaller ash particles to remain in the flue gas rather than falling out into the water tray or heavy fly ash tee section.

The elemental analysis of the ash revealed higher levels of sulphur throughout the ashes collected for the biomass case likely due to higher KCl content. SiO_2 , Al_2O_3 and FeO_3 were significantly higher for the coal case across all collection locations, but were also a considerable quantity for biomass. Concentrations of MgO , K_2O , Mn_3O_4 , P_2O_5 and SO_3 remained higher for ashes from the biomass trial.

Ashes collected from the last location in the flue gas, the candle filter, will show the highest similarity to those encountered by a carbon capture plant. Interestingly at this location concentrations of Cl, K_2O and SO_3 appear to increase and differences between the two trials seem to disappear for CaO and MgO . Which would typically be expected to be larger for the biomass trial.

Potassium is shown to be the largest major elemental oxide contributor in Figure 6.6. With a concentration of K_2O at twelve times larger than coal ashes and double that of ashes prepared in the laboratory, suggesting that the large contributions of potassium and chlorine at the candle filter for the biomass case are likely due to the volatilisation of potassium in the combustion furnace to KCl as identified in chapter 3. Previous work on metal aerosols from the same experimental set-up found potassium to be the only metal in higher concentration for the biomass case (Finney et al., 2018). This increase in K, Cl and S at the candle filter is likely due to the build-up of ash of the filter material, resulting in a caked ash layer on the outside (Basu, 2013). Such a caked layer can provide a surface for the condensation of aerosol species such as KCl and may explain the high quantities of these elements and moisture measured here.

The quantities of ash generated by the pilot-scale facilities used in this study can enable comparisons and very rough estimates of the amounts of ash and volatile species being generated at a full-scale power plant. The pilot-scale facility uses slightly less than 1 tonne of biomass fuel per day, resulting in roughly 7 kg of ash being generated per day (based on a biomass fuel with 0.7% ash being used). Whereas, Drax power station is currently combusting a comparative 20,000 tonnes

of biomass each day which would generate approximately 140 tonnes of ash per day or 5.8 t/hr.

6.4.2 Quantities of K escaping removal

Both candle filters and ESPs, used at Drax, can achieve collection efficiencies of 99.9% (Roddy, 2010). Since 13.5% of total ash particles was captured by the candle filter in these pilot scale experiments, the 0.1% of ash particles that will escape capture equates to approximately 0.0135% of the total ash particles generated, as illustrated in Figure 6.10. Consisting of approximately 20% K_2O , CaO and SO_3 . Hence making 0.0027% of the total ash mass or 200 grams of K_2O per day for PACT.

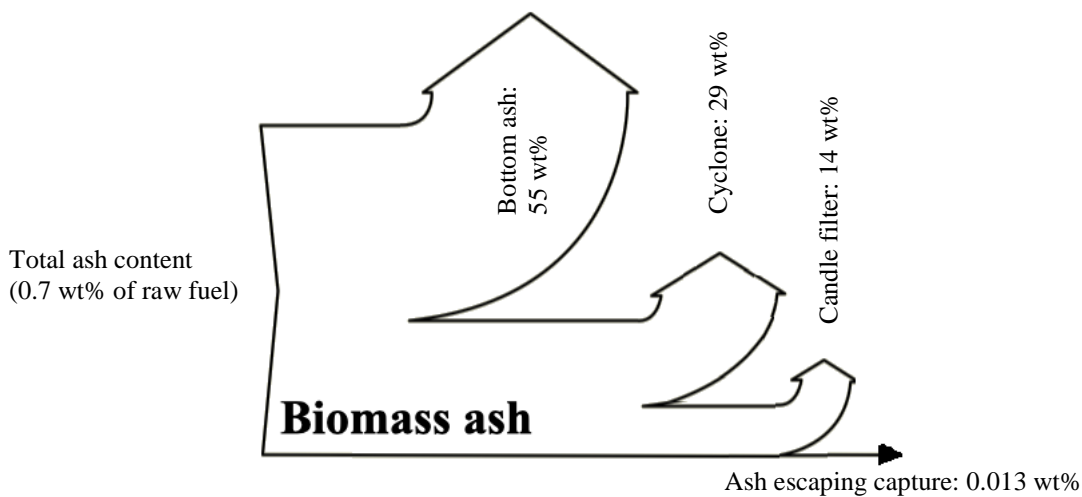


Figure 6.10 Biomass ash flow at PACT facilities

However, based on the findings of chapter 4, white wood particles are expected to release roughly 60% of their original K content during combustion to become volatile K. In such a case, the daily one tonne of white wood pellet would be expected to generate 8 kg of ash, composed of 10% K_2O i.e. 800 g of K_2O per day. 480 g of which be expected to be released during combustion, whereas 320 g will be retained in the solid phase ash.

A lot of the solid phase potassium can be expected to be in the unmeasured ashes of the furnace water tray – approximately 4 kg of unaccounted for ash per day at 10 wt% K_2O . However the 480 g of expected volatile K can be accounted for partially by the 200 g at the candle filter (1 kg per day at 21 wt% K_2O), leaving

approximately 280 g of unaccounted for volatile K likely escaping removal and remaining in the flue gas until carbon capture.

6.4.3 K in solvents

Results of the elemental analysis for metals accumulating in MEA solvents from the pilot-scale facility find high quantities of K, Ca and Cr in solution from the biomass trial compared to the coal trial, whereas MEA samples from the coal trial were found to have more Si, Fe and Na.

The accumulation of potassium in the solvent is clear for the biomass case. The measured concentration of 27 mg/L for a solvent volume of approximately 470 litres (UKCCSRC, 2019), accounts for a deposition of 12.7 g of elemental K over the 3 day (30 hour) trial. This is small relative to the quantities of unaccounted for volatile K, however much of this would likely have condensed on cooling surfaces encountered by the flue gas prior to the carbon capture process. If 0.42 g of K is accumulating in the carbon capture system for every hour of operation, then roughly 300 g would be expected to accumulate per month of full time operation.

Scaling this up to the size of a full-scale power facility from the 1 tonne a day of biomass burned at the pilot facility could provide some insight as to what could be expected by such a facility. Drax currently burns 20,000 tonnes of biomass, by assuming that a similar quantity of volatile K would end up in carbon capture systems, this would predict that approximately 6 tonnes of elemental K would be deposited in the amine every month.

6.5 Conclusions

MEA solvent is known to degrade when exposed to coal-fired power plant flue gas. Biomass and coal fly ash generally contain the same inorganic oxides such as SiO_2 , Al_2O_3 , Fe_2O_3 , CaO , MgO , Na_2O , K_2O and P_2O_5 . Although flue gas treatment technologies have very high particulate removal rates, their efficiency can still be affected by flue gas temperature, moisture content, dew point, particle size distribution and fly ash composition (IEA Clean Coal Centre, 2016). As shown in this chapter, it is still feasible that biomass fly ash particles or gas phase potassium can reach a post combustion capture (PCC) plant and react with the solvents used to possibly inhibit the solvent.

Similar quantities of the main thermal degradation product, HEIA, are seen for both pilot-scale combustion cases. Suggesting that the temperatures that both solvent were exposed to were similar and that temperature was not a factor in the differences in degradation.

Analysis of the samples obtained from the pilot-plant facilities identified a different mix of degradation products formed compared to laboratory experiments. This is unsurprising given the varying temperature and oxygen conditions experienced by the cyclical processing of solvent from a CO₂ capture plant. The pilot plant was not run for a long period thus not enabling the in depth comparison of the full degradation path between coal and biomass flue gases. However these results show the early formation of oxidative degradation products (HEF and HEINO). Analysis suggests that the catalytic effects of coal flue gas on the formation of HEINO is not matched by the use of MEA with biomass flue gases.

Real world PCC processes are not simple. Amines encounter fluctuating temperatures, varying flue gas composition and differences in ambient conditions which can impact on performance. The biomass and coal combustion campaigns were completed using the same equipment and fuel feed rates. However the campaigns were complete at different times, and the SO_x removal equipment was not operative for 1 day for the coal combustion campaign which may influence the sulphur concentration and degradation seen in these solvent samples.

Mitigating degradation in a full-scale industry CCS plant would reduce the operational costs associated with running such a plant and could thus make it more attractive to investors in the power industry. Analysis of the products generated by oxidative degradation can enable us to assess the different reactions undertaken during degradation. Some metals such as copper, chromium, nickel and iron have been found to speed up this oxidative degradation of MEA, these metals are often found in the alloys or corrosion inhibitors used by amine absorber columns.

This work has examined the impact that fly ashes from biomass combustion will have on amine degradation compared to coal fly ashes. The results of laboratory testing in this study has found biomass ashes from white wood combustion to reduce the formation of the major oxidative degradation products. Samples obtained from 3-day pilot-scale air-biomass and air-coal trials at the UKCCSRC's PACT facilities support these finding of less HEINO and HEF formation. Carbon capture processes

are complex and more research is required before conclusions can be drawn on the degradation of amines in a full scale BECCS plant. However these initial findings suggest the carbon capture applied to flue gases from white wood biomass combustion may observe less amine degradation, and thus reduced regeneration costs, than coal or olive biomass plant combustion.

Chapter 7

Overall conclusions

7.1 Overarching key findings

The overarching key findings of this thesis map onto the aims and objectives of the project set out in Chapter 2. Potassium (K) is a crucial element in the combustion of biomass for power generation. K is present in particularly high concentrations in biomass fuel relative to coal and can become volatile during the high temperatures of combustion, though this can be effectively controlled with the use of additives as demonstrated in Chapter 4. This work develops our current understanding of the fate of potassium from the combustion of white wood, wheat straw and olive cake in line with aim 1 of the project.

Volatile K in the fuel gas can be difficult to remove using traditional particle removal technologies, which can result in large quantities of K accumulation within carbon capture processes. Chapter 5 found that potassium deposited into MEA solvents has little impact on the CO₂ absorbance capacity of the solvent. However it also found that biomass ash appears to slow the rate of oxidative MEA product formation, an important result from aim 2 of the project. The work in this chapter also meets the objective of aim 3 by characterising known degradation products and identifying a previously unidentified product which is present in significant quantities.

Chapter 6 scaled up the experimental work in this project to the pilot scale in line with aim 4. Samples of ashes from the UKCCSRC's PACT facilities enabled the tracking of elemental species through different stages of flue gas treatment. While MEA samples from the pilot carbon capture plant confirmed that potassium was the element most likely to be present in high quantities at a BECCS plant. However, this potassium does not appear to catalyse the thermal or oxidative degradation of MEA. These results suggest that using post combustion carbon capture with air fired biomass combustion on a large scale should not have a significant impact on MEA degradation.

7.2 Relevance to industrial applications of BECCS

Based on the findings of the pilot-scale experiments, rough estimates for the amounts of ash and volatile species that would be generated at a full-scale BECCS power plant can be predicted, whilst accounting for the large amounts of these flue gas species that are removed during the flue gas treatment process. Large-scale generation facilities may be fitted with different pollutant removal technologies, such as electrostatic precipitators, which may affect the quantities of volatile K and other species that are removed from biomass flue gases.

These findings suggest that potassium is a key element that is likely to encounter the solvents of carbon capture facilities due to its volatility. High quantities of K, Ca and Cr were found to accumulate in the MEA solution from the pilot-scale biomass trial when compared to the coal trial. However, laboratory testing on the impacts of the key potassium compound, KCl, and biomass ashes found no evidence of catalytic effects on the thermal and oxidative degradation of MEA. Also no impacts were seen on the capacity of the solvent to absorb CO₂ with the addition of KCl. Whilst coal ashes were found to catalyse oxidative degradation, in line with previous literature.

7.3 Concluding remarks

Real world BECCS applications are not simple. There are a variety of technical and non-technical considerations regarding the successful coupling of post-combustion capture with the combustion of biomass to remove CO₂ from the atmosphere. Nevertheless, the recent announcement by Drax power station to continue with significant financial investment into BECCS technology (Drax Group Plc, 2019a) shows promise for the technology. Mitigating degradation in a full-scale industry BECCS plant would reduce the operational costs associated with running such a plant and could thus make it attractive to investors in the power industry.

This work has found biomass ashes from white wood combustion to reduce the formation of the major oxidative degradation products, suggesting that post-combustion carbon capture applied to flue gases from white wood biomass combustion may observe less amine degradation, and thus reduced regeneration costs than coal combustion.

7.4 Future research

7.4.1 Combustion

The combustion experiments identify the volatility of potassium under high temperatures, highlighting its potential to escape particle removal technologies. This work has addressed options for mitigating the release of potassium into the volatile phase using an aluminosilicate additive. As identified by the aims of this work this will reduce slagging and fouling of the furnace. However, further investigation may be required to assess the impact on flue gas treatment technologies such as particle filters, carbon capture solvents and facilities from adding coal ash to the combustion of biomass.

7.4.2 Amine degradation

The results of Chapter 5 and 6 suggest that the use of CCS with biomass combustion instead of coal will not have any significant impacts on CO₂ capture performance or degradation of amines. However, these results are not conclusive in terms of the success of an amine capture system on a BECCS power plant. Further pilot-scale testing would be a logical step in assessing the impacts of biomass flue gases on amine degradation over a prolonged period.

This work has found biomass ashes from white wood combustion to reduce the formation of the major oxidative degradation products for MEA, however other amines and solvents have not been tested in this work. Many leading solvent systems used for industrial carbon capture make use of secondary/tertiary amines or non-amine liquids; these may react differently with potassium salts or biomass ash and thus will require individual testing.

Chapter 8

Experimental Details

8.1 Introduction

This chapter provides the specific details of the experimental apparatus and operation used in this project. The chapter begins with a detailed description of the fuel and ash composition analysis techniques used, followed by specifics of the combustion analysis apparatus. Later in the chapter, the experimental procedure for the degradation of monoethanolamine is described and further details on the identification and quantification of degradation products are given.

8.2 Biomass combustion experimental details

8.2.1 Fuel selection

The three biomass fuels selected for the experimental work of this project are shown in Figure 8.1. These were selected to cover a range of biomass that could be used for power generation in the future. It can be seen that the North American white wood pellet, UK wheat straw and European olive cake were supplied in various forms which required sample preparation in order to obtain a homogeneous sample for experiments.



Figure 8.1 Biomass fuel samples used by this work; a) North American white wood pellet; b) UK wheat straw; c) olive cake.

8.2.2 Sample preparation

8.2.2.1 Retsch SM300 cutting mill



Figure 8.2 Retsch SM300 Cutting Mill

A Retsch SM300 cutting mill, Figure 8.2, was used to first break up the biomass to a particle size <5 mm from their original fuel state for the wood pellet and wheat straw. The olive cake did not require milling as it was already <5 mm. The fuel samples were loaded into the top of the cutter, where the fuel flows down the feeder with the use of two rams (located on the top left and right of the equipment) to a rotor with three stainless steel blades spinning at 1300 rpm. The biomass particles must then pass through a 5mm sieve prior to collection in the bottom pot.

8.2.2.2 SPEX 6770 Freezer mill



Figure 8.3 SPEX 6770 freezer mill

The SPEX 6770 Freezer mill (Figure 8.3) is cryogenic laboratory mill that cools samples to cryogenic temperatures using liquid nitrogen, before pulverising samples by magnetically shuttling a steel impactor. The mill was used to provide particles $<90\mu\text{m}$ for use in ultimates analysis and single particle combustion experiments of chapter 4. The mill components were precooled with liquid nitrogen prior to loading a vial with 3-4g of milled sample. The cryomill was set on a 14 minute milling cycle, after which the sample was passed through a $90\mu\text{m}$ sieve to check satisfactory milling. Any biomass too large to pass through the sieve was milled again.

8.2.2.3 SPECAC 15.011 laboratory manual hydraulic press



Figure 8.4 SPECAC 15.011 laboratory manual hydraulic press

The SPECAC 15.011 laboratory manual hydraulic press is capable of loadings of up to 15 Tonnes. However, for the purpose of these experiments a 5mm diameter pellet die was used with a maximum rating of 2 Tonnes. The die was loaded with 20–60mg of the biomass and additive blends using a spatula and the maximum load of 2 tonnes applied to the die for 30 seconds before removal. Each pellet was made in triplicate as the pellets were fragile and easily broken.

8.2.2.4 Hand drill

A hand drill was used to create a 0.8mm diameter hole in the centre of each pellet for the attachment of the pellet to a 0.5mm diameter needle on the single particle combustion rig. Pellets were fragile and easily broken so a slow, manual drilling approach was employed. The 0.8mm drill bit used to contact the pellet was stainless steel.

8.2.3 Fuel characterisation

Characterisation of the fuels used for this project allows for the interpretation of which key characteristic traits could explain certain behaviours observed during experimental analysis. Characterisation of fuels are complete in accordance with the

European Standard methods detailed below. This enables the identification of major differences between the fundamental composition of fuels prior to experimentation.

8.2.3.1 Proximate analysis

The proximate analysis provides an overview of the main components of the fuel in terms of moisture, volatiles, fixed carbon and ash contents. Moisture content is defined as the mass of water held within the “as received” fuel that is removable through oven drying at 105 °C over a prolonged period (up to 3 hours). Volatile matter is taken to be the mass loss of a small sample (approximately 1g) when rapidly heated upon placement in a 900°C furnace for 7 minutes in a crucible with a loose lid. Volatile matter on a dry basis is adjusted to account for moisture content. ‘Fixed carbon’ is the quantity of material remaining in the sample after the release of volatiles and excluding ash – predominantly considered to be non-volatile organic compounds. Ash is the solid residue remaining after the complete combustion of all carbon and volatile compounds present in the biomass. Ash is measured as the mass remaining after heating a small sample (approximately 1g) in a furnace to a temperature of 250°C for 1 hour and then to 550°C for a further two hours to obtain complete combustion. All fuels were characterized using a Carbolite AAF 1100 furnace and Carbolite moisture oven in accordance with the European Standard methods (EN 18134-1, EN 18122, EN 18123). All samples were run in duplicate and fixed carbon content calculated by mass difference. Dry and dry ash free basis proximate contents were determined by discounting the average values of moisture and ash measured in the sample.

8.2.3.2 Ultimate analysis

Ultimate analysis provides an overview of the elemental composition of the biomass fuels used. For raw ligno-cellulosic biomass these main elemental components are carbon (C), hydrogen (H) and oxygen (O). Nitrogen (N) and sulphur (S) are present in much smaller quantities but are measured due to the oxide gases (NO_x and SO_x) they form during combustion. These were complete using a CE Instruments Flash EA 1112 Series elemental analyser in Figure 8.5 for elemental values, with O calculated by difference after accounting for the ash content. These analysers combust the sample at 900°C to produce CO₂, H₂O, NO₂ and SO₂. These gases then pass through a gas-chromatography column which separates the gases so that the relative percentages of each gas can be detected using a thermal conductivity

detector (TCD). The absolute masses of C, H, N and S in the original sample can then be calculated.

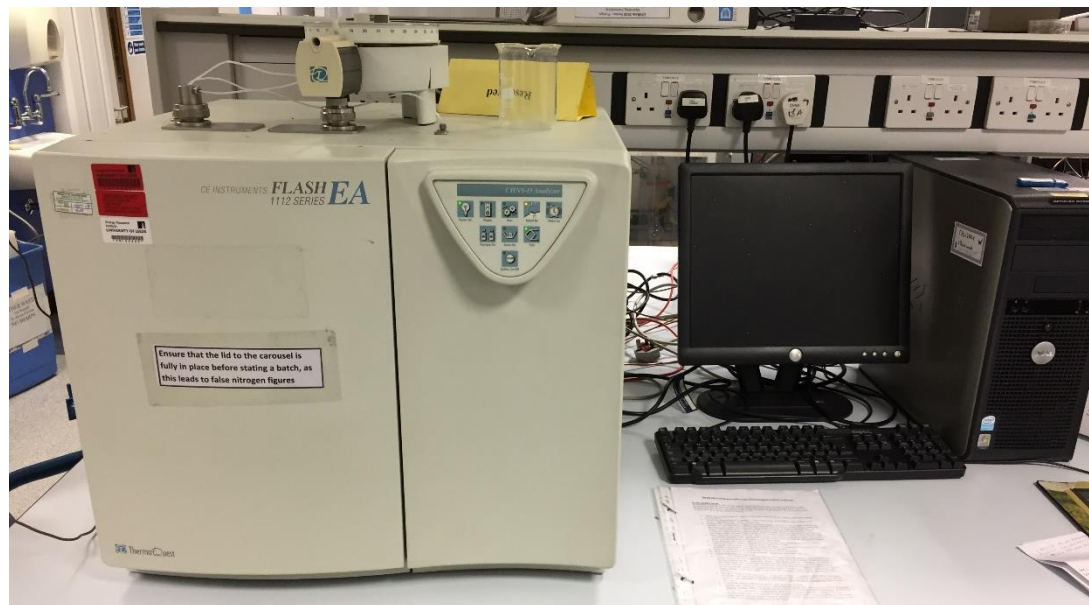


Figure 8.5 CE Instrument Flash EA 112 Series elemental analyser

Samples were run in duplicate in accordance with EN 16948. Weighed samples (2-4mg) of <math><90\mu\text{m}</math> sample were added into small tin capsules which were folded to remove any air. Calibration standard materials were used to calibrate the equipment prior to the running of samples. The calibration standards used for the raw biomass fuels were: atropine, methionine, cystine, sulphanilamide and 2,5-bis(5-tert-butyl-benzoxazol-2-yl)thiophene.

Ash samples were also run using this method to analyse the quantities of unburned carbon in some ash samples. Different calibration standards were used for these experiments due to the lower wt% of carbon present in the samples. For these samples, soil and sediment standards were used to compliment the calibration of the analyser.

8.2.3.3 Inorganic content



Figure 8.6 Varian AA240FS atomic absorption spectrophotometer

Measuring the inorganic content of fuels can be completed by various experimental methods. Inorganics (Na, Mg, Al, K, Ca, Mn, Fe) were measured in this project using atomic absorption spectroscopy (AAS) on ashes digested in accordance with EN 16967:2015. Digested samples were analysed in duplicate and a coal ash reference material was used to validate the data. A Varian AA240FS atomic absorption spectrophotometer was used to measure the major ash components in parts per million (ppm). This is used to calculate an inferred potassium oxide (K_2O) weight percentage in the ash as per equation (8.1) below:

$$K_2O \text{ (wt\%)} = \frac{K \text{ (ppm)} \times \text{Volume (L)} \times 1.205 \text{ (Oxide conversion factor)}}{\text{Ash weight (g)}} \quad (8.1)$$

Ashes were digested prior to AAS using the following procedure: 0.4 g of the sample was weighed to 4 decimal places into a 60 mL polypropylene beaker. 2 mL of distilled water was added to the beaker and swirled, followed by 10 mL of hydrofluoric (HF) acid. The beaker was then placed on a steam bath until all the HF had been evaporated. To the dry residue, 10 mL of hydrochloric (HCl) acid was added, the beaker was then covered with a lid and placed back on the steam bath for 10 minutes. After which approximately 30 mL of distilled water was added into the beaker and allowed to cool. The contents of the beaker were transferred to a 400 mL

Pyrex beaker - washing out carefully. The Pyrex beaker was then placed on a hot plate and evaporated to dryness. The beaker was then removed from the hotplate and allowed to cool before the addition of 5 mL 1:1 H₂SO₄. The beaker was then put back on the hotplate with a clockglass to cover. White sulphuric acid fumes were allowed to persist for at least 5 minutes before removal of the beaker from the hotplate and allowing to cool before 200 mL of distilled water was added to the beaker and left back on the hotplate for 30 minutes. After cooling the solution was transferred to a 250ml volumetric flask and made up to volume and was stored in a plastic bottle.

8.2.4 Single Particle Combustion (SPC) rig

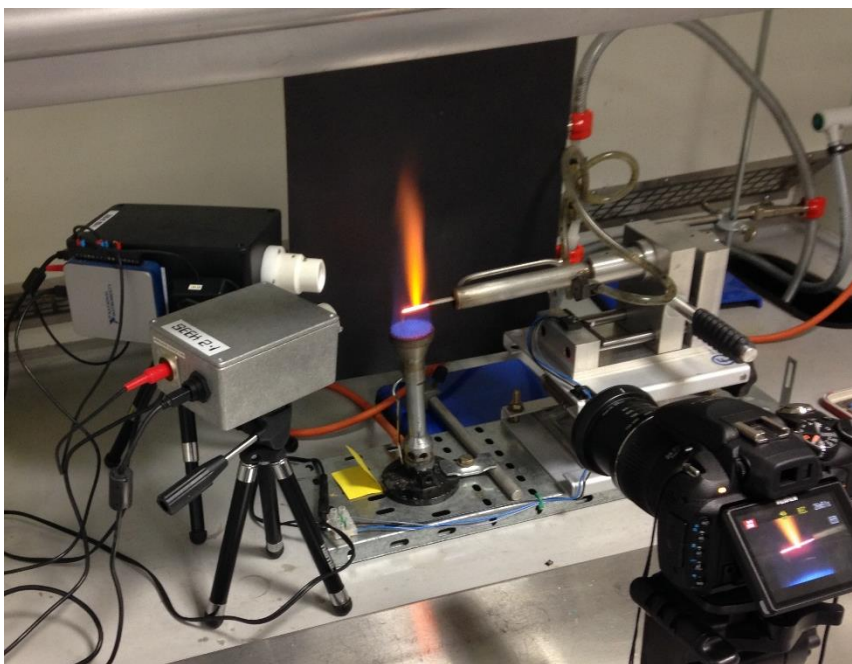


Figure 8.7 Single Particle Combustion Rig

The behaviour of solid fuels during combustion can be examined by exposing single particles of fuel to a high temperature flame. This requires the use of a support rig to hold the particle in the centre of the flame during the combustion, the single particle combustion (SPC) rig used by this project is seen in Figure 8.7. The SPC rig was designed and built at the University of Leeds by Dr. Patrick Mason and full details of the experimental method used by this work are described in (Mason et al., 2015). It is fitted with a water-cooled sleeve, a high-speed video camera (FujiFilm Finepix HS10 camera), a high-speed thermal imaging camera (FLIR A655sc) and two custom-built photodetector devices. The retractable, water-cooled sleeve is used to protect the particle from high temperatures until the desired start of experiment. The high-speed thermal imaging camera and video camera were used to track the

temperature of the pellet and to visually inspect the combustion events after experimentation. While the photodetectors with an optical band-pass filter was used to measure the relative intensity of the spectral emissions at 750 nm and 766 nm wavelengths. 766 nm is characteristic of potassium and 750 nm was used to measure background wavelengths emissions not specifically associated with potassium e.g. soot (Mason, Jones, et al., 2016). Thermal imaging used an emissivity factor of 0.85 for the biomass chars in line with previous work using this thermal imaging camera (Mason, 2016).

8.2.5 Laboratory ash preparations

The method of ash generation used in this work utilised three stainless steel trays (approximately 300 mm length × 150 mm width) to spread the milled raw biomass over a large surface area prior to combustion in a Carbolite AAF 1100 furnace at 550 °C for 5 hours. This method helped to minimize carbon in ash. Samples were weighed before and after ashing.

From Table 8.1 it can be seen that the ash content of all of the biomass fuels decreases with higher temperatures, thus changing the proportions of the ash dilution. The ash content of the additive at elevated temperatures was used to calculate the equivalent mass of the biomass ash in accordance with equation (8.2). This was used to calculate the ratios of biomass ash to additive and thus undo the dilution effects of the additive.

$$(Biomass\ blend\ ash\ weight)_T = (Biomass\ ash\ weight)_T + (Additive\ ash\ weight)_T \quad (8.2)$$

Data acquired from the atomic absorption spectrometer for the measurement of potassium retained in the ash was recorded in parts per million which is used to calculate a potassium oxide (K₂O) percentage. An average of the duplicates was taken prior to accounting for the ash dilution effects of the additive. The addition of a mitigant to the biomass prior to ash generation will result a dilution effect on the biomass ash generated due to the high ash content (96% on an as received basis) of the additive.

Table 8.1 Theoretical and measured ash contents of the biomass with additive blends

Sample and additive wt%	Ash: additive ratio (based on 550°C ash)	Theoretical ash yield (additive) wt%				Actual ash yield, wt%			
		550	850	1000	1150	550	850	1000	1150
Temperature of Ashing (°C)		550	850	1000	1150	550	850	1000	1150
Wood	100%	0.7	0.5	0.4	0.3	0.7	0.5	0.4	0.3
Wood + 5 wt%	11.9%	5.5	5.3	5.2	5.1	5.4	5.3	5.3	5.2
Wood + 15 wt%	5.8%	15.1	14.9	14.7	14.7	15.3	15.2	15.1	15.0
Wood + 25 wt%	4.8%	24.7	24.5	24.3	24.2	25.2	25.1	25.0	24.9
Wheat Straw	100%	5.1	4.5	3.9	3.4	5.1	4.5	3.9	3.4
Wheat Straw + 5 wt%	50.7%	9.9	9.3	8.7	8.2	9.7	9.4	9.3	9.0
Wheat straw + 15 wt%	26.6%	19.5	18.9	18.2	17.7	19.6	19.2	19.0	18.9
Wheat straw + 25 wt%	18.3%	29.1	28.5	27.8	27.3	29.4	29.2	28.5	28.4
Olive	100%	8.1	6.1	5.9	4.7	8.1	6.1	5.9	4.7
Olive + 5 wt%	62.2%	12.9	10.9	10.6	9.5	12.7	10.9	10.4	10.2
Olive + 15 wt%	35.3%	22.5	20.5	20.2	19.0	22.2	20.7	20.5	19.8
Olive + 25 wt%	25.9%	32.1	30.1	29.7	28.6	32.4	30.7	30.4	29.9

8.3 Amine degradation experimental

8.3.1 General experimental

All solvents and reagents were obtained from a commercial supplier without the need for distillation before use. Solvents were removed under reduced pressure using a diaphragm pump with Buchi rotary evaporator. Traces of solvent were removed by drying under high vacuum at 25mbar using a Genevac personal evaporator.

MEA solutions were prepared by adding monoethanolamine (99%), purchased from Alfa Aesar to distilled water (18.2 M Ω cm) to make a 30 wt% solutions. For the thermal degradation experiments 32.45 g of MEA was combined with 75.96 g of distilled water to make a 30 wt% MEA solution which was bubbled with CO₂ at 0.3 L/min for 120 minute using a needle in a 250 mL round bottom flask. 30 wt% MEA solutions for oxidative degradations were typically made up using ~105 g of MEA combined with 350 g of distilled water on the day of the degradation experiment starting.

MEA samples contaminated with potassium salts for VLE experiments were measured to the desired molarity using a four figure balance and mixed until dissolved using an orbital shaker. For example, the 150ml required for the VLE experiments were made up by measuring 5.96 g, 11.92 g and 17.89 g of KCl into 160 mL of 30 wt% MEA solution to produce 0.5 M, 1.0 M and 1.5 M solutions. Ashes or potassium salts added to thermal and oxidative degradation experiments were measured into weighing boat on a four figure balance (3.4g of ash per kilogram of solvent) before being added to the 30 wt% MEA solution which was hand shaken prior to the degradation experiments.

8.3.2 Spectroscopy and chromatography procedures

8.3.2.1 Nuclear Magnetic Resonance (NMR) spectroscopy



Figure 8.8 Bruker Avance III HD-400 NMR spectrometer

NMR spectra were obtained using Bruker Avance III HD-400 spectrometer pictured in Figure 8.8, operating at 400 MHz for ^1H and 100 MHz for ^{13}C . D_2O was employed as the NMR solvent which provided a deuterium lock for the spectrometer and 4,4-dimethyl-4-silapentane-1-sulfonic acid (DSS) was used as a reference peak, with $\delta = 0$. A solution of 13 mg of DSS was prepared in 10ml D_2O for the addition of 75 μL to each NMR tube. Chemical shifts were recorded downfield from this DSS peak at 0 ppm. Proton and carbon assignments in this work are based on an appropriate combination of COSY, HMQC and HMBC spectra analysis with data reported using the following abbreviations; s = singlet, d = doublet, t = triplet.

NMR spectra were integrated with respect to the known quantity of 4,4-dimethyl-4-silapentane-1-sulfonic acid (DSS), in order to calculate the quantities of each degradation product. DSS contains three methyl groups attached to Si as seen in Figure 8.9 which results in a strong peak at chemical shift 0.00 ppm. Since the peak is from three methyl groups it must be attributed to the nine identical protons.

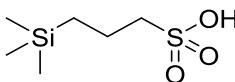


Figure 8.9 Structure of 4,4-dimethyl-4-silapentane-1-sulfonic acid

The number of moles of DSS in each NMR tube, 4.97×10^{-7} , can be calculated by dividing the mass of DSS, 0.0975 mg, by its molar mass, 196.34 g/mol. Each peak from the NMR analysis was integrated respective to the DSS peak and thus must be multiplied by 9 and the number of DSS moles to calculate the number of protons at the single peak. Integrated NMR data provided in Appendix 1. This is divided by Avogadro's number to find the quantity of moles are present for the peak, assuming that 1 peak equates to 1 molecule. This is then multiplied by the molar mass of the product and 0.575 (to account for the dilution of 75 μ L of D₂O added to each 0.5 ml NMR tube).

Thermal and oxidative degradation products (OZD, HEEDA, HEIA, HEI, HEA, HEF and BHEOX) were purchased from Sigma Aldrich and typically 100 mg of each was placed in 0.5 ml of D₂O in order to obtain a clean NMR spectra for each product. Degraded MEA samples were also individually spiked with a 10 mg of each degradation product to confirm the suspected chemical shifts under sample conditions, where factors such as pH can influence shift measurements.

8.3.2.2 High Resolution Mass Spectrometry (HRMS)

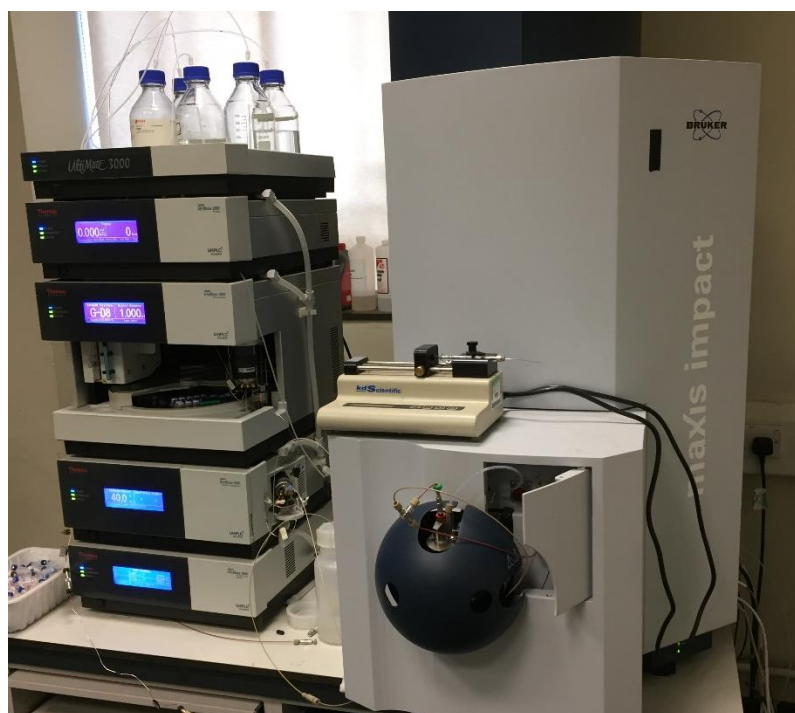


Figure 8.10 Bruker maxis impact spectrometer

Mass spectra (HRMS) were recorded using the Bruker maxis impact instrument pictured in Figure 8.10, with electron spray ionisation (ESI) operating in positive ion mode. Pure compounds (1mg) were diluted in 1ml of MeOH, before a further ten times dilution for injection into the MS. Scans were measured between 50 m/z and 1500 m/z.

8.3.2.3 Infrared (IR) spectroscopy



Figure 8.11 Bruker Alpha FT-IR spectrometer

Infrared (IR) spectra were recorded on a Bruker Alpha FT-IR spectrometer as pure oily liquid samples. Vibrational frequencies are reported in wavenumbers (cm^{-1}).

8.3.2.4 GC-MS degradation product analysis



Figure 8.12 Perkin Elmer Clarus GC-MS with autosampler

A Perkin Elmer Clarus 580 gas chromatograph equipped with an autosampler and Perkin Elmer Clarus 560 mass spectrometer (inert XL EI/CI MSD with triple axis detector). A Rtx-35 Amine Column (30m x 0.32 mm x 1.00 μm) with Helium carrier gas was used for separation of the degradation products with an initial oven temperature of 100°C held for 10 minutes, followed by a ramp rate of 5°C/min to 250°C where it was held for 10 min, (InjAuto=250°C, Split=5:1, Solvent Delay=2.50 min, Transfer Temp=250°C -- Source Temp=180°C, Scan: 10 to 300Da). 1 mL of the thermally degraded solvents was placed in the 2mL borosilicate glass vials before being covered with aluminium crimp seals and loaded in to the GC-MS autosampler.

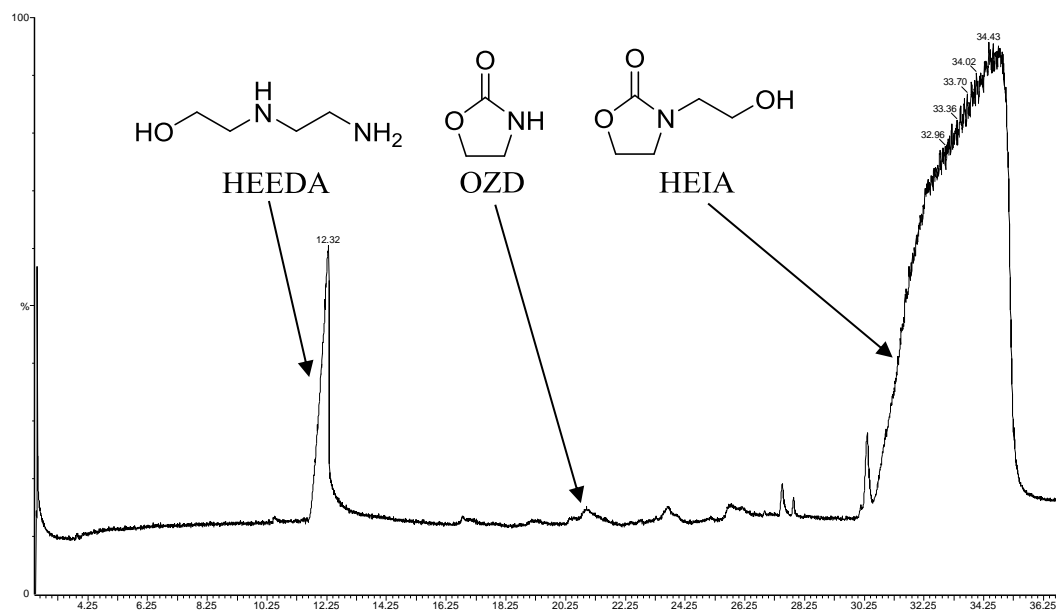


Figure 8.13 Example GC-MS chromatogram of thermally degraded MEA solvent

Example chromatograms from the analysis of thermal and oxidative degradations are provided in Figure 8.13 and Figure 8.14, respectively. Peaks are clearly observed for HEEDA and HEIA in the thermal degradation case. Whereas HEF and HEI are the two clear peaks in the oxidative case, with small peaks observed for the OZD, N-oxide and HEIA.

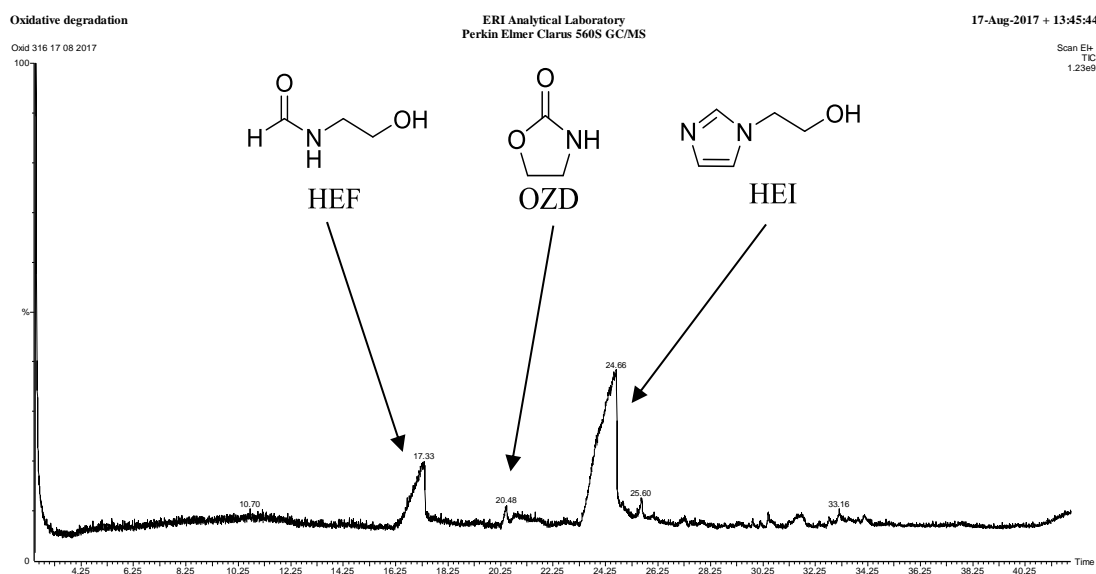


Figure 8.14 Example GC-MS chromatogram of MEA solvent degraded through oxidation

8.3.2.5 Ion Chromatography (IC)



Figure 8.15 Dionex ICS-900 ion chromatography system

Heat stable salts were detected using the Dionex ICS-900 ion chromatography system pictured in Figure 8.15. It consists of a pump, an injection valve and a conductivity cell with an eluent of 5 mM NaOH used for these experiments. Acetate, formate, glycolate, sulphate, oxalate, nitrite and nitrate standards for IC at 1000 mg/L were purchased from Sigma Aldrich. Standards were used to calibrate the system at ion concentrations of 1, 20, 250, 500 and 1000 mg/L. The background conductivity was less than 1 μ S with a system pressure greater than 260 psi. Degraded samples were diluted by 100 for the analysis, similar to literature (Vevelstad et al., 2012).

8.3.3 CO₂ absorption procedures

8.3.3.1 CO₂ absorption procedure for VLE measurements

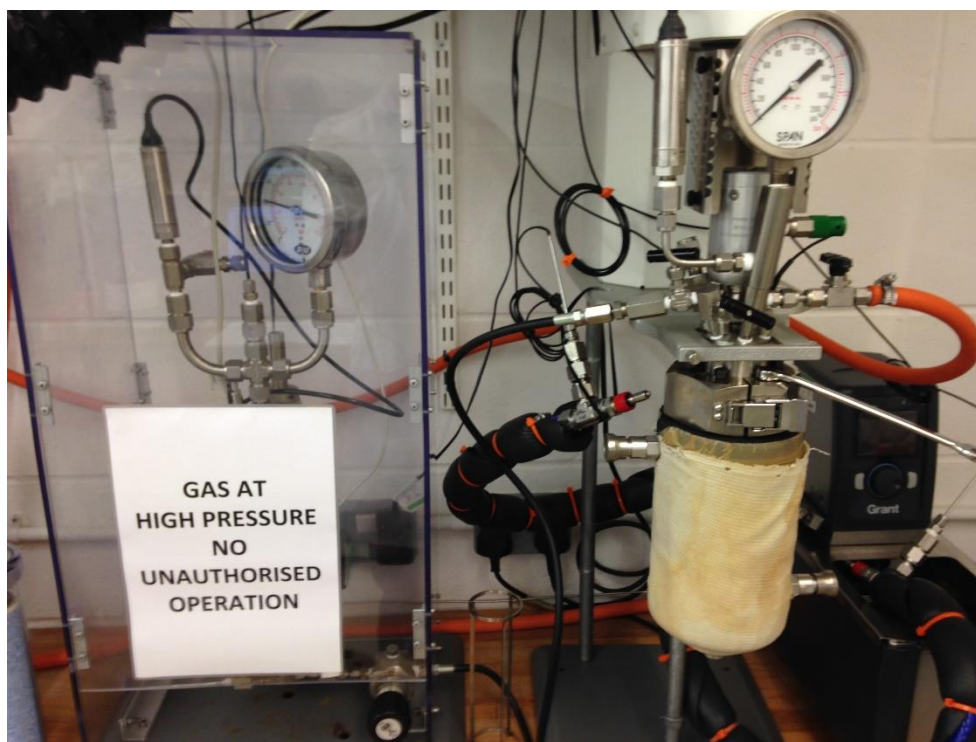


Figure 8.16 Vapour-liquid equilibrium (VLE) apparatus at C-Capture Ltd.

The vapour-liquid equilibrium (VLE) apparatus enables the measurement of CO₂ distribution between the vapour phase and absorbed liquid phase within a sealed vessel. The apparatus used was designed and assembled by C-Capture Ltd. and incorporates a CO₂ gas supply from a storage reservoir to provide gaseous CO₂ to the reactor vessel. The vessel is fitted with a mechanical stirrer and stainless steel jacketed reactor for temperature control using a water/oil heater unit (Grant Instruments). Temperature and pressure probes are also fitted to the reactor to measure the pressure and temperature change within the vessel as CO₂ absorbed by the solvent. These provide an electrical signal reading from the gauges back to data acquisition software (Labview) during the experiments so that the amount of CO₂ removed from the burette can be measured. The number of moles (n) of carbon dioxide absorbed in the experiments is calculated from the ideal gas equation. The rate of reaction is obtained from the data collected based on the number of millimoles of CO₂ absorbed per second.

A set procedure was followed for the running of the VLE apparatus. Each day the apparatus was pressure checked under vacuum for leakages. Pressure inside the

vessel was set to 1 bar using a pressure regulating valve and the partial pressure of CO₂ was set to 0.14 bar to replicate conditions of a solid fuel flue gas. The vessel pressure was set using data acquisition software (Labview), which also tracked the drop in pressure from the CO₂ storage burette over the course of the experiment.

Upon setting the temperature of the experiments to 40 °C, 16 repeated runs of 30% w/w virgin MEA were complete on VLE. From which, the overall capacity for virgin MEA was found to be 2.24 mol/L ± 0.045 (2%) and the rate of absorption: 1.34 mMol/s ± 0.06 (4.5%).

8.3.4 Degradation procedures

8.3.4.1 Thermal degradation procedure and NMR spectra

Tri-clamp stainless steel tubing was used for the thermal degradation experiments. However, as these experiments involve heating a sealed vessel to high temperatures the pressure built up within the vessel is an important consideration. The vapour pressure of 30% w/w MEA can be calculated from the pressure/temperature curve using Antoine's parameters. Based on the data and parameters from literature (S. Wu et al., 2013) for 30-70 °C the pressure temperature curve in Figure 8.17 can be extrapolated. This data was verified as a suitable match for the MEA solutions used by this project by comparing the boiling points at atmospheric pressure, which were matched at 104°C. As can be seen from the curve; the contributing solvent pressures predicted at 120°C, 130°C and 140°C are 1.795bar, 2.46bar, 3.32bar, respectively.

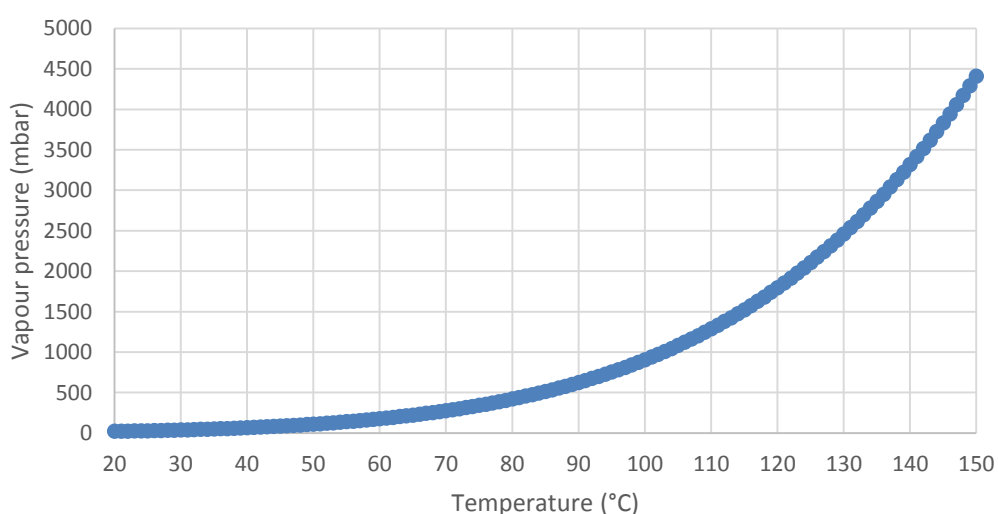


Figure 8.17 Vapour pressure of MEA against temperature

The contribution of solvent vapour pressure to the pressure within the stainless steel vessel is an important contributor to the total pressure. However, in addition to this, the air space left within the vessel at atmospheric pressure will also contribute. To calculate the size of this contribution we must assume the gas behaves under ideal conditions and therefore follows the ideal gas equation (8.3).

$$pV = nRT \quad (8.3)$$

Since the volume (V), moles of gas (n) and the gas constant (R) will remain unchanged over the experiment we can use the difference in temperature (in Kelvin), from before the vessels are sealed (T_1) to after the vessels are in the oven (T_2), to calculate the pressure rise due to this trapped air. From this the pressures from the air trapped within the vessels at suitable temperatures for thermal degradation experiment (120°C, 130°C and 140°C) are calculated as seen in Table 8.2, allowing for the total pressures expected at each of these temperatures to be predicted.

Table 8.2 Total pressures calculated for various degradation experiment temperatures

Temp (°C)	Solvent vapour pressure (bar)	Air pressure (bar)	Total (bar)
120°C	1.7956	1.3646	3.1602
130°C	2.4609	1.3993	3.8602
140°C	3.3193	1.434	4.7533

8.3.4.2 Oxidative degradation procedure



Figure 8.18 Oxidative degradation apparatus set-up

The experimental set-up pictured in Figure 8.18 was used to investigate the oxidative degradation of MEA. This apparatus arrangement is based on previous MEA oxidation experiments was used (Da Silva et al., 2012). Two 500 ml round bottom flasks were used to contain 250 ml of distilled water and the 30% w/w MEA ready for degradation. Compressed air firstly flowed through water to saturate the air and minimize any moisture losses in the solvent reactor which would affect the measured MEA concentrations in solution. Volumes of solvent were measured before and after experiments, however no significant water losses were seen throughout the degradation experiments.

Prior to the start of each experiment, 250 ml of the amine solvent was located in a 500mL round bottom and with the combustion ashes added and hand shaken. The flask was then held at 40 °C and a 0.5 ml aliquot taken for NMR analysis. The

solvent was initially sparged with 0.3 L/min of CO₂ for 2 hours with 0.5 ml taken for NMR after 30 minutes, 1 hour and 2 hours. This was followed by a sparging of compressed air at 0.15L/min for 21 days, with sparging of CO₂ (0.3L/min for 30 minutes) every 3 days to maintain a high carbamate levels. Aliquots of 0.5 ml were taken before each periodic CO₂ sparging and 5 ml aliquots were taken after for GC-MS and IC analysis

8.3.5 Purification of oxidative degradation products

8.3.5.1 Distillation

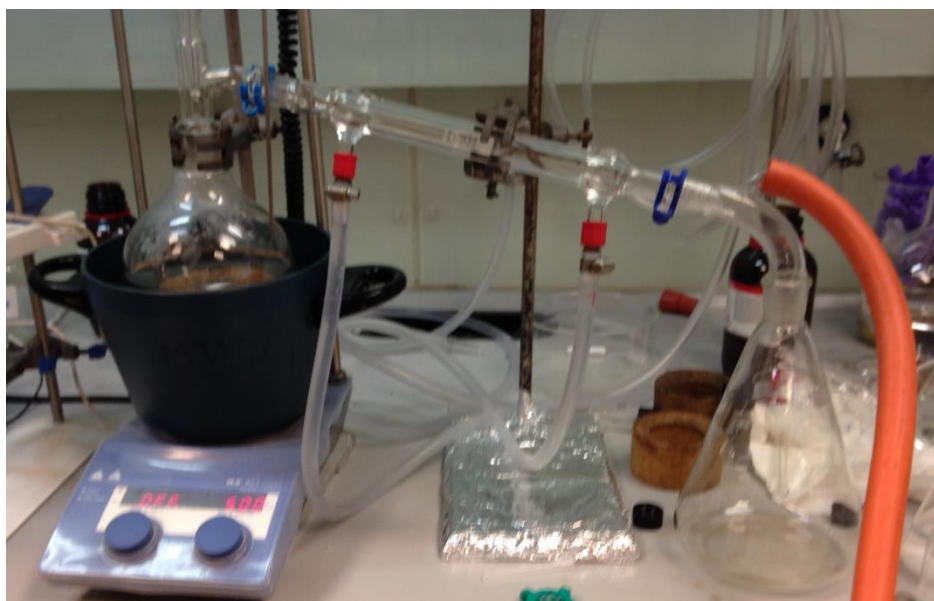


Figure 8.19 Distillation apparatus set-up

Distillation of the degraded MEA solvent using the set-up pictured in Figure 8.18 to remove CO₂, water and MEA and leave the concentrated mixture of degradation products. This residue was useful for the 2D NMR analysis of degradation products in order to established associates carbon and proton chemical shifts. A 500 ml round bottom flask was used to hold the degraded solvent while the water bath was slowly heated across the period of 4-5 hours to a maximum temperature of 60 °C. The distillation was completed under vacuum of 0.8 mbar with a water cooled condenser and conical flask for the collection of the evaporated fraction. Dry ice was used to cool condensers located prior to the pump. The residue was used in attempts to isolate the unknown compound, the mass of residue after distillation was not measured.

8.3.5.2 Preparative High Performance Liquid Chromatography (HPLC)



Figure 8.20 Agilent 1260 Mass Directed Preparative HPLC

Preparative HPLC was complete using an Agilent 1260 connected to a Agilent 6120 quadrupole liquid chromatography mass spectrometer (LC/MS) system for separation of the unidentified compound from the distillation mixture. By specifying the mass N-(2-hydroxyethyl)imidazole (HEI) it was expected that the unknown compound could be purified. Masses were observed at M+1 of 113, 129 and 143 which were intended to be separated into different collection vials however the separation proved ineffective. A Kinetex Reversed Phase C18 HPLC column (5.0 cm x 2.1 mm x 2.6 μm) was used with a gradient acetonitrile (5 to 50%) in water solvent system with 0.1% formic acid. Collected fractions were rotary evaporated at 55 °C to remove acetonitrile and high vacuum used to remove water.

8.3.5.3 Thin-Layer Chromatography (TLC)

Thin-layer chromatography (TLC) of the degradation products were complete using 20 x 5 cm glass TLC plates coated with silica gel from Merck. A mobile phase of 20 % MeOH, 80% DCM and 5 % Triethylamine was used to elute the degradation products from the start point, where the distilled mixture was deposited using a capillary tube and MeOH to dilute the mixture. The deposited material was allowed to dry before the 60 minute separation, the result can be seen in Figure 8.21. After which the silica gel was scraped from the desired sections of the glass plate. Compounds attached to the silica sections were individually extracted in 10 ml of MeOH prior to filtration of the silica. The methanol was removed from these samples using reduced pressure rotary evaporation to afford the separated degradation products. Products were in D₂O for NMR spectroscopy analysis.

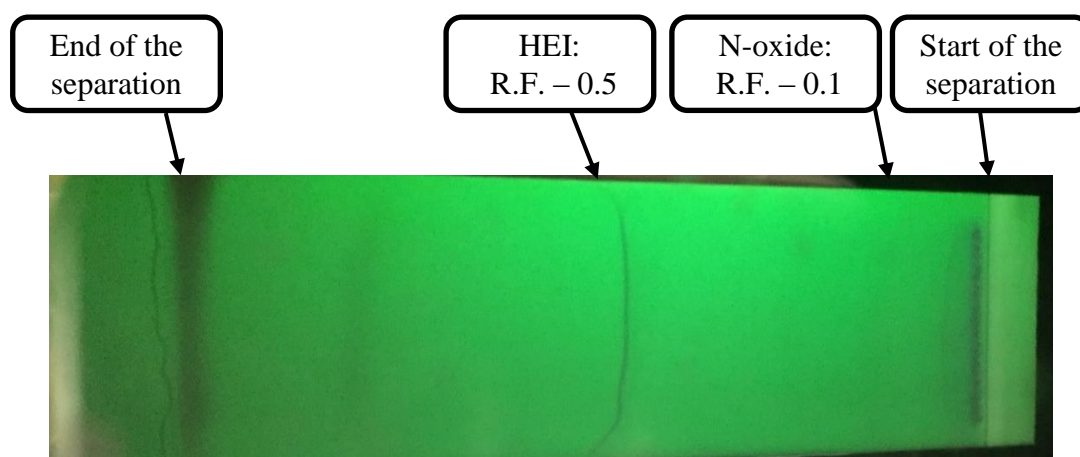
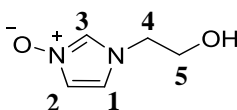


Figure 8.21 Thin-layer chromatography (TLC) of degradation products in 20 % MeOH, 80% DCM and 5 % Triethylamine.

8.3.6 Synthesis of imidazole-N-oxide



A solution of N-(2-hydroxyethyl)imidazole (0.336 g, 1.0 mmol) was prepared in CH_2Cl_2 (1 mL) and cooled to 0 °C. A solution of *m*CPBA (75% *m*CPBA, 0.618 g, 3.0 mmol) in CH_2Cl_2 (1 mL) was added dropwise to the imidazole solution over a period of 5 minutes and the reaction was stirred vigorously for 3h whilst returning to room temperature. Purification was achieved by column chromatography (eluting with 20% MeOH- CH_2Cl_2) which obtained the N-oxide compound (0.062 g, 0.5 mmol, 20%) as a colourless oil; **R_f** 0.10 (20% MeOH- CH_2Cl_2) **¹H NMR** (D_2O , 400 MHz): δ 3.85 (2H, t, $^3J_{\text{HH}} = 5.2$ Hz, O- CH_2), 4.15 (2H, t, $^3J_{\text{HH}} = 5.2$ Hz, N- CH_2), 7.16 (1H, t, $^3J_{\text{HH}} = 5.2$ Hz, N⁺-CH), 7.20 (1H, t, $^3J_{\text{HH}} = 5.2$ Hz, N-CH), 8.25 (1H, t, $^3J_{\text{HH}} = 5.2$ Hz, N⁺-CH-N), **¹³C NMR** (D_2O , 100 MHz): δ 51.2 (N- CH_2) 60.2 (O- CH_2), 118.9 (N-CH), 120.3 (N⁺-CH), 127.8 (N⁺-CH-N); **m/z (ESI)** (Found MH^+ , 128.0656 $\text{C}_5\text{H}_8\text{N}_2\text{O}_2$ requires MH 128.0665). **IR** 3132, 2940, 2854, 1656, 1545, 1477, 1307, 1162, 1135, 1068, 1025, 940, 868, 724, 637.

References

- Aaron, D. and Tsouris, C. 2005. Separation of CO₂ from flue gas: A review In: Separation Science and Technology., pp. 321–348.
- Abanades, J.C., Rubin, E.S. and Anthony, E.J. 2004. Sorbent Cost and Performance in CO₂ Capture Systems. *Industrial & Engineering Chemistry Research*. 43, pp.3462–3466.
- Adams, D. Flue Gas Treatment for CO₂ Capture; IEA Clean Coal Centre: London, UK, 2010.
- Aho, M. and Silvennoinen, J. 2004. Preventing chlorine deposition on heat transfer surfaces with aluminium–silicon rich biomass residue and additive. *Fuel*. 83(10), pp.1299–1305.
- Akbar, S., Schnell, U. and Scheffknecht, G. 2010. Modelling potassium release and the effect of potassium chloride on deposition mechanisms for coal and biomass-fired boilers. *Combustion Theory and Modelling*. 14(3), pp.315–329.
- Akram, M., Ali, U., Best, T., Blakey, S., Finney, K.N. and Pourkashanian, M. 2016. Performance evaluation of PACT Pilot-plant for CO₂ capture from gas turbines with Exhaust Gas Recycle. *International Journal of Greenhouse Gas Control*. 47, pp.137–150.
- Al-Qayim, K.A.J. 2017. Combustion Behaviour of Biomass in Air and Oxy-fuel Environments and Techno-economic Analysis of Biomass Energy with Carbon Capture. (Doctoral dissertation, University of Sheffield).
- Anderson, K. and Peters, G. 2016. The trouble with negative emissions. *Science*. 354(6309), pp.182–183.
- Aronu, U.E., Gondal, S., Hessen, E.T., Haug-Warberg, T., Hartono, A., Hoff, K.A. and Svendsen, H.F., 2011. Solubility of CO₂ in 15, 30, 45 and 60 mass% MEA from 40 to 120 C and model representation using the extended UNIQUAC framework. *Chemical Engineering Science*, 66(24), pp.6393-6406.
- Azzi, M., Day, S., French, D., Halliburton, B., Element, A., Farrell, O. and Feron, P. 2013. Impact of Flue Gas Impurities on Amine - based PCC Plants Final

Report.

- Barth, D., Tondre, C., Lappal, G. and Delpuech, J.J. 1981. Kinetic Study of Carbon Dioxide Reaction with Tertiary Amines in Aqueous Solutions. *The Journal of Physical Chemistry*. 258, pp.3660–3667.
- Basu, P. 2013. *Biomass Gasification, Pyrolysis and Torrefaction: Practical Design and Theory*.
- Baxter, L.L., Miles, T.R., Miles Jr, T.R., Jenkins, B.M., Milne, T., Dayton, D., Bryers, R.W. and Oden, L.L. 1998. The behavior of inorganic material in biomass-fired power boilers: field and laboratory experiences. *Fuel Processing Technology*. 54, p.32.
- BEIS 2018a. *Energy Trends: June 2018* [Online].
- BEIS 2017a. *The Clean Growth Strategy: Leading the way to a low carbon future* [Online].
- BEIS 2019. *UK becomes first major economy to pass net zero emissions law* [Online].
- BEIS 2018b. *Updated energy and emissions projections: 2017* [Online].
- BEIS 2017b. *Updated short-term traded carbon values used for UK policy appraisal 2017* [Online].
- Blomberg, T., 2006. Which are the right test conditions for the simulation of high temperature alkali corrosion in biomass combustion? *Materials and Corrosion*, 57(2), pp.170-175.
- Boot-Handford, M.E., Abanades, J.C., Anthony, E.J., Blunt, M.J., Brandani, S., Mac Dowell, N., Fernández, J.R., Ferrari, M.C., Gross, R., Hallett, J.P., Haszeldine, R.S., Heptonstall, P., Lyngfelt, A., Makuch, Z., Mangano, E., Porter, R.T.J., Pourkashanian, M., Rochelle, G.T., Shah, N., Yao, J.G. and Fennell, P.S. 2014. Carbon capture and storage update. *Energy and Environmental Science*. 7(1), pp.130–189.
- Brack, D. 2017. *The Impacts of the Demand for Woody Biomass for Power and Heat on Climate and Forests*. Chatham House Report. [Online].
- Bridgwater, A.V. and Boocock, D.G.. 2013. *Developments in Thermochemical Biomass Conversion: Volume 1*. Springer Science & Business.

- Bryers, R. 1996. Fireside slagging, fouling, and high-temperature corrosion of heat-transfer surface due to impurities in steam-raising fuels. *Progress in energy and combustion science*.
- Bui, M., Adjiman, C.S., Bardow, A., Anthony, E.J., Boston, A., Brown, S., Fennell, P.S., Fuss, S., Galindo, A., Hackett, L.A., Hallett, J.P., Herzog, H.J., Jackson, G., Kemper, J., Krevor, S., Maitland, G.C., Matuszewski, M., Metcalfe, I.S., Petit, C., Puxty, G., Reimer, J., Reiner, D.M., Rubin, E.S., Scott, S.A., Shah, N., Smit, B., Trusler, J.P.M., Webley, P., Wilcox, J. and Mac Dowell, N. 2018. Carbon capture and storage (CCS): the way forward. *Energy & Environmental Science*, pp.1062–1176.
- CBC News 2018. SaskPower looking for help to fix ‘high cost’ Boundary Dam carbon capture flaw. [Online].
- Chandan, P., Richburg, L., Bhatnagar, S., Remias, J.E. and Liu, K. 2014. Impact of fly ash on monoethanolamine degradation during CO₂ capture. *International Journal of Greenhouse Gas Control*. 25, pp.102–108.
- Chen, H. 2014. Chemical Composition and Structure of Natural Lignocellulose In: *Biotechnology of Lignocellulose* pp. 25–71. Springer, Dordrecht.
- Ciftja, A.F., Hartono, A., Grimstedt, A. and Svendsen, H.F. 2012. NMR study on the oxidative degradation of MEA in presence of Fe²⁺. *Energy Procedia*. 23(1876), pp.111–118.
- CO2CRC 2018. Retrofitting an Australian brown coal power station with post-combustion capture [Online].
- Coda, B., Aho, M., Berger, R. and Hein, K.R.G. 2001. Behavior of chlorine and enrichment of risky elements in bubbling fluidized bed combustion of biomass and waste assisted by additives. *Energy and Fuels*. 15(3), pp.680–690.
- Committee on Climate Change 2018a. Biomass in a low-carbon economy [Online].
- Committee on Climate Change 2018b. Reducing UK emissions – 2018 Progress Report to Parliament [Online].
- Committee on Climate Change 2016. UK climate action following the Paris agreement [Online].
- Cozier, M., 2016. Reactions to the UK's cut to CCS funding: Does CCS have a

- future in the UK?. *Greenhouse Gases: Science and Technology*, 6(1), pp.3-6.
- Damoe, A.J., Wu, H., Frandsen, F., Glarborg, P. and Sander, B., 2012. Combustion aerosols from full-scale suspension-firing of wood pellets. In *International Conference on Impacts of Fuel Quality on Power Production and Environment*.
- Dang, H. and Rochelle, G.T., 2003. CO₂ absorption rate and solubility in monoethanolamine/piperazine/water. *Separation science and technology*, 38(2), pp.337-357.
- Darvell, L.I., Jones, J.M., Gudka, B., Baxter, X.C., Saddawi, A., Williams, A. and Malmgren, A. 2010. Combustion properties of some power station biomass fuels. *Fuel*. 89(10), pp.2881–2890.
- Davidsson, K.O., Steenari, B.M. and Eskilsson, D. 2007. Kaolin addition during biomass combustion in a 35 MW circulating fluidized-bed boiler. *Energy and Fuels*. 21(4), pp.1959–1966.
- Davis, J. and Rochelle, G. 2009. Thermal degradation of monoethanolamine at stripper conditions. *Energy Procedia.*, pp.327–333.
- Desideri, U. and Fantozzi, F., 2013. Biomass combustion and chemical looping for carbon capture and storage. In *Technologies for converting biomass to useful energy: combustion, gasification, pyrolysis, torrefaction and fermentation* (pp. 129-167). CRC Press New York.
- Drax Group Plc 2017. Annual Report 2017 [Online].
- Drax Group Plc 2019a. C-Capture raises £3.5m in funding round led by BP, Drax and IP Group [Online].
- Drax Group Plc 2019b. Environment [Online].
- Drax Group Plc 2018. Drax to pilot Europe's first carbon capture storage project [Online].
- Drax Group Plc 2016. The biggest balls of electricity generation [Online].
- Dumée, L., Scholes, C., Stevens, G. and Kentish, S., 2012. Purification of aqueous amine solvents used in post combustion CO₂ capture: A review. *International Journal of Greenhouse Gas Control*, 10, pp.443-455.
- ECOFYS 2018. Assessing the potential of CO₂ utilisation in the UK [Online].

- Element Energy 2018. Shipping CO₂ – UK Cost Estimation Study [Online].
- Energy Technologies Institute 2016. Progressing Development of the UK's Strategic Carbon Dioxide Storage Resource [Online].
- Estevan Mercury 2017. What was wrong with BD3, and how they fixed it. [Online]. Available from: <https://www.estevanmercury.ca/news/business-energy/what-was-wrong-with-bd3-and-how-they-fixed-it-1.19977450>.
- Eurostat 2018. Agricultural production – crops [Online].
- Fajardy, M., Chiquier, S. and Mac Dowell, N., 2018. Investigating the BECCS resource nexus: delivering sustainable negative emissions. *Energy & Environmental Science*, 11(12), pp.3408-3430.
- Fajardy, M., Chiquier, S. and Mac Dowell, N., 2018. Investigating the BECCS resource nexus: delivering sustainable negative emissions. *Energy & Environmental Science*, 11(12), pp.3408-3430.
- Fajardy, M. and Mac Dowell, N. 2017. Can BECCS deliver sustainable and resource efficient negative emissions? *Energy and Environmental Science*. 10(6), pp.1389–1426.
- Fennell, P. and Anthony, B. eds., 2015. Calcium and chemical looping technology for Power Generation and Carbon Dioxide (CO₂) Capture. Elsevier.
- Finney, K., Szuhánszki, J., Darvell, L., Dooley, B., Milkowski, K., Jones, J.M. and Pourkashanian, M. 2018. Entrained Metal Aerosol Emissions from Air-Fired Biomass and Coal Combustion for Carbon Capture Applications. *Materials*. 11, pp.1819–34.
- Flower, M. and Gibbins, J. 2009. A radiant heating wire mesh single-particle biomass combustion apparatus. *Fuel*. 88(12), pp.2418–2427.
- Fuss, S., Canadell, J.G., Peters, G.P., Tavoni, M., Andrew, R.M., Ciais, P., Jackson, R.B., Jones, C.D., Kraxner, F., Nakicenovic, N., Quéré, C. Le, Raupach, M.R., Sharifi, A., Smith, P. and Yamagata, Y. 2014. Betting on negative emissions. *Nature Publishing Group*. 4(10), pp.850–853.
- Schulz, G., Luedemann, H., Goetze, W. and Wolf, P., BASF SE, 1973. Production of mixtures of monoethanolamine and triethanolamine. U.S. Patent 3,723,530.
- Global CCS Institute 2012. CO₂ Capture Technologies - PostCombustion Capture

(PCC) [Online].

- Goetze, W., Luedemann, H., Schulz, G. and Wolf, P. 1970. Production of mixtures of monoethanolamine and triethanolamine.
- Goff, G.S. and Rochelle, G.T. 2006. Oxidation inhibitors for copper and iron catalyzed degradation of monoethanolamine in CO₂ capture processes. *Industrial and Engineering Chemistry Research*. 45(8), pp.2513–2521.
- Gurvich, L.V., Bergman, G. a., Gorokhov, L.N., Iorish, V.S., Leonidov, V.Y. and Yungman, V.S. 1997. Thermodynamic properties of alkali metal hydroxides. Part 2. Potassium, Rubidium and Cesium Hydroxides. *J. Phys. Chem. Ref. Data*. 26, pp.1031–1110.
- Gutknecht, V., Snæbjörnsdóttir, S.Ó., Sigfússon, B., Aradóttir, E.S. and Charles, L., 2018. Creating a carbon dioxide removal solution by combining rapid mineralization of CO₂ with direct air capture. *Energy Procedia*, 146, pp.129-134.
- Heck, V., Gerten, D., Lucht, W. and Popp, A. 2018. Biomass-based negative emissions difficult to reconcile with planetary boundaries. *Nature Climate Change*. 8(2), pp.151–155.
- Heldebrant, D.J., Koech, P.K., Glezakou, V.A., Rousseau, R., Malhotra, D. and Cantu, D.C., 2017. Water-lean solvents for post-combustion CO₂ capture: fundamentals, uncertainties, opportunities, and outlook. *Chemical reviews*, 117(14), pp.9594-9624.
- Höfer, I. and Kaltschmitt, M., 2019. Assessment of additives avoiding the release of problematic species into the gas phase during biomass combustion—development of a fast screening method based on TGA. *Biomass Conversion and Biorefinery*, 9(1), pp.21-33.
- Huang, L., Li, L., Dong, W., Liu, Y. and Hou, H. 2008. Removal of ammonia by OH radical in aqueous phase. *Environmental Science and Technology*. 42(21), pp.8070–8075.
- Huang, Q., Thompson, J., Bhatnagar, S., Chandan, P., Remias, J.E., Selegue, J.P. and Liu, K. 2014. Impact of flue gas contaminants on monoethanolamine thermal degradation. *Industrial and Engineering Chemistry Research*. 53(2), pp.553–563.

- IEA 2013. Technology Roadmap: Carbon Capture and Storage [Online].
- IEA 2017. World Energy Outlook 2017 [Online].
- IEAGHG 2015. Integrated carbon capture and storage project at Saskpower's boundary dam power station [Online].
- IEAGHG 2007. Post Combustion Carbon Capture From Coal Fired Power Plant - Solvent Scrubbing [Online].
- IEAGHG 2011. Potential for biomass and carbon dioxide capture and storage [Online].
- IEA 2016. 20 Years of carbon capture and storage: Accelerating future deployment [Online].
- IPCC 2014a. 5th Assessment Report: Summary for Policymakers [Online].
- IPCC 2005. Carbon Dioxide Capture and Storage [Online].
- IPCC 2014b. Climate Change 2014 Synthesis Report. Summary for Policymakers [Online].
- IPCC 2018. Global Warming of 1.5 °C - Summary for Policymakers [Online].
- Jasinski, M., Mloston, G., Mucha, P., Linden, A. and Heimgartner, H. 2007. Synthesis of New Bis-imidazole Derivatives. *Helvetica Chimica Acta*. 90, pp.1765–1780.
- Jenkins, B.M. and Baxter, L.L., 1998. TRM Jr (Vol. 54, pp. 17-46). and TR Miles, "Combustion properties of biomass," *Fuel Processing Technology*.
- Jensen, P.A., Frandsen, F.J., Dam-Johansen, K. and Sander, B., 2000. Experimental investigation of the transformation and release to gas phase of potassium and chlorine during straw pyrolysis. *Energy & Fuels*, 14(6), pp.1280-1285.
- Jones, J.M., Darvell, L.I., Bridgeman, T.G., Pourkashanian, M. and Williams, A., 2007. An investigation of the thermal and catalytic behaviour of potassium in biomass combustion. *Proceedings of the Combustion Institute*, 31(2), pp.1955-1963.
- Kakeshpour, T., Bailey, J.P., Jenner, M.R., Howell, D.E., Staples, R.J., Holmes, D., Wu, J.I. and Jackson, J.E. 2017. High-Field NMR Spectroscopy Reveals Aromaticity-Modulated Hydrogen Bonding in Heterocycles. *Angewandte*

- Chemie - International Edition. 56(33), pp.9842–9846.
- Keddy, P.A., 2010. Wetland ecology: principles and conservation. Cambridge University Press.
- Keith, D.W., Holmes, G., Angelo, D.S. and Heidel, K., 2018. A Process for Capturing CO₂ from the Atmosphere. *Joule*, 2(8), pp.1573-1594.
- Kemper, J. 2015. Biomass and carbon dioxide capture and storage: A review. *International Journal of Greenhouse Gas Control*. 40, pp.401–430.
- Klass, D.L. 1998. Biomass for Renewable Energy, Fuels and Chemicals. Elsevier.
- Knudsen, J.N., Jensen, P.A. and Dam-Johansen, K. 2004. Transformation and release to the gas phase of Cl, K, and S during combustion of annual biomass. *Energy and Fuels*. 18(5), pp.1385–1399.
- Koelbl, B.S., van den Broek, M.A., Faaij, A.P.C. and van Vuuren, D.P. 2014. Uncertainty in Carbon Capture and Storage (CCS) deployment projections: A cross-model comparison exercise. *Climatic Change*. 123(3–4), pp.461–476.
- Kubacki, M.L., 2007. Co-Pyrolysis and co-combustion of coal and biomass (Doctoral dissertation, University of Leeds).
- Langat, J., Bellayer, S., Hudrlik, P., Hudrlik, A., Maupin, P.H., Gilman, J.W. and Raghavan, D. 2006. Synthesis of imidazolium salts and their application in epoxy montmorillonite nanocomposites. *Polymer*. 47(19), pp.6698–6709.
- Lashof, D. a and Ahuja, D.R. 1990. Relative Contributions of Greenhouse Gas Emissions to Global Warming. *Nature*. 344(6266), pp.529–531.
- Lebuis, A.-M., Young, J.M.C. and Beauchamp, A.L. 1993. Non-stoichiometric chloride salts of dioxotetrakis(imidazole)rhenium (V) cations. *Canadian Journal of Chemistry*. 71(12), pp.2070–2078.
- Lepaumier, H., Picq, D. and Carrette, P.-L. 2009. New Amines for CO₂ Capture. II. Oxidative Degradation Mechanisms. *Industrial & Engineering Chemistry Research*. 48(20), pp.9068–9075.
- Lepaumier, H., Picq, D. and Carrette, P.L. 2009. Degradation study of new solvents for CO₂ capture in post-combustion. *Energy Procedia*. 1(1), pp.893–900.
- Lepaumier, H., da Silva, E.F., Einbu, A., Grimstvedt, A., Knudsen, J.N., Zahlsen, K.

- and Svendsen, H.F., 2011. Comparison of MEA degradation in pilot-scale with lab-scale experiments. *Energy Procedia*, 4, pp.1652-1659.
- Li, L., Zhao, N., Wei, W. and Sun, Y., 2013. A review of research progress on CO₂ capture, storage, and utilization in Chinese Academy of Sciences. *Fuel*, 108, pp.112-130.
- Lin, Y.S., Liu, C.W. and Tsai, T.Y.R. 2005. 1-Methylimidazole 3-N-oxide as a new promoter for the Morita-Baylis-Hillman reaction. *Tetrahedron Letters*. 46(11), pp.1859–1861.
- van Lith, S.C., Jensen, P.A., Frandsen, F.J. and Glarborg, P. 2008. Release to the gas phase of inorganic elements during wood combustion. Part 2: Influence of fuel composition. *Energy and Fuels*. 22(3), pp.1598–1609.
- Loo, S. Van and Koppejan, J. 2008. *The handbook of biomass combustion and co-firing*. Routledge.
- Lovett, A., Sünnerberg, G. and Dockerty, T. 2014. The availability of land for perennial energy crops in Great Britain. *GCB Bioenergy*. 6(2), pp.99-107.
- Ma'mun, S., Jakobsen, J.P., Svendsen, H.F. and Juliussen, O. 2006. Experimental and Modeling Study of the Solubility of Carbon Dioxide in Aqueous 30 Mass % 2-((2-Aminoethyl)amino)ethanol Solution. *Industrial & Engineering Chemistry Research*. 45(8), pp.2505–2512.
- MacDowell, N., Florin, N., Buchard, A., Hallett, J., Galindo, A., Jackson, G., Adjiman, C.S., Williams, C.K., Shah, N. and Fennell, P. 2010. An overview of CO₂ capture technologies. *Energy & Environmental Science*. 3(11), pp.1645.
- Mancini, I., Guella, G., Debitus, C., Waikedre, J. and Pietra, F. 1996. 172. From inactive nortopsentin D, a novel bis(indole) alkaloid isolated from the axinellid sponge *Dragmacidon* sp. from deep waters south of new caledonia, to a strongly cytotoxic derivative. *Helvetica Chimica Acta*. 79(8), pp.2075–2082.
- Markewitz, P., Kuckshinrichs, W., Leitner, W., Linssen, J., Zapp, P., Bongartz, R., Schreiber, A. and Müller, T.E. 2012. Worldwide innovations in the development of carbon capture technologies and the utilization of CO₂. *Energy & Environmental Science*. 5(6), p.7281.
- Mason, P.E. 2016. *On the combustion of solid biomass fuels for large scale power*

- generation*. (Doctoral dissertation, University of Leeds).
- Mason, P.E., Darvell, L.I., Jones, J.M., Pourkashanian, M. and Williams, A. 2015. Single particle flame-combustion studies on solid biomass fuels. *Fuel*. 151, pp.21–30.
- Mason, P.E., Darvell, L.I., Jones, J.M. and Williams, A. 2016. Observations on the release of gas-phase potassium during the combustion of single particles of biomass. *Fuel*. 182, pp.110–117.
- Mason, P.E., Darvell, L.I., Jones, J.M. and Williams, A. 2017. Release of gas phase potassium during combustion of biomass - experimental and modelling observations. *VGB PowerTech Journal*. 1, pp.1–8.
- Mason, P.E., Jones, J.M., Darvell, L.I. and Williams, A., 2017. Gas phase potassium release from a single particle of biomass during high temperature combustion. *Proceedings of the Combustion Institute*, 36(2), pp.2207-2215.
- McCann, N., Phan, D., Wang, X., Conway, W., Burns, R., Attalla, M., Puxty, G. and Maeder, M. 2009. Kinetics and mechanism of carbamate formation from CO₂(aq), carbonate species, and monoethanolamine in aqueous solution. *Journal of Physical Chemistry A*. 113, pp.5022–5029.
- Miller, B.G. 2005. *Introduction to Coal In: Coal Energy Systems*. Academic Press.
- Mohan, D., Pittman, C.U. and Steele, P.H. 2006. Pyrolysis of wood/biomass for bio-oil: A critical review. *Energy and Fuels*. 20(3), pp.848–889.
- Monteiro, J., Stellwag, I., Mohana, M., Huizinga, A., Khakharia, P., van Os, P. and Goetheer, E., 2018, October. De-Oxygenation as Countermeasure for the Reduction of Oxidative Degradation of CO₂ Capture Solvents. In 14th Greenhouse Gas Control Technologies Conference Melbourne (pp. 21-26).
- Murray, J. 2016. Preparation of 1-methylimidazole-N-oxide (NMI-O). *Organic Syntheses*. 93, pp.331–340.
- Neele, F., Mikunda, T., Seebregts, A., Santen, S., Van Der Burgt, A., Stiff, S. and Hustad, C. 2013. A roadmap towards a European CO₂ transport infrastructure In: *Energy Procedia*., pp. 7774–7782.
- NERC 2017. *Greenhouse Gas Removal from the Atmosphere* [Online].
- Nielsen, H.P., Frandsen, F.J., Dam-Johansen, K. and Baxter, L.L. 2000. Implications

of chlorine-associated corrosion on the operation of biomass-fired boilers. *Progress in Energy and Combustion Science*. 26(3), pp.283–298.

Nussbaumer, T., 2003. Combustion and co-combustion of biomass: fundamentals, technologies, and primary measures for emission reduction. *Energy & fuels*, 17(6), pp.1510-1521.

Ofgem 2018. Biomass Sustainability Dataset 2016-17 [Online].

Öhman, M. and Nordin, A. 2000. The Role of Kaolin in Prevention of Bed Agglomeration during Fluidized Bed Combustion of Biomass Fuels. *Energy & Fuels*. 14(3), pp.618–624.

Olsson, J.G., Ja, U. and Pettersson, J.B.C. 1997. Alkali Metal Emission during Pyrolysis of Biomass. *Energy & Fuels*. 11(7), pp.779–784.

Olsson, J.G., Pettersson, J.B.C., Padban, N. and Bjerle, I. 1998. Alkali Metal Emissions from Filter Ash and Fluidized Bed Material from PFB Gasification of Biomass. *Energy & Fuels*. 12, pp.626–630.

Pereira, H. ed., 2011. *Cork: biology, production and uses*. Elsevier.

Peters, M., Köhler, B., Kuckshinrichs, W., Leitner, W., Markewitz, P. and Müller, T.E. 2011. Chemical technologies for exploiting and recycling carbon dioxide into the value chain. *ChemSusChem*. 4(9), pp.1216–1240.

Plaza, P., 2013. The development of a slagging and fouling predictive methodology for large scale pulverised boilers fired with coal/biomass blends (Doctoral dissertation, Cardiff University).

Pretsch, E., Bühlmann, P. and Badertscher, M. 2009. Structure determination of organic compounds: Tables of spectral data. Springer-Verlag Berlin Heidelberg.

Puxty, G., Rowland, R., Allport, A., Yang, Q., Bown, M., Burns, R., Maeder, M. and Attalla, M. 2009. Carbon dioxide post combustion capture: a novel screening study of the carbon dioxide absorption performance of 76 amines. *Environmental science & technology*. 43(16), pp.6427–6433.

Reynolds, A.J., Verheyen, T.V., Adeloju, S.B., Chaffee, A.L. and Meuleman, E. 2015. Evaluation of methods for monitoring MEA degradation during pilot scale post-combustion capture of CO₂. *International Journal of Greenhouse Gas*

- Control. 39, pp.407–419.
- Riaza, J., Gibbins, J. and Chalmers, H. 2017. Ignition and combustion of single particles of coal and biomass. *Fuel*. 202, pp.650–655.
- Roddy, D.J. 2010. *Advanced power plant materials, design and technology*. Elsevier.
- Röder, M., Thiffault, E., Martínez-Alonso, C., Senez-Gagnon, F., Paradis, L. and Thornley, P. 2019. Understanding the timing and variation of greenhouse gas emissions of forest bioenergy systems. *Biomass and Bioenergy*. 121, pp.99–114.
- Röder, M., Whittaker, C. and Thornley, P. 2014. How certain are greenhouse gas reductions from bioenergy? Life cycle assessment and uncertainty analysis of wood pellet-to-electricity supply chains from forest residues. *Biomass and Bioenergy*. 79, pp.50–63.
- Rodrigues, P.C.R. and Silva Fernandes, F.M.S. 2007. Phase diagrams of alkali halides using two interaction models: A molecular dynamics and free energy study. *Journal of Chemical Physics*. 126(2), pp.1–10.
- Rooney, P.C., Dow Chemical Co, 1999. Amine heat stable salt neutralization having reduced solids. U.S. Patent 5,912,387.
- Rooney, P.C., Dupart, M.S. and Bacon, T.R. 1998. Oxygen's role in alkanolamine degradation. *Hydrocarbon Processing*. 77(7), pp.109–113.
- Saddawi, A., Jones, J.M., Williams, A. and Le Coeur, C. 2012. Commodity fuels from biomass through pretreatment and torrefaction: Effects of mineral content on torrefied fuel characteristics and quality In: *Energy and Fuels*., pp. 6466–6474.
- Sánchez, J.R., Rodriguez, J.M., Alvaro, A. and Estevez, A.M., 2007. The capture of fly ash particles using circular and noncircular cross-section fabric filters. *Environmental Progress*, 26(1), pp.50-58.
- Scott, A., 2015. Learning to love CO₂. *Chemical & Engineering News*, 93(45), pp.10-16.
- Sexton, A. and Rochelle, G. 2006. Oxidation products of amines in CO₂ capture. 8th International Conference on Greenhouse Gas Control Technologies., pp.1–6.

- Sexton, A.J. and Rochelle, G.T. 2009. Catalysts and inhibitors for MEA oxidation. *Energy Procedia*. 1, pp.1179–1185.
- Shao, Y., Wang, J., Preto, F., Zhu, J. and Xu, C. 2012. Ash Deposition in Biomass Combustion or Co-Firing for Power/Heat Generation. *Energies*. 5(12), pp.5171–5189.
- Da Silva, E.F., Lepaumier, H., Grimstvedt, A., Vevelstad, S.J., Einbu, A., Vernstad, K., Svendsen, H.F. and Zahlsen, K. 2012. Understanding 2-ethanolamine degradation in postcombustion CO₂ capture. *Industrial and Engineering Chemistry Research*. 51(41), pp.13329–13338.
- Song, Y., Jiang, G., Chen, Y., Zhao, P. and Tian, Y., 2017. Effects of chloride ions on corrosion of ductile iron and carbon steel in soil environments. *Scientific reports*, 7(1), p.6865.
- Steenari, B.M. and Karlfeldt Fedje, K. 2010. Addition of kaolin as potassium sorbent in the combustion of wood fuel - Effects on fly ash properties. *Fuel*. 89(8), pp.2026–2032.
- Strazisar, B.R., Anderson, R.R. and White, C.M. 2003. Degradation pathways for monoethanolamine in a CO₂ capture facility. *Energy and Fuels*. 17(9), pp.1034–1039.
- Supap, T., Idem, R. and Tontiwachwuthikul, P. 2011. Mechanism of formation of heat stable salts (HSSs) and their roles in further degradation of monoethanolamine during CO₂ capture from flue gas streams. *Energy Procedia*. 4, pp.591–598.
- Szuhánszki, J., 2014. Advanced oxy-fuel combustion for carbon capture and sequestration (Doctoral dissertation, University of Leeds).
- The Royal Society 2018. Greenhouse Gas Removal [Online].
- Thompson, J.G., Bhatnagar, S., Combs, M., Abad, K., Onneweer, F., Pelgen, J., Link, D., Figueroa, J., Nikolic, H. and Liu, K., 2017. Pilot testing of a heat integrated 0.7 MWe CO₂ capture system with two-stage air-stripping: Amine degradation and metal accumulation. *International Journal of Greenhouse Gas Control*, 64, pp.23-33.
- Thornley, P., Tomei, J., Upham, P., Panoutsou, C. and Yates, N., 2008. Supergen

- Biomass & Bioenergy Consortium: Theme 6 Resource Assessment Feedstock Properties. Supergen, Tyndall Centre Manchester, Kings College, London.
- Tilman, D., Socolow, R., Foley, J.A., Hill, J., Larson, E., Lynd, L., Pacala, S., Reilly, J., Searchinger, T., Somerville, C. and Williams, R., 2009. Beneficial biofuels—the food, energy, and environment trilemma. *Science*, 325(5938), pp.270-271.
- UKCCSRC 2019. Overview of the amine plant facility at UKCCSRC PACT for use in modelling studies [Online].
- UNEP 2017. The Emissions Gap Report 2017 - A UN Environment Synthesis Report. [Online].
- UNFCCC 2017. Paris Agreement - Status of Ratification. [Online].
- Uyanga, I.J. and Idem, R.O. 2007. Studies of SO₂ - and O₂ -Induced Degradation of Aqueous MEA during CO₂ Capture from Power Plant Flue Gas Streams.
- Vassilev, S. V., Baxter, D. and Vassileva, C.G. 2014. An overview of the behaviour of biomass during combustion: Part II. Ash fusion and ash formation mechanisms of biomass types. *Fuel*. 117, pp.152–183.
- Vaughan, N.E. and Gough, C. 2016. Expert assessment concludes negative emissions scenarios may not deliver. *Environmental Research Letters*. 11(9).
- Vaughan, N.E., Gough, C., Mander, S., Littleton, E.W., Welfle, A., Gernaat, D.E.H.J. and Van Vuuren, D.P. 2018. Evaluating the use of biomass energy with carbon capture and storage in low emission scenarios. *Environmental Research Letters*. 13(4).
- Vega, F., Sanna, A., Navarrete, B., Maroto-Valer, M.M. and Cortés, V.J., 2014. Degradation of amine-based solvents in CO₂ capture process by chemical absorption. *Greenhouse Gases: Science and Technology*, 4(6), pp.707-733.
- Veltman, K., Singh, B. and Hertwich, E.G. 2010. Human and Environmental Impact Assessment of Post combustion CO₂ Capture Focusing on Emissions from Amine-Based Scrubbing Solvents to Air. 44(4), pp.1496–1502.
- Vevelstad, S.J., Grimstvedt, A., Elnan, J., da Silva, E.F. and Svendsen, H.F. 2013. Oxidative degradation of 2-ethanolamine: The effect of oxygen concentration and temperature on product formation. *International Journal of Greenhouse Gas*

- Control. 18, pp.88–100.
- Vevelstad, S.J., Grimstvedt, A., Knuutila, H., da Silva, E.F. and Svendsen, H.F. 2014. Influence of experimental setup on amine degradation. *International Journal of Greenhouse Gas Control*. 28, pp.156–167.
- Vevelstad, S.J., Grimstvedt, A., Lepaumier, H., Zahlsen, K., Kjos, M.S., Knudsen, J.N. and Svendsen, H.F., 2012. Identification and quantification of degradation products by ion chromatography. In *ACS Symp. Ser (Vol. 1097, pp. 239-247)*.
- Wang, L., Hustad, J.E., Skreiberg, Ø., Skjevraak, G. and Grønli, M. 2012. A Critical Review on Additives to Reduce Ash Related Operation Problems in Biomass Combustion Applications. *Energy Procedia*. 20(1876), pp.20–29.
- Wang, X., Conway, W., Burns, R., McCann, N. and Maeder, M. 2009. Comprehensive Study of the Hydration and Dehydration Reactions of Carbon Dioxide in Aqueous Solution. *The Journal of Physical Chemistry A*. 114, pp.1734–1740.
- Wheatley, J.E., 2017. *Fundamental Chemistry of Carbon Dioxide Capture (Doctoral dissertation, University of Leeds)*.
- Wu, H., Bashir, M.S., Jensen, P.A., Sander, B. and Glarborg, P. 2013. Impact of coal fly ash addition on ash transformation and deposition in a full-scale wood suspension-firing boiler. *Fuel*. 113, pp.632–643.
- Wu, S.H., Caparanga, A.R., Leron, R.B. and Li, M.H., 2013. Vapor pressures of aqueous blended-amine solutions containing (TEA/AMP/MDEA) + (DEA/MEA/PZ) at temperatures (303.15–343.15) K. *Experimental Thermal and Fluid Science*, 48, pp.1-7.
- Xing, P., 2016. *Modelling ash deposition during air firing of high percentages of biomass with coal (Doctoral dissertation, University of Leeds)*.
- Xing, P., Mason, P.E., Chilton, S., Lloyd, S., Jones, J.M., Williams, A., Nimmo, W. and Pourkashanian, M. 2016. A comparative assessment of biomass ash preparation methods using X-ray fluorescence and wet chemical analysis. *Fuel*. 182, pp.161–165.
- Yao, Z.T., Ji, X.S., Sarker, P.K., Tang, J.H., Ge, L.Q., Xia, M.S. and Xi, Y.Q., 2015. A comprehensive review on the applications of coal fly ash. *Earth-Science*

Reviews, 141, pp.105-121.

Yu, C. and Zhang, W. 2001. Modeling potassium release in biomass pyrolysis. *Progress in Thermochemical Biomass Conversion.*, pp.1107–1115.

Yu, C. and Zhang, W., 2008. Modeling potassium release in biomass pyrolysis. In *Fifth International Conference on Thermochemical Biomass Conversion.* Blackwell science.

Zhang, X., Yang, W. and Blasiak, W. 2011. Modeling study of woody biomass: Interactions of cellulose, hemicellulose, and lignin. *Energy and Fuels.* 25(10), pp.4786–4795.

Appendix 1

Integrated NMR values respective to DSS peak for oxidative degradation products, and CO₂ loadings.

Degradation compound: NMR shift:	Formic acid ppm	HEINO ppm	HEF ppm	HEI ppm	Moles of CO ₂ /moles of MEA
MEA alone					
0 days (post-loading)	0.00	0.00	0.00	0.00	0.50
3 days (pre-loading)	0.02	0.31	0.24	0.06	0.35
3 days (post-loading)	0.02	0.35	0.32	0.05	0.50
6 days (pre-loading)	0.22	0.36	2.12	1.01	0.35
6 days (post-loading)	0.13	0.31	2.22	1.06	0.50
9 days (pre-loading)	0.59	0.47	4.25	2.15	0.34
9 days (post-loading)	-	-	-	-	-
12 days (pre-loading)	1.38	0.69	7.5	2.75	0.35
12 days (post-loading)	1.51	0.84	7.93	3.59	0.50
15 days (pre-loading)	1.71	0.73	8.87	4.59	0.36
MEA + Olive ash					
0 days (post-loading)	0.00	0.00	0.00	0.00	0.50
3 days (pre-loading)	0.06	2.73	1.15	0.67	0.27
3 days (post-loading)	0.02	2.97	1.06	0.58	0.50
6 days (pre-loading)	0.20	6.17	2.41	1.28	0.35
6 days (post-loading)	0.20	4.95	2.2	1.05	0.50
9 days (pre-loading)	0.47	7.50	3.69	1.81	0.34
9 days (post-loading)	0.43	6.85	3.44	1.64	0.50
12 days (pre-loading)	0.82	9.36	5.15	2.52	0.35
12 days (post-loading)	0.77	9.06	4.80	2.17	0.50
15 days (pre-loading)	1.11	11.50	6.10	2.75	0.34
15 days (post-loading)	1.95	16.62	8.76	3.81	0.50
18 days (pre-loading)	2.03	17.07	9.38	4.17	0.34
18 days (post-loading)	4.605	20.61	12.80	4.91	0.51
21 days (pre-loading)	3.14	21.97	12.50	5.48	0.35

MEA + Coal ash #1					
0 days (post-loading)	0.00	0.00	0.00	0.00	0.50
3 days (pre-loading)	0.07	1.69	0.72	0.36	0.35
3 days (post-loading)	0.04	1.79	0.82	0.34	0.50
6 days (pre-loading)	0.20	4.05	1.97	1.24	0.35
6 days (post-loading)	0.20	4.29	2.23	1.20	0.50
9 days (pre-loading)	0.42	6.05	3.53	2.16	0.34
9 days (post-loading)	0.70	7.95	4.66	2.39	0.49
12 days (pre-loading)	0.74	9.16	5.17	2.81	0.35
12 days (post-loading)	0.96	9.05	5.36	2.75	0.50
15 days (pre-loading)	1.22	10.85	6.56	3.61	0.33
15 days (post-loading)	1.67	11.56	7.13	3.52	0.50
18 days (pre-loading)	1.76	12.50	7.69	4.23	0.33
18 days (post-loading)	3.07	17.88	12.10	5.50	0.50
21 days (pre-loading)	3.65	16.49	11.00	5.66	0.35

MEA + PACT Biomass ash					
0 days (post-loading)	0.00	0.00	0.00	0.00	0.50
3 days (pre-loading)	0.00	0.00	0.28	0.00	0.35
3 days (post-loading)	0.00	0.00	0.24	0.00	0.50
6 days (pre-loading)	0.06	0.00	0.91	0.24	0.35
6 days (post-loading)	0.03	0.00	0.85	0.00	0.50
9 days (pre-loading)	0.18	0.00	1.84	0.65	0.34
9 days (post-loading)	0.24	0.00	2.70	0.75	0.49
12 days (pre-loading)	0.38	0.00	2.93	1.48	0.35
12 days (post-loading)	0.31	0.00	4.17	1.22	0.50
15 days (pre-loading)	0.76	0.00	5.50	2.70	0.33
15 days (post-loading)	0.76	0.00	5.19	2.16	0.50
18 days (pre-loading)	0.96	0.00	5.39	3.17	0.33
18 days (post-loading)	0.84	0.00	5.85	2.52	0.50
21 days (pre-loading)	1.95	0.00	8.70	4.05	0.34

MEA + PACT Coal ash					
0 days (post-loading)	0.00	0.00	0.00	0.00	0.50
3 days (pre-loading)	0.06	0.43	1.07	1.19	0.35
3 days (post-loading)	0.00	0.66	1.58	1.61	0.50
6 days (pre-loading)	0.22	1.02	2.89	3.32	0.35
6 days (post-loading)	0.29	1.27	3.72	3.82	0.50
9 days (pre-loading)	0.71	2.09	6.2	6.83	0.34
9 days (post-loading)	1.11	3.38	8.57	8.52	0.50
12 days (pre-loading)	1.18	2.88	8.42	9.55	0.35
12 days (post-loading)	1.79	4.02	11.20	10.59	0.50
15 days (pre-loading)	1.68	3.31	10.50	10.94	0.36
15 days (post-loading)	1.89	3.51	10.56	9.84	0.34
18 days (pre-loading)	2.31	3.69	11.70	12.23	0.33
18 days (post-loading)	2.58	4.02	12.50	11.50	0.50
21 days (pre-loading)	3.11	4.35	15.51	15.11	0.35
MEA + KCl					
0 days (post-loading)	0.00	0.00	0.00	0.00	0.50
3 days (pre-loading)	0.00	0.00	0.12	0.04	0.34
3 days (post-loading)	0.00	0.00	0.46	0.14	0.49
6 days (pre-loading)	0.30	0.06	2.24	1.01	0.35
6 days (post-loading)	0.23	0.02	2.17	0.95	0.50
9 days (pre-loading)	0.76	0.19	4.39	1.83	0.34
9 days (post-loading)	0.59	0.16	4.81	2.33	0.49
12 days (pre-loading)	1.37	0.26	6.73	2.77	0.33
12 days (post-loading)	1.44	0.48	7.50	2.93	0.50
15 days (pre-loading)	1.81	0.42	8.31	3.48	0.33
15 days (post-loading)	2.65	0.95	13.5	5.00	0.50
18 days (pre-loading)	2.54	0.54	9.85	4.31	0.33
18 days (post-loading)	3.35	0.89	11.7	4.73	0.50
21 days (pre-loading)	3.72	0.86	12.9	5.45	0.35